A New Solution for an Edge Dislocation with Applications to the Stress and Fracture Analysis of Multilayered Media

By

Aditya Khanna

B.Eng. (Mechanical)

A thesis submitted for the degree of Doctor of Philosophy at the

School of Mechanical Engineering

The University of Adelaide

Australia

Submitted: 1st of December, 2015

Accepted: 16th of March, 2016

Abstract

The stress and fracture analysis of multilayered materials and structures containing crack-like defects is of interest in many research areas, such as composites, bio-mechanics, and geomechanics, and engineering applications, such as coatings, electronics, and adhesive joints. The main objective of this thesis is to further develop a general methodology and utilise it for the examination of fracture problems in multilayered materials. The general methodology is based upon the distributed dislocation technique and edge dislocation solutions obtained within the framework of plane theory of linear elasticity. This methodology has been shaped by the seminal contributions of many researchers over the past fifty years and currently represents a powerful tool for the analysis of crack problems.

New theoretical models and techniques are developed in the present thesis for a range of multi-disciplinary problems utilising the adopted methodology. The research gaps and objectives are formulated specifically for each problem and discussed in separate chapters of this thesis. The solution of each of these problems represents an original and substantial contribution towards the respective area of research. The significant outcomes of this thesis include: a new approach for the analysis of reinforced cracks in layered media, a new mechanism for height control of hydraulic fractures in layered hydrocarbon reservoirs, and a new predictive model for skier-triggered avalanches.

The original contributions of this thesis also include a new fundamental solution for an interfacial edge dislocation, which recovers all previously published solutions for edge dislocations in isotropic multilayered media. The obtained solution can be utilised to derive the governing integral equations for a wide variety of quasi-static crack problems in linearly elastic and isotropic multilayered materials, without any restrictions on the crack orientation or number of elastic layers. Therefore, the newly obtained solution further extends the general

methodology to effectively solve a wide class of fracture problems in multilayered materials and structures.

This thesis is presented in the form of a compendium of publications in high impact specialist journals. The main body of the thesis contains four articles which are united by the above mentioned theme and methodology. Three appendices are also included, which represent a compilation of the candidate's publications on related topics. A complete publication list is provided in the forthcoming pages.

Declaration

I certify that this thesis contains no material which has been accepted for the award of any other degree or diploma in my name in any university or other tertiary institution and, to the best of my knowledge and belief, contains no material previously published or written by another person, except where due reference has been made in the text. In addition, I certify that no part of this thesis will, in the future, be used in a submission in my name for any other degree or diploma in any other university or other tertiary institution without the prior approval of the University of Adelaide.

I give consent to this copy of my thesis when deposited in the University library, being made available for loan and photocopying, subject to the provisions of the Copyright Act 1968. I acknowledge that copyright of the published works contained within this thesis resides with the copyright holder(s) of those works.

I also give permission for the digital version of my thesis to be made available on the web, via the University's digital research repository, the Library Search and also through web search engines.

Aditya Khanna Date

Acknowledgements

I would like to begin by thanking A/Prof Andrei Kotousov for his mentorship and continuous efforts towards my professional development. Over the years, Andrei not only acted as my research supervisor but also provided me with several career enhancing opportunities. For that, I am very grateful to him. I hope that our collaboration is long lasting.

The research undertaken in this thesis would not have been possible without the financial support in the form of the Australian Postgraduate Award administered by the University of Adelaide on behalf of the Department of Education and Training of the Australian government. The additional financial support from the School of Mechanical Engineering in the form of causal teaching-assistant and lecturing positions is also greatly acknowledged. I would like to thank A/Prof Colin Kestell, Dr Antoni Blazewicz, Mr Gareth Bridges, A/Prof Andrei Kotousov, Dr John Codrington, A/Prof Zonghan Xie, and Dr Zhao Tian for offering me these positions.

I greatly appreciate the guidance and support received from Prof Pavel Bedrikovetsky during my candidature. I would also like to thank the editors and anonymous reviewers for their constructive and valuable feedback during the peer-review of manuscripts included in this thesis. Special thanks go to Ms Tracy Miller for proof-reading the thesis prior to submission.

I dedicate the thesis to my parents, Vijay and Renu Khanna and my sister, Maulshree Khanna. It is due to their continued support that I was able to pursue my interests freely.

List of publications

This thesis is comprised of published and submitted journal articles in accordance with the Academic Program Rules 2015 of The University of Adelaide. A complete list of articles written during the candidature is presented here. The main body of the thesis is based on the following journal articles:

1) **A. Khanna** and A. Kotousov (2015), A new predictive model for the onset of skier-triggered avalanches, *Geophys. Res. Lett.*, revised manuscript under review.

2) **A. Khanna** and A. Kotousov (2015), The stress field due to an interfacial edge dislocation in a multi-layered medium, *Int. J. Solids Struct.*, 72, 1-10, doi: 10.1016/j.ijsolstr.2015.06.030.

3) **A. Khanna** and A. Kotousov (2015), Controlling the height of multiple hydraulic fractures in layered media. *SPE J.*, SPE-176017-PA, 1-8, doi: 10.2118/176017-PA.

4) **A. Khanna** and A. Kotousov (2014), Stress analysis of a crack in a fiber-reinforced layered composite, *Compos. Struct.*, 118, 139-148, doi: 10.1016/j.compstruct.2014.07.024.

The following journal articles are of closely related to the main topic of research and are included in the thesis as appendices:

5) L. Bortolan Neto, **A. Khanna** and A. Kotousov (2015), Conductivity and performance of hydraulic fractures partially filled with compressible proppant packs. *Int. J. Rock Mech. Mining Sci.*, 74, 1-9, doi: 10.1016/j.ijrmms.2014.11.005.

6) **A. Khanna**, L. Bortolan Neto and A. Kotousov (2014), Effect of residual opening on the inflow performance of a hydraulic fracture, *Int. J. Eng. Sci.*, 74, 80-90, doi: 10.1016/j.ijengsci.2013.08.012.

7) A. Kotousov, L. Bortolan Neto and **A. Khanna** (2014), On a rigid inclusion pressed between two elastic half spaces, *Mech. Mater.*, 68, 38-44, doi: 10.1016/j.mechmat.2013.08.004.

The remaining journal articles authored by the candidate are not related to the main topic of the thesis. These articles are listed below but not included in the thesis.

8) **A. Khanna**, A. Keshavarz, K. Mobbs, M. Davis and P.Bedrikovetsky (2013), Stimulation of the natural fracture system by graded proppant injection, *J. Pet. Sci. Eng.*,111, 71-77, doi: 10.1016/j.petrol.2013.07.004.

9) L. Bortolan Neto and **A. Khanna** (2013), The performance of hydraulic fractures partially filled with compressible proppant, *Aust. J. Multidiscip. Eng.*, 10(2), 185-197.

10) **A. Khanna**, A. Kotousov, J. Sobey and P. Weller (2012), Conductivity of narrow fractures filled with a proppant monolayer, *J. Pet. Sci. Eng.*, 100: 9-13, doi: 10.1016/j.petrol.2012.11.016.

The outcomes of the undertaken research were also presented at several international peer-reviewed conferences. The complete list of conference articles is provided below, however these articles are not included in the thesis.

11) M. Mohabuth, D. Chang and **A. Khanna**, Experimental study on local plastic collapse in a plate weakened by two collinear cracks, Proceedings of the 4th International Conference on Advances in Mechanics Engineering (ICAME 2015), 20-21 July 2015, Madrid , Spain, doi: 10.1051/bioconf/20152801002.

12) **A. Khanna** and A. Kotousov, A mathematical model for interfacial defects in snow layers, Proceedings of the 4th International Conference on Advances in Mechanics Engineering (ICAME 2015), 20-21 July 2015, Madrid , Spain, doi: 10.7763/IJMMM.2016.V4.256.

13) **A. Khanna** and A. Kotousov, Numerical implementation of an interfacial edge dislocation solution in a multi-layered medium, Proceedings of the 17th International Conference on Applied Mechanics and Mechanical Engineering (ICAMME 2015), 13-14 July 2015, Stockholm, Sweden.

14) A. Kotousov, **A. Khanna** and S. Bun, An analysis of elasto-plastic fracture criteria, Recent Advances in Structural Integrity Analysis - Proceedings of the International

Congress (APCF/SIF-2014), 9-12 December 2014, Sydney, Australia, doi: 10.1533/9780081002254.67.

15) **A. Khanna**, Stress analysis of a crack near an elastic layer, Proceedings of the 8th Australasian Congress on Applied Mechanics (ACAM 8), 23-26 November 2014, Melbourne, Australia.

16) A. Keshavarz, **A. Khanna**, T. Hughes, M. Boniciolli, A. Cooper and P. Bedrikovetsky, Mathematical model for stimulation of cbm reservoirs during graded proppant injection, Proceedings of the SPE/EAGE European Unconventional Resources Conference and Exhibition, 25-27 February 2014, Vienna, Austria, doi: 10.2118/167758-MS.

17) L. Bortolan Neto, **A. Khanna** and A. Kotousov, A new approach to evaluate the performance of partially propped hydraulic fractures, Proceedings of the 2013 APPEA Conference and Exhibition, 26-29 May 2013, Brisbane, Australia.

18) A. Keshavarz, K. Mobbs, **A. Khanna** and P. Bedrikovetsky, Stress-based mathematical model for graded proppant injection in coal bed methane reservoirs, Proceedings of the 2013 APPEA Conference and Exhibition, 26-29 May 2013, Brisbane, Australia.

19) **A. Khanna**, M. Mohabuth and A. Kotousov, On the residual opening of a hydraulic fracture, Proceedings of the 8th International Conference on Structural Integrity and Fracture (SIF 2013), 11-12 July 2013, Melbourne, Australia.

20) P. Bedrikovetsky, A. Keshavarz, **A. Khanna**, K. Mckenzie and A. Kotousov, Stimulation of natural cleats for gas production from coal beds by graded proppant injection, Proceedings of the SPE Asia Pacific Oil and Gas Conference and Exhibition, 22-24 October 2012, Perth, Australia, doi: 10.2118/158761-MS.

21) **A. Khanna** and A. Kotousov, Steady flow towards a row of collinear hydraulic fractures, Proceedings of the 7th Australasian Congress on Applied Mechanics (ACAM 7), 9-12 December 2012, Adelaide, Australia.

Table of Contents

Chapter 1

Introduction

Chapter 1

Introduction

In this introductory chapter, an overview of multilayered materials and structures is presented, focussing on their engineering applications and prevalence in nature. It is highlighted that the stress and fracture analysis of these materials and structures is important in a number of engineering and research contexts. The fracture mechanisms of multilayered media as well as the common methods for the solution of crack problems are also reviewed. Descriptive summaries of the subsequent chapters are presented to highlight the specific research gaps addressed in each chapter of this thesis.

1.1 Multilayered materials

Multilayered materials and structures find a variety of applications in modern engineering. For example, composite laminates, which are formed by stacking several layers of fiber-reinforced plies, are increasingly used in the design of various structural components across many industries. Composite laminates offer many advantages in comparison with traditional structural materials. These include high strength combined with low weight, improved stiffness and durability (Reddy, 2004). Other advantages include better manufacturability, which is important in the fabrication of aerodynamically-efficient shapes for aerospace and automotive applications (Soutis, 2005). Additionally, the layered arrangement readily permits for the integration of actuators, smart sensors, processors and interconnections within the composite laminates, transforming them into "intelligent structures" (Crawley, 1994).

Another important category of multilayered media is protective surface coatings for structures operating in a harsh environment. Examples include the wear-resistant coatings for machining and cutting tools (Dolinšek et al., 2001), anticorrosive coatings used in construction and marine applications (Sørensen et al., 2009) and thermal barrier coatings in gas turbine engines, nuclear power plants, space shuttles, etc. (Nguyen et al., 2010; Miller, 1987). The application of protective coating can significantly increase the lifespan and integrity of the structures without increasing their weight and cost (Stern, 1996).

In other engineering applications, multilayered structures are selected for reasons other than the strength and durability considerations. These include periodically layered mechanical filters for vibration isolation (Zhuang et al., 2003; Sackman et al., 1989), piezoelectric multilayer actuators (Pritchard et al., 2001) and microelectromechanical systems or MEMS (Dunn et al., 2002). These structures may face integrity problems due to the mismatch in material properties and experience failure under thermal or electro-magnetic loading.

Multilayered arrangements are also prevalent in nature, ranging in length scale from a few micrometres to several kilometres. Hierarchical biological materials, such as sea shells, glass sponges, nacre and tooth enamel, possess a layered microstructure (Dunlop and Fratzl, 2010). An understanding of the unique toughening mechanisms of these biological materials has led to the development of a new class of bio-inspired synthetic composites, which possess a combination of high strength and toughness (Mirkhalaf et al., 2014; Walley et al., 2012; Barthelat and Zhu, 2011; Espinosa et al., 2011; Bonderer et al., 2008; Munch et al., 2008; Podsiadlo et al., 2007; Tang et al., 2003).

Geological materials, such as sedimentary rocks, soil, ice and snow also display a multilayered or stratified arrangement on the macro-scale (Reading, 1996). Sedimentary rocks are exploited for natural resources like coal, fossil fuels and mineral ores and the study of the sequence of strata in sedimentary rock and

ice sheets is the main source of scientific knowledge about the Earth's history (Boggs, 2006). The layered structure of soils and sedimentary rocks is an important consideration in the design of foundations and other sub-surface structures (Hansbo, 1994).

To improve the reliability, integrity and fracture resistance of engineering multilayered structures, an understanding of their mechanical behaviour and fracture mechanisms is required. This understanding is also essential in the interpretation and forecasting of natural events such as snow avalanches, mudslides or fault propagation in rocks. In the next section, common fracture mechanisms of multilayered materials are briefly reviewed.

1.2 Fracture mechanisms in multilayered materials

The fracture of materials is generally considered from two different points of view (Erdogan, 1972). In the first approach, the failure conditions of the structure are estimated by using probabilistic strength theories, which assume that the material is statistically homogeneous and the existing imperfections (which are unavoidable) are randomly distributed. In the second approach, one is interested in the initiation of fracture from 'localized' imperfections, which are known, or assumed, to exist in the material. This approach is deterministic in nature and the fracture conditions are identified by an appropriate equality or criterion. In this criterion, a calculated fracture controlling parameter, such as stress intensity factor, is compared with the corresponding material constant obtained experimentally. Problems belonging to the second category are of interest in this thesis.

The 'localized' defects or imperfections found in multilayered materials are typically in the form of voids, cracks and inclusions. In composite laminates, delamination is the most intrinsic form of localized damage and can be formed as an intra-layer crack, or as an interfacial crack between two adjacent layers of the laminate (Garg, 1988). Delamination damage can be introduced at the

manufacturing stage due to improper curing or as a result of machining operations for creating fastener holes and cut-outs in the laminates (Ho-Cheng and Dharan, 1990). During operation, these defects may be caused by low speed impact e.g. dropped tools (Lin and Lee, 1990), thermal fatigue loading or differential swelling of layers in the presence of moisture (Evans and Hutchinson, 2007; Teh, et al. 2005).

Depending on the structural loading, delamination may or may not be a critical failure mode. In composite laminates, which are designed to carry large in-plane stresses and negligible transverse or interlaminar stresses, delamination is usually a secondary failure mode leading to the overall reduction in strength and stiffness of the component as well as promoting out-of-plane buckling under compression (Short et al., 2002; Melin and Schon, 2001; Gaudenzi, 1997; Bolotin 1996; Nilsson et al., 1993; Hutchinson and Suo, 1991). In the case of layered snow covers on mountain slopes, significant transverse shear stresses exist due to gravitational loads and the delamination of weak interfaces under skier loading has been linked to triggering of avalanches (Schweizer and Camponovo, 2001; McClung and Schweizer, 1999).

When transverse cracking is the predominant failure mode, multilayered structures can exhibit a higher resistance to fracture than their homogenous constituents. This is attributed to different toughening mechanisms, such as the deflection and branching of the transverse crack at interfaces and crack-tip blunting within ductile layers. These toughening mechanisms are responsible for the remarkable fracture resistance of some biological materials, such as nacre, tooth enamel and mollusc shells (Fratzl et al., 2007; Menig et al., 2000). These toughening mechanisms also play an important role in propagation, arrest and containment of fluid driven fractures, such as dykes, mineral veins, pressurised joints and man-made hydraulic fractures in subterranean rocks (Philipp et al., 2013; Gudmundsson et al., 2010; Lam and Cleary, 1984). To prevent structural failure by transverse cracking, multilayered composite structures can also be

designed to promote crack deflection at interfaces (Li, 2000; Gupta et al., 1992; He and Hutchinson, 1989) or crack-tip blunting in ductile layers (Zechner and Kolednik, 2013; Markaki and Clyne, 2002).

1.3 Numerical solution techniques

The analysis of crack problems in multilayered media, such as those mentioned above, often requires the use of numerical techniques. The accurate analysis of stresses in multilayered structures is challenging (Pagano, 1978) and in the presence of cracks, there is the additional complexity of correctly modelling the singular behaviour at the crack tip.

The finite element method presents an attractive approach for modelling crack problems in multilayered structures. However, the implementation of standard FE techniques requires the entire domain of the problem geometry to be discretised, which can be computationally expensive and often impractical in the case of multilayered structures composed of a large number of layers. Mesh refinement is required to capture the high stress gradients around material interfaces and other stress concentrators, which adds to the computational cost. Another shortcoming of the finite element method is that the conventional singular finite elements do not explicitly account for the different strengths of singular behaviour as well as the possible oscillatory nature of the near crack tip stress and displacement field, which can occur at bimaterial interfaces (Suo, 1990; Bogy, 1971; Williams, 1959). As a result, the relevant fracture parameters can only be estimated using a highly refined mesh, which is both computationally expensive and error-prone (Raju, 1987). Recent developments in the element formulations addressing these shortcoming are reviewed in Carrera and Demasi (2002), Cho and Averill (2000), and Her (2000). However, even with the advanced formulations a benchmarking solution is still required to verify FE calculations.

An alternative approach to the solution of crack problems in multilayered materials is the distributed dislocation technique (DDT). In this approach, which

will be described further in the next chapter, only the crack boundary needs to be discretised and the exact nature of the stress singularity can be built into the solution of the governing integral equations (Hills et al., 1996; Erdogan et al., 1973). Material anisotropy can also be included in the formulation at the expense of mathematical complexity and increased computational effort (Chen and Pindera, 2006; Azhdari et al., 2000; Pindera, 1991). Although the analysis of multilayered media using DDT is still quite challenging, this method is more efficient than the finite element analysis, specifically when parametric investigations need to be conducted or benchmarking solutions are required.

During the 1970s, Erdogan and co-workers pioneered the application of the DDT and provided the integral equation formulations for a variety of crack problems in multilayered materials, some of which are reviewed in Erdogan (1972). Hutchinson and co-workers also utilised this approach to consider the problems of crack path selection in two or three layered systems composed of isotropic or orthotropic layers and their results are summarised in Hutchinson and Suo (1991). The present work builds upon the seminal contributions of past researchers and utilises DDT to examine a set of crack problems in multilayered media, which have not been considered previously.

Other numerical techniques in which only the boundaries of the problem geometry need to be discretised include the boundary collocation method and the boundary element method. These methods are not reviewed here and the reader is referred to Aliabadi and Rooke (1991).

1.4 Methodology and details of publications

The methodology implemented throughout the thesis is based on the systematic application of DDT for the analysis of crack problems in multilayered media. Although the adopted methodology is quite general, the scope of the present research is restricted to the examination of quasi-static crack problems in linearly elastic and isotropic multilayer materials and structures.

The problems under consideration in the present thesis are diverse and multi-disciplinary in nature. For this reason, research gaps and objectives are formulated within each chapter rather than identifying a set of global research objectives at the outset. The order in which these chapters are presented has been chosen to best show the progression of the research, which involves the derivation and validation of a new dislocation solution (Chapter 3) and the development of new theoretical models using DDT (Chapters 4-6). Brief summaries containing the context, specific research gaps, method and outcomes of each of the articles are provided next.

Chapter 3: The stress field due to an interfacial edge dislocation in a multilayered medium

This chapter is concerned with the development and validation of a new fundamental solution for an interfacial edge dislocation which can be applied within the framework of DDT to analyse crack problems in general multilayered media without any restrictions on the crack orientation and number of layers. Currently available integral equation formulations for general multilayered materials can only be applied for the analysis of delamination problems, in which the cracks are located along or parallel to the interfaces (Chen and Pindera, 2006; Kucherov and Ryvkin, 2002; Erdogan and Gupta, 1971a, 1971b). The analysis of arbitrarily oriented, kinking or branching cracks using the distributed dislocation approach is limited to the rather simple case of a bimaterial medium i.e. an elastic medium composed of two perfectly bonded and dissimilar elastic half planes (Hills et al, 1996; Hutchinson and Suo, 1991; Erdogan, 1972). The obtained solution addresses these shortcomings and can be applied to all of the above mentioned situations.

The complex potential method of Muskhelishvili and Fourier transform techniques are applied to obtain the new solution. The multilayered medium under consideration is composed of perfectly bonded, linearly elastic and isotropic

layers. The obtained solution recovers all previous solutions for embedded or interfacial edge dislocations in isotropic layered media (Kuo, 2014; Savage, 1998; Kelly et al., 1995; Fleck et al., 1991; Suo and Hutchinson, 1990; Comninou and Dundurs, 1983; Lee and Dundurs, 1973). Within the DDT framework, the current solution is employed to derive the governing singular integral equations for an interfacial crack in an arbitrary multilayered medium. The results obtained by Kucherov and Ryvkin (2002) and Erdogan and Gupta (1971b) for specific geometries are recovered from the appropriate solutions of the governing singular integral equations.

The edge dislocation solution and the governing singular equations developed in this chapter generalise the specific approaches developed in the following chapters. For example, Chapters 4 and 5 utilise the solution for an edge dislocation in an elastic layer obtained by Fleck et al. (1991). The more general solution presented in this chapter recovers the latter solution in its exact form. A new screw dislocation solution presented in Chapter 6 was also obtained using the approach developed in this chapter.

Chapter 4: Stress analysis of a crack in a fiber-reinforced layered composite

In this chapter, the plane elasticity problem of an elastic layer bonded to two dissimilar elastic half-planes is considered. The elastic layer contains an embedded crack, which is oriented perpendicular to the interfaces and reinforced by bridging fibers. The problem of a crack reinforced by bridging tractions has been examined previously in the context of fiber-reinforced composites (Budiansky et al., 1986; Marshall et al., 1985) and also in the context of crack repair by adhesively bonded composite patches (Rose, 1982). However, the problem of a reinforced crack in a layered medium has not been examined previously. The latter problem may arise, for example, in structural engineering applications where one needs to estimate the residual strength of a fiber-reinforced cement structure containing a macroscopic

defect near the free surface or near a bonded interface with another steel structure (Shah and Ouyang, 1991).

The DDT is used to formulate the crack problem and the displacement-dependant bridging tractions along the crack faces are incorporated into the governing singular integral equation. The Gauss-Chebyshev quadrature is applied to reduce the singular integral equation to a system of non-linear algebraic equations and the Newton-Raphson iterative scheme is implemented to obtain a numerical solution to the resulting system of non-linear algebraic equations.

The dependence of the critical applied stress required to initiate matrix fracture and fiber failure upon the mismatch in elastic properties is established though a parametric study. It is demonstrated that any reduction in failure stress due to material mismatch can be alleviated by increasing the bridging traction on the crack faces, for example, by increasing the volume fraction of the fibers or by selecting fibers with greater stiffness.

Chapter 5: Height control of multiple hydraulic fractures in layered media

This chapter is related to the hydraulic fracturing of hydrocarbon bearing rock layers. In particular, the problem of height containment of multiple hydraulic fractures emanating from a horizontal wellbore is considered. Horizontal well drilling is a key production technology for extracting hydrocarbons from thin reservoirs situated in layered rock formations (Joshi, 1991) and the horizontal wells are often fractured at multiple sites to enhance the production rate from these reservoirs (Economides and Martin, 2010). It is desirable to contain the hydraulic fractures within the target layer, since uncontrolled fracture growth diminishes the overall efficiency of the fracturing treatment and affects the environment negatively (Warpinski et al., 1982).

Several mechanisms for fracture height control have been examined previously, focussing on a single hydraulic fracture emanating from a vertical

wellbore (Cleary, 1980). However, the more practical problem, which involves multiple closely-spaced hydraulic fractures, has not received much attention. To address this gap, the plane problem of an elastic layer containing multiple equidistant cracks and bonded to dissimilar elastic half-planes is considered and fracturing fluid pressure control is proposed as a possible mechanism for height control during hydraulic fracturing. The theoretical model is based on DDT and it incorporates not only the effect of mismatch in elastic properties between the reservoir and the bounding layers, but also the interaction effect between the neighbouring cracks.

It is demonstrated that when the fracture spacing becomes comparable to the fracture height, the interaction between the fractures produces a shielding effect. In this case, the fracturing fluid pressure that ensures fracture containment is greater and the fracture opening is smaller, in comparison to the case of a single isolated fracture. The dependence of the fracturing fluid pressure and fracture opening upon the fracture spacing is established through dimensionless parametric studies as well as case studies. The obtained results can assist in the selection of the fracture spacing and proppant size for a fracturing treatment involving multiple hydraulic fractures.

Chapter 6: A new predictive model for the onset of skier-triggered avalanches

This chapter is concerned with the onset conditions for skier-triggered dry snow slab avalanches in stratified snow slopes. Dry snow slab avalanches involve the release of large volumes of cohesive snow that slide down the mountain slope and often lead to fatalities and property damage. Such avalanches originate from localized initial failure in a weak layer beneath the cohesive snow slab followed by rapid crack propagation within this weak layer (van Herwijnen and Jamieson, 2007; Schweizer et al., 2003).

Several previous models for the fracture failure of the weak layer assume the failure initiation to occur in mode II from a pre-existing defect or deficit zone

(Bažant et al., 2003; Bader and Salm, 1990; McClung, 1979, 1981). In this chapter, any assumptions regarding pre-existing defects of unknown shape are avoided. Instead, it is suggested that crack-like defects of high aspect-ratio may be generated under skier loading as a result of 'localized' weak layer failure. The high aspect-ratio of the skier induced defect would promote the failure initiation of the weak layer in mode III rather than in mode II.

All existing models for the onset of snow avalanches are based on beam theories and energy balance equations, which, strictly speaking, are only applicable when the defect length is significantly greater than the slab thickness. However, these models predict a critical defect size of the order of 0.1 – 10 m, which is of the same order of magnitude as the thickness of the snow slab obtained from several field observations (Perla, 1977). This contradicts the basic assumptions of beam theories.

In this chapter, a new model based on the DDT is developed to address the above discussed shortcomings. The anti-plane problem of an elastic layer bonded to a rigid substrate and containing an embedded crack parallel to the interface is considered and the critical crack length is evaluated using the brittle fracture criterion. The solution for a screw dislocation in the same geometry is utilised to develop the governing integral equation and the solution approach is analogous to the approach developed in Chapter 3 for an interfacial edge dislocation in a multilayered medium. The size of the skier-induced defect is evaluated from the solution for a concentrated line load acting normal to the surface of an elastic layer bonded to a rigid substrate in conjunction with a simple compressive failure criterion. For a range of values of the snowpack properties, the critical defect size is compared with the size of the skier-induced defect to identify conditions favourable for avalanche onset.

1.5 Concluding remarks

In this introductory chapter, the overall significance of the undertaken research was highlighted. A chapter-wise summary of the specific research gaps addressed in this thesis was also provided. The research methodology is elaborated further in the next chapter, in which the fundamentals of LEFM and DDT are presented.

References

Aliabadi, M.H. and D.P. Rooke (1991), Numerical Fracture Mechanics, Kluwer Academic Publishers, Dordrecht, The Netherlands.

Azhdaria, A, M. Obatab and S. Nemat-Nasser (2000), Alternative solution methods for crack problems in plane anisotropic elasticity, with examples, *Int. J. Solids Struct.*, 37, 6433-6478, doi: 10.1016/S0020-7683(99)00137-7.

Bader, H.P. and B., Salm (1990), On the mechanics of snow slab release, *Cold Reg. Sci. Technol.*, 17(3), 287-300, doi: 10.1016/S0165-232X(05)80007-2.

Barthelat, F. and D. Zhu (2012), A novel biomimetic material duplicating the structure and mechanics of natural nacre, *J. Mater. Res.*, 26(10), 1203-1215, doi: 10.1557/jmr.2011.65.

Bažant, Z.P., G. Zi and D. McClung (2003), Size effect law and fracture mechanics of the triggering of dry snow slab avalanches, *J. Geophys. Res*., 108(B2), 2119, doi: 10.1029/2002JB001884.

Bilby, B. and J. Eshelby (1968), Dislocations and the theory of fracture, in Fracture: An Advanced Treatise, vol. 1, edited by H. Liebowitz, pp. 99-182, Academic Press, New York.

Boggs, S. (2006), Principles of Sedimentology and Stratigraphy, 4th edition, Pearson Prentice Hall, Upper Saddle River, NJ.

Bogy, D.B. (1971), On the plane elastostatic problem of a loaded crack terminating at a material interface, *J. Appl. Mech.*, 38, 911-918, doi: 10.1115/1.3408975.

Bolotin, V.V. (1996), Delaminations in composite structures: its origin, buckling, growth and stability, *Composites*, 27(2), 129-145, doi: 10.1016/1359-8368(95)00035-6.

Bonderer, L.J., A.R. Studart and L.J. Gauckler (2008), Bioinspired Design and Assembly of Platelet Reinforced Polymer Films, *Science*, 319 (5866), 1069-1073, doi: 10.1126/science.1148726.

Budiansky, B., J.W. Hutchinson and A.G. Evans (1986), Matrix fracture in fiber-reinforced ceramics, *J. Mech. Phys. Solids*, 34(2), 167-189, doi: 1016/0022-5096(86)90035-9.

Carrera, E. and L. Demasi (2002), Classical and advanced multilayered plate elements based upon PVD and RMVT. Part 1: Derivation of finite element matrices, *Int. J. Numer. Methods Eng.*, 55, 191-231, doi: 10.1002/nme.492.

Chen, L. and M.J. Pindera (2006), Plane Analysis of finite multilayered media with multiple aligned cracks - Part I: Theory, *J. Appl. Mech*., 74(1), 128-143, doi: 10.1115/1.2201883.

Cho, Y.B. and R.C. Averill (2000), First-order zig-zag sublaminate plate theory and finite element model for laminated composite and sandwich panels, *Compos. Struct*., 50(1), 1-15, doi: 10.1016/S0263-8223(99)00063-X.

Cleary, M.P. (1980), Analysis Of Mechanisms And Procedures For Producing Favourable Shapes Of Hydraulic Fractures. SPE Paper 9260 presented at SPE Annual Technical Conference and Exhibition, Dallas, Texas, 21-24 September, doi: 10.2118/9260-MS.

Comninou, M. and J. Dundurs (1983) Partial closure of a crack at the interface between a layer and a half space, *Eng. Fract. Mech*., 18(2), 315-323, doi: 10.1016/0013-7944(83)90142-X.

Crawley, E.P. (1994), Intelligent structures for aerospace - a technology overview and assessment, *AIAA J*., 32(8), 1689-1699, doi: 10.2514/3.12161.

Dolinšek, S., B. Šuštaršič and J. Kopač (2001), Wear mechanisms of cutting tools in high-speed cutting processes, *Wear*, 250, 349-356, doi: 10.1016/S0043-1648(01)00620-2.

Dunlop, J.W.C. and P. Fratzl (2010), Biological Composites, *Annu. Rev. Mater. Res.*, 40, 1-24, doi: 10.1146/annurev-matsci-070909-104421.

Dunn, M.L., Y. Zhang and V.M. Bright (2002), Deformation and structural stability of layered plate microstructures subjected to thermal loading, *J. Microelectromech. Syst*., 11(4), 372-384, doi: 10.1109/JMEMS.2002.800932.

Economides, M.J. and A.N. Martin (2010), How to decide between horizontal transverse, horizontal longitudinal and vertical fracture completion. SPE Paper 134424 presented at the SPE Annual Technical Conference and Exhibition, Florence, Italy, 19-22 September, doi: 10.2118/134424-MS.

Erdogan, F. (1972), Fracture problems in composite materials, *Eng. Fract. Mech.*, 4(4), 811-840, doi: 10.1016/0013-7944(72)90018-5.

Erdogan, F. and G. Gupta (1971), The stress analysis of multilayered composites with a flaw, *Int. J. Solids Struct.*, 7(1), 39-61, doi: 10.1016/0020-7683(71)90017-5.

Erdogan, F. and G.D. Gupta (1971), Layered composites with an interface flaw, *Int. J. Solids Struct.*, 7(8), 1089-1107, doi: 10.1016/0020-7683(71)90082-5.

Erdogan, F., G.D. Gupta and T.S. Cook (1973), Numerical solution of singular integral equations, in Mechanics of Fracture, vol. 1, edited by G.C. Sih , pp. 368-425, Noordhoff International, Leyden, The Netherlands.

Espinosa, H.D., A.L. Juster, F.J. Latourte, O.Y. Loh, D. Gregoire and P.D. Zavattieri (2011), Tablet-level origin of toughening in abalone shells and translation to synthetic composite materials, *Nat. Commun.*, 2, doi: 10.1038/ncomms1172.

Evans, A.G. and J.W. Hutchinson (2007), The mechanics of coating delamination in thermal gradients, *Surf. Coat. Technol.*, 201(18), 7905-7916, doi: 10.1016/j.surfcoat.2007.03.029.

Fleck, N.A., J.W. Hutchinson and Z. Suo (1991), Crack path selection in a brittle adhesive layer, *Int. J. Solids Struct.*, 27(13), 1683-1703, doi: 10.1016/0020-7683(91)90069-R.

Fratzl P., H.S. Gupta, F.D. Fischer and O. Kolednik (2007), Hindered crack propagation in materials with periodically varying Young's modulus: lessons from biological materials, *Adv. Mater*., 19, 2657-61, doi: 10.1002/adma.200602394.

Garg, A.C. (1988), Delamination–a damage mode in composite structures, *Eng. Fract. Mech*., 29, 557-584, doi: 10.1016/0013-7944(88)90181-6.

Gaudenzi, P. (1997), On delamination buckling of composite laminates under compressive loading, Compos. Struct., 39, 21-30, doi: 10.1016/S0263-8223(98)80017-2.

Gudmundsson, A., T.H. Simmenes, B. Larsen and S.L. Philipp (2010), Effects of internal structure and local stresses on fracture propagation, deflection, and arrest in fault zones, *J. Struct. Geol.*, 32(11), 1643-1655, doi: 10.1016/j.jsg.2009.08.013.

Gupta, G.D. (1973), A layered composite with a broken laminate, *Int. J. Solids Struct.*, 9(10), 1141-1154, doi: 10.1016/0020-7683(73)90108-X.

Gupta, V., A.S. Argon and Z. Suo (1992), Crack deflection at an interface between two orthotopic media, *J. Appl. Mech.*, 59(2S), S79-S87, doi: 10.1115/1.2899511.

Hansbo, S. (1994), Foundation Engineering, Elsevier Science B.V., The Netherlands.

He M.Y. and J.W. Hutchinson (1989), Crack deflection at an interface between dissimilar elastic materials, *Int. J. Solids Struct.*, 25(9), 1053-1067, doi: 10.1016/0020-7683(89)90021-8.

Her, S.C. (2000), Fracture analysis of interfacial crack by global-local finite element, *Int. J. Fract.*, 106(2), 177-193, doi: 10.1023/A:1007682601766.

Hills, D.A., P.A. Kelly, D.N. Dai and A.M. Korsunsky (1996), Solution of Crack Problems: The Distributed Dislocation Technique, Kluwer Academic Publishers, Dordrecht, The Netherlands.

Ho-Cheng, H.H. and C.H. Dharan (1990), Delamination during drilling in composite laminates, *ASME J. Eng. Ind.*, 112(3), 236-239, doi:10.1115/1.2899580.

Hutchinson, J.W. and Z. Suo (1991), Mixed mode cracking in layered materials, in Advances in Applied Mechanics, Vol. 29, p. 63-191, edited by: J.W. Hutchinson and T.Y. Wu, Academic Press Inc., doi: 10.1016/S0065-2156(08)70164-9.

Joshi, S.D. (1991), Horizontal well technology, PennWell Publishing Company, Tulsa, Oklahoma.

Kelly, P.A., J.J. O'Connor and D.A. Hills (1995), Stress field due to a dislocation in layered media, *J. Phys. D - Appl. Phys.*, 28(3), 530-534, doi: 10.1088/0022-3727/28/3/013.

Kucherov, L. and M. Ryvkin (2002), Interface crack in periodically layered bimaterial composite, *Int. J. Fract.*, 117(2), 175-194, doi: 10.1023/A:1020914902780.

Kuo, C.-H. (2014), Elastic field due to an edge dislocation in a multilayered composite, *Int. J. Solids Struct.*, 51, 1421-1433, doi: 10.1016/j.ijsolstr.2013.12.032.

Lam, K.Y. and M. P. Cleary (1984), Slippage and re-initiation of (hydraulic) fractures at frictional interfaces, *Int. J. Numer. Anal. Methods Geomech*., 8(6), 589-604, doi: 10.1002/nag.1610080607.

Lee, M.-S. and J. Dundurs (1973), Edge dislocation in a surface layer, *Int. J. Eng. Sci.*, 11(1), 87-94, doi: 10.1016/0020-7225(73)90071-2.

Li J. (2000), Debonding of the interface as 'crack arrestor', Int. J. Fract., 105(1), 57-79, doi: 10.1023/A:1007603809972.

Lin, H.J. and Y.J. Lee (1990) Impact induced fracture of laminated plates and shells, *J. Compos. Mater.*, 24,1179-1199, doi: 10.1177/002199839002401105.

Markaki, A.E., T.W. Clyne (2002), Energy absorption during failure of layered metal foam/ceramic laminates, *Mat. Sci. Eng. A - Struct*., 323(1-2), 260-269, doi: 10.1016/S0921-5093(01)01344-2.

Marshall, D.B., B.N. Cox and A.G. Evans (1985), The mechanics of matrix cracking in brittle-matrix fiber composites, *Acta. Metall*., 33(11), 2013–2021, doi: 10.1016/0001-6160(85)90124-5.

McClung, D. and J. Schweizer (1999), Skier triggering, snow temperatures and the stability index for dry-slab avalanche initiation, *J. Glaciol*., 45(150), 190-200, doi: 10.3189/002214399793377121.

McClung, D.M. (1979), Shear fracture precipitated by strain softening as a mechanism of dry slab avalanche release, *J. Geophys. Res*., 84(B7), 3519-3525, doi: 10.1029/JB084iB07p03519.

McClung, D.M. (1981), Fracture mechanical models of dry slab avalanche release, *J. Geophys. Res*., 86(B11), 10783-10790, doi: 10.1029/JB086iB11p10783.

Melin, L.G. and J. Schon (2001), Buckling behaviour and delamination growth in impacted composite specimens under fatigue load: an experimental study, *Compos. Sci. Technol*., 61(13), 1841-52, doi: 10.1016/S0266-3538(01)00085-9.

Menig, R., M.H. Meyers, M.A. Meyers and K.S. Vecchio (2000), Quasi-static and dynamic mechanical response of *Haliotis rufescens* (abalone) shells, *Acta Mater*., 48, 2383-98, doi: 10.1016/S1359-6454(99)00443-7.

Miller, R.A. (1987), Current status of thermal barrier coatings - an overview, *Surf. Coat. Technol.*, 30(1), 1-11, doi: 10.1016/0257-8972(87)90003-X.

Mirkhalaf, M., A. Khayer Dastjerdi and F. Barthelat (2014), Overcoming the brittleness of glass through bio-inspiration and micro-architecture, *Nat. Commun.*, 5, doi: 10.1038/ncomms4166.

Munch, E., M.E. Launey, D.H. Alsem, E. Saiz, A.P. Tomsia and R.O. Ritchie (2008), Tough, Bio-Inspired Hybrid Materials, *Science*, 322 (5907), 1516-1520, doi: 10.1126/science.1164865.

Nguyen, P., A. Kotousov, S.-Y. Ho and S. Wildy (2010), Investigation of thermo-mechanical properties of slurry based thermal barrier coatings under repeated thermal shock, *Key Eng. Mater*., 417-418, 197-200, doi: 10.4028/www.scientific.net/KEM.417-418.197.

Nilsson, K.F., J.C. Thesken, P. Sindelar, A.E. Giannakopoulos and B. Storakers (1993), A theoretical and experimental investigation of buckling induced delamination growth, *J. Mech. Phys. Solids*, 41, 749-782, doi: 10.1016/0022-5096(93)90025-B.

Pagano, N.J. (1978), Stress fields in composite laminates, *Int. J. Solids Struct*., 14, 385-400, doi: 10.1016/0020-7683(78)90020-3.

Perla, R. (1977), Slab avalanche measurements, *Can. Geotech. J*., 14(2), 206-213, doi: 10.1139/t77-021.

Philipp, S.L., F. Afşar and A. Gudmundsson (2013), Effects of mechanical layering on hydrofracture emplacement and fluid transport in reservoirs, *Front. Earth Sci*., 1, 4, doi: 10.3389/feart.2013.00004.

Pindera, M.J. (1991), Local/global stiffness matrix formulation for composite materials and structures, *Compos. Eng.*, 1(2), 69-83, doi: 10.1016/0961-9526(91)90028-Q.

Podsiadlo, P., A.K. Kaushik, E.M. Arruda, A.M. Waas, B.S. Shim, J. Xu, H. Nandivada, B.G. Pumplin, J. Lahann, A. Ramamoorthy and N.A. Kotov (2007), Ultrastrong and Stiff

Layered Polymer Nanocomposites, *Science*, 318 (5847), 80-83, doi: 10.1126/science.1143176.

Pritchard, J., C.R. Bowen and F. Lowrie (2001), Multilayer actuators: review, *Br. Ceram. Trans.*, 100(6), 265-273, doi: 10.1179/bct.2001.100.6.265.

Raju, I.S. (1987), Calculation of strain-energy release rates with higher order and singular finite elements, *Eng. Fract. Mech.*, 28(3), 251-274, doi: 10.1016/0013-7944(87)90220-7.

Reading, H.G. (1996), Sedimentary environments: processes, facies and stratigraphy, 3rd edition, Blackwell Publishing, Oxford.

Reddy, J.N. (2004), Mechanics of laminated composite plates and shells: theory and analysis, 2nd edition, CRC Press LLC.

Rose, L.R.F. (1982), A cracked plate repaired by bonded reinforcements, *Int. J. Fract.*, 18(2), 135-144, doi: 10.1007/BF00019638.

Sackman, J.L., J.M. Kelly and A.E. Javid (1989), A layered notch filter for high-frequency dynamic isolation, *J. Pressure Vessel Technol*., 111(1), 17-24, doi: 10.1115/1.3265634.

Savage, J.C. (1998), Displacement field for an edge dislocation in a layered half-space, *J. Geophys. Res*., 103 (B2), 2439-2446, doi: 10.1029/97JB02562.

Schweizer, J. and C. Camponovo (2001), The skier's zone of influence in triggering slab avalanches, Ann. Glaciol., 32(1), 314-320, doi: 10.3189/172756401781819300.

Schweizer, J., J.B. Jamieson and M. Schneebeli (2003), Snow avalanche formation, *Rev. Geophys*., 41(4), 1016, doi: 10.1029/2002RG000123.

Shah, S. P. and C. Ouyang (1991), Mechanical Behavior of Fiber-Reinforced Cement-Based Composites, *J. Am. Ceram. Soc.*, 74, 2727-2953, doi:10.1111/j.1151-2916.1991.tb06836.x.

Short G.J., F.J. Guild and M.J. Pavier (2002), Delaminations in flat and curved composite laminates subjected to compressive load, *Compos. Struct.*, 58(2), 249-258, doi: 10.1016/S0263-8223(02)00052-1.

Sørensen, P.A., S. Kiil, K. Dam-Johansen and C. E. Weinell (2009), Anticorrosive coatings: a review, *J. Coat. Technol. Res*., 6(2), 135-176, doi: 10.1007/s11998-008-9144-2.

Soutis, C. (2005), Fibre reinforced composites in aircraft construction, *Prog. Aerosp. Sci.*, 41(2), 143-151, doi: 10.1016/j.paerosci.2005.02.004.

Stern, K.H. (1996), Metallurgical and Ceramic Protective Coatings, Chapman and Hall, Suffolk.

Suo, Z. (1990), Singularities, interfaces and cracks in dissimilar anisotropic media, *Proc. R. Soc. London, Ser. A*, 427(1873), doi: 10.1098/rspa.1990.0016.

Suo, Z. and J.W. Hutchinson (1990), Interface crack between two elastic layers, *Int. J. Fract.*, 43(1), 1-18, doi: 10.1007/BF00018123.

Tang, Z., N.A. Kotov, S. Magonov and B. Ozturk (2003), Nanostructured artificial nacre, *Nat. Mater.*, 2, 413-418, doi: 10.1038/nmat906.

Teh, L.K., M. Teo, E. Anto, C.C. Wong, S.G. Mhaisalkar, P.S. Teo and E.H. Wong (2005), Moisture-induced failures of adhesive flip chip interconnects, *IEEE Trans. Compon. Packag. Technol.*, 28(3), 506-516, doi: 10.1109/TCAPT.2005.848572

van Herwijnen, A., and B. Jamieson (2007), Snowpack properties associated with fracture initiation and propagation resulting in skier-triggered dry snow slab avalanches, *Cold Reg. Sci. Technol.*, 50(1-3), 13-22, doi: 10.1016/j.coldregions.2007.02.004.

Walley, P., Y. Zhang and J.R.G. Evans (2012), Self-assembly of montmorillonite platelets during drying, *Bioinspiration Biomimetics*, 7(4), doi: 10.1088/1748-3182/7/4/046004.

Warpinski, N.R., R.A. Schmidt, and D.A. Northrop (1982), In-Situ Stresses: The Predominant Influence on Hydraulic Fracture Containment, *J. Pet. Technol*., 34 (3), 653-664, doi: 10.2118/8932-PA.

Williams, M.L. (1959), Stresses around a fault or crack in dissimilar media, *Bull. Seism. Soc. Am.*, 49, 199-204,

Zechner, J. and O. Kolednik (2013), Fracture resistance of aluminum multilayer composites, *Eng. Fract. Mech*., 110, 489-500, doi: 10.1016/j.engfracmech.2012.11.007.

Zhuang, S.M., G. Ravichandran and D.E.W. Grady (2003), An experimental investigation of shock wave propagation in periodically layered composites, *J. Mech. Phys. Solids*, 51(2), 245-265, doi: 10.1016/S0022-5096(02)00100-X.

Chapter 2

Background on LEFM and DDT

Chapter 2

Background on LEFM and DDT

In the present chapter, a brief overview of the key concepts of Linear Elastic Fracture Mechanics (LEFM) and interfacial fracture mechanics is provided and the general approach for the solution to crack problems using the Distributed Dislocation Technique (DDT) and dislocation solutions is described. Although the present chapter intends to provide the necessary background information on the methodology adopted in this thesis, it is assumed that the reader is already familiar with LEFM, interfacial fracture mechanics and DDT. Parts of this background chapter are based on more in-depth and complete references, particularly Hills et al. (1996) and Erdogan et al. (1973).

2.1 Basic concepts of LEFM

LEFM pertains to the examination of solid bodies weakened by cracks under the idealisation of linearly-elastic material behaviour and small deformations. One of the fundamental results of LEFM is that the stress fields around sharp crack tips are singular in nature. In the analysis of plane crack problems, the stress singularity has the general form of r^{λ}, where r is the radial distance from the crack or notch tip and λ is a real or complex number and $\mathrm{Re}(\lambda) \geq -1$. The latter condition arises from the finite strain energy considerations in the area encapsulating the crack tip under the plane assumptions of the theory of elasticity. The order or strength of the singularity, λ, is established numerically from analysis of near-tip region ($r \to 0$) or analytically utilising, for example, the eigenfunction expansion technique. A review of some well-known results is provided later in this chapter.

Under plane stress or plane strain assumptions the solution near the crack tip can be represented in the form of an infinite series with a singular leading term. Therefore, there exists a small region surrounding the crack tip in which the singular term of the asymptotic solution dominates the stress and strain fields. The normalised magnitude of this singular term is often referred to as the stress intensity factor, K and the region in which the stress intensity factor fully characterises the stress and displacement fields is known as the K-dominance region. The near-tip stress distribution in the K-dominance region has a universal form (see for e.g. Table 1). The problem geometry and loading influence the stresses within the K-dominance zone only through the stress intensity factor, K, or combination of stress intensity factors corresponding to different fracture modes.

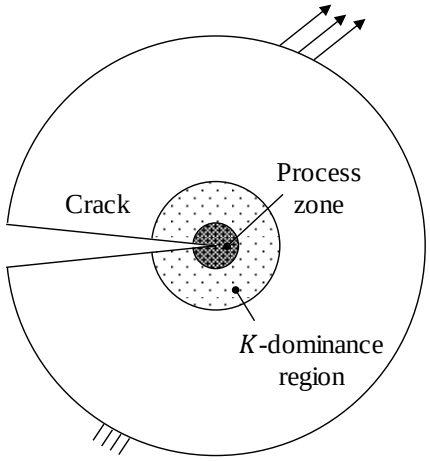

Fig. 1: Schematic representation of small-scale yielding at the crack tip.

It should be highlighted that the stress singularities predicted within the framework of LEFM arise from the assumptions of a linear elastic continuum, small deformations and a perfectly sharp crack tip. In reality, the material cannot sustain infinitely large stresses and a 'process-zone' or region, characterised by non-linear and discontinuous deformations, always exist in the close vicinity of the crack tip, which also cannot be perfectly sharp. Nonetheless, the singular elastic solution can adequately represent the actual stress field around the crack tip,

provided that the tip radius or the characteristic length associated with the process-zone are negligible in size when compared to the size of the K-dominance region, as illustrated in Fig. 1. Under these conditions, referred to as 'small scale yielding', the fracture/crack extension criteria can be fully characterised in terms of the stress intensity factor alone (Irwin, 1957). For this reason, a variety of analytical, numerical and experimental approaches have been developed over the past decades for the evaluation of the stress intensity factor as a function of the problem geometry and loading conditions. One of these approaches, based on the DDT is discussed in more detail later in this chapter.

2.2 Stress singularities in plane elasticity

Within the plane elasticity framework, the stresses directly ahead of a crack tip in a homogenous, isotropic linear elastic plate have an inverse square root singular behaviour, as shown in Table 1. This fundamental result was obtained by Williams (1957) using the eigenfuntion series expansion method. The order of the stress singularity is the same for a crack tip embedded in a homogenous, anisotropic medium (Sih and Liebowitz, 1968) or a non-homogenous, linearly elastic material with continuous and piece-wise differentiable material properties (Jin and Noda, 1994; Eischen, 1987).

If the material properties are discontinuous at the crack tip, the stress singularity may no longer be of the form $r^{-1/2}$. A classic example is an interfacial crack between two dissimilar isotropic materials under in-plane (Mode I or Mode II) remote loading. Here the crack tip stresses and displacement take the following asymptotic form as $r \to 0$ (Williams, 1959)

$$\begin{aligned} \sigma_{rr}, \sigma_{\theta\theta}, \sigma_{r\theta} &\sim r^{-1/2+i\epsilon} = r^{-1/2}[\cos(\epsilon \ln r) + i \sin(\epsilon \ln r)], \\ u_r, u_\theta &\sim r^{1/2}[\cos(\epsilon \ln r) + i \sin(\epsilon \ln r)], \end{aligned} \tag{1}$$

where,

Table 1: Summary of two-dimensional asymptotic solutions inside the K-dominance zone for a crack tip embedded in a homogenous material (Hills et al., 1996).

Cartesian	Polar
Mode I	*Mode II*
$\sigma_{xx} = \frac{K_I}{\sqrt{2\pi r}} \cos\frac{\theta}{2}\left[1 - \sin\frac{\theta}{2}\sin\frac{3\theta}{2}\right]$	$\sigma_{rr} = \frac{K_I}{\sqrt{2\pi r}}\left(\frac{5}{4}\cos\frac{\theta}{2} - \frac{1}{4}\cos\frac{3\theta}{2}\right)$
$\sigma_{yy} = \frac{K_I}{\sqrt{2\pi r}} \cos\frac{\theta}{2}\left[1 + \sin\frac{\theta}{2}\sin\frac{3\theta}{2}\right]$	$\sigma_{\theta\theta} = \frac{K_I}{\sqrt{2\pi r}}\left(\frac{3}{4}\cos\frac{\theta}{2} + \frac{1}{4}\cos\frac{3\theta}{2}\right)$
$\sigma_{xy} = \frac{K_I}{\sqrt{2\pi r}} \sin\frac{\theta}{2}\cos\frac{\theta}{2}\cos\frac{3\theta}{2}$	$\sigma_{r\theta} = \frac{K_I}{\sqrt{2\pi r}}\left(\frac{1}{4}\sin\frac{\theta}{2} + \frac{1}{4}\sin\frac{3\theta}{2}\right)$
$u_x = \frac{K_I}{2\mu}\sqrt{\frac{r}{2\pi}}\cos\frac{\theta}{2}(\kappa - \cos\theta)$	$u_r = \frac{K_I}{4\mu}\sqrt{\frac{r}{2\pi}}\left[(2\kappa - 1)\cos\frac{\theta}{2} - \cos\frac{3\theta}{2}\right]$
$u_y = \frac{K_I}{2\mu}\sqrt{\frac{r}{2\pi}}\sin\frac{\theta}{2}(\kappa - \cos\theta)$	$u_\theta = \frac{K_I}{4\mu}\sqrt{\frac{r}{2\pi}}\left[-(2\kappa + 1)\sin\frac{\theta}{2} + \sin\frac{3\theta}{2}\right]$
Mode II	*Mode II*
$\sigma_{xx} = -\frac{K_{II}}{\sqrt{2\pi r}} \sin\frac{\theta}{2}\left[2 + \cos\frac{\theta}{2}\cos\frac{3\theta}{2}\right]$	$\sigma_{rr} = \frac{K_{II}}{\sqrt{2\pi r}}\sin\frac{\theta}{2}\left(1 - 3\sin^2\frac{\theta}{2}\right)$
$\sigma_{yy} = \frac{K_{II}}{\sqrt{2\pi r}} \sin\frac{\theta}{2}\cos\frac{\theta}{2}\cos\frac{3\theta}{2}$	$\sigma_{\theta\theta} = \frac{K_{II}}{\sqrt{2\pi r}}\left(-3\sin\frac{\theta}{2}\cos^2\frac{\theta}{2}\right)$
$\sigma_{xy} = \frac{K_{II}}{\sqrt{2\pi r}} \cos\frac{\theta}{2}\left[1 - \sin\frac{\theta}{2}\sin\frac{3\theta}{2}\right]$	$\sigma_{r\theta} = \frac{K_{II}}{\sqrt{2\pi r}}\cos\frac{\theta}{2}\left(1 - 3\sin^2\frac{\theta}{2}\right)$
$u_x = \frac{K_{II}}{2\mu}\sqrt{\frac{r}{2\pi}}\sin\frac{\theta}{2}(2 + \kappa + \cos\theta)$	$u_r = \frac{K_{II}}{4\mu}\sqrt{\frac{r}{2\pi}}\left[-(2\kappa - 1)\sin\frac{\theta}{2} + 3\sin\frac{3\theta}{2}\right]$
$u_y = \frac{K_{II}}{2\mu}\sqrt{\frac{r}{2\pi}}\cos\frac{\theta}{2}(2 - \kappa - \cos\theta)$	$u_\theta = \frac{K_{II}}{4\mu}\sqrt{\frac{r}{2\pi}}\left[-(2\kappa + 1)\cos\frac{\theta}{2} - 3\cos\frac{3\theta}{2}\right]$
Mode III	*Mode III*
$\sigma_{xz} = -\frac{K_{III}}{\sqrt{2\pi r}}\sin\frac{\theta}{2}$	$\sigma_{rz} = -\frac{K_{III}}{\sqrt{2\pi r}}\sin\frac{\theta}{2}$
$\sigma_{yz} = \frac{K_{III}}{\sqrt{2\pi r}}\cos\frac{\theta}{2}$	$\sigma_{\theta z} = \frac{K_{III}}{\sqrt{2\pi r}}\cos\frac{\theta}{2}$
$u_z = \frac{2K_{III}}{\mu}\sqrt{\frac{r}{2\pi}}\sin\frac{\theta}{2}$	
$\kappa = (3 - \nu)/(1 + \nu)$ in plane stress	$\kappa = 3 - 4\nu$ in plane strain

$$\epsilon = \frac{1}{2\pi}\ln\left[\left(\frac{\kappa_1}{\mu_1}+\frac{1}{\mu_2}\right)\Big/\left(\frac{\kappa_2}{\mu_2}+\frac{1}{\mu_1}\right)\right].$$

The form of the Eq. (1) implies that the behaviour of the stress and displacement fields is oscillatory in nature leading to interpenetration of crack faces. England (1965) has demonstrated that under remote general loading this inadmissible physical phenomenon is confined to a very small region of order 10^{-4} of crack length and can be disregarded in most practical situations. For combinations of material properties, when the parameter $\epsilon = 0$, the inverse square root singularity ($r^{-1/2}$) is recovered. It should also be noted that this oscillating singular behaviour does not occur for an interfacial crack under anti-plane (Mode III) loading for any combination of material properties.

For a more general plane elasticity problem of a straight crack terminating at a straight interface at an arbitrary angle, the order of the singularity depends upon the elastic constants of the constituents as well as the angle of incidence. The dominant term(s) in the series expansion for the stress field as $r \to 0$ is of the order of r^{λ}, where the eigenvalue(s) λ can be real or complex and $\mathrm{Re}(\lambda) \geq -1$. For a bimaterial isotropic composite, Bogy (1971a) derived the following characteristic equation for obtaining λ (Hills et al., 1996):

$$\begin{aligned} 0 = {} & [A\beta^2 - (2A - B)\beta + A - B + 1]\alpha^2 \\ & + [(-2A + B + C)\beta^3 + (4A - 2B - C + D + 2)\beta^2 - (2A - B - C)\beta + C - D]\alpha \\ & + (A - B - C + D + E + 1)\beta^4 - (2A - B - C)\beta^3 + (A + C - D - 2E)\beta^2 - C\beta + E, \end{aligned} \tag{2}$$

where,

$$A(\theta,\lambda) = 4(1+\lambda)^4 \sin^4\theta + \sin^2[(1+\lambda)(2\theta - \pi)],$$

$$B(\theta,\lambda) = 4(1+\lambda)^2 \sin^2\theta + 2\sin^2[(1+\lambda)(2\theta - \pi)],$$

$$C(\theta,\lambda) = 4(1+\lambda)^2 \sin^2\theta \{\sin^2[(1+\lambda)\theta] + \sin^2[(1+\lambda)(\theta - \pi)] - 1\},$$

$$D(\theta,\lambda) = 2\{\sin^2[(1+\lambda)\theta] + \sin^2[(1+\lambda)(\theta - \pi)] - 1\},$$

$E(\theta,\lambda) = \cos^2(\lambda\pi)$,

and α and β are Dundur's parameter

$$\alpha = \frac{\mu_2(\kappa_1+1)-\mu_1(\kappa_2+1)}{\mu_2(\kappa_1+1)+\mu_1(\kappa_2+1)}, \quad \beta = \frac{\mu_2(\kappa_1-1)-\mu_1(\kappa_2-1)}{\mu_2(\kappa_1+1)+\mu_1(\kappa_2+1)}.$$

Setting $\theta = 0, \pm 2\pi$ the above equations recover the case of the crack lying along the interface yielding $\lambda = -1/2 \pm i\epsilon$. If $\alpha = \beta = 0$ is substituted in the above equation, the expected result of $\lambda = -1/2$ is obtained.

Another commonly encountered singularity is associated with the kinking of a straight crack. If the crack is open in the vicinity of the kink, the singularity at the kink is the same as that at the apex of a wedge. Bogy (1971b) derived the characteristic equation for the bonded bimaterial wedge geometry, which can be utilised to identify the order of singularity for a crack going through an interface or kinking at an interface. The latter solution also recovers Williams' (1952) results for a homogenous wedge or an angular corner in an infinite plate. A review of methods for finding the stress singularities at the apex of isotropic elastic wedges is provided by Dempsey and Sinclair (1981). The equivalent problem of anisotropic bimaterial wedges was considered by Kuo and Bogy (1974a, 1974b). The singularities at a crack-tip terminating at the interface in an anisotropic bimaterial are examined by Ting and Hoang (1984) for a crack lying perpendicular to the interface and by Deng (1993), Suo (1990) and Ting (1986) for an interfacial crack. In the present thesis only plane crack problems are considered. A review of stress singularities arising in three-dimensional fracture mechanics can be found in Pook (2013), Kotousov et al. (2013) and Kotousov and Lew (2006).

2.3 Fundamentals of DDT

DDT is a powerful semi-analytical approach for obtaining accurate solutions to plane crack problems using the principle of superposition. The technique originated from the pioneering work of Bilby, Cottrell and Swinden (1963), and Bilby and Eshelby (1968) and involves the representation of the displacement discontinuity along the crack faces by a continuous distribution of 'strain nuclei'. These strain nuclei can be edge and screw dislocations or their dipoles for two-dimensional problems or dislocation loops for three dimensional problems (Hills et al., 1996).

The technique can be introduced in a simple manner through the example problem of a straight crack in an infinite plane subjected to remote tensile loading, as illustrated in Fig. 2. From Bueckner's theorem (Cartwright and Rooke, 1979; Bueckner, 1958), the solution to this problem can be obtained by a superposition of two problems, shown in Figs. 2b and 2c, respectively. The first problem involves finding the stresses arising in the uncracked body due to the applied or external loading, and particularly, the tractions at the location of the crack, as shown in Fig. 2b. In the second problem, the cracked body, which is free from the applied loading, is considered and rigid material is inserted between the crack faces in a manner such that the resulting tractions along the location of the crack are equal and opposite to the ones found in the first problem.

The inserted material between the crack faces can be visualised as a combination of infinitesimally thin strips, the first strip beginning at one crack tip and extending along the crack direction, as illustrated in Fig. 3a. By adding more strips of material along the crack (Fig. 3b) and by taking others away (Fig. 3c), the exact crack geometry can be reproduced (Fig. 3d) (Codrington, 2008). The single inserted strip of material is called an edge dislocation, and although it has precisely the same characteristics as the edge dislocation arising as a lattice defect, in the present context the material is treated as a continuum, i.e. the presence of any lattice defects is not implied.

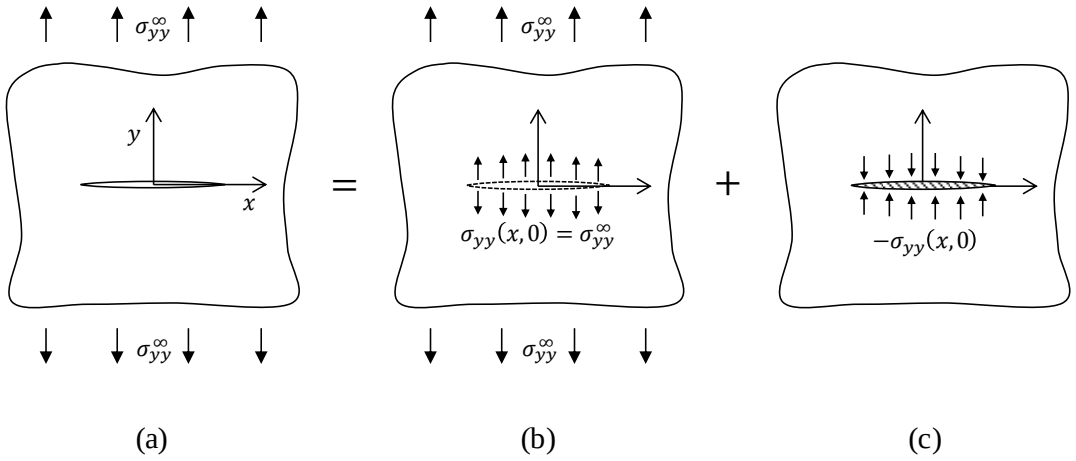

Fig. 2: Application of Bueckner's superposition principle: (a) overall problem, (b) stresses in the perfect body, (c) corrective tractions on crack faces.

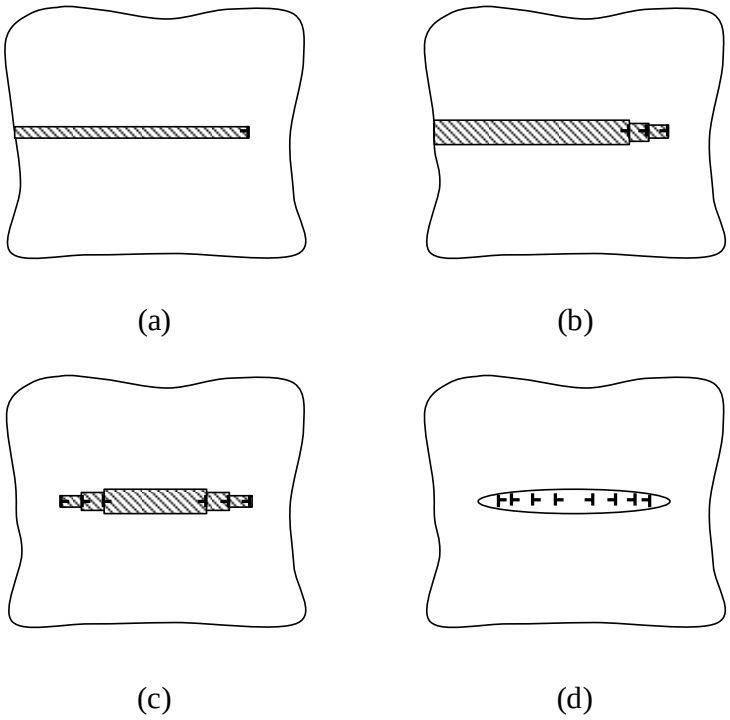

Fig. 3: The insertion of material between crack faces, (a) a single edge dislocation, (b) addition of more dislocations, (c) removal of dislocations, and (d) final crack geometry (adapted from Codrington, 2008).

The stress and displacement fields generated by a continuous distribution of dislocations (Fig. 3d) can be obtained by integrating the solution for a single edge dislocation over the length of the crack. The net state of stress in the cracked body can then be obtained using superposition, as illustrated in Fig. 2. The requirement of zero net traction on the crack faces yields a singular integral equation for determining the distributed dislocation density along the crack. In general, the governing integral equations need to be solved numerically and the methods relevant to the present thesis are discussed in Section 2.6. The complete solution for stress and displacement fields in the cracked body as well as the crack tip stress intensity factors can be inferred from the solution for the dislocation density (Hills et al., 1996). In the next section, some of the fundamental edge and screw dislocation solutions in multilayered elastic media are reviewed. These solutions are required to formulate the governing integral equation for crack problems in various geometries.

2.4 Review of dislocation solutions in multilayered media

The fundamental solutions for edge and screw dislocations in homogenous elastic media of infinite extent are well known (Weertman, 1996). These plane solutions were also extended to the case of finite thickness plates by Kotousov and Wang, (2002). Although these solutions are quite useful, most problem geometries of practical interest involve boundaries along which certain traction and displacement conditions need to be satisfied. A number of plane dislocation solutions are available for such problems, for e.g. dislocations near elastic inclusions of arbitrary shape (Shi and Li, 2003; Li and Shi, 2002) and a crack (Zhang et al., 1995; Ohr et al., 1985) and in a bimaterial wedge (Kelly et al., 1994; Hein and Erdogan, 1971).

In this section, attention is focussed on dislocation solutions in multilayered media, which are composed of two or more linearly elastic materials perfectly bonded along straight interfaces. Dislocation solutions for these geometries are

needed to obtain the governing integral equations for a variety of plane crack problems discussed in Chapter 1. The solutions for edge and screw dislocations in both isotropic and anisotropic multilayers are reviewed below.

Perhaps the simplest problem geometry involving a straight interface is a bimaterial elastic medium composed of two perfectly bonded half-planes. The solutions for an edge dislocation in this medium were obtained by Dundurs and Mura (1964), Dundurs and Sendeckyj (1965) and Comninou (1977) for the isotropic case, and by Barnett and Lothe (1974), Qu and Li (1991), and Ting (1992) for the anisotropic case. The corresponding solutions for a screw dislocation were given by Head (1953), and Martin and McGee (1969), for an isotropic bimaterial and by Chou (1966), Chou and Pande (1973) and Barnett and Lothe (1974), for the anisotropic case. Nakahara et al. (1972) and Suo (1990) presented the general approach for obtaining the stress fields due to various singularities, such as point force, screw dislocation and edge dislocation at a bimaterial interface for the isotropic and anisotropic cases, respectively.

An elastic layer of finite width, which is bonded to dissimilar elastic half-planes on both sides, represents the next step in terms of complexity of the problem geometry. The problem of an edge dislocation in an isotropic elastic strip was considered by Nabarro and Kostlan (1978), Moss and Hoover (1978), and Suo and Hutchinson (1990). Chu (1982) obtained the analogous solution for the case of a screw dislocation. The similar problem for anisotropic strips was considered by Chou (1963) and Wu and Chiu (1994) for edge dislocations and Lee et al. (2001) for screw dislocations. The problems involving edge dislocations in isotropic layer-substrate media have been examined by Weeks et al. (1968), Lee and Dundurs (1973), and Kelly et al. (1995). The solutions for edge and screw dislocations in anisotropic layer-substrate systems was derived by Wu and Wang (2007) and Wang and Wu (2005), respectively. A general method for obtaining the stress fields due to singularities in isotropic and anisotropic trimaterials, composed

of an elastic strip sandwiched between two dissimilar elastic half-planes, was suggested by Choi and Earmme (2001, 2002).

The above mentioned solutions are restricted to two or three layer geometries. Several researchers have presented methodologies for the analysis of general or periodic multilayer geometries. For e.g. the method for obtaining the solution for an edge dislocation in isotropic multilayers was presented by Khanna and Kotousov (2015) and Kuo (2014). Alshits and Kirchner (1995a, 1995b) proposed theoretical solutions for line defects in anisotropic multilayers based on Fourier transform method, but reported computational difficulties in the numerical evaluation of Fourier integrals. Wang et al. (2007) presented an alternative approach for the derivation of screw and edge dislocation solutions in a general anisotropic multilayered medium. In the proposed method, a continuous distribution of virtual dislocations is placed along the interfaces and the equilibrium and continuity conditions along the interfaces are utilised to formulate the governing system of singular integral equations. These equations are converted to non-singular Fredholm integral equations of the second kind using special integral transforms, which are solved numerically. Further, the authors also present selected numerical results for two and three layer anisotropic media. However, a direct application of the developed solutions to solve crack problems in anisotropic media is still lacking.

2.5 General form of singular integral equations under consideration

Singular integral equations arise in the formulation of mixed boundary value problems in several areas of applied mechanics and physics. In particular, they play an important role in the solution of a variety of contact and crack problems in solid mechanics. The problems under consideration in the present thesis all deal with embedded or interfacial cracks in multilayered media. For this group of problems, the system of singular integral equation contains kernels with simple

Cauchy-type singularities and can be expressed in the following general form (Erdogan et al., 1973):

$$A(x)\psi(x) + \frac{1}{\pi}\int_a^b B(t)\psi(t)\frac{dt}{t-x} + \int_a^b K(x,t)\psi(t)\mathrm{d}t = f(x), \quad (a < x < b) \qquad (3)$$

where $\psi = (\psi_i),\ (i = 1, \dots, N)$ is the set of unknown function which can be interpreted as the dislocation densities, the square matrices $A = \left(a_{ij}\right)$ and $B = \left(b_{ij}\right),\ (i, j = 1, \dots, N)$ are known with $A \pm B$ non-singular in $a < x < b$, the elements $k_{ij}(x,t)$ of the square matrix K are Fredholm kernels, and the vector $f = (f_i),\ (i = 1, \dots, N)$ consists of the known functions which can be interpreted as the traction components on the crack surface.

For the problems in which the crack kinks, terminates or deflects at an interface, or penetrates several layers, the kernels k_{ij} no longer remain simple Fredholm kernels and become unbounded as x and t approach the irregular point simultaneously. In this case, the principal part of the system of equations (3) is said to have a generalised Cauchy kernel (Erdogan et al., 1973). In the latter case, the matrix of the fundamental functions (which characterise the order of the singularity of the unknown functions ψ_i) can be obtained by a direct application of the function theoretic methods to the integral equations or by the asymptotic analysis of the solution at the irregular point (Hills et al., 1996; Erdogan et al., 1973). Problems of this kind are not examined in the present thesis. Hence, the forthcoming discussion of the numerical solution techniques focusses only on integral equations containing kernels with simple Cauchy-type singularities.

2.6 Numerical solution techniques

In the general system of singular integral equations (3), diagonalising the matrices A and B simultaneously, the principal part of the system can be uncoupled (Erdogan et al., 1973). Thus, any numerical technique developed for the solution of a single equation may be generalised for application to a system of equations. It is then sufficient to review the numerical solution methods only for the following integral equation:

$$A\phi(x) + \frac{B}{\pi}\int_{-1}^{1}\frac{\phi(t)}{t-x}dt + \int_{-1}^{1}k(x,t)\phi(t)dt = f(x), \quad (-1 < x < 1), \tag{4}$$

where the original interval (a, b) is normalised to be $(-1,1)$ without any loss of generality, and A and B are known constants. The functions ϕ, k, f, and the constants A, B may be real or complex. The fundamental function of the principal part of the integral Eq. (4) can be obtained as (Erdogan et al., 1973; Muskhelishvili, 1953)

$$w(x) = (1-x)^{\alpha}(1+x)^{\beta}, \tag{5}$$

where

$$\alpha = \frac{1}{2\pi \mathrm{i}}\log\left(\frac{A-\mathrm{i}B}{A+\mathrm{i}B}\right) + N,$$

$$\beta = -\frac{1}{2\pi \mathrm{i}}\log\left(\frac{A-\mathrm{i}B}{A+\mathrm{i}B}\right) + M,$$

$$-1 < \mathrm{Re}(\alpha) < 1, \quad -1 < \mathrm{Re}(\beta) < 1,$$

$$\kappa = -(\alpha+\beta) = -(N+M),$$

and N and M are integers. The index of the integral equation κ is either -1, 0 or $+1$, and is determined from the physical nature of the problem. In the case of $\kappa = 1$, the solution contains one arbitrary constant that is determined from an equilibrium or compatibility condition of the form

$$\int_{-1}^{1} \phi(t)\mathrm{d}t = C. \tag{6}$$

If the known constant C is taken to be zero, the above condition may be interpreted as the requirement of no relative displacement (opening or sliding) at the crack tips. For $\kappa = 0$, the inversion of Eq. (4) does not contain any arbitrary constants. When $\kappa = -1$, the solution does not contain any arbitrary constants, but the following consistency equation must be satisfied (Erdogan et al., 1973)

$$\int_{-1}^{1} [f(x) - \int_{-1}^{1} k(x,t)\phi(t)\mathrm{d}t] \frac{\mathrm{d}x}{w(x)} = 0. \tag{7}$$

In the problems under consideration in the present thesis, only the integral equations with index $+1$ are encountered. Therefore, the discussion on numerical solution methods is restricted to the case of $\kappa = +1$. The details of the solution procedures for the other cases are similar, and covered in Erdogan et al. (1973).

Solution by Jacobi polynomials (used in Chapter 3)

The solution for the unknown function $\phi(x)$ in Eq. (4), may be expressed in terms of the fundamental function, $w(x)$ as follows:

$$\phi(x) = w(x)g(x), \tag{8}$$

where $g(x)$ is a bounded continuous function in the closed interval [-1,1] and can always be represented in terms of an infinite series. Observing that $w(x)$ defined in Eq. (5) is the weight function of the Jacobi polynomial $P_n^{(\alpha,\beta)}(x)$, $(n = 0,1,\dots)$, the function $\phi(x)$ may be written as

$$\phi(x) = \sum_{0}^{\infty} c_n w(x) P_n^{(\alpha,\beta)}(x), \tag{9}$$

where c_n $(n = 0,1,\dots)$ are undetermined constants. Using the following result valid for $\kappa = (-1,0,1)$ (Erdogan et al., 1973; Tricomi, 1957):

$$\frac{1}{\pi}\int_{-1}^{1} w(t)P_n^{(\alpha,\beta)}(t)\frac{dt}{t-x} = -\frac{A}{B}w(x)P_n^{(\alpha,\beta)}(x) \\ -2^{-\kappa}\frac{\Gamma(\alpha)\Gamma(1-\alpha)}{\pi}P_{n-\kappa}^{(-\alpha,-\beta)}(x), \quad (|x|<1), \tag{10}$$

and substituting Eq. (9) into Eq. (4), the following equation can be obtained:

$$\sum_{0}^{\infty} c_n\left[-\frac{2^{-\kappa}b}{\sin\pi\alpha}P_{n-\kappa}^{(-\alpha,-\beta)}(x) + h_n(x)\right] = f(x), \\ h_n(x) = \int_{-1}^{1} w(t)P_n^{(\alpha,\beta)}(t)k(x,t)dt\,, \quad (-1<x<1). \tag{11}$$

The functional Eq. (11) can be reduced to an infinite system of algebraic equations with respect to c_n by expanding both sides into series of Jacobi polynomials $P_k^{(-\alpha,-\beta)}(x)$ $(k = 0,1,...)$. Using orthogonality relations for Jacobi polynomials and truncating the series to the first $N+1$ terms results in (Erdogan et al., 1973):

$$-\frac{2^{-1}b}{\sin\pi\alpha}\theta_k^{(-\alpha,-\beta)}c_{k+1} + \sum_{k=0}^{N} d_{nk}c_n = F_k, \quad (k = 0,1,\dots,N) \tag{12}$$

where

$$\theta_k^{(\alpha,\beta)} = \frac{2^{\alpha+\beta+1}}{2k+\alpha+\beta+1}\frac{\Gamma(k+\alpha+1)\Gamma(k+\beta+1)}{k!\,\Gamma(k+\alpha+\beta+1)},$$

$$d_{nk} = \int_{-1}^{1} P_k^{(-\alpha,-\beta)}(x)w(-\alpha,-\beta,x)h_n(x)dx,$$

$$F_k = \int_{-1}^{1} P_k^{(-\alpha,-\beta)}(x)w(-\alpha,-\beta,x)f(x)dx,$$

and

$w(-\alpha,-\beta,x)=(1-x)^{-\alpha}(1+x)^{-\beta}=w^{-1}(x)$.

For $\kappa=+1$, the $N+1$ equations given by (12) contain $N+2$ unknown constants, $c_0,\dots,c_{N+1}$. The additional equation for a unique solution can be obtained from the equilibrium or compatibility condition given by Eq. (6) as follows:

$$c_0\theta_0(\alpha,\beta)=C. \tag{13}$$

The general solution procedure described above can also be applied for solution of singular integral equations of the first kind of the form

$$\frac{1}{\pi}\int_{-1}^{1}\frac{\phi(t)}{t-x}dt+\int_{-1}^{1}k(x,t)\phi(t)dt=f(x),\quad(-1<x<1), \tag{14}$$

which correspond to the more specific case of $A=0$ and $B=1$ in Eq. (4). However, in the present thesis another method is utilised to solve integral equations of this type, which is described next.

Solution by Gauss-Chebyshev quadrature (used in Chapters 4-6)

The singular integral Eq. (14) can be reduced to the following algebraic system (Erdogan et al., 1973):

$$\frac{1}{\pi}\sum_{j=1}^{n}W_j g(t_j)\left[\frac{1}{t_j-x_i}+\pi k(x_i,t_j)\right]=f(x_i),\quad(i=1,\dots,n-\kappa), \tag{15}$$

where κ is the index of the integral equation, t_j are the integration points and x_i are the collocation points. Only the case of $\kappa=1$ is considered here and it corresponds to the integrable singularities at both ends, i.e. $\alpha=-1/2=\beta$ in Eq. (5). In this case, the fundamental function $w(x)$ becomes the weight function of the Chebyshev polynomials of the first kind (T_n). The integration and collocation points in Eq. (15) are chosen as roots of the Chebyshev polynomials according to (Erdogan et al., 1973):

$$W_j = \pi/n\,,$$
$$T_n(t_j) = 0, \quad t_j = \cos\left(\pi\frac{2j-1}{2n}\right), \quad (j = 1, \dots, n), \tag{16}$$
$$U_{n-1}(x_i) = 0, \quad x_i = \cos\frac{\pi i}{n}, \quad (i = 1, \dots, n-1).$$

The additional condition given by Eq. (5) can be represented as

$$\sum_{1}^{n} W_j g(t_j) = C. \tag{17}$$

Eqs. (15) and (17) provide n linear algebraic equations to determine $g(t_j)$, $(j = 1, \dots, n)$.

2.7 Concluding remarks

In this chapter, the fundamentals of LEFM and the DDT were briefly discussed in the context of the current research topic, which is the analysis of crack problems in multilayered elastic media. In addition, the two-dimensional dislocation solutions in multilayered elastic media were reviewed. A new fundamental solution for edge dislocation in multilayered media to be presented in the next chapter represents a natural extension of the previous results. The next and following chapters are a collection of the candidate's publications based on the general methodology described above.

References

Alshits, V.I. and H.O.K. Kirchner (1995), Elasticity of multilayers I. Basic equations and solutions, *Philos. Mag. A*, 72, 1431-1444, doi: 10.1080/01418619508243922.

Alshits, V.I. and H.O.K. Kirchner (1995), Elasticity of multilayers II. Strips, coatings and sandwiches, *Philos. Mag. A*, 72, 1445-1470, doi: 10.1080/01418619508243923.

Barnett, D.M. and J. Lothe (1974), An image force theorem for dislocations in anisotropic bicrystals, *J. Phys. F: Met. Phys*., 4, 1618-1635, doi: 10.1088/0305-4608/4/10/010.

Bilby, B. and J. Eshelby (1968), Dislocations and the theory of fracture, in Fracture: An Advanced Treatise, vol. 1, edited by H. Liebowitz, pp. 99-182, Academic Press, New York.

Bilby, B.A., A.H. Cottrell and K.H. Swinden (1963), The spread of plastic yield from a notch, *Proc. R. Soc. London, Ser. A*, 272, 304-314, doi: 10.1098/rspa.1963.0055.

Bogy, D.B. (1971a), On the plane elastostatic problem of a loaded crack terminating at a material interface, *J. Appl. Mech.*, 38, 911-918, doi: 10.1115/1.3408975.

Bogy, D.B. (1971b), Two edge bonded elastic wedges of different materials and wedge angles under surface tractions, *J. Appl. Mech.*, 38, 911-918, doi: 10.1115/1.3408786.

Bueckner, H.F. (1958), The propagation of cracks and energy of elastic deformation, *Trans. ASME*, 80, 1225-1230.

Cartwright, D.J., and Rooke, D.P. (1979), Green's functions in fracture mechanics, in Fracture Mechanics: Current Status, Future Prospects, edited by R.A. Smith, pp. 91-123, Pergamon, Oxford.

Choi, S.T. and Y.Y. Earmme (2001), Elastic study on singularities interacting with interfaces using alternating technique: Part I. Anisotropic trimaterial, *Int. J. Solids Struct*., 39, 943-957, doi: 10.1016/S0020-7683(01)00230-X.

Choi, S.T. and Y.Y. Earmme (2002), Elastic study on singularities interacting with interfaces using alternating technique: Part II. Isotropic trimaterial, *Int. J. Solids Struct*., 39, 1199-1211, doi: 10.1016/S0020-7683(01)00231-1.

Chou, Y.T. (1963), Planar stress field of a dislocation in an anisotropic plate, *J. Appl. Phys.*, 34, 3608-3614, doi: 10.1063/1.1729266.

Chou, Y.T. (1966), Screw dislocations in and near lamellar inclusions, *Phys. Status Solidi B*, 17, 509-516, doi: 10.1002/pssb.19660170206.

Chou, Y.T. and C.S. Pande (1973), Interfacial screw dislocation in anisotropic two-phase media, *J. Appl. Phys*., 44, 3355-3356, doi: 10.1063/1.1662761.

Chu, S.N.G. (1982), Screw dislocation in a two phase isotropic thin film, *J. Appl. Phys*., 53, 3019-3023, doi: 10.1063/1.331043.

Codrington, J. (2008), Non-linear individual and interaction phenomena associated with fatigue crack growth, PhD thesis, The University of Adelaide.

Comninou, M. (1977), A property of interface dislocation, *Phil. Mag.*, 36, 281-283, doi: 10.1080/14786437708239797.

Dempsey, J.P. and G.B. Sinclair (1981), On the singular behaviour at the vertex of a bi-material wedge, *J. Elast.*, 11(3), 317-327, doi: 10.1007/BF00041942.

Deng, X. (1993), General Crack-Tip Fields for Stationary and Steadily Growing Interface Cracks in Anisotropic Bimaterials, *J. Appl. Mech.*, 60, 183-189, doi: 10.1115/1.2900743.

Dundurs, J. and G.P. Sendeckyj (1965), Behaviour of an edge dislocation near a bimetallic interface, *J. Appl. Phys*., 36, 3353-3354, doi: 10.1063/1.1702981.

Dundurs, J. and T. Mura (1964), Interaction between an edge dislocation and a circular inclusion, *J. Mech. Phys. Solids,* 12, 177-189, doi: 10.1016/0022-5096(64)90017-1.

Eischen, J.W. (1987), Fracture of nonhomogenous materials, *Int. J. Fract.*, 34, 3-22, doi: 10.1007/BF00042121.

Erdogan, F. (1972), Fracture problems in composite materials, *Eng. Fract. Mech.*, 4(4), 811-840, doi: 10.1016/0013-7944(72)90018-5.

Erdogan, F. and G.D. Gupta (1972), On the numerical solution of singular integral equations, *Quart. Appl. Math.*, 30, p. 525-534.

Erdogan, F., G.D. Gupta and T.S. Cook (1973), Numerical solution of singular integral equations, in Mechanics of Fracture, vol. 1, edited by G.C. Sih , pp. 368-425, Noordhoff International, Leyden, The Netherlands, doi: 10.1007/978-94-017-2260-5_7.

Head, A.K. (1953), The interaction of dislocations and boundaries, *Phil. Mag.*, 44, 92-94, doi: 10.1080/14786440108520278.

Hein, V.L. and F. Erdogan (1971), Stress singularities in a two-material wedge, *Int. J. Frac. Mech*., 7, 317-330, doi: 10.1007/BF00184307.

Hills, D.A., P.A. Kelly, D.N. Dai and A.M. Korsunsky (1996), Solution of Crack Problems: The Distributed Dislocation Technique, Kluwer Academic Publishers, Dordrecht, The Netherlands.

Irwin, G.R. (1957), Analysis of stresses and strains near the end of a crack traversing a plate, *J. Appl. Mech*., 24, 361-364.

Jin, Z.-H. and N. Noda (1994), Crack-tip singular fields in nonhomogenous materials, *J. Appl. Mech.*, 61, 738-740, doi: 10.1115/1.2901529.

Kelly, P., D.A. Hills and D. Nowell (1994), The complete stress field due to a dislocation anywhere in two bonded quarter-planes, *J. Appl. Mech*., 61, 992-993, doi: 10.1115/1.2901596.

Kelly, P.A., J.J. O'Connor and D.A. Hills (1995), The stress field due to a dislocation in layered media, *J. Phys. D: Appl. Phys*., 28, 530-534, doi: 10.1088/0022-3727/28/3/013.

Khanna, A. and A. Kotousov (2015), The stress field due to an interfacial edge dislocation in a multi-layered medium, *Int. J. Solids Struct*., 72, 1-10, doi: 10.1016/j.ijsolstr.2015.06.030.

Kotousov, A. and C.H. Wang (2002), Fundamental solutions for the generalised plane strain theory, *Int. J. Eng. Sci*., 40, 1775-1790, doi: 10.1016/S0020-7225(02)00041-1.

Kotousov, A. and Y.T. Lew (2006), Stress singularities resulting from various boundary conditions in angular corners of plates of arbitrary thickness in extension, *Int. J. Solids Struct.*, 43(17), 5100-5109, doi: 10.1016/j.ijsolstr.2005.06.037.

Kotousov, A., P. Lazzarin, F. Berto and L.P. Pook (2013), Three-dimensional stress states at crack tip induced by shear and anti-plane loading, *Eng. Fract. Mech.*, 108, 65-74, doi: 10.1016/j.engfracmech.2013.04.010.

Kuo, C.-H. (2014), Elastic field due to an edge dislocation in a multi-layered composite, *Int. J. Solids Struct*., 51, 1421-1433, doi: 10.1016/j.ijsolstr.2013.12.032.

Kuo, M.C. and D.B. Bogy (1974a), Plane solutions for traction problems on orthotropic unsymmetrical wedges and symmetrically twinned wedges, *J. Appl. Mech.*, 41, 203-208, doi: 10.1115/1.3423225.

Kuo, M.C. and D.B. Bogy (1974b), Plane solutions for the displacement and traction-displacement problems for anisotropic elastic wedges, *J. Appl. Mech.*, 41, 197-203, doi: 10.1115/1.3423223.

Lee, K.W., J.H. Lim, Y.Y. Earmme (2001), A screw dislocation interacting with an interfacial crack in two anisotropic thin films with finite thickness, *Mech. Mater*., 33, 97-103, doi: 10.1016/S0167-6636(00)00061-2.

Lee, M.S. and J. Dundurs (1973), Edge dislocation in a surface layer, *Int. J. Eng. Sci*., 11, 87-94, doi: 10.1016/0020-7225(73)90071-2.

Li, Z. and J. Shi (2002), The interaction of a screw dislocation with inclusion analyzed by Eshelby equivalent inclusion method, *Scr. Mater*., 47, 371-375, doi: 10.1016/S1359-6462(02)00113-6.

Ma, C.-C. and R.-L. Lin (2002), Full field analysis of a planar anisotropic layered half-plane for concentrated forces and edge dislocations, *Proc. R. Soc. London, Ser. A*, 458, 2369-2392, doi: 10.1098/rspa.2002.0974.

Martin, D.M. and T.D. McGee (1969), The interaction of dislocations and boundaries, *Acta Metall*., 17(8), 929-932, doi: 10.1016/0001-6160(69)90037-6.

Moss, W.C. and W.G. Hoover (1978), Edge-dislocation displacements in an elastic strip, *J. Appl. Phys*., 49, 5449-5451, doi: 10.1063/1.324512.

Muskhelishvili, N.I. (1953), Singular Integral Equations, P. Noordhoff, Groningen, The Netherlands.

Nabarro, F.R.N. and E.J. Kostlan (1978), The stress fields of a dislocation lying in a plate, *J. Appl. Phys*., 49, 5445-5448, doi: 10.1063/1.324511.

Nakahara, S., J.B.C. Wu and J.C.M. Li (1972), Dislocations in a welded interface between two isotropic media, *Mater. Sci. Eng*., 10, 291-296, doi: 10.1016/0025-5416(72)90101-2.

Ohr, S.M., S.-J. Chang and R. Thompson (1985), Elastic interaction of a wedge crack with a screw dislocation, *J. Appl. Phys*., 57, 1839-1843, doi: 10.1063/1.334412.

Pook, L.P. (2013), A 50-year retrospective review of three-dimensional effects at cracks and sharp notches, *Fatigue Fract. Eng. Mater. Struct*., 36(8), 699-723, doi: 10.1111/ffe.12074.

Qu, J. and Q. Li (1991), Interfacial dislocation and its applications to interface cracks in anisotropic bimaterials, *J. Elast*., 26, 169-195, doi: 10.1007/BF00041220.

Shi, J.-Y. and Z.-H. Li (2003), The interaction of an edge dislocation with an inclusion of arbitrary shape analyzed by the Eshelby inclusion method, *Acta Mech*., 161, 31-37, doi: 10.1007/s00707-002-0987-9.

Sih, G.C. and H. Liebowitz (1968), Mathematical theories of brittle fracture, in Fracture: An Advanced Treatise, vol. 2, edited by H. Liebowitz, pp. 67-190, Academic Press, New York.

Suo, Z. (1990), Singularities, Interfaces and Cracks in Dissimilar Anisotropic Media, *Proc. R. Soc. London, Ser. A*, 427, 331-358, doi: 10.1098/rspa.1990.0016.

Suo, Z. and J.W. Hutchinson (1990), Interface crack between two elastic layers, *Int. J. Fract.*, 43, 1-18, doi: 10.1007/BF00018123.

Ting, T.C.T. (1986), Explicit solution and invariance of the singularities at an interface crack in anisotropic composites, *Int. J. Solids Struct.*, 22(9), 965-983, doi: 10.1016/0020-7683(86)90031-4, doi: 10.1016/0020-7683(86)90031-4.

Ting, T.C.T. (1992), Image singularities of Green's functions for anisotropic elastic half-spaces and bimaterials, *Q. J. Mech. Appl. Math*., 45, 119-139, doi: 10.1093/qjmam/45.1.119.

Ting, T.C.T. and P.H. Hoang (1984), Singularities at the tip of a crack normal to the interface of an anisotropic layered composite, *Int. J. Solids Struct*., 20, 439-454, doi: 10.1016/0020-7683(84)90011-8.

Tricomi, F.G. (1957), Integral equations, Interscience, New York.

Wang, H.Y. and M.S. Wu (2005), Green's function for an anisotropic film-substrate embedded with a screw dislocation, *Eng. Anal. Boundary Elem*., 29, 624-635, doi: 10.1016/j.enganabound.2005.01.013.

Wang, H.Y., M.S. Wu and H. Fan (2007), Image decomposition method for the analysis of a mixed dislocation in a general multilayer, *Int. J. Solids Struct.*, 44, 1563-1581, doi: 10.1016/j.ijsolstr.2006.06.042.

Weeks, R., J. Dundurs and M. Stippes (1968), Exact analysis of an edge dislocation near a surface layer, *Int. J. Eng. Sci*., 6, 365-372, doi: 10.1016/0020-7225(68)90016-5.

Weertman, J. (1996), Dislocation based fracture mechanics, World Scientific, Singapore.

Williams, M.L. (1952), Stress singularities resulting from various boundary conditions in angular corners of plates in extension, *J. Appl. Mech.*, 19, 526-528.

Williams, M.L. (1957), On the stress distribution at the base of a stationary crack, *J. Appl. Mech*., 24, 109-114.

Williams, M.L. (1959), Stresses around a fault or crack in dissimilar media, *Bull. Seism. Soc. Am.*, 49, 199-204.

Wu, K.-C. and Y.-T. Chiu (1994), The elastic fields of a dislocation in an anisotropic strip, *Int. J. Solids Struct*., 32, 543-552, doi: 10.1016/0020-7683(94)00115-D.

Wu, M.S. and H.Y. Wang (2007), Solutions for Edge Dislocation in Anisotropic Film-substrate System by the Image Method, *Math. Mech. Solids*, 12, 183-212, doi: 10.1177/1081286505055756.

Zhang, T.-Y., P. Tong, H. Quyang and S. Lee (1995), Interaction of an edge dislocation with a wedge crack, *J. Appl. Phys*., 78, 4873-4880, doi: 10.1063/1.359775.

Chapter 3

The stress field due to an interfacial edge dislocation in a multi-layered medium

Statement of Authorship

Title of Paper	The stress field due to an interfacial edge dislocation in a multi-layered medium
Publication Status	☑ Published ☐ Accepted for Publication ☐ Submitted for Publication ☐ Unpublished and Unsubmitted work written in manuscript style
Publication Details	International Journal of Solids and Structures, 72, 1-10, doi: 10.1016/j.ijsolstr.2015.06.030 Submitted: 10 Mar 2015, Submitted in revised form: 2 Jun 2015, Accepted: 28 Jun 2015

Principal Author

Name of Principal Author (Candidate)	Aditya Khanna		
Contribution to the Paper	Performed all analyses and wrote manuscript.		
Overall percentage (%)	80		
Certification:	This paper reports on original research I conducted during the period of my Higher Degree by Research candidature and is not subject to any obligations or contractual agreements with a third party that would constrain its inclusion in this thesis. I am the primary author of this paper.		
Signature		Date	10/04/2016

Co-Author Contributions

By signing the Statement of Authorship, each author certifies that:

i. the candidate's stated contribution to the publication is accurate (as detailed above);

ii. permission is granted for the candidate in include the publication in the thesis; and

iii. the sum of all co-author contributions is equal to 100% less the candidate's stated contribution.

Name of Co-Author	Andrei Kotousov		
Contribution to the Paper	Checked the derivation of the dislocation solution. Assisted in the preparation of the manuscript.		
Overall percentage (%)	20		
Signature		Date	10/04/2016

International Journal of Solids and Structures 72 (2015) 1–10

Contents lists available at ScienceDirect

International Journal of Solids and Structures

journal homepage: www.elsevier.com/locate/ijsolstr

The stress field due to an interfacial edge dislocation in a multi-layered medium

Aditya Khanna *, Andrei Kotousov

School of Mechanical Engineering, The University of Adelaide, Adelaide, SA 5005, Australia

ARTICLE INFO

Article history:
Received 10 March 2015
Received in revised form 2 June 2015
Available online 9 July 2015

Keywords:
Edge dislocation
Multi-layered composite
Interface
Delamination
Distributed dislocation technique

ABSTRACT

We consider the problem of a multi-layered medium composed of an arbitrary number of perfectly bonded isotropic layers, with different thicknesses and elastic properties, when an edge dislocation of arbitrary orientation is present along one of the interfaces. A new effective solution is obtained for the complete stress and displacement fields induced by the interfacial edge dislocation in the multi-layered medium. The solution for the stress field due to the interfacial edge dislocation can be utilized to formulate governing equations for multiple interacting cracks in a multi-layered medium, with no restriction on the crack orientation, position and loading. The edge dislocation solution is validated directly by comparing it to available edge dislocation solutions and indirectly by revisiting some previously examined interfacial crack problems.

1. Introduction

Many modern composites and advanced material systems, such as protective coatings, laminated ceramics, microelectronic devices, layered nanofilms, functionally graded materials and adhesive joints, are examples of multi-layered structures (Sackman et al. 1989; Holleck et al. 1990; Roeder and Sun, 2001; Chen and Pindera, 2006; Khanna and Kotousov, 2014). These structures are also prevalent in nature, ranging from the nano-scale structures, which provide unique properties to bio-materials such as nacre, tooth enamel and bone (Sellinger et al. 1998; Gao et al. 2003) to the large scale structures such as stratified rock formations in the earth's crust (Daneshy, 1978; Gudmundsson et al. 2010; Khanna and Kotousov, 2015).

Accurate analysis of fracture problems in multi-layered laminates is of great practical interest in many engineering applications, for example, in the study of delamination damage (Bolotin, 1996; Garg, 1988), in the design of crack arresting interfaces (Cook et al. 1964; He and Hutchinson, 1989; Gupta et al. 1992; Li, 2000), when describing the toughness behavior of natural composites (Okumura and de-Gennes, 2001) and in the modeling of hydraulic fracture propagation in heterogeneous oil/gas reservoirs (Cleary, 1978).

The distributed dislocation technique (DDT), which is based on the pioneering work of Bilby and Eshelby (1968), can provide an efficient procedure for analyzing a variety of crack problems in such multi-layered structures. In this technique, the mixed boundary-value crack problem is reduced to a system of coupled singular integral equations of the Cauchy type with kernels formulated in terms of the unknown displacement discontinuities. The literature is replete with solutions to crack problems in multi-layered composites obtained by the distributed dislocation approach (for e.g. Erdogan and Gupta, 1971a,b; Erdogan, 1972; Kucherov and Ryvkin, 2002; Chen and Pindera, 2006). In every case we find that there is some restriction on the geometry tackled; either because the crack is chosen to be normal or parallel to the interfaces. However, several crack problems of practical interest in multi-layered structures may require the analysis of inclined, kinking or branching cracks (Garg, 1988).

In this paper, we consider a general multi-layered composite, composed of perfectly bonded isotropic elastic layers, and present the solution for the elastic field induced by an interfacial edge dislocation. The present solution is more general than other available solutions for embedded or interfacial edge dislocations in: a film-substrate medium (Savage, 1998; Kelly et al., 1995; Comninou and Dundurs, 1983; Lee and Dundurs, 1973), a layer joining two substrates (Fleck et al. 1991), two bonded layers (Suo and Hutchinson, 1990) and a general multilayered composite (Kuo, 2014). The obtained solution can be implemented using the framework of the distributed dislocation technique to formulate the governing singular integral equations for a wide variety of

* Corresponding author. Tel.: +61 8 8313 6385.
E-mail addresses: aditya.khanna@adelaide.edu.au (A. Khanna), andrei.kotousov@adelaide.edu.au (A. Kotousov).

http://dx.doi.org/10.1016/j.ijsolstr.2015.06.030
0020-7683/

crack problems in multi-layered media, in particular problems involving inclined or kinking cracks. The obtained solution can also be used to study the interaction between 'real' edge dislocations and interfaces in multilayered composites (Nix, 1998; Misra et al. 1998; Misra and Kung, 2001).

The present solution is developed using the complex potential method of Muskhelishvili and the Fourier transform method for strip problems, based on the approach outlined by Fleck et al. (1991) for an embedded dislocation in an elastic layer. The details of the solution are covered in Sections 2–4 and Appendix A. In Section 5, the solution is validated against the solution obtained by Kelly et al. (1995) for an interfacial edge dislocation in a layer-substrate medium. To demonstrate the application of the present solution, the problem of an interfacial crack in a general multilayered composite is formulated in Section 6. Selected numerical results are presented for the interfacial crack problem and compared with classical solution obtained by Erdogan and Gupta (1971b) and more recent results of Kucherov and Ryvkin (2002).

2. Problem formulation

Consider the plane elasticity problem of a multi-layered medium, composed of $m+n$ layers, as shown in Fig. 1. The elastic properties of the layers are defined by the shear modulus, μ and Poisson's ratio, ν. The top and bottom layers are of infinite extent and the intermediate layers are of arbitrary thickness. Free boundaries can be modeled by setting the shear modulus of elasticity of the top and bottom layers to a very small value approaching zero, while the embedded dislocation corresponds to the case when $\mu_{-1}=\mu_1$ and $\nu_{-1}=\nu_1$. The layers are perfectly bonded, except for an edge dislocation along the interface between layers L_1 and L_{-1}. The origin of the coordinate system lies at the location of the edge dislocation and the x -axis is aligned with the interfaces.

The solution to the plane elasticity problem shown in Fig. 1 is obtained using the approach outlined by Fleck et al. (1991). First, we consider a composite medium composed of two homogenous elastic half-planes, with a bimaterial interface along $y=0$. The elastic properties of the material above the interface ($y>0$) are denoted by μ_1,ν_1 and those of the material below the interface ($y<0$) are denoted by μ_{-1},ν_{-1}. The stress and displacement field due to an interfacial edge dislocation in this medium are well known.

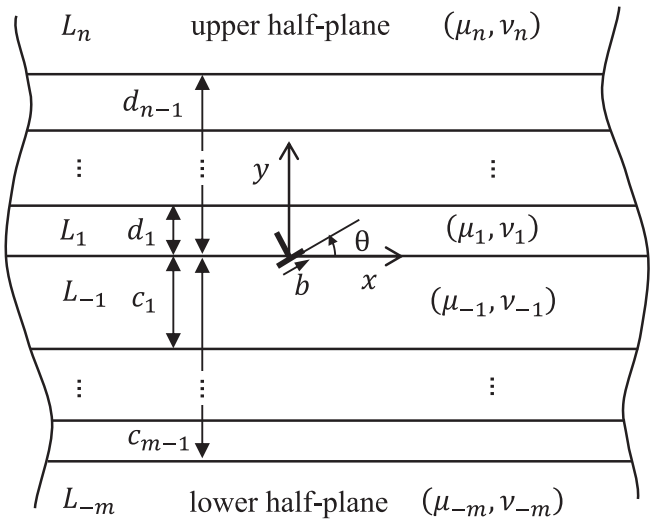

Fig. 1. An edge dislocation in a multi-layered composite.

The material in the region, $d_i<y<d_{i+1}$, is then allowed to transform to material μ_{i+1},ν_{i+1} $(i=1,\ldots,n-1)$ and the material in the region, $-c_{j+1}<y<-c_j$, is allowed to transform to material $\mu_{-(j+1)},\nu_{-(j+1)}$ $(j=1,\ldots,m-1)$. The transformation occurs in a manner which does not alter the stress state anywhere, but generates a displacement mismatch at the interfaces. The displacement jump at the interfaces is denoted by $\Delta u(x,d_i)+i\Delta v(x,d_i)$ for $y>0$ and $\Delta u(x,-c_j)+i\Delta v(x,-c_j)$ for $y<0$.

Finally, the problem of the multi-layered medium is considered, with the displacement jumps prescribed at the interfaces equal in magnitude but opposite in sign to those obtained previously. The corrective stress field required to generate these displacement jumps is then evaluated. The net stress field is obtained as a superposition of this corrective stress field and the known solution for stress field in a bimaterial due to an interfacial edge dislocation.

3. Problem 1: Edge dislocation at a bimaterial interface

Consider a composite medium with a planar interface along $y=0$, with an interfacial dislocation at the origin. The elastic properties of the material above the interface ($y>0$) are denoted by μ_1,ν_1 and those of the material below the interface ($y<0$) are denoted by μ_{-1},ν_{-1}. The displacement field in the medium is continuous everywhere, except for the half-plane given by $x<0$ and $y=0$, along which it is discontinuous. The jump in displacement is given by

$$u(x,0^+)+\mathrm{i}v(x,0^+)-u(x,0^-)-\mathrm{i}v(x,0^-)=(b_x+\mathrm{i}b_y)H(-x), \tag{1}$$

where b_x and b_y are the glide and climb components of the Burger's vector and $H(x)$ is the Heaviside step function.

3.1. Stress and displacement fields

The stress and displacement fields in each region can be conveniently expressed in terms of Muskhelishvili's complex potentials $\varphi(z)$ and $\psi(z)$ according to Muskhelishvili (1958)

$$\sigma_{xx}+\sigma_{yy}=2[\varphi'(z)+\overline{\varphi'(z)}], \tag{2}$$

$$\sigma_{yy}-\sigma_{xx}+2i\sigma_{xy}=2[\bar{z}\varphi''(z)+\psi'(z)], \tag{3}$$

$$2\mu(u+iv)=\kappa\varphi(z)-z\overline{\varphi'(z)}-\overline{\psi(z)}. \tag{4}$$

where μ is the shear modulus, $\kappa=3-4\nu$ is Kolosov's constant.

For an interfacial edge dislocation, as shown in Fig. 2, the complex potentials are given by Zhang and Li (1992), Hui and Lagoudas (1990) as

$$\varphi_1(z)=\Gamma_1\frac{b}{\mathrm{i}\pi}\ln z,\quad \psi_1(z)=\Gamma_{-1}\frac{\bar{b}}{-\mathrm{i}\pi}\ln z, \tag{5}$$

in region 1 ($y>0$) and

$$\varphi_{-1}(z)=\Gamma_{-1}\frac{b}{\mathrm{i}\pi}\ln z,\quad \psi_{-1}(z)=\Gamma_1\frac{\bar{b}}{-\mathrm{i}\pi}\ln z, \tag{6}$$

in region 2 ($y<0$), respectively. Here $z=x+\mathrm{i}y$, $b=b_x+\mathrm{i}b_y$ and the constants Γ_1 and Γ_{-1} are defined as

$$\Gamma_1=\frac{\mu_1\mu_{-1}}{\mu_1+\mu_{-1}\kappa_1}=\frac{\mu_1}{\kappa_1+1}\frac{1+\alpha}{1-\beta},\quad \Gamma_{-1}=\frac{\mu_1\mu_{-1}}{\mu_1\kappa_{-1}+\mu_{-1}}=\frac{\mu_1}{\kappa_1+1}\frac{1+\alpha}{1+\beta}. \tag{7}$$

The constants α and β are Dundur's elastic mismatch parameters, which are defined as:

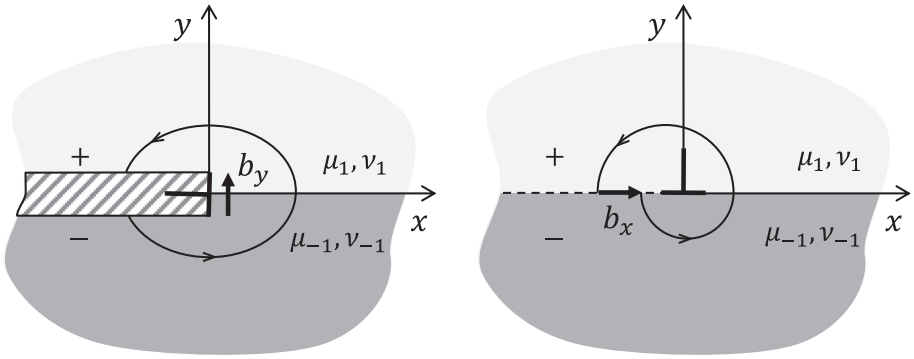

Fig. 2. The climb (b_y) and glide (b_x) component of an interfacial edge dislocation.

$$\alpha = \frac{\mu_1(\kappa_{-1}+1) - \mu_{-1}(\kappa_1+1)}{\mu_1(\kappa_{-1}+1) + \mu_{-1}(\kappa_1+1)}, \quad \beta = \frac{\mu_1(\kappa_{-1}-1) - \mu_{-1}(\kappa_1-1)}{\mu_1(\kappa_{-1}+1) + \mu_{-1}(\kappa_1+1)}, \tag{8}$$

By substituting Eq. (5) into Eqs. (2) and (3), the stress field in the upper half-space, $y > 0$, can be obtained as

$$\sigma_{xx}(x, y>0) = \frac{b_x}{\pi}\left[-\frac{y}{r^4}\{(5\Gamma_1+\Gamma_{-1})x^2 + (\Gamma_1+\Gamma_{-1})y^2\}\right] + \frac{b_y}{\pi}\left[+\frac{x}{r^4}\{(3\Gamma_1-\Gamma_{-1})x^2 - (\Gamma_1+\Gamma_{-1})y^2\}\right], \tag{9}$$

$$\sigma_{yy}(x, y>0) = \frac{b_x}{\pi}\left[+\frac{y}{r^4}\{(\Gamma_1+\Gamma_{-1})x^2 - (3\Gamma_1-\Gamma_{-1})y^2\}\right] + \frac{b_y}{\pi}\left[+\frac{x}{r^4}\{(\Gamma_1+\Gamma_{-1})x^2 + (5\Gamma_1+\Gamma_{-1})y^2\}\right], \tag{10}$$

$$\sigma_{xx}(x, y>0) = \frac{b_x}{\pi}\left[+\frac{x}{r^4}\{(\Gamma_1+\Gamma_{-1})x^2 - (3\Gamma_1-\Gamma_{-1})y^2\}\right] + \frac{b_y}{\pi}\left[+\frac{y}{r^4}\{(3\Gamma_1-\Gamma_{-1})x^2 - (\Gamma_1+\Gamma_{-1})y^2\}\right]. \tag{11}$$

Similarly, the displacement field in region 1 ($y > 0$) can be obtained by substituting Eq. (5) into Eq. (4), which yields

$$2\mu_1 u(x, y>0) = \frac{1}{\pi}\left[\left\{(\kappa_1\Gamma_1+\Gamma_{-1})\tan^{-1}\frac{y}{x} + \Gamma_1\frac{2xy}{x^2+y^2}\right\}b_x + \left\{\left(\frac{\kappa_1\Gamma_1-\Gamma_{-1}}{2}\right)\ln(x^2+y^2) - \Gamma_1\frac{x^2-y^2}{x^2+y^2}\right\}b_y\right] \tag{12}$$

$$2\mu_1 v(x, y>0) = \frac{1}{\pi}\left[-\left\{\left(\frac{\kappa_1\Gamma_1-\Gamma_{-1}}{2}\right)\ln(x^2+y^2) + \Gamma_1\frac{x^2-y^2}{x^2+y^2}\right\}b_x + \left\{(\kappa_1\Gamma_1+\Gamma_{-1})\tan^{-1}\frac{y}{x} - \Gamma_1\frac{2xy}{x^2+y^2}\right\}b_y\right]. \tag{13}$$

In Eqs. (12) and (13), κ is Kolosov's constant, which is defined in terms of the Poisson's ratio ν as

$$\kappa = \begin{cases} 3-4\nu & \text{in plane strain,} \\ \frac{3-\nu}{1+\nu} & \text{in plane stress.} \end{cases} \tag{14}$$

The stresses and displacements in the lower half-space, i.e. $y < 0$, can be obtained by interchanging the subscripts 1 and −1 in Eqs. (9)–(14) or by replacing β with $-\beta$ if Dundur's parameters are used. In the case when $\mu_1 = \mu_{-1} = \mu_0$ and $\kappa_1 = \kappa_{-1} = \kappa_0$, then $\Gamma_1 = \Gamma_{-1} = \mu_0/(\kappa_0+1)$ and Eqs. (9)–(13) yield the standard results for the elastic fiend due to an edge dislocation in an infinite homogenous medium.

3.2. Displacement discontinuities induced at the interfaces

The material in the region, $d_i < y < d_{i+1}$, is then allowed to transform to material μ_{i+1}, ν_{i+1} $(i = 1, \ldots, n-1)$ and the material in the region, $-c_{j+1} < y < -c_j$, is allowed to transform to material $\mu_{-(j+1)}, \nu_{-(j+1)}$ $(j = 1, \ldots, m-1)$. However, the Muskhelishvili potentials given by Eqs. (5) and (6) are kept fixed. As a result, the stresses given by Eqs. (2) and (3) remain unaltered but displacement jumps are registered at the interfaces when using Eq. (4) across a material interface. The resulting displacement jump is defined as

$$\Delta u(x, d_i) + i\Delta v(x, d_i) = u(x, d_i^+) + \mathrm{i}\, v(x, d_i^+) - u(x, d_i^-) - \mathrm{i}\, v(x, d_i^-) \tag{15}$$

for an interface located above the origin, i.e. $y > 0$ and

$$\Delta u(x, -c_j) + i\Delta v(x, -c_j) = u(x, -c_j^+) + \mathrm{i}\, v(x, -c_j^+) - u(x, -c_j^-) - \mathrm{i}\, v(x, -c_j^-) \tag{16}$$

for an interface located below the origin, i.e. $y < 0$. The usual convention is adopted for evaluating the one-sided limits, i.e. $y \to d_i^+$ means that y approaches d_i from above and $y \to d_i^-$ means that y approaches d_i from below.

In boundary matching problem, such as the present one, the displacement mismatch is expressed more conveniently in differential from, thus avoiding the integration constants associated with rigid-body motions. The jump in displacement gradient at an interface located in the region $y > 0$, can be evaluated substituting Eqs. (12) and (13) into Eq. (15), which yields

$$\Delta\frac{\partial u}{\partial x}(x, d_i) = -\frac{b_x}{\pi}\left[\left(\frac{\kappa_{i+1}\Gamma_1+\Gamma_{-1}}{2\mu_{i+1}} - \frac{\kappa_i\Gamma_1+\Gamma_{-1}}{2\mu_i}\right)\frac{d_i}{(x^2+d_i^2)} + \left(\frac{\Gamma_1}{2\mu_{i+1}} - \frac{\Gamma_1}{2\mu_i}\right)\frac{2d_i(x^2-d_i^2)}{(x^2+d_i^2)^2}\right] + \frac{b_y}{\pi}\left[\left(\frac{\kappa_{i+1}\Gamma_1-\Gamma_{-1}}{2\mu_{i+1}} - \frac{\kappa_i\Gamma_1-\Gamma_{-1}}{2\mu_i}\right)\frac{x}{(x^2+d_i^2)} - \left(\frac{\Gamma_1}{2\mu_{i+1}} - \frac{\Gamma_1}{2\mu_i}\right)\frac{4xd_i^2}{(x^2+d_i^2)^2}\right], \tag{17}$$

and

$$\Delta\frac{\partial v}{\partial x}(x,d_i)=-\frac{b_x}{\pi}\left[\left(\frac{\kappa_{i+1}\Gamma_1-\Gamma_{-1}}{2\mu_{i+1}}-\frac{\kappa_i\Gamma_1-\Gamma_{-1}}{2\mu_i}\right)\frac{x}{(x^2+d_i^2)}+\left(\frac{\Gamma_1}{2\mu_{i+1}}-\frac{\Gamma_1}{2\mu_i}\right)\frac{4xd_i^2}{(x^2+d_i^2)^2}\right]-\frac{b_y}{\pi}\left[\left(\frac{\kappa_{i+1}\Gamma_1+\Gamma_{-1}}{2\mu_{i+1}}-\frac{\kappa_i\Gamma_1+\Gamma_{-1}}{2\mu_i}\right)\frac{d_i}{(x^2+d_i^2)}-\left(\frac{\Gamma_1}{2\mu_{i+1}}-\frac{\Gamma_1}{2\mu_i}\right)\frac{2d_i(x^2-d_i^2)}{(x^2+d_i^2)^2}\right],\tag{18}$$

where $i=1,\ldots,n-1$. The jump in displacement gradient at an interface located in the region $y<0$, can be evaluated in a similar manner as

$$\Delta\frac{\partial u}{\partial x}(x,-c_j)=\frac{b_x}{\pi}\left[\left(\frac{\kappa_{-j}\Gamma_{-1}+\Gamma_1}{2\mu_{-j}}-\frac{\kappa_{-(j+1)}\Gamma_{-1}+\Gamma_1}{2\mu_{-(j+1)}}\right)\frac{c_j}{(x^2+c_j^2)}+\left(\frac{\Gamma_{-1}}{2\mu_{-j}}-\frac{\Gamma_{-1}}{2\mu_{-(j+1)}}\right)\frac{2c_j(x^2-c_j^2)}{(x^2+c_j^2)^2}\right]+\frac{b_y}{\pi}\left[\left(\frac{\kappa_{-j}\Gamma_{-1}-\Gamma_1}{2\mu_{-j}}-\frac{\kappa_{-(j+1)}\Gamma_{-1}-\Gamma_1}{2\mu_{-(j+1)}}\right)\frac{x}{(x^2+c_j^2)}-\left(\frac{\Gamma_{-1}}{2\mu_{-j}}-\frac{\Gamma_{-1}}{2\mu_{-(j+1)}}\right)\frac{4xc_j^2}{(x^2+c_j^2)^2}\right],\tag{19}$$

and

$$\Delta\frac{\partial v}{\partial x}(x,-c_j)=-\frac{b_x}{\pi}\left[\left(\frac{\kappa_{-j}\Gamma_{-1}-\Gamma_1}{2\mu_{-j}}-\frac{\kappa_{-(j+1)}\Gamma_{-1}-\Gamma_1}{2\mu_{-(j+1)}}\right)\frac{x}{(x^2+c_j^2)}+\left(\frac{\Gamma_{-1}}{2\mu_{-j}}-\frac{\Gamma_{-1}}{2\mu_{-(j+1)}}\right)\frac{4xc_j^2}{(x^2+c_j^2)^2}\right]+\frac{b_y}{\pi}\left[\left(\frac{\kappa_{-j}\Gamma_{-1}+\Gamma_1}{2\mu_{-j}}-\frac{\kappa_{-(j+1)}\Gamma_{-1}+\Gamma_1}{2\mu_{-(j+1)}}\right)\frac{c_j}{(x^2+c_j^2)}-\left(\frac{\Gamma_{-1}}{2\mu_{-j}}-\frac{\Gamma_{-1}}{2\mu_{-(j+1)}}\right)\frac{2c_j(x^2-c_j^2)}{(x^2+c_j^2)^2}\right],\tag{20}$$

where $j=1,\ldots,m-1$.

4. Problem 2: Dislocation-free strip problem

The displacement field should be continuous across a perfectly bonded interface. However, using the same Muskhelishvili complex potential for layers with different material properties introduces discontinuity or jump in the displacement field at the bimaterial interfaces. These jumps are prescribed in gradient form by Eqs. (17)–(20). In this section, we consider the bonded system shown in Fig. 1, having stress-free infinite boundaries and prescribed displacement jumps at the interfaces, equal in magnitude, and of opposite sign to those obtained previously. The latter problem is treated with the Airy stress function formulation. The unknown Airy stress function, $\varphi(x,y)$ is determined by matching the free boundary conditions in the far field and by satisfying the traction equilibrium and displacement jump conditions at the interfaces. The corrective stresses and displacement field can be obtained in terms of the solution for $\varphi(x,y)$.

4.1. General solution for stress and displacement fields in a strip

In the absence of body forces, the general solution for Airy's stress function, $\varphi(x,y)$, in a strip can be obtained as the following Fourier integral (Selvadurai, 2000)

$$\varphi(x,y)=\frac{1}{\sqrt{2\pi}}\int_{-\infty}^{\infty}[(A(\xi)+B(\xi)y)e^{-|\xi|y}+(C(\xi)+D(\xi)y)e^{+|\xi|y}]e^{-i\xi x}d\xi.\tag{21}$$

where the unknown constants A, B, C and D are determined by applying the boundary conditions and regularity conditions applicable to a particular problem. Without loss of generality, the unknown constants A, B, C and D, in the general solution for $\varphi(x,y)$ can be decomposed according to

$$A(\xi)=\sqrt{\tfrac{\pi}{2}}\left[\tfrac{b_x}{|\xi|^2}A_x(\xi)+i\tfrac{b_y}{|\xi|^2}A_y(\xi)\right],\quad B(\xi)=\sqrt{\tfrac{\pi}{2}}\left[\tfrac{b_x}{|\xi|}B_x(\xi)+i\tfrac{b_y}{|\xi|}B_y(\xi)\right],$$
$$C(\xi)=\sqrt{\tfrac{\pi}{2}}\left[\tfrac{b_x}{|\xi|^2}C_x(\xi)+i\tfrac{b_y}{|\xi|^2}C_y(\xi)\right],\quad D(\xi)=\sqrt{\tfrac{\pi}{2}}\left[\tfrac{b_x}{|\xi|}D_x(\xi)+i\tfrac{b_y}{|\xi|}D_y(\xi)\right],\tag{22}$$

such that A_x, B_x, C_x and D_x are even functions of the variable ξ, whereas, A_y, B_y, C_y and D_y are odd functions of ξ. The constants b_x and b_y are the components of the Burger's vector of the edge dislocation.

By substituting Eq. (22) into Eq. (21), the solution for $\varphi(x,y)$ can be decomposed into its even and odd components according to

$$\varphi(x,y)=\varphi_{b_x}(x,y)+\varphi_{b_y}(x,y),\tag{23}$$

where

$$\varphi_{b_x}(x,y)=b_x\int_0^{\infty}\left[\left(\frac{A_x}{\xi^2}+\frac{B_x}{\xi}y\right)e^{-\xi y}+\left(\frac{C_x}{\xi^2}+\frac{D_x}{\xi}y\right)e^{\xi y}\right]\cos(\xi x)d\xi,\tag{24}$$

and

$$\varphi_{b_y}(x,y)=b_y\int_0^{\infty}\left[\left(\frac{A_y}{\xi^2}+\frac{B_y}{\xi}y\right)e^{-\xi y}+\left(\frac{C_y}{\xi^2}+\frac{D_y}{\xi}y\right)e^{\xi y}\right]\sin(\xi x)d\xi.\tag{25}$$

The corrective stress components can be obtained as follows

$$\sigma_{xx}^*=b_x\int_0^{\infty}[(A_x+(\xi y-2)B_x)e^{-\xi y}+(C_x+(\xi y+2)D_x)e^{\xi y}]\cos(\xi x)d\xi+b_y\int_0^{\infty}[(A_y+(\xi y-2)B_y)e^{-\xi y}+(C_y+(\xi y+2)D_y)e^{\xi y}]\sin(\xi x)d\xi,\tag{26}$$

$$\sigma_{yy}^*=-b_x\int_0^{\infty}[(A_x+\xi yB_x)e^{-\xi y}+(C_x+\xi yD_x)e^{\xi y}]\cos(\xi x)d\xi-b_y\int_0^{\infty}[(A_y+\xi yB_y)e^{-\xi y}+(C_y+\xi yD_y)e^{\xi y}]\sin(\xi x)d\xi,\tag{27}$$

$$\sigma_{xy}^*=b_x\int_0^{\infty}[(-A_x+(1-\xi y)B_x)e^{-\xi y}+(C_x+(1+\xi y)D_x)e^{\xi y}]\sin(\xi x)d\xi-b_y\int_0^{\infty}[(-A_y+(1-\xi y)B_y)e^{-\xi y}+(C_y+(1+\xi y)D_y)e^{\xi y}]\cos(\xi x)d\xi.\tag{28}$$

The displacement components are given in gradient form as follows

$$\frac{\partial u^*}{\partial x}=\frac{b_x}{2\mu}\int_0^\infty\left[\left(A_x+\left(\xi y-\frac{\kappa+1}{2}\right)B_x\right)e^{-\xi y}+\left(C_x+\left(\xi y+\frac{\kappa+1}{2}\right)D_x\right)e^{\xi y}\right]\times\cos(\xi x)d\xi+\frac{b_y}{2\mu}\int_0^\infty\left[\left(A_y+\left(\xi y-\frac{\kappa+1}{2}\right)B_y\right)e^{-\xi y}+\left(C_y+\left(\xi y+\frac{\kappa+1}{2}\right)D_y\right)e^{\xi y}\right]\sin(\xi x)d\xi, \tag{29}$$

$$\frac{\partial v^*}{\partial x}=\frac{b_x}{2\mu}\int_0^\infty\left[\left(-A_x+\left(1-\xi y-\frac{\kappa+1}{2}\right)B_x\right)e^{-\xi y}+\left(C_x+\left(1+\xi y-\frac{\kappa+1}{2}\right)D_x\right)e^{\xi y}\right]\sin(\xi x)d\xi-\frac{b_y}{2\mu}\int_0^\infty\left[\left(-A_y+\left(1-\xi y-\frac{\kappa+1}{2}\right)B_y\right)e^{-\xi y}+\left(C_y+\left(1+\xi y-\frac{\kappa+1}{2}\right)D_y\right)e^{\xi y}\right]\cos(\xi x)d\xi. \tag{30}$$

4.2. Bimaterial interface conditions

The unknown constants A, B, C and D in the general solution for $\varphi(x,y)$ associated with each layer can be obtained by utilizing the conditions of displacement continuity and traction equilibrium, written as

$$u(x,y^+)+\mathrm{i}v(x,y^+)=u(x,y^-)+\mathrm{i}v(x,y^-), \tag{31}$$

$$\sigma_{yy}(x,y^+)+\mathrm{i}\sigma_{xy}(x,y^+)=\sigma_{yy}(x,y^-)+\mathrm{i}\sigma_{xy}(x,y^-). \tag{32}$$

Since the general solution for $\varphi(x,y)$ is a Fourier integral, the unknown constants can be determined more readily if the bimaterial interface conditions are expressed in the Fourier domain. The traction equilibrium condition Eq. (32) yields the following bimaterial interface conditions

$$\tilde{\sigma}^*_{yy}(x,d_i^+)=\tilde{\sigma}^*_{yy}(x,d_i^-),\quad \tilde{\sigma}^*_{xy}(x,d_i^+)=\tilde{\sigma}^*_{xy}(x,d_i^-), \tag{33}$$

$$\tilde{\sigma}^*_{yy}(x,-c_j^+)=\tilde{\sigma}^*_{yy}(x,-c_j^-),\quad \tilde{\sigma}^*_{xy}(x,-c_j^+)=\tilde{\sigma}^*_{xy}(x,-c_j^-), \tag{34}$$

and

$$\tilde{\sigma}^*_{yy}(x,0)=\tilde{\sigma}^*_{yy}(x,0),\quad \tilde{\sigma}^*_{xy}(x,0)=\tilde{\sigma}^*_{xy}(x,0). \tag{35}$$

where $i=1,\ldots,n-1$, $j=1,\ldots,m-1$ and the tilde symbol represents the Fourier transform with respect to the variable x. The displacement continuity condition Eq. (31) requires that

$$\Delta\frac{\partial\tilde{u}^*}{\partial x}(x,d_i)=-\Delta\frac{\partial\tilde{u}}{\partial x}(x,d_i),\quad \Delta\frac{\partial\tilde{v}^*}{\partial x}(x,d_i)=-\Delta\frac{\partial\tilde{v}}{\partial x}(x,d_i), \tag{36}$$

$$\Delta\frac{\partial\tilde{u}^*}{\partial x}(x,c_j)=-\Delta\frac{\partial\tilde{u}}{\partial x}(x,c_j),\quad \Delta\frac{\partial\tilde{v}^*}{\partial x}(x,c_j)=-\Delta\frac{\partial\tilde{v}}{\partial x}(x,c_j), \tag{37}$$

and

$$\Delta\frac{\partial\tilde{u}^*}{\partial x}(x,0)=0,\quad \Delta\frac{\partial\tilde{v}^*}{\partial x}(x,0)=0. \tag{38}$$

i.e. the displacement gradient jump due to the correction field must be equal and opposite to the displacement gradient jump due to the dislocation field, given by Eqs. (17)–(20).

Each layer has four constants A, B, C and D associated with it. Hence, there are a total of $4(m+n)$ constants to be determined. The interface conditions provide a total of $4(m+n-1)$ equations and the remaining four equations are supplied by the far-field boundary conditions, i.e. $\sigma^*_{xy}(x,y\to\pm\infty)=0$ and $\sigma^*_{yy}(x,y\to\pm\infty)=0$. To make the presentation of these equations more manageable, the effects of b_x and b_y are considered separately and the equations are presented in Appendix A.

5. Validation of the dislocation solution

The problem of an edge dislocation in an elastic layer bonded to a half-space has been considered previously by several researchers (Savage, 1998; Kelly et al. 1995; Comninou and Dundurs, 1983; Lee and Dundurs, 1973). As a verification example, we consider the particular case when the edge dislocation lies at the interface between the elastic layer and the half-plane and compare the obtained result for corrective tractions along the interface to those obtained using the solution of Kelly et al. (1995). The corrective tractions along the interface can be obtained by letting $y=0$ in Eqs. (27) and (28)

$$\sigma^*_{yy}(x,0)=-b_x\int_0^\infty(A_x^1+C_x^1)\cos(\xi x)d\xi-b_y\int_0^\infty(A_y^1+C_y^1)\sin(\xi x)d\xi, \tag{39}$$

$$\sigma^*_{xy}(x,0)=b_x\int_0^\infty(-A_x^1+B_x^1+C_x^1+D_x^1)\sin(\xi x)d\xi-b_y\int_0^\infty(-A_y^1+B_y^1+C_y^1+D_y^1)\cos(\xi x)d\xi. \tag{40}$$

The Fourier integrals in Eqs. (39) and (40) are evaluated numerically by truncating the upper limit of the integrals to $\xi=\xi^*$. The unknown constants in these integrals are obtained by setting $d_1=h$, $c_1\to\infty$ and $\mu_2/\mu_1\to 0$ (see Fig. 1) and then solving the system of linear equations given in Appendix A at each value of ξ. The corresponding results for corrective tractions based on the solution of Kelly et al. (1995) can be obtained by setting $d=0$ and $y=0$ in Eq. B1 of the original paper and then following the procedure described in the paper. The corrective tractions at the interface obtained using the two methods are compared in Fig. 3 and an excellent agreement is observed. This implies that the general solution obtained in the present work correctly recovers the simpler case considered previously. Further validation is also conducted in Section 6.3.

6. Interfacial crack in an arbitrarily layered medium

The obtained solution for an interfacial edge dislocation can be utilized to solve a variety of crack problems in an arbitrarily layered composite using the framework of the distributed dislocation technique. As an example, the problem of an interfacial crack with oscillatory singularity is considered.

6.1. Main definitions

For an interfacial crack of length $2a$, the complex stress intensity factor K can be defined as (Rice, 1988)

$$K=K_1+\mathrm{i}K_2=\lim_{r\to 0}\left\{r^{+\mathrm{i}\varepsilon}\sqrt{2\pi r}[\sigma_{yy}(r)+\mathrm{i}\sigma_{xy}(r)]\right\}, \tag{41}$$

where r is the distance ahead of the crack tip and ε is the oscillatory index defined as

$$\varepsilon=\frac{1}{2\pi}\log\left(\frac{1+\beta}{1-\beta}\right). \tag{42}$$

The right hand crack tip, located at $x=a$, will be considered hereafter for definiteness. The local $r-\theta$ coordinate system under consideration has its origin at $x=a, y=0$. The crack tip stresses, the relative displacement of the crack faces and the displacement gradients in the K-dominance zone are as follows (Hills et al., 1996):

$$\sigma_{yy}(r)+\mathrm{i}\sigma_{xy}(r)=\frac{K}{\sqrt{2\pi r}}r^{-\mathrm{i}\varepsilon}, \tag{43}$$

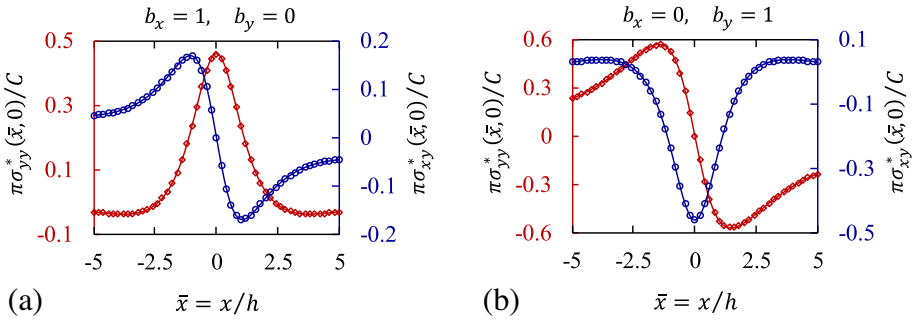

Fig. 3. The numerical results for the corrective tractions along the interface for the case of (a) a glide dislocation, and (b) a climb dislocation. The solid lines correspond to the proposed solution and the dotted lines correspond to the solution obtained by Kelly et al. (1995). The calculations were performed for obtained for $\alpha = 0.8$, $\beta = 0.2$ and $h = 1$.

$$\delta_x(r) + \mathrm{i}\delta_y(r) = \{u(r,+\pi) - u(r,-\pi)\} + \mathrm{i}\{v(r,+\pi) - v(r,-\pi)\} = K\sqrt{\frac{2r}{\pi}}\frac{r^{-\mathrm{i}\varepsilon}}{(1-2\mathrm{i}\varepsilon)C\sqrt{1-\beta^2}}, \tag{44}$$

$$B(r) = B_x(r) + \mathrm{i}B_y(r) = \frac{\partial}{\partial r}[\delta_x(r) + \mathrm{i}\delta_y(r)] = \mathrm{i}\frac{\bar{K}}{\sqrt{2\pi r}}\frac{r^{+\mathrm{i}\varepsilon}}{C\sqrt{1-\beta^2}}, \tag{45}$$

where $\bar{K}$ is the complex conjugate of K and C is the effective bimaterial modulus, defined as

$$C = \frac{2\mu_1}{(\kappa_1+1)}\frac{1-\alpha}{1-\beta^2} = \frac{2\mu_{-1}}{(\kappa_{-1}+1)}\frac{1+\alpha}{1-\beta^2}. \tag{46}$$

For interfacial cracks, the quantity that is physically more important is the strain energy release rate G, which is related to the absolute value of the complex stress intensity factor, $|K| = K\bar{K}$, as

$$G = \frac{|K|}{4C}. \tag{47}$$

The energy release rate, G is uninfluenced by oscillatory character of the solution and the crack-face interpenetration implied by the open model, if the zone of interpenetration is fully encapsulated within the zone of K dominance. It is convenient to normalize G by the known result for a crack at the bimaterial interface between two elastic half-planes, subjected to uniform remote loading (Rice and Sih, 1965)

$$K_b = (\sigma^\infty_{yy} + \mathrm{i}\sigma^\infty_{xy})(1-2\mathrm{i}\varepsilon)\sqrt{\pi a}(2a)^{+\mathrm{i}\varepsilon}. \tag{48}$$

Denoting the corresponding energy release rate by G_b, the normalized energy release rate can be written as

$$\hat{G} = \frac{G}{G_b} = \frac{K\bar{K}}{(1+4\varepsilon^2)(\pi a)(\sigma^{\infty 2}_{yy} + \sigma^{\infty 2}_{xy})}. \tag{49}$$

6.2. Governing singular integral equations

We assume that the loading is predominantly tensile, so that any stress oscillations or material interpenetration are confined to a region very close to the crack tips, and the open crack formulation can be implemented. If the crack faces are open at all points, the tractions must vanish along the entire crack, and the governing integral equations are (Hills et al., 1996; Erdogan et al., 1973)

$$-\frac{\pi}{C}\breve{\sigma}_{yy}(x) = -\beta\pi B_x(x) + \int_{-a}^{+a}\frac{B_y(\lambda)}{x-\lambda}d\lambda + \int_{-a}^{+a}[B_x(\lambda)K_{xyy}(x,\lambda) + B_y(\lambda)K_{yyy}(x,\lambda)]d\lambda, \quad |x| < a, \tag{50}$$

$$-\frac{\pi}{C}\breve{\sigma}_{xy}(x) = +\beta\pi B_y(x) + \int_{-a}^{+a}\frac{B_x(\lambda)}{x-\lambda}d\lambda + \int_{-a}^{+a}[B_x(\lambda)K_{xxy}(x,\lambda) + B_y(\lambda)K_{yxy}(x,\lambda)]d\lambda, \quad |x| < a, \tag{51}$$

where $\breve{\sigma}_{yy}(x)$ and $\breve{\sigma}_{xy}(x)$ are the normal and shear stresses at the crack location in the absence of the crack. The kernels $K_{ijk}(x,\lambda)$ are regular bounded functions describing the influence of the layered structure, and can be obtained from Eqs. (39) and (40) as

$$K_{xyy}(x,\lambda) = -\frac{\pi}{C}\int_0^\infty (A^1_x + C^1_x)\cos[\xi(x-\lambda)]d\xi, \tag{52}$$

$$K_{yyy}(x,\lambda) = -\frac{\pi}{C}\int_0^\infty (A^1_y + C^1_y)\sin[\xi(x-\lambda)]d\xi, \tag{53}$$

$$K_{xxy}(x,\lambda) = \frac{\pi}{C}\int_0^\infty (-A^1_x + B^1_x + C^1_x + D^1_x)\sin[\xi(x-\lambda)]d\xi, \tag{54}$$

$$K_{yxy}(x,\lambda) = -\frac{\pi}{C}\int_0^\infty (-A^1_y + B^1_y + C^1_y + D^1_y)\cos[\xi(x-\lambda)]d\xi. \tag{55}$$

The governing equations, Eqs. (50) and (51), can be normalized by setting $s = \lambda/a$ and $t = x/a$ and combined into one single complex equation as follows:

$$F(t) = -\beta B(t) - \frac{\mathrm{i}}{\pi}\int_{-1}^{+1}\frac{B(s)}{t-s}ds + \int_{-1}^{1}[B(s)K'_1(t,s) + \overline{B(s)}K'_2(t,s)]ds, \tag{56}$$

where,

$$F(t) = -\frac{1}{C}[\breve{\sigma}_{yy}(t) - \mathrm{i}\breve{\sigma}_{xy}(t)], \tag{57}$$

$$B(t) = B_x(t) + \mathrm{i}B_y(t), \tag{58}$$

and

$$K'_1(t,s) = \frac{a}{2\pi}\{(K'_{xyy} - K'_{yxy}) - \mathrm{i}(K'_{yyy} + K'_{xxy})\}, \tag{59}$$

$$K'_2(t,s) = \frac{a}{2\pi}\{(K'_{xyy} + K'_{yxy}) + \mathrm{i}(K'_{yyy} - K'_{xxy})\}. \tag{60}$$

The over-bar denotes the complex conjugate, i.e. $\overline{B(s)} = B_x(s) - \mathrm{i}B_y(s)$. The crack must have no net dislocation content, i.e. the crack faces must physically come together at both ends. This condition requires that

$$\int_{-1}^{+1} B(s)ds = 0. \tag{61}$$

The solution for the complex dislocation density function, $B(x)$, can be obtained by solving the governing Eq. (56) subject to the uniqueness condition (61). Here, the method for solving integral equations of second kind given by Erdogan et al. (1973) is used.

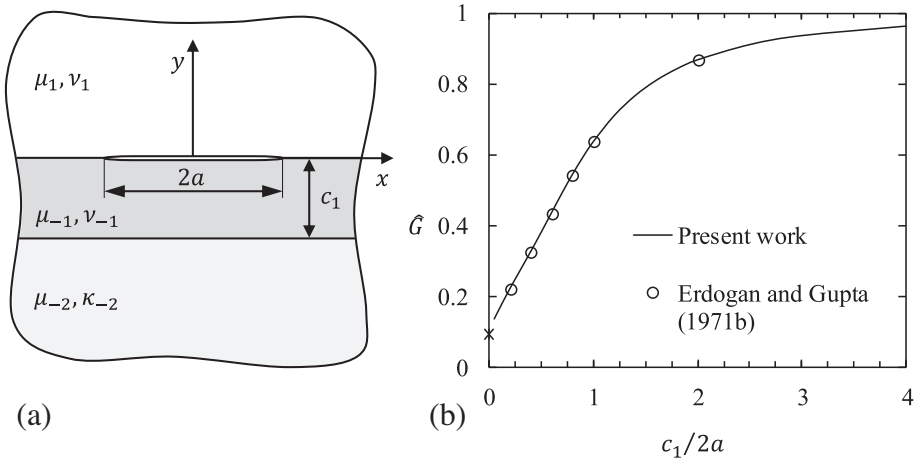

Fig. 4. (a) Interfacial crack in a layer-substrate sandwich, and (b) Normalized energy release rate vs. normalized layer thickness for Aluminum–Epoxy–Aluminum composite. The cross symbol represents theoretical bound for $c_1/2a \to 0$.

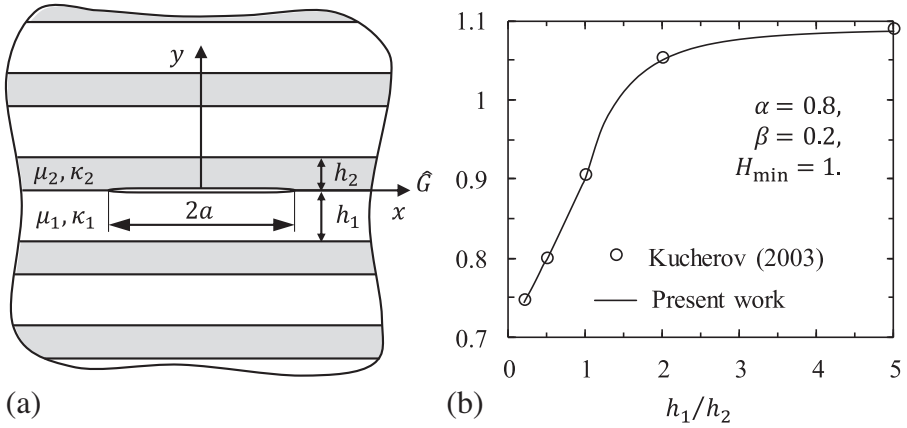

Fig. 5. (a) Interfacial crack in periodic bimaterial medium, and (b) Normalized energy release rate vs. layer thickness ratio.

An alternative method, as discussed by Ma and Korsunsky (2004) can also be implemented. Once the solution for $B(x)$ is known, the complex stress intensity factor and energy release rate can be determined in terms of the obtained solution for the dislocation density function.

6.3. Verification examples

The edge dislocation solution obtained in the present work is applied to some previously considered plane strain problems of an interfacial crack in multi-layered media. The first of these is a composite medium comprising of a single layer bounded by two half-spaces and with crack along one of the two bimaterial interfaces (Fig. 4a). This problem was solved previously by Erdogan and Gupta (1971b), also using the method described in Section 6.2, however using a different dislocation solution. Fig. 4b shows the numerical results for the normalized energy release rate, $\hat{G}$ as a function of the normalized layer thickness, $c_1/2a$. The results are evaluated for an Aluminum–Epoxy–Aluminum composite, i.e. $\mu_1 = \mu_{-2} = 26.52$ GPa, $\mu_{-1} = 1.15$ GPa, $\nu_1 = \nu_{-2} = 0.3$ and $\nu_{-1} = 0.35$. The results obtained by Erdogan and Gupta (1971b) were retrieved from Table 3 of the latter paper.

The second problem involves an interfacial crack in a composite medium comprising of alternating layers of two materials (Fig. 5a). This problem was considered more recently by Kucherov and Ryvkin (2002) and Kucherov (2003). The numerical results for the normalized energy release rate, $\hat{G}$, as a function of the layer thickness ratio, h_1/h_2, are shown in Fig. 5b. The results are evaluated for Dundur's parameters, $\alpha = 0.8$ and $\beta = 0.2$ and $H_{\min} = \min\{h_1/2a, h_2/2a\} = 1$. The corresponding results were retrieved from Fig. 5.4 of Kucherov (2003).

For both crack problems, there is close agreement between the numerical results obtained using the present dislocation solution and the numerical results obtained in previous studies using a different approach. This serves as an indirect validation of the obtained edge dislocation solution and also demonstrates the application of the solution to crack problems.

7. Concluding Remarks

In this paper, we consider a general multi-layered composite, composed of perfectly bonded isotropic elastic layers, and present the solution for the elastic field induced by an interfacial edge dislocation. Composite structures with a finite number of layers can be modeled by setting the shear modulus of elasticity of the top and bottom layers to a very small value approaching zero, while the embedded dislocation corresponds to the case when $\mu_{-1} = \mu_1$ and $\nu_{-1} = \nu_1$. The obtained solution for an interfacial edge dislocation in a multi-layered medium can be used in conjunction with the distributed dislocation technique (DDT) to solve crack problems involving multiple interacting cracks in a multi-layered medium, with no restriction on the crack orientation, position and loading. Several validation examples are included to demonstrate the accuracy of the obtained solution.

Appendix A. Equations of compatibility and equilibrium at the interfaces

Case 1: $b_x = 1$, $b_y = 0$.

The system of four equations associated with an interface located at $y = d_i$ is given by

$$(A_x^i + \xi d_i B_x^i)e^{-\xi d_i} + (C_x^i + \xi d_i D_x^i)e^{\xi d_i} - (A_x^{i+1} + \xi d_i B_x^{i+1})e^{-\xi d_i} - (C_x^{i+1} + \xi d_i D_x^{i+1})e^{\xi d_i} = 0, \tag{A.1}$$

$$-(-A_x^i + (1-\xi d_i)B_x^i)e^{-\xi d_i} - (C_x^i + (1+\xi d_i)D_x^i)e^{\xi d_i} + (-A_x^{i+1} + (1-\xi d_i)B_x^{i+1})e^{-\xi d_i} + (C_x^{i+1} + (1+\xi d_i)D_x^{i+1})e^{\xi d_i} = 0, \tag{A.2}$$

$$-\frac{1}{2\mu_i}\left(A_x^i + \left(\xi d_i - \frac{\kappa_i+1}{2}\right)B_x^i\right)e^{-\xi d_i} - \frac{1}{2\mu_i}\left(C_x^i + (\xi d_i + \frac{\kappa_i+1}{2})D_x^i\right)e^{\xi d_i} + \frac{1}{2\mu_{i+1}}\left(A_x^{i+1} + \left(\xi d_i - \frac{\kappa_{i+1}+1}{2}\right)B_x^{i+1}\right)e^{-\xi d_i} + \frac{1}{2\mu_{i+1}}\left(C_x^{i+1} + \left(\xi d_i + \frac{\kappa_{i+1}+1}{2}\right)D_x^{i+1}\right)e^{\xi d_i} = -\Delta\frac{\partial\tilde{u}}{\partial x}(x, d_i), \tag{A.3}$$

and

$$-\frac{1}{2\mu_i}\left(-A_x^i + \left(1 - \xi d_i - \frac{\kappa_i+1}{2}\right)B_x^i\right)e^{-\xi d_i} - \frac{1}{2\mu_i}\left(C_x^i + \left(1 + \xi d_i - \frac{\kappa_i+1}{2}\right)D_x^i\right)e^{\xi d_i} + \frac{1}{2\mu_{i+1}}\left(-A_x^{i+1} + \left(1 - \xi d_i - \frac{\kappa_{i+1}+1}{2}\right)B_x^{i+1}\right)e^{-\xi d_i} + \frac{1}{2\mu_{i+1}}\left(C_x^{i+1} + \left(1 + \xi d_i - \frac{\kappa_{i+1}+1}{2}\right)D_x^{i+1}\right)e^{\xi d_i} = -\Delta\frac{\partial\tilde{v}}{\partial x}(x, d_i). \tag{A.4}$$

where $i = 1, \ldots, n-1$. The right hand side of Eqs. (A3) and (A4) can be evaluated by taking the appropriate Fourier transforms of Eqs. (17) and (18), respectively. For $b_x = 1$ and $b_y = 0$,

$$\Delta\frac{\partial\tilde{u}}{\partial x}(x, d_i) = \frac{2}{\pi}\int_0^\infty \Delta\frac{\partial u}{\partial x}(x, d_i)\cos(\xi x)dx = \frac{1}{\pi}\left[-\left(\frac{\kappa_{i+1}\Gamma_1 + \Gamma_{-1}}{2\mu_{i+1}} - \frac{\kappa_i\Gamma_1 + \Gamma_{-1}}{2\mu_i}\right) + 2\left(\frac{\Gamma_1}{2\mu_{i+1}} - \frac{\Gamma_1}{2\mu_i}\right)\xi d_i\right]e^{-\xi d_i}, \tag{A.5}$$

And

$$\Delta\frac{\partial\tilde{v}}{\partial x}(x, d_i) = \frac{2}{\pi}\int_0^\infty \Delta\frac{\partial u}{\partial x}(x, d_i)\sin(\xi x)dx = -\frac{1}{\pi}\left[\left(\frac{\kappa_{i+1}\Gamma_1 - \Gamma_{-1}}{2\mu_{i+1}} - \frac{\kappa_i\Gamma_1 - \Gamma_{-1}}{2\mu_i}\right) + 2\left(\frac{\Gamma_1}{2\mu_{i+1}} - \frac{\Gamma_{-1}}{2\mu_i}\right)\xi d_i\right]e^{-\xi d_i} \tag{A.6}$$

Similarly, the system of four equations associated with an interface located at $y = -c_j$ is given by

$$\left(A_x^{-(j+1)} - \xi c_j B_x^{-(j+1)}\right)e^{\xi c_j} + \left(C_x^{-(j+1)} - \xi c_j D_x^{-(j+1)}\right)e^{-\xi c_j} - \left(A_x^{-j} - \xi c_j B_x^{-j}\right)e^{\xi c_j} - \left(C_x^{-j} - \xi c_j D_x^{-j}\right)e^{-\xi c_j} = 0, \tag{A.7}$$

$$-\left(-A_x^{-(j+1)} + (1+\xi c_j)B_x^{-(j+1)}\right)e^{\xi c_j} - \left(C_x^{-(j+1)} + (1-\xi c_j)D_x^{-(j+1)}\right)e^{-\xi c_j} + \left(-A_x^{-j} + (1+\xi c_j)B_x^{-j}\right)e^{\xi c_j} + \left(C_x^{-j} + (1-\xi c_j)D_x^{-j}\right)e^{-\xi c_j} = 0, \tag{A.8}$$

$$-\frac{1}{2\mu_{-(j+1)}}\left(A_x^{-(j+1)} + \left(-\xi c_j - \frac{\kappa_{-(j+1)}+1}{2}\right)B_x^{-(j+1)}\right)e^{\xi c_j} - \frac{1}{2\mu_{-(j+1)}}\left(C_x^{-(j+1)} + \left(-\xi c_j + \frac{\kappa_{-(j+1)}+1}{2}\right)D_x^{-(j+1)}\right)e^{-\xi c_j} + \frac{1}{2\mu_{-j}}\left(A_x^{-j} + \left(-\xi c_j - \frac{\kappa_{-j}+1}{2}\right)B_x^{-j}\right)e^{\xi c_j} + \frac{1}{2\mu_{-j}}\left(C_x^{-j} + \left(-\xi c_j + \frac{\kappa_{-j}+1}{2}\right)D_x^{-j}\right)e^{-\xi c_j} = -\Delta\frac{\partial\tilde{u}}{\partial x}(x, -c_j), \tag{A.9}$$

and

$$-\frac{1}{2\mu_{-(j+1)}}\left(-A_x^{-(j+1)} + \left(1 + \xi c_j - \frac{\kappa_{-(j+1)}+1}{2}\right)B_x^{-(j+1)}\right)e^{\xi c_j} - \frac{1}{2\mu_{-(j+1)}}\left(C_x^{-(j+1)} + \left(1 - \xi c_j - \frac{\kappa_{-(j+1)}+1}{2}\right)D_x^{-(j+1)}\right)e^{-\xi c_j} + \frac{1}{2\mu_{-j}}\left(-A_x^{-j} + \left(1 + \xi c_j - \frac{\kappa_{-j}+1}{2}\right)B_x^{-j}\right)e^{\xi c_j} + \frac{1}{2\mu_{-j}}\left(C_x^{-j} + \left(1 - \xi c_j - \frac{\kappa_{-j}+1}{2}\right)D_x^{-j}\right)e^{-\xi c_j} = -\Delta\frac{\partial\tilde{v}}{\partial x}(x, -c_j) \tag{A.10}$$

where $j = 1, \ldots, m-1$. The right hand side of Eqs. (A9) and (A10) can be evaluated by taking the appropriate Fourier transforms of Eqs. (19) and (20), respectively. For $b_x = 1$ and $b_y = 0$,

$$\Delta\frac{\partial\tilde{u}}{\partial x}(x, -c_j) = \frac{2}{\pi}\int_0^\infty \Delta\frac{\partial u}{\partial x}(x, -c_j)\cos(\xi x)dx = -\frac{1}{\pi}\left[-\left(\frac{\kappa_{-j}\Gamma_{-1} + \Gamma_1}{2\mu_{-j}} - \frac{\kappa_{-(j+1)}\Gamma_{-1} + \Gamma_1}{2\mu_{-(j+1)}}\right) + 2\left(\frac{\Gamma_{-1}}{2\mu_{-j}} - \frac{\Gamma_{-1}}{2\mu_{-(j+1)}}\right)\xi c_j\right]e^{-\xi c_j}, \tag{A.11}$$

and

$$\Delta\frac{\partial\tilde{v}}{\partial x}(x, -c_j) = \frac{2}{\pi}\int_0^\infty \Delta\frac{\partial u}{\partial x}(x, -c_j)\sin(\xi x)dx = -\frac{1}{\pi}\left[\left(\frac{\kappa_{-j}\Gamma_{-1} - \Gamma_1}{2\mu_{-j}} - \frac{\kappa_{-(j+1)}\Gamma_{-1} - \Gamma_1}{2\mu_{-(j+1)}}\right) + 2\left(\frac{\Gamma_{-1}}{2\mu_{-j}} - \frac{\Gamma_{-1}}{2\mu_{-(j+1)}}\right)\xi c_j\right]e^{-\xi c_j}. \tag{A.12}$$

The system of equations for the interface located along $y = 0$ are given by

$$A_x^{-1} + C_x^{-1} - A_x^1 - C_x^1 = 0, \tag{A.13}$$

$$A_x^{-1} - B_x^{-1} - C_x^{-1} - D_x^{-1} - A_x^1 + B_x^1 + C_x^1 + D_x^1 = 0, \tag{A.14}$$

$$-\frac{1}{2\mu_{-1}}\left(A_x^{-1} - \frac{\kappa_{-1}+1}{2}B_x^{-1}\right) - \frac{1}{2\mu_{-1}}\left(C_x^{-1} + \frac{\kappa_{-1}+1}{2}D_x^{-1}\right) + \frac{1}{2\mu_1}\left(A_x^1 - \frac{\kappa_1+1}{2}B_x^1\right) + \frac{1}{2\mu_1}\left(C_x^1 + \frac{\kappa_1+1}{2}D_x^1\right) = 0, \tag{A.15}$$

And

$$-\frac{1}{2\mu_{-1}}\left(-A_x^{-1} + \left(1 - \frac{\kappa_{-1}+1}{2}\right)B_x^{-1}\right) - \frac{1}{2\mu_{-1}}\left(C_x^{-1} + \left(1 - \frac{\kappa_{-1}+1}{2}\right)D_x^{-1}\right) + \frac{1}{2\mu_1}\left(-A_x^1 + \left(1 - \frac{\kappa_1+1}{2}\right)B_x^1\right) + \frac{1}{2\mu_1}\left(C_x^1 + \left(1 - \frac{\kappa_1+1}{2}\right)D_x^1\right) = 0. \tag{A.16}$$

Finally, the far-field boundary conditions, i.e. $\sigma_{xy}^*(x, y \to \pm\infty) = 0$ and $\sigma_{yy}^*(x, y \to \pm\infty) = 0$, imply that

$$C_x^n = 0, \quad D_x^n = 0, \tag{A.17}$$

$$A_x^{-m} = 0, \quad B_x^{-m} = 0. \tag{A.18}$$

For an arbitrary medium composed of $m+n$ layers, a system of $4(m+n)$ linear equation can be obtained from Eqs. (A1)–(A18). A global matrix can then be assembled in an appropriate manner to find the $4(m+n)$ unknown constants associated with an edge dislocation of strength $b_x = 1$ and $b_y = 0$.

Case 2: $b_x = 0$, $b_y = 1$.

The system of equations for this case take the exact same form as Case 1, except the constants A_x, B_x, C_x and D_x need to be replaced by A_y, B_y, C_y and D_y, respectively. Also, the right hand sides of Eqs. (A3), (A4), (A9) and (A10) need to be replaced by

$$\begin{aligned} -\Delta\frac{\partial \tilde{u}}{\partial x}(x,d_i) &= -\frac{2}{\pi}\int_0^\infty \Delta\frac{\partial u}{\partial x}(x,d_i)\sin(\xi x)dx \\ &= \frac{1}{\pi}\left[-\left(\frac{\kappa_{i+1}\Gamma_1-\Gamma_{-1}}{2\mu_{i+1}}-\frac{\kappa_i\Gamma_1-\Gamma_{-1}}{2\mu_i}\right)+2\left(\frac{\Gamma_1}{2\mu_{i+1}}-\frac{\Gamma_1}{2\mu_i}\right)\xi d_i\right]e^{-\xi d_i}, \end{aligned} \tag{A.19}$$

$$\begin{aligned} +\Delta\frac{\partial \tilde{v}}{\partial x}(x,d_i) &= \frac{2}{\pi}\int_0^\infty \Delta\frac{\partial u}{\partial x}(x,d_i)\cos(\xi x)dx \\ &= -\frac{1}{\pi}\left[\left(\frac{\kappa_{i+1}\Gamma_1+\Gamma_{-1}}{2\mu_{i+1}}-\frac{\kappa_i\Gamma_1+\Gamma_{-1}}{2\mu_i}\right)+2\left(\frac{\Gamma_1}{2\mu_{i+1}}-\frac{\Gamma_{-1}}{2\mu_i}\right)\xi d_i\right]e^{-\xi d_i}. \end{aligned} \tag{A.20}$$

$$\begin{aligned} -\Delta\frac{\partial \tilde{u}}{\partial x}(x,-c_j) &= -\frac{2}{\pi}\int_0^\infty \Delta\frac{\partial u}{\partial x}(x,-c_j)\sin(\xi x)dx \\ &= \frac{1}{\pi}\left[-\left(\frac{\kappa_{-j}\Gamma_{-1}-\Gamma_1}{2\mu_{-j}}-\frac{\kappa_{-(j+1)}\Gamma_{-1}-\Gamma_1}{2\mu_{-(j+1)}}\right)\right. \\ &\quad \left.+2\left(\frac{\Gamma_{-1}}{2\mu_{-j}}-\frac{\Gamma_{-1}}{2\mu_{-(j+1)}}\right)\xi c_j\right]e^{-\xi c_j}, \end{aligned} \tag{A.21}$$

and

$$\begin{aligned} +\Delta\frac{\partial \tilde{v}}{\partial x}(x,-c_j) &= \frac{2}{\pi}\int_0^\infty \Delta\frac{\partial u}{\partial x}(x,-c_j)\cos(\xi x)dx \\ &= \frac{1}{\pi}\left[\left(\frac{\kappa_{-j}\Gamma_{-1}+\Gamma_1}{2\mu_{-j}}-\frac{\kappa_{-(j+1)}\Gamma_{-1}+\Gamma_1}{2\mu_{-(j+1)}}\right)\right. \\ &\quad \left.+2\left(\frac{\Gamma_{-1}}{2\mu_{-j}}-\frac{\Gamma_{-1}}{2\mu_{-(j+1)}}\right)\xi c_j\right]e^{-\xi c_j}, \end{aligned} \tag{A.22}$$

respectively.

References

Bilby, B., Eshelby, J., 1968. Dislocations and the theory of fracture. In: Liebowitz, H. (Ed.), Fracture: An Advanced Treatise, vol. 1. Academic Press, New York (USA).

Bolotin, VV., 1996 (Delaminations in composite structures: its origin, buckling, growth and stability). Compos Part B - Eng 27 (2), 129–145. http://dx.doi.org/10.1016/1359-8368(95)00035-6.

Chen, L., Pindera, M.J., 2006. Plane Analysis of finite multilayered media with multiple aligned cracks - Part I: Theory. J. Appl. Mech. 74 (1), 128–143. http://dx.doi.org/10.1115/1.2201883.

Cleary M.P., 1978. Primary factors governing hydraulic fractures in heterogeneous stratified porous formations. No. UCRL-13884; CONF-781112-10. Massachusetts Inst. of Tech., Cambridge (USA).

Comninou, M., Dundurs, J., 1983. Partial closure of a crack at the interface between a layer and a half space. Eng. Fract. Mech. 18 (2), 315–323. http://dx.doi.org/10.1016/0013-7944(83)90142-X.

Cook, J., Gordon, J.E., Evans, C.C., Marsh, D.M., 1964. A Mechanism for the control of crack propagation in all-brittle systems. P Roy. Soc. London A - Mat. 282 (1391), 508–520. http://dx.doi.org/10.1098/rspa.1964.0248.

Daneshy, A.A., 1978. Hydraulic fracture propagation in layered formations. SPE J. 18 (1), 33–41. http://dx.doi.org/10.2118/6088-PA.

Erdogan, F., Gupta, G., 1971a. The stress analysis of multi-layered composites with a flaw. Int. J. Solids Struct. 7 (1), 39–61. http://dx.doi.org/10.1016/0020-7683(71)90017-5.

Erdogan, F., Gupta, G.D., 1971b. Layered composites with an interface flaw. Int. J. Solids Struct. 7 (8), 1089–1107. http://dx.doi.org/10.1016/0020-7683(71)90082-5.

Erdogan, F., 1972. Fracture problems in composite materials. Eng. Fract. Mech. 4 (4), 811–840. http://dx.doi.org/10.1016/0013-7944(72)90018-5.

Erdogan, F., Gupta, G.D., Cook, T.S., 1973. Numerical solution of singular integral equations. In: Sih, G.C. (Ed.), Mechanics of Fracture, vol. 1. Noordhoff International Publishing, Leyden (The Netherlands).

Fleck, N.A., Hutchinson, J.W., Suo, Z., 1991. Crack path selection in a brittle adhesive layer. Int. J. Solids Struct. 27 (13), 1683–1703. http://dx.doi.org/10.1016/0020-7683(91)90069-R.

Gao, H., Ji, B., Jäger, I.L., Arzt, E., Fratzl, P., 2003. Materials become insensitive to flaws at nanoscale: Lessons from nature. Proc. Natl. Acad. Sci. USA 100 (10), 5597–5600. http://dx.doi.org/10.1073/pnas.0631609100.

Garg, A.C., 1988. Delamination - a damage mode in composite structures. Eng. Fract. Mech. 29 (5), 557–584. http://dx.doi.org/10.1016/0013-7944(88)90181-6.

Gudmundsson, A., Simmenes, T.H., Larsen, B., Philipp, S.L., 2010. Effects of internal structure and local stresses on fracture propagation, deflection, and arrest in fault zones. J. Struct. Geol. 32, 1643–1655. http://dx.doi.org/10.1016/j.jsg.2009.08.013.

Gupta, V., Argon, A.S., Suo, Z., 1992. Crack Deflection at an Interface Between Two Orthotopic Media. J. Appl. Mech. 59 (2S), S79–S87. http://dx.doi.org/10.1115/1.2899511.

He, M.-Y., Hutchinson, J.W., 1989. Crack deflection at an interface between dissimilar elastic materials. Int. J. Solids Struct. 25 (9), 1053–1067. http://dx.doi.org/10.1016/0020-7683(89)90021-8.

Hills, D.A., Kelly, P.A., Dai, D.N., Korsunsky, A.M., 1996. Solution of Crack Problems: The Distributed Dislocation Technique. Kluwer Academic Publishers, Dordrecht (The Netherlands).

Holleck, H., Lahres, M., Woll, P., 1990. Multilayer coatings – influence of fabrication parameters on constitution and properties. Surf. Coat. Technol. 41, 179–190. http://dx.doi.org/10.1016/0257-8972(90)90166-A.

Hui, C.-Y., Lagoudas, D.C., 1990. Stress Fields of Interface Dislocations. J. Appl. Mech. 57 (1), 247–248. http://dx.doi.org/10.1115/1.2888311.

Kelly, P.A., O'Connor, J.J., Hills, D.A., 1995. Stress field due to a dislocation in layered media. J. Phys. D – Appl. Phys. 28 (3), 530–534. http://dx.doi.org/10.1088/0022-3727/28/3/013.

Khanna, A., Kotousov, A., 2014. Stress analysis of a crack in a fiber-reinforced layered composite. Compos. Struct. 118, 139–148. http://dx.doi.org/10.1016/j.compstruct.2014.07.024.

Khanna, A., Kotousov, A., 2015. Controlling the height of multiple hydraulic fractures in layered media. SPE J. http://dx.doi.org/10.2118/176017-PA.

Kucherov L., 2003. Delamination in periodically layered bi-material composites (PhD Thesis), Tel Aviv University, Israel.

Kucherov, L., Ryvkin, M., 2002. Interface crack in periodically layered bimaterial composite. Int. J. Fract. 117 (2), 175–194. http://dx.doi.org/10.1023/A:1020914902780.

Kuo, C.-H., 2014. Elastic field due to an edge dislocation in a multi-layered composite. Int. J. Solids Struct. 51, 1421–1433. http://dx.doi.org/10.1016/j.ijsolstr.2013.12.032.

Lee, M.-S., Dundurs, J., 1973. Edge dislocation in a surface layer. Int. J. Eng. Sci. 11 (1), 87–94. http://dx.doi.org/10.1016/0020-7225(73)90071-2.

Li, J., 2000. Debonding of the interface as 'crack arrestor'. Int. J. Fract. 105 (1), 57–79. http://dx.doi.org/10.1023/A:1007603809972.

Ma, L., Korsunsky, A.M., 2004. A note on the Gauss–Jacobi quadrature formulae for singular integral equations of the second kind. Int. J. Fract. 126 (4), 399–405. http://dx.doi.org/10.1023/B:FRAC.0000031158.62052.3c.

Misra, A., Verdier, M., Lu, Y.C., Kung, E., Mitchell, T.E., Nastasi, M., Embury, J.D., 1998. Structure and mechanical properties of Cu–X (X = Nb, Cr, Ni) nanolayered composites. Scr. Mater. 39, 555–560. http://dx.doi.org/10.1016/S1359-6462(98)00196-1.

Misra, A., Kung, H., 2001. Deformation behaviour of nanostructured metallic multilayers. Adv. Eng. Mater. 3, 217–222. http://dx.doi.org/10.1002/1527-2648(200104)3:4<217::AID-ADEM217>3.0.CO;2-5.

Muskhelishvili, N.L., 1958. Some Basic Problems of Mathematical Theory of Elasticity. P. Noordhoff, Groningen (The Netherlands).

Nix, W.D., 1998. Yielding and strain hardening of thin metal films on substrates. Scr. Mater. 39, 545–554. http://dx.doi.org/10.1016/S1359-6462(98)00195-X.

Okumura, K., de Gennes, P.-G., 2001. Why is nacre strong? Elastic theory and fracture mechanics for biocomposites with stratified structures. Eur. Phys. J. E 4 (1), 121–127. http://dx.doi.org/10.1007/s101890170150.

Rice, J.R., Sih, G.C., 1965. Plane problems of cracks in dissimilar media. J. Appl. Mech. 32 (2), 418–423. http://dx.doi.org/10.1115/1.3625816.

Rice, J.R., 1988. Elastic fracture mechanics concepts for interfacial cracks. J. Appl. Mech. 55 (1), 98–103. http://dx.doi.org/10.1115/1.3173668.

Roeder, B.A., Sun, C.T., 2001. Dynamic penetration of Alumina/aluminium laminates: experiments and modelling. Int. J. Impact Eng. 25 (2), 169–185. http://dx.doi.org/10.1016/S0734-743X(00)00031-2.

Sackman, J.L., Kelly, J.M., Javid, A.E., 1989. A layered notch filter for high-frequency dynamic isolation. J. Press. Vessel Technol. 111 (1), 17–24. http://dx.doi.org/10.1115/1.3265634.

Savage, J.C., 1998. Displacement field for an edge dislocation in a layered half-space. J. Geophys. Res. 103 (B2), 2439–2446. http://dx.doi.org/10.1029/97JB02562.

Selvadurai, A.P.S., 2000. Partial Differential Equations in Mechanics 2: The Biharmonic Equation, Poisson's Equation. Springer.
Sellinger, I., Weiss, P.M., Nguyen, A., Lu, Y., Assink, R.A., Gong, W., Brinker, C.J., 1998. Continuous self-assembly of organic–inorganic nanocomposite coatings that mimic nacre. Nature 394, 256–260. http://dx.doi.org/10.1038/28354.
Suo, Z., Hutchinson, J.W., 1990. Interface crack between two elastic layers. Int. J. Fract. 43 (1), 1–18. http://dx.doi.org/10.1007/BF00018123.
Zhang, T.-Y., Li, J.C.M., 1992. Interaction of an edge dislocation with an interfacial crack. J. Appl. Phys. 72 (6), 2215–2226. http://dx.doi.org/10.1063/1.351614.

Chapter 4

Stress analysis of a crack in a fiber-reinforced layered composite

Statement of Authorship

Title of Paper	Stress analysis of a crack in a fiber-reinforced layered composite
Publication Status	☑ Published ☐ Accepted for Publication ☐ Submitted for Publication ☐ Unpublished and Unsubmitted work written in manuscript style
Publication Details	Composite structures, 188, 139-148, doi: 10.1016/j.compstruct.2014.07.024 Submitted: 22 Apr 2014, Submitted in revised form: 14 Jul 2014, Accepted: 17 July 2014

Principal Author

Name of Principal Author (Candidate)	Aditya Khanna		
Contribution to the Paper	Performed all analyses and wrote manuscript.		
Overall percentage (%)	80		
Certification:	This paper reports on original research I conducted during the period of my Higher Degree by Research candidature and is not subject to any obligations or contractual agreements with a third party that would constrain its inclusion in this thesis. I am the primary author of this paper.		
Signature		Date	10/04/2016

Co-Author Contributions

By signing the Statement of Authorship, each author certifies that:

i. the candidate's stated contribution to the publication is accurate (as detailed above);

ii. permission is granted for the candidate in include the publication in the thesis; and

iii. the sum of all co-author contributions is equal to 100% less the candidate's stated contribution.

Name of Co-Author	Andrei Kotousov		
Contribution to the Paper	Supervised the development of the theoretical models and assisted in the preparation of the manuscript.		
Overall percentage (%)	20		
Signature		Date	10/04/2016

Composite Structures 118 (2014) 139–148

Contents lists available at ScienceDirect

Composite Structures

journal homepage: www.elsevier.com/locate/compstruct

Stress analysis of a crack in a fiber-reinforced layered composite

Aditya Khanna *, Andrei Kotousov

School of Mechanical Engineering, The University of Adelaide, Adelaide, SA 5005, Australia

ARTICLE INFO

Article history:
Available online 27 July 2014

Keywords:
Bonded ceramic
Fiber reinforced matrix
Distributed dislocation technique

ABSTRACT

Brittle matrix composites such as fiber-reinforced cements and ceramics are often bonded to dissimilar materials such as metals or other ceramics. The mismatch in elastic properties can affect the growth of matrix cracks located near the bonded interface. In this paper, a bonded system comprising of an elastic layer sandwiched between two identical elastic half-spaces is considered. A mathematical model is developed based on the distributed dislocation technique, for the analysis of a bridged straight crack embedded in the elastic layer. The bridging tractions are considered to be dependent on the crack opening displacement. The stress field is assumed to be plane stress or plane strain and all three-dimensional effects are disregarded.

The numerical results include the critical stress required to initiate failure of the matrix and the failure of fibers bridging the crack. The dependencies of these critical values upon the thickness of the composite layer as well as the mismatch in elastic properties are presented in dimensionless form. The results can be used to estimate the residual strength of bonded composites with a flaw near the material interface.

1. Introduction

The problem of crack bridging by reinforcements has been treated extensively in the literature over the past fifty years. There are several practical contexts where the residual strength of a component is controlled by a reinforced macro-crack. The reinforcements can be attributed, as in the present case, to fibers in a brittle-matrix composite [1,2] or they can be externally applied, as in the case of adhesively bonded patches often utilized to repair damaged composite plate or shell structures [3–5]. The bridging reinforcement obstructs the opening of the crack and hence, leads to a reduction in the stress intensity factors at the crack tips restricting the crack growth and reducing the risk of failure of the structural components [6]. The analytical procedure for evaluating the stress intensity factor associated with the bridging reinforcement involves the application of a displacement-dependent traction constraint over the crack faces and solving the resultant integral equation for crack opening [7].

There are several studies characterizing the failure mechanics of reinforced brittle matrix composites containing pre-existing cracks [8–11]. The problems addressed in these studies involve cracks in a homogenous material. However, brittle matrix composites such as fiber-reinforced cements and ceramics are often bonded to dissimilar materials such as metals or other ceramics [12,13]. The mismatch in elastic properties can affect the growth of cracks located at or near the bonded interface. To obtain the solution to such problems, one can readily adapt or extend the existing solutions to crack problems in composite materials without fiber reinforcement (see for e.g. Chen and Sih [14], Erdogan [15] and Hills et al. [16]). The system of governing singular integral equations needs be modified to incorporate the traction on the crack faces due to reinforcement. Such an approach has been utilized previously to solve the problem of a fiber-reinforced slant crack located near a free surface [17] and the problem of a fiber-reinforced interfacial crack in a bi-material composite [18].

In the present work a different problem is considered, which is a bonded system comprising of an elastic layer sandwiched between two identical half-spaces. Stress analysis is conducted for a straight crack embedded in the composite layer and located perpendicular to the material interfaces. A number of governing dimensionless parameters are identified in order to establish the effect of (1) the distance of the crack tips from the material interfaces, and (2) the mismatch in elastic properties on the stress intensity factor. The developed method based on the distributed dislocation technique, is extended to two other related problems which are solved in the Appendices. The first is the stress analysis of a crack in an aircraft panel repaired by a composite patch and the second problem involves a crack in a bonded ceramic lying perpendicular to a bi-material interface.

* Corresponding author. Tel.: +61 8 8313 6385.
E-mail addresses: aditya.khanna@adelaide.edu.au (A. Khanna), andrei.kotousov@adelaide.edu.au (A. Kotousov).

http://dx.doi.org/10.1016/j.compstruct.2014.07.024
0263-8223/

Nomenclature

Symbol	description (Dimensions)
x	co-ordinate along the length of the crack [L]
y	co-ordinate perpendicular to the crack [L]
$2a$	length of the crack [L]
$2h$	width of the elastic layer containing the crack [L]
μ	shear modulus [$ML^{-1}T^{-2}$]
κ	Kolosov's constant [–]
$\sigma_{xx},\sigma_{xy},\sigma_{yy}$	the stresses in the composite at a point (x,y) [$ML^{-1}T^{-2}$]
$u_y(x,0^+)$	displacement of the positive crack face in the y-direction [L]
$\delta(x)$	crack opening displacement [L]
f	volume fraction of the bridging fibers [–]
S	strength of individual fibers [$ML^{-1}T^{-2}$]
R	radius of individual fibers [L]
τ	frictional stress at the fiber/matrix interface [$ML^{-1}T^{-2}$]
η	micro-mechanical constant [$ML^{-3/2}T^{-2}$]
$\sigma_f(x)$	average stress in the bridging fibers along the crack [$ML^{-1}T^{-2}$]
$p(x)$	bridging traction due to the fibers [$ML^{-1}T^{-2}$]
σ_∞	remote tensile load opening the crack [$ML^{-1}T^{-2}$]
σ_{ult}	bridging traction required to initiate fiber failure [$ML^{-1}T^{-2}$]
u_{ult}	crack face displacement required to initiate fiber failure [L]
$b_y(x)$	distributed dislocation density [–]
t	dummy integration variable along the crack length [L]
$G^{(2)}_{yyy}$	dislocation influence function [L^{-1}]

Dimensionless parameters

α,β	Dundur's parameters
X	normalized co-ordinate along crack length
Σ_∞	normalized remote tensile load
$\Sigma_{yy}(X,0)$	normalized bridging traction along the crack
Σ_k	value of Σ_∞ required to initiate matrix cracking
Σ_s	value of Σ_∞ required to initiate fiber failure
A	normalized crack length
H	normalized width of elastic layer
$U(X)$	normalized crack face displacement
$B_y(X)$	normalized distributed dislocation density
K_N	normalized stress intensity factor

Subscripts

1	region outside the elastic layer, i.e. $x < -h$, $x > h$
2	region inside the elastic layer, i.e. $\|x\| < h$

Superscripts

(1)	region 1, located along $x < -h$
(2)	region 2, located along $\|x\| < h$
(3)	region 3, located along $x > h$

2. Problem formulation

Consider the bonded structure shown in Fig. 1. The problem is 2D and all three-dimensional effects are disregarded, such as, the corner (vertex) singularity [19], scale effect [20] and variation of the stress intensity factor across the crack front [21]. Only Mode I loading of the crack is considered. The elastic layer of thickness $2h$ contains a straight crack of length $2a < 2h$ and the crack lies perpendicular to the material interface. The half-planes occupy region 1 ($x < -h$) and region 3 ($x > h$) and have identical elastic constants, denoted by κ_1 and μ_1. The elastic layer, which contains the crack, occupies region 2 ($|x| < h$) and described by elastic constants denoted as κ_2 and μ_2. Here κ is the Kolosov's constant and μ is the shear modulus of the material. The composite material is uniformly loaded perpendicular to the crack faces, such that

$$\sigma_{xx} = \sigma_{xy} = 0, \quad x^2 + y^2 \to \infty \tag{1a}$$

$$\sigma^{(2)}_{yy} = \sigma_\infty, \quad x^2 + y^2 \to \infty \tag{1b}$$

$$\sigma^{(1)}_{yy} = \sigma^{(3)}_{yy} = \sigma_\infty \frac{\mu_1}{\mu_2}\frac{(\kappa_2+1)}{(\kappa_1+1)}, \quad x^2 + y^2 \to \infty, \tag{1c}$$

where the super-script (1) indicates region 1 ($x < -h$), the super-script (2) indicates region 2 ($|x| < h$) and the super-script (3) indicates region 3 ($x > h$). For this particular remote loading, the crack is subjected to failure mode I (opening failure mode) only.

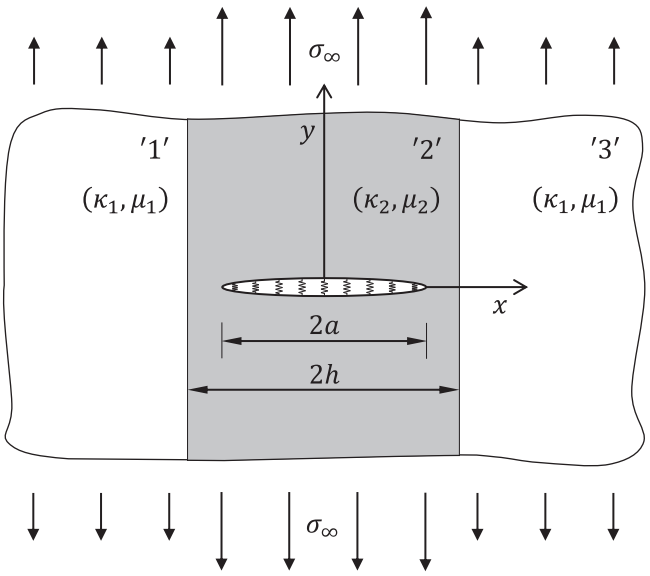

Fig. 1. Formulation of the problem: a bridged crack symmetrically embedded in an elastic layer perpendicular to the material interfaces.

The crack is bridged by uni-directional fibers, which are aligned perpendicular to its length. The bridging fibers restrain the opening of the crack and consequently, causes a reduction in the stress intensities at the crack tip. In continuum approximation (crack length ≫ fiber spacing), the bridging traction due to the individual fibers can be replaced by a continuous distribution of bridging tractions, $p(x)$ on the crack surface [1]. Hence, the boundary conditions along the crack face i.e. $y = 0$ can be represented as

$$\sigma^{(2)}_{yy}(x, y = 0) = p(x), \quad |x| < a \tag{2a}$$

$$\sigma^{(2)}_{xy}(x, y = 0) = 0, \quad -\infty < x < \infty \tag{2b}$$

$$u_y(x, y = 0) = 0, \quad x \leqslant -a,\ x \geqslant a. \tag{2c}$$

where $p(x)$ is the net bridging traction on the crack face.

The bridging traction $p(x)$ at a location x is defined as $p(x) = f\sigma_f(x)$, where f is the volume fraction of the fibers and $\sigma_f(x)$ is the average stress in the fibers [1]. Failure of individual fibers occurs when the stress σ_f in the fibers exceeds the fiber strength, S. Thus, fiber failure within the crack occurs when $p(x) > fS = \sigma_{ult}$.

The bridging traction $p(x)$ is dependent upon the crack opening displacement $\delta(x)$, or equivalently on the crack face displacement defined as $u(x) = \delta(x)/2 = u_y(x,y \to 0+)$. In the present case, the traction law proposed by Marshall et al. [1] for frictionally bonded composites is utilized:

$$p(x) = \eta\sqrt{u(x)}\mathrm{H}(u_{ult} - u(x)), \quad \mathrm{H}(u_{ult} - u(x)) = \begin{cases} 1, & u(x) \leqslant u_{ult}, \\ 0, & u(x) > u_{ult}. \end{cases} \tag{3}$$

In the above model, the bridging traction is proportional to the square root of the crack face displacement and the failure of fibers occurs when $u(x) > u_{ult}$. Here η is a constant, $u_{ult} = (fS/\eta)^2$ and H(.) is the Heaviside step function. The constant η was determined by a one-dimensional analysis of the frictional bond between the fiber and matrix by Marshall et al. [1] as:

$$\eta = \left[\frac{4\tau f^2 E_f E_c}{RE_m(1-f)}\right]^{1/2}, \tag{4}$$

where τ is the frictional stress between the fiber and matrix in the region of fiber/matrix sliding, f is the volume fraction of the fibers and R is the radius of the individual fibers. The constants E_c, E_m and E_f are the Young's moduli of the composite, matrix and fibers respectively, related according to the mixture rule as $E_c = fE_f + (1-f)E_m$.

3. Governing integral equation

Following the procedure of Bilby and Eshelby [22], the governing integral equation for crack opening can be written in terms of the distributed dislocation density function, $b_y(x)$. The distributed dislocation density is related to the crack face displacement according to:

$$u(x) = -\frac{1}{2}\int_{-\infty}^{x} b_y(t)dt, \quad b_y(x) = -2\frac{du(x)}{dx}. \tag{5}$$

The normal stress along the crack length can be written as a superposition of two auxiliary problems: (1) the normal stress in the absence of the crack (i.e. in a perfect body), σ_∞ and (2) the normal stress in the elastic layer due to a continuous distribution of edge dislocations of density $b_y(x)$ along the crack length, $\bar{\sigma}^{(2)}_{yy}(x,0)$. Thus,

$$\sigma^{(2)}_{yy}(x,0) = \sigma_\infty + \bar{\sigma}^{(2)}_{yy}(x,0), \quad |x| \leqslant a, \tag{6}$$

where $\bar{\sigma}^{(2)}_{yy}(x,0)$ is given by:

$$\bar{\sigma}^{(2)}_{yy}(x,0) = \frac{2\mu_2}{\pi(\kappa_2+1)}\int_{-a}^{+a} b_y(t)\left[\frac{1}{x-t} + G^{(2)}_{yyy}(x-t,0)\right]dt. \tag{7}$$

In the above integral equation, the first singular term relates to the homogeneous dislocation solution and the second bounded part of the kernel, $G^{(2)}_{yyy}$, describes the influence of the material interfaces located along $x = \pm h$. An expression for $G^{(2)}_{yyy}$ was derived by Fleck et al. [23] using Airy's stress function approach and Fourier transform method and their method of determining the influence function is summarized briefly in Appendix C for the sake of completeness of this paper. The influence function $G^{(2)}_{yyy}(x,0)$ is dependent on the thickness of the elastic layer $2h$, the crack length $2a$, and Dundur's parameters α and β, which are defined as

$$\alpha = \frac{\mu_1(\kappa_2+1) - \mu_2(\kappa_1+1)}{\mu_2(\kappa_1+1) + \mu_1(\kappa_2+1)}, \quad \beta = \frac{\mu_1(\kappa_2-1) - \mu_2(\kappa_1-1)}{\mu_2(\kappa_1+1) + \mu_1(\kappa_2+1)}.$$

These parameters characterize the degree of mismatch in the elastic properties between materials 1 and 2.

Substituting Eq. (7) into Eq. (6) and utilizing the boundary condition (2a), the governing integral equation in terms of the unknown dislocation density function, $b_y(t)$, can be obtained as

$$\frac{2\mu_2}{\pi(\kappa_2+1)}\int_{-a}^{+a} b_y(t)\left[\frac{1}{x-t} + G^{(2)}_{yyy}(x-t,0)\right]dt + \sigma_\infty - p(x) = 0, \quad |x| \leqslant a, \tag{8}$$

where the bridging traction $p(x)$ is given by Eq. (3). The unknown dislocation density function, $b_y(x)$ must also satisfy the condition [24]:

$$\int_{-a}^{+a} b_y(t)dt = 0, \tag{9}$$

which corresponds to the physical condition that the crack should have no net dislocation content or the faces of the crack come together at $x = \pm a$.

4. Dimensionless form of the governing integral equation

To facilitate numerical solution, the scaled coordinate X is introduced such that $x = aX$. Similarly a dummy integration variable ξ is introduced such that $t = a\xi$. Also, the following dimensionless parameters are introduced:

$$\Sigma_\infty = \frac{\sigma_\infty}{\sigma_n}, \quad A = \frac{a}{a_n}, \quad H = \frac{h}{a}, \quad U = \frac{u}{u_n}, \quad B_y = \frac{a}{u_n}b_y, \quad K_N = \frac{K}{K_c}. \tag{10}$$

Here, Σ_∞ is the normalized tensile stress, A is the normalized crack length, H is the normalized thickness of the elastic layer, U is the normalized crack face displacement, B_y is the normalized distributed dislocation density function and K_N is the normalized stress intensity factor at the crack tip. The normalizing parameters used in this study are the same as those introduced by Marshall and Cox [8] in order to facilitate the comparison of numerical results. These are defined as:

$$\sigma_n = \left[\frac{3\eta^2 K_c^2}{\bar{E}_1}\right]^{1/3}, \quad a_n = \frac{\pi}{4}\left[\frac{9\bar{E}_1 K_c}{\eta^2}\right]^{2/3}, \quad u_n = \frac{\sigma_\infty^2}{\eta^2}, \tag{11}$$

where K_c is the fracture toughness of the fiber–matrix composite, which occupies region 2, see Fig. 1.

In non-dimensional form, the relationship between the crack opening and distributed dislocation density given by Eq. (5), can be written as

$$U(X) = \frac{1}{2}\int_X^1 B_y(\xi)d\xi, \quad -1 \leqslant X \leqslant 1. \tag{12}$$

Similarly, the governing integral Eq. (8) can be written in non-dimensional form as:

$$\frac{\Sigma_\infty}{3\pi^2 A}\int_{-1}^{1} B_y(\xi)\left[\frac{1}{X-\xi} + G^{(2)}_{yyy}(X-\xi,0)\right]d\xi + F(X) = 0, \quad -1 \leqslant X \leqslant 1, \tag{13}$$

where the function $F(X)$ is given by

$$F(X) = 1 - \sqrt{U(X)}\mathrm{H}\left(\frac{\sigma_{ult}}{\sigma_n} - \Sigma_\infty\sqrt{U(X)}\right).$$

The criterion for fiber failure is $\Sigma_\infty\sqrt{U(X)} = \sigma_{ult}/\sigma_n$. Finally, Eq. (9) can be re-written as:

$$\int_{-1}^{1} B_y(\xi)d\xi = 0. \tag{14}$$

An efficient numerical solution to the system of Eqs. (15) and (17), can be obtained by utilizing the Gauss–Chebyshev quadrature method, which reduces the governing singular Eqs. (13) and (14) to a system of non-linear algebraic equations, which can be readily solved using Newton–Raphson iteration method and Gaussian elimination [25].

5. Numerical solution procedure

The interval $-1 \leqslant X \leqslant 1$ is discretized into N points and a set of indices are defined as $i = 1 \ldots N$ and $j = 1 \ldots N-1$. The integration and collocation points over the interval $-1 \leqslant X \leqslant 1$ are given by $s_i = \cos(\pi(2i-1)/2N)$ and $t_j = \cos(\pi\ j/N)$ respectively. The asymptotic behavior at the crack tips is built into the solution for $B_y(X)$ by writing the edge dislocation density function as $B_y(X) = W(X)\Phi(X)$ where $W(X) = (1-X)^{-1/2}$ is the fundamental solution and $\Phi(X)$ is an unknown regular function to be determined at N points along the interval $-1 \leqslant X \leqslant 1$. The Eq. (13) can be discretized into a system of $N-1$ equations with N unknowns as:

$$\frac{\Sigma_\infty}{3\pi AN}\sum_{i=1}^{N}\Phi(s_i)\left[\frac{1}{t_j - s_i} + G^{(2)}_{yyy}(t_j - s_i, 0)\right] + F(t_j) = 0, \tag{15}$$

where,

$$F(t_j) = 1 - \sqrt{U(t_j)}\,\mathrm{H}\left(\frac{\sigma_{ult}}{\sigma_n} - \Sigma_\infty\sqrt{U(t_j)}\right).$$

The normalized crack opening $U(t_j)$ can be obtained from Eq. (12) as:

$$U(t_j) = \frac{\pi}{2N}\sum_{i=1}^{j}\Phi(s_i). \tag{16}$$

Similarly, Eq. (14) can be discretized to obtain the Nth equation:

$$\frac{\pi}{N}\sum_{i=1}^{N}\Phi(s_i) = 0. \tag{17}$$

The system of $N \times N$ non-linear equations given by (15) and (17) is solved using the Newton–Raphson iterative scheme, as follows. Let the array $\{\Phi\} = [\Phi(s_1), \Phi(s_2), \ldots \Phi(s_N)]^T$ contain the unknown values of the function Φ at the N points along the length of the crack. Then, the kth iteration for $\{\Phi\}$ is given by:

$$\{\Phi\}_k = \{\Phi\}_{k-1} - [J]^{-1}_{k-1}\{S\}_{k-1}, \quad k = 1, 2, \ldots \tag{18}$$

The vector $\{S\}_{k-1}$ is the L.H.S. of Eq. (15) evaluated for $\{\Phi\} = \{\Phi\}_{k-1}$. The $N \times N$ matrix $[J]$ is the Jacobian matrix containing partial derivatives, the elements of which are given by:

$$J_{j,i} = \frac{\Sigma_\infty}{3\pi AN}\left[\frac{1}{t_j - s_i} + G^{(2)}_{yyy}(t_j - s_i, 0)\right] - \frac{\pi}{4N}\frac{1}{\sqrt{U(t_j)}}\,\mathrm{H}(j-i)H\left(\frac{\sigma_{ult}}{\sigma_n} - \Sigma_\infty\sqrt{U(t_j)}\right), \quad J_{N,i} = \frac{\pi}{N}. \tag{19}$$

For the first iteration, i.e. $k = 1$, an initial guess $\{\Phi\}_0$ is required. The initial guess $\{\Phi\}_0$ must be chosen such that $U(t_j)$ is non-zero for all t_j. This is because the components of the Jacobian matrix contain the term $U(t_j)^{-1/2}$ which is singular for $U(t_j) = 0$. In this paper, $\{\Phi\}_0 = [s_1, s_2, \ldots s_N]^T$ was chosen, where $s_i = \cos(\pi(2i-1)/2N)$. It provides rapid convergence for the entire range of governing parameters considered in the numerical study. The solution for $\{\Phi\}$ is considered to be converged when $\|\{\Phi\}_k - \{\Phi\}_{k-1}\|/\|\{\Phi\}_{k-1}\| < \epsilon$. The parameter ϵ can be chosen to be arbitrarily small and it controls the accuracy and convergence of the calculations. In the present calculations. $\epsilon = 10^{-10}$.

Once a converged solution for the function Φ is obtained, the normal stress along the crack i.e. $-1 \leqslant X \leqslant 1$, $y = 0$ is given by:

$$\frac{\Sigma_{yy}(t_j)}{\Sigma_\infty} = \frac{\Sigma_\infty}{3\pi AN}\sum_{i=1}^{N}\Phi(s_i)\left[\frac{1}{t_j - s_i} + G^{(2)}_{yyy}(t_j - s_i, 0)\right] + 1, \tag{20}$$

and the normalized stress intensity factors at the crack tips i.e. at $X = \pm 1$ are given by:

$$K_N(\pm 1) = \pm\frac{\Sigma^2_\infty}{2\sqrt{A}}\Phi(\pm 1). \tag{21}$$

The value of normalized tensile stress Σ_∞ for which $K_N = 1$ is denoted by Σ_k. At this stress, matrix failure occurs in material 1. Also, the value of normalized tensile stress Σ_∞ for which $(\sigma_{ult}/\sigma_n) = \Sigma_\infty\sqrt{\max(U)}$ is denoted by Σ_s. At this stress, fiber failure is initiated within the crack. The values of Σ_k and Σ_s depend upon the normalized thickness of the elastic layer H and Dundurs' parameters α and β which characterize the degree of mismatch in the elastic properties. In the next section, selected numerical results are presented, which demonstrate the most interesting features of the obtained solution.

6. Numerical results

The numerical procedure described previously was applied to solve the governing Eqs. (13) and (14) for a fully bridged straight crack. The solution procedure involves guessing the unknown crack length over which fiber failure occurs, in order to obtain self-consistent solutions for the normalized crack opening, $U(X)$ and the normal stress along the crack location, $\Sigma_{yy}(X)$. The number of integration points N is kept sufficiently high in order to ensure that the results are accurate up to four significant figures.

Firstly, the solutions for Σ_k and Σ_s were obtained for the case of no material interface, i.e. $H \to \infty$. The results are shown in Fig. 2 along with the numerical results for a penny shaped crack obtained by Marshall and Cox [8]. Due to the difference in the problem geometry (straight crack considered in the present work vs. penny shaped crack considered by Marshall and Cox [8]), the numerical values in the two sets of curves differ slightly. However, in both cases, the normalized stress required for matrix cracking, Σ_k converges to a value of 0.794 (Fig. 2(a)) and the value of applied stress required to initiate fiber failure, Σ_s converges to the value of the normalized fiber strength, Σ_{ult} (Fig. 2(b)). This comparison serves as a validation of the numerical procedure presented in this paper.

Next, the effect of crack tip distance from the interface on the solutions for Σ_k and Σ_s was examined. The results are presented in Fig. 3 for two extreme cases: when $\alpha = -1$, i.e. the crack lies close to a free boundary ($\mu_1 = 0$) and when $\alpha = +1$, i.e. the crack lies close to a rigid boundary ($\mu_1 \to \infty$). In both cases, the value of β is taken as $\alpha/4$. All other material combinations are expected to lie in between these two extremes. The calculations are performed for $H = 1.01$, 1.5 and 2.0 ($H = 1$ corresponds to the crack tip touching the interface and $H \to \infty$ corresponds to the absence of a material interface). The solution for the applied stress required to initiate matrix cracking Σ_k is presented in Fig. 3(a). At this stress, the normalized stress intensity factor at the crack tips $K_N = 1$. The following observations can be made from the figure:

1. When the crack lies close to the free surface, the stress intensity factor at the crack tips increases and hence, the stress required to initiate matrix cracking Σ_k, decreases. The opposite is true when the crack lies close to a rigid boundary. However, the effect of the boundary diminishes as H increases and can be ignored for $H > 2$. This observation is in agreement with the general trend observed in crack problems in bonded composite materials [15].
2. For the chosen values of the parameter H, the stress required to initiate matrix failure Σ_k changes only slightly as H goes from ∞ to 2. It changes quite significantly as H goes from 2 to 1.5 and the change is more pronounced as H goes from 1.5 to 1.01. Hence, the rate of change of the stress intensity factor increases rapidly as the crack tip approaches the boundary or as $H \to 1$.

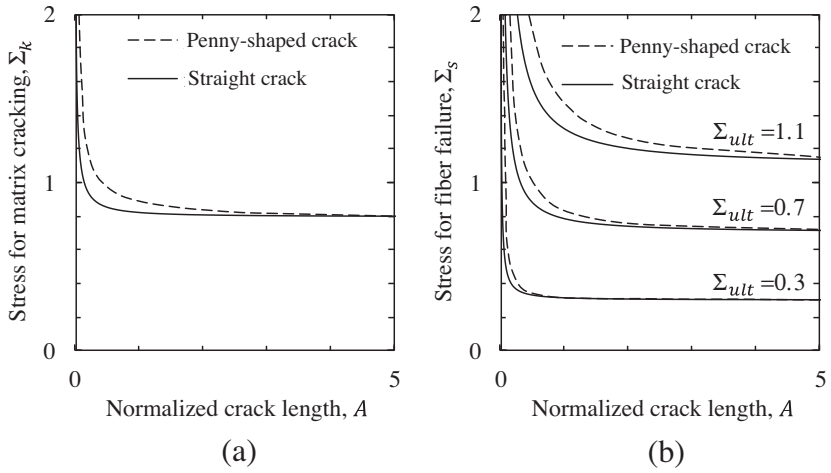

Fig. 2. Solution for Σ_k and Σ_s for a fully bridged matrix crack disregarding the material interfaces. The solid curves correspond to the numerical results obtained for a straight crack in the present work and the dotted curves correspond to the results for a penny shaped crack obtained by Marshall and Cox [8].

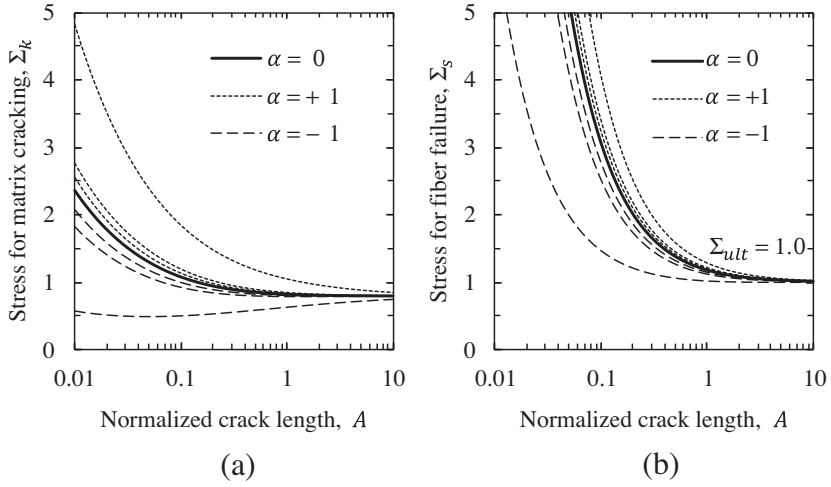

Fig. 3. Solution for Σ_k and Σ_s for a fully bridged crack for various values of the normalized thickness of the elastic layer, H. The curves furthest away from the solid curve correspond to $H = 1.01$. The curves closest to the solid curve correspond to $H = 2$. The intermediate curves correspond to $H = 1.05$.

3. With increasing normalized crack length A, the solution for Σ_k in the layered composite approaches the solution for Σ_k in a homogenous material. Based on Eqs. (10) and (11), the parameter $A \propto \eta^{4/3}$, where η is the constant of proportionality appearing in Eq. (3). Keeping other parameters constant, an increase in the bridging traction corresponds to an increase in η and subsequently, an increase in the normalized crack length A. Thus, the effect of the material interface diminishes with increased bridging traction. This result agrees with the findings of Ni and Nemat-Nasser [18] and Lee [17] for different problem geometries.

The solution for the applied stress required to initiate fiber failure Σ_s, which is presented in Fig. 3(b), follows the same trends as described previously. At this stress, the fiber failure criterion is satisfied at the point of maximum opening within the crack i.e. $\Sigma_{ult} = \Sigma_\infty \sqrt{U(0)}$. As the normalized crack length A increases, the value of Σ_s converges to the value of Σ_{ult}.

To demonstrate the effect of the elastic property mismatch, the solutions for Σ_k and Σ_s are evaluated for $H = 1.01$ and different values of Dundur's parameters α and β. The chosen values of α are $|\alpha| = 1$, 0.75, 0.50, 0.25 and 0. The value of β is taken as $\alpha/4$ in all cases, which implies that the Poisson's ratios of the two materials are chosen to be identical and the condition of plain strain dominates the stress state near the crack. The results are presented in Fig. 4 and the following observations can be made from the figure:

1. When $\alpha < 0$, the stress intensity factor at the crack tips as well as the maximum crack opening displacement increase. Hence, the stress required to initiate matrix cracking and fiber failure, Σ_k and Σ_s decrease. The opposite is true when $\alpha > 0$.
2. As $|\alpha|$ varies from 0 to 1, the change in values of Σ_k and Σ_s is quite uniform, unlike the change in values of Σ_k and Σ_s with H (shown in Fig. 3).
3. As before, the effect of the material interface diminishes with increasing the normalized crack length, A.

The distributed dislocation technique is also applied to solve the related problem a crack in an aircraft panel repaired by a composite patch in Appendix A. The results for a crack in a bonded ceramic lying perpendicular to a bi-material interface are given in Appendix B. A related problem of a crack located at an arbitrary

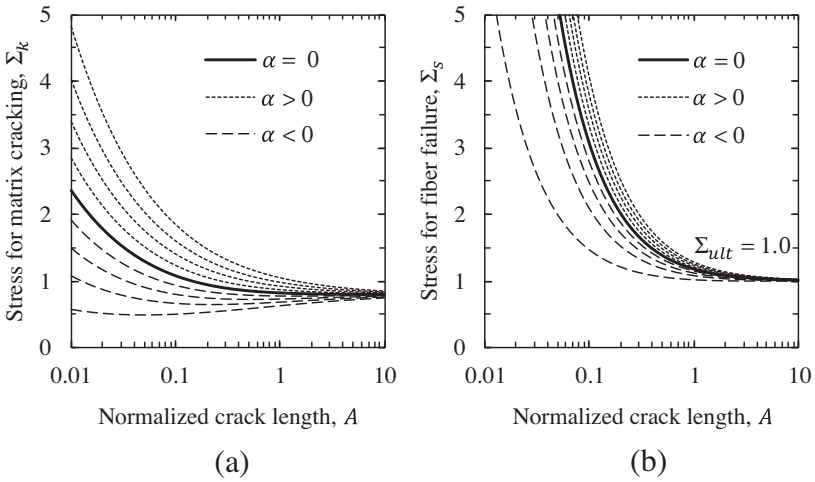

Fig. 4. Solution for Σ_k and Σ_s for a fully bridged matrix crack for $H = 1.01$ and various values of Dundur's parameter, α. Four curves each are presented for $\alpha > 0$ ($\mu_1 > \mu_2$) and $\alpha < 0$($\mu_1 < \mu_2$). These correspond to $|\alpha| = 1$ (outermost), 0.75, 0.50 and 0.25 (innermost). The solid curves correspond to the solution for $\alpha = 0$ i.e. $\mu_1 = \mu_2$.

angle in an elastic layer can also be solved using the dislocation solution outlined in Appendix C.

7. Concluding remarks

The mismatch in elastic properties between adjacent layers of a bonded structure can influence the stress intensity factor solution when the crack is located near the material interface. In the present work, a simple 2D problem geometry (shown in Fig. 1) was considered in order to demonstrate this effect. The general trends observed for unbridged cracks in bonded composite materials [15] were found applicable to the present problem as well. For example, the effect of the boundaries is significant only when the distance from the boundary is of the order of the crack length. Also, the effect of the boundary on the stress intensity factor rapidly increases as the crack tip approached the material interface. In addition, the effect of the material interface was found to diminish with increasing bridging traction, as demonstrated in previous studies [17,18].

The related problem of a cracked plate repaired by a composite patch was also considered and analyzed with the developed method. It was found that for typical material combinations, the mismatch in elastic properties between the patched and unpatched regions of the plate leads to an increase in the stress intensity factor (and hence, crack growth rate) when the crack tips were in the vicinity of the patch boundaries.

The novelty of the present work is that the governing integral equations for the crack problem were written in terms of the edge dislocation density rather than the crack opening displacement. The governing integral equations obtained in this form were solved readily using the numerical procedure outlined previously and the solution procedure did not experience the computational difficulties outlined by Marshall and Cox [8]. The developed method can be easily generalized to a number of other problem geometries, which can be handled in the similar manner due to the abundance of dislocation solutions available in the literature (for e.g. [16,15]).

Appendix A. Crack repaired by a composite patch

The mathematical formulation present in within the paper can be readily extended solve the problem of a crack in an aircraft panel repaired by a composite patch. The problem geometry is essentially the same as that shown in Fig. 1. A strip of composite material of width $2h$ is bonded to the aircraft panel along $|x| \leqslant h$. The thickness of the plate is denoted by t_P and the thickness of the patch is denoted by t_R. A straight crack of length $2a < 2h$ lies within the patched region, perpendicular to the boundaries of the patch. Additionally, the plate is restrained against out-of-plane bending either with the use of stiffeners or due to symmetry in the case of the two-sided patch repair.

The reinforced region of the plate can be treated as an elastic inclusion of higher stiffness than the surrounding plate [26]. The applicability of the inclusion analogy to bonded reinforcements has been verified numerically and experimentally [27]. The plate and the reinforcement are taken to be isotropic materials with equal Poisson's ratios. This considerably simplifies the presentation of the results, however it is acknowledged that the reinforcement and plate can be orthotropic. The elastic constants of the inclusion are then given by:

$$\mu_I = (\mu_P t_P + \mu_R t_R)/t_I, \quad \kappa_I = \kappa_P = \kappa_R, \tag{A1}$$

where (κ_P, μ_P) and (κ_R, μ_R) are the elastic constants of the plate and reinforcement, respectively. The thickness of the inclusion, t_I can be chosen arbitrarily and was chosen to be $t_I = t_P + t_R$ by Muki and Sternberg [28]. In the present context, it is chosen to be equal to the plate thickness, i.e. $t_I = t_P$ since the latter implies continuity of stress across the inclusion boundaries [26].

The elastic constants of the unrepaired regions of the plate, i.e. the half-planes occupying region 1 ($x < -h$) and region 3 ($x > h$) are identical and denoted by $(\kappa, \mu_1) \equiv (\kappa_P, \mu_P)$. The elastic inclusion, which contains the crack, occupies region 2 ($|x| < h$) and has elastic constants denoted by $(\kappa, \mu_2) \equiv (\kappa_I, \mu_I)$.

The governing integral equation is identical to Eq. (8), except the bridging traction $p(x)$ is modeled by elastic-perfectly plastic springs [29]:

$$p(x) = \begin{cases} \frac{8\mu_2}{(\kappa+1)} k u(x), & u(x) < u_P, \\ \frac{8\mu_2}{(\kappa+1)} k u_P \equiv \sigma_P, & u(x) \geqslant u_P. \end{cases} \tag{A2}$$

In the above constitutive model, k is a constant with dimension $(\text{Length})^{-1}$ characterizing the spring stiffness in the linear range, u_P is the characteristic displacement beyond which the spring response changes from being elastic to perfectly plastic and σ_P can be interpreted as the yield stress for the springs. Also, the dimensionless parameters are redefined as:

$$\Sigma_\infty = \frac{\sigma_\infty}{\sigma_P}, \quad A = \frac{4ka}{\pi}, \quad H = \frac{h}{a}, \quad U = \frac{u}{u_P}, \quad K_N = \frac{K\sqrt{k}}{\pi\sigma_P}. \tag{A3}$$

To obtain some numerical results corresponding to typical material combinations, the values of Dundur's parameters need to be

estimated. For example, consider an aluminium plate of thickness $t_P = 1.5$ mm, Young's Modulus $E_P = 69$ GPa and Poisson's ratio $\nu_P = 0.33$ which is bonded to a boron-epoxy laminate of thickness $t_R = 0.75$ mm. The boron-epoxy laminate is an orthotropic material containing uni-directional fibers, which are aligned perpendicular to the crack. The material properties are: $E_{Rx} = 19$ GPa, $E_{Ry} = 210$ GPa, $\mu_{Rxy} = 4.8$ GPa and $\nu_{yx} = 0.35$ [3]. To simplify the analysis, the reinforcement is treated as an isotropic material with Young's modulus equal to its longitudinal Young's modulus E_{Ry} i.e. $E_R = 210$ GPa and Poisson's ratio equal to that of the plate, i.e. $\nu_R = 0.33$. The corresponding values of the shear moduli of the plate, reinforcement and inclusion are $\mu_P = 26$ GPa, $\mu_R = 79$ GPa and $\mu_I = 65.5$ GPa, respectively. The values of Dundur's parameters are calculated as $\alpha = -0.4317$ and $\beta = -0.1087$. The dependence of the stress intensity factor at the crack tip upon the distance from the material interface is demonstrated in Fig. A1 for this particular set of values of the Dundur's parameters.

The results obtained for the present case converge to the results obtained by Cox and Rose [29] for large distance from patch boundaries ($H \to \infty$). However, it can be observed that up until $H = 1.5$, the effect of patch boundaries is insignificant for a range of values of applied stress. Thus, for a patch of width 1.5 times or greater than the crack length, the effect of patch boundaries on stress intensity factor and crack growth rate can be disregarded. As the crack approaches the patch boundary ($H = 1.01$), there is a significant increase in the stress intensity factor at the crack tips. Other factors, such as the high stresses in the plate, adhesive and laminate near the edges of the laminate, owing to the finite geometry of the patch (edge effect), would also contribute to the increase in stress intensity factor at such a distance [30].

Appendix B. Crack near a bi-material interface

For a straight crack, lying perpendicular to a bi-material interface, as shown in Fig. B1, the governing integral equation for this crack problem is given by

$$\frac{2\mu_2}{\pi(\kappa_2+1)}\int_{b-a}^{b+a} b_y(t)\left[\frac{1}{x-t}+G^{(2)}_{yyy}(x,t)\right]dt+\sigma_\infty-p(x)=0,\quad b-a\leqslant x\leqslant b+a. \tag{B1}$$

where the influence function is given by [16]

$$G^{(2)}_{yyy}=\frac{\alpha+\beta^2}{1-\beta^2}\frac{1}{x+t}+\frac{\beta-\alpha}{1+\beta}\left[-\frac{2t}{(x+t)^2}+\frac{4t^2}{(x+t)^3}\right],$$

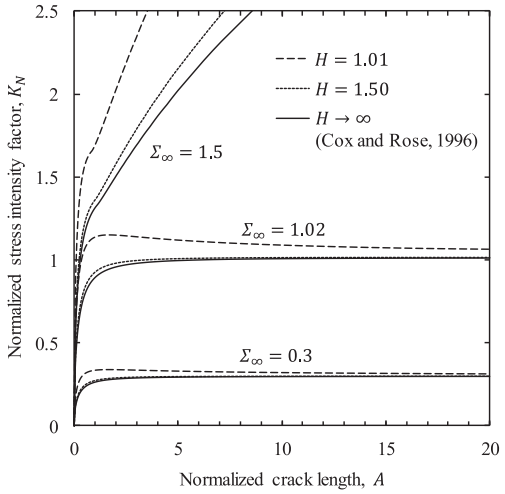

Fig. A1. The effect of the distance from the patch boundary on the stress intensity factor. Calculations were performed for Dundur's parameters $\alpha = -0.4317$ and $\beta = -0.1087$.

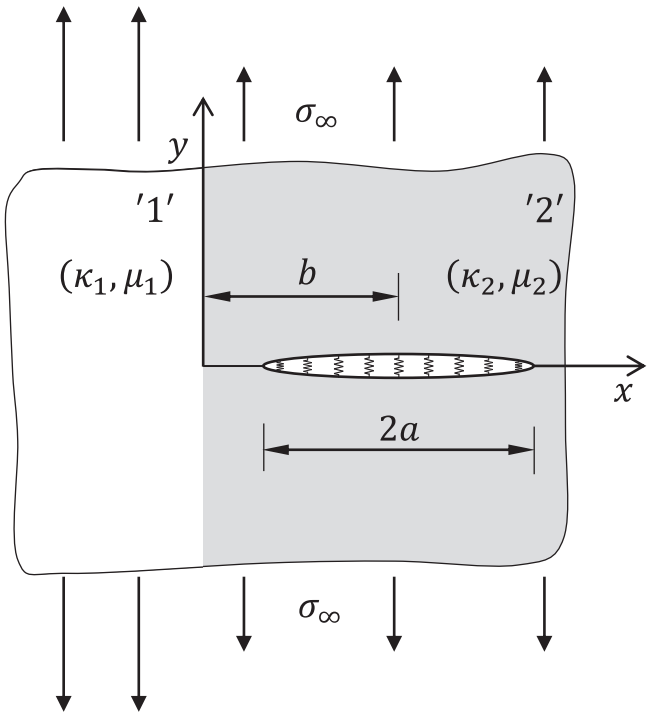

Fig. B1. A bridged crack located perpendicular to a bi-material interface.

and the normalized distance from the interface is defined as $B = b/a$.

Due to the asymmetry of the problem, the stress intensity factor at the two crack tips are different and subsequently the solution for Σ_k or the stress required to initiate matrix cracking are different at the two crack tips. The dimensionless parameters for this problem are also given by Eq. (10). The results are shown in Fig. B2 for $B = 1.01$ and $\alpha = \pm 1$.

It can be observed from Fig. B2 that the solution for Σ_k differs significantly at the two crack tips in the case a crack located near a bi-material interface (Fig. B1). The effect of the material interface is more pronounced at the crack tip close to the interface and is not quite significant at the far crack tip, even for small values of the

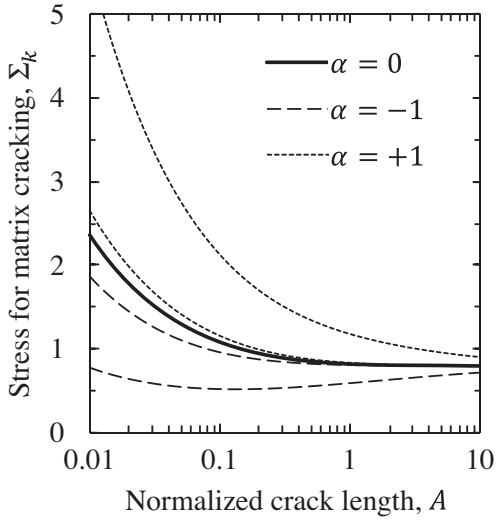

Fig. B2. Solution for Σ_k for a fully bridged matrix crack for $B = 1.01$. The curves adjacent to the solid curve correspond to the solution for Σ_k at the crack tip away from the interface. The curves away from the solid curve correspond to the crack tip near the interface.

normalized crack length A. As before, the solution for Σ_k approaches the solution in the absence of a material interface, as the value of the normalized crack length increases. In other words, the effect of the material interface diminishes as the bridging traction increases.

Appendix C. Solution for an edge dislocation in an elastic layer bounded by two identical elastic half-spaces

The solution for an edge dislocation in an elastic layer sandwiched between two identical elastic half-planes (Fig. C1) was utilized to derive the governing integral Eq. (8). The dislocation solution used in the present work was originally obtained by Fleck et al. [23] using Airy's stress function approach and Fourier transforms. It is briefly presented here for the sake of completeness.

Consider an edge dislocation with components b_x and b_y, which is located at the origin of the coordinate system. It lies at a distance c from the boundary between regions 2–3 and at a distance d from the boundary between regions 1–2. The thickness of the elastic layer containing the dislocation is $2h = c + d$.

The stresses induced at a point (x,y) due to an edge dislocation located at the origin (as shown in Fig. C1) are given by [16]:

$$\sigma_{xx}^{(i)}(x,y)=\frac{2\mu_2}{\pi(\kappa_2+1)}\left\{b_x\left[G_{xxx}^{(i)}-\frac{y}{r^4}(3x^2+y^2)\right]+b_y\left[G_{yxx}^{(i)}+\frac{x}{r^4}(x^2-y^2)\right]\right\}, \quad (C1)$$

$$\sigma_{xy}^{(i)}(x,y)=\frac{2\mu_2}{\pi(\kappa_2+1)}\left\{b_x\left[G_{xxy}^{(i)}+\frac{x}{r^4}(x^2-y^2)\right]+b_y\left[G_{yxy}^{(i)}+\frac{y}{r^4}(x^2-y^2)\right]\right\}, \quad (C2)$$

$$\sigma_{yy}^{(i)}(x,y)=\frac{2\mu_2}{\pi(\kappa_2+1)}\left\{b_x\left[G_{xyy}^{(i)}+\frac{y}{r^4}(x^2-y^2)\right]+b_y\left[G_{yyy}^{(i)}+\frac{x}{r^4}(x^2+3y^2)\right]\right\}, \quad (C3)$$

where the influence functions $G_{lmn}^{(i)}$ depend upon the problem geometry. For the problem shown in Fig. C1, a total of 18 influence functions need to be listed, 6 associated with each region. The stresses in region '1' are given by taking $i = 1$, the stresses in region '2' by taking $i = 2$ and in region '3' by taking $i = 3$. The first subscript of the influence function $G_{lmn}^{(i)}$ corresponds to the component of the Burger's vector of the edge dislocation, and the second and third subscripts correspond to the component of stress induced. The influence functions obtained by Fleck et al. [23] are listed as follows:

$$\frac{2\mu_2 G_{xxx}^{(i)}(x,y)}{\pi(\kappa_2+1)}=\int_0^\infty\left[-\left(B_1^i-\lambda x B_2^i\right)e^{\lambda x}-\left(B_3^i-\lambda x B_4^i\right)e^{-\lambda x}\right]\sin\lambda y\,d\lambda. \quad (C4)$$

$$\frac{2\mu_2 G_{xxy}^{(i)}(x,y)}{\pi(\kappa_2+1)}=\int_0^\infty\left[\left(B_1^i-(\lambda x+1)B_2^i\right)e^{\lambda x}-\left(B_3^i-(\lambda x-1)B_4^i\right)e^{-\lambda x}\right]\cos\lambda y\,d\lambda, \quad (C5)$$

$$\frac{2\mu_2 G_{xyy}^{(i)}(x,y)}{\pi(\kappa_2+1)}=\int_0^\infty\left[\left(B_1^i-(\lambda x+2)B_2^i\right)e^{\lambda x}+\left(B_3^i-(\lambda x-2)B_4^i\right)e^{-\lambda x}\right]\sin\lambda y\,d\lambda, \quad (C6)$$

$$\frac{2\mu_2 G_{yxx}^{(i)}(x,y)}{\pi(\kappa_2+1)}=\int_0^\infty\left[-\left(A_1^i-\lambda x A_2^i\right)e^{\lambda x}-\left(A_3^i-\lambda x A_4^i\right)e^{-\lambda x}\right]\cos\lambda y\,d\lambda, \quad (C7)$$

$$\frac{2\mu_2 G_{yxy}^{(i)}(x,y)}{\pi(\kappa_2+1)}=\int_0^\infty\left[-\left(A_1^i-(\lambda x+1)A_2^i\right)e^{\lambda x}+\left(A_3^i-(\lambda x-1)A_4^i\right)e^{-\lambda x}\right]\sin\lambda y\,d\lambda, \quad (C8)$$

$$\frac{2\mu_2 G_{yyy}^{(i)}(x,y)}{\pi(\kappa_2+1)}=\int_0^\infty\left[\left(A_1^i-(\lambda x+2)A_2^i\right)e^{\lambda x}+\left(A_3^i-(\lambda x-2)A_4^i\right)e^{-\lambda x}\right]\cos\lambda y\,d\lambda. \quad (C9)$$

There are a total of 8 constants associated with each region of the material. Let the constants A_j^i be designated by C_j in region '1', D_j in region '2' and E_j in region '3'. Similarly, let the constants B_j^i be designated by F_j in region '1', G_j in region '2' and H_j in region '3'. The outer regions (regions '1' and '3', made of material 1) are semi-infinite and their far-field boundaries are free of stresses and displacement gradients. This implies that as $x \to -\infty$, the influence functions $G_{lmn}^{(1)}$ must vanish i.e. the constants $C_3 = C_4 = 0$ and $F_3 = F_4 = 0$. Similarly, as $x \to \infty$, the influence functions $G_{lmn}^{(3)}$ must vanish i.e. the constants $E_1 = E_2 = 0$ and $H_1 = H_2 = 0$ in region '3'. There remains a total of 16 constants to be determined, of which 8 correspond to region '2' or the elastic layer and 4 constants correspond to each of the two half-spaces. These constants were

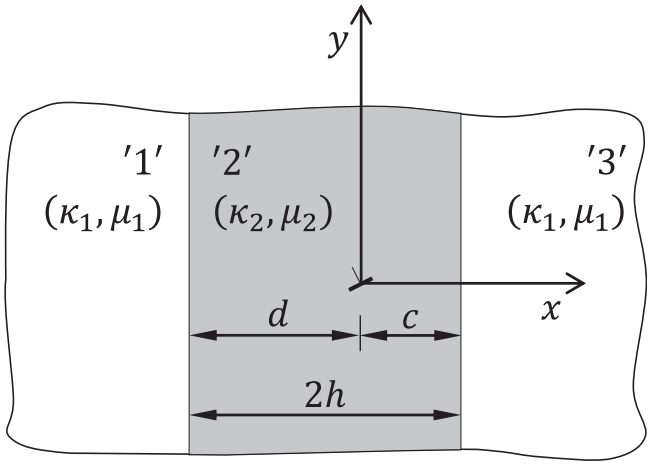

Fig. C1. Edge dislocation in an elastic layer.

determined by Fleck et al. [23] by matching tractions and displacement gradients at the strip boundaries $x = -d$ and $x = c$, which were written in terms of the Fourier transformation variable, λ. In symbolic form, the unknown constants are related to the known displacement gradient mismatch as

$$\begin{bmatrix}\mathbf{M_1} & \mathbf{M_2} & \mathbf{0}\\ \mathbf{M_3} & \mathbf{0} & \mathbf{M_4}\end{bmatrix}\begin{bmatrix}\mathbf{D}\\ \mathbf{E}\\ \mathbf{C}\end{bmatrix}=\begin{bmatrix}\mathbf{v_1}\\ \mathbf{v_2}\end{bmatrix}, \quad (C10)$$

and

$$\begin{bmatrix}\mathbf{M_1} & \mathbf{M_2} & \mathbf{0}\\ \mathbf{M_3} & \mathbf{0} & \mathbf{M_4}\end{bmatrix}\begin{bmatrix}\mathbf{G}\\ \mathbf{H}\\ \mathbf{F}\end{bmatrix}=\begin{bmatrix}\mathbf{w_1}\\ \mathbf{w_2}\end{bmatrix}, \quad (C11)$$

where the constants are contained in the vectors

$$\mathbf{C}=\begin{bmatrix}C_1\\ C_2\end{bmatrix},\quad \mathbf{D}=\begin{bmatrix}D_1\\ D_2\\ D_3\\ D_4\end{bmatrix},\quad \mathbf{E}=\begin{bmatrix}E_3\\ E_4\end{bmatrix},\quad \mathbf{F}=\begin{bmatrix}F_1\\ F_2\end{bmatrix},$$

$$\mathbf{G}=\begin{bmatrix}G_1\\ G_2\\ G_3\\ G_4\end{bmatrix},\quad \mathbf{H}=\begin{bmatrix}H_3\\ H_4\end{bmatrix},$$

and the matrices are defined as [23]:

$$\mathbf{M_1}=e^{-\lambda d}\begin{bmatrix}-1 & \lambda c & -e^{-2\lambda c} & \lambda c e^{-2\lambda c}\\ -1 & (1+\lambda c) & e^{-2\lambda c} & (1-\lambda c)e^{-2\lambda c}\\ 0 & \frac{\Pi_1}{2} & 0 & -\frac{\Pi_1}{2}e^{-2\lambda c}\\ 0 & \frac{\Pi_1}{2} & 0 & \frac{\Pi_1}{2}e^{-2\lambda c}\end{bmatrix},$$

$$\mathbf{M_2}=e^{-\lambda(2h+c)}\begin{bmatrix}1 & -\lambda c\\ -1 & (\lambda c-1)\\ -\Pi_2 & \Pi_2\lambda c+\frac{1}{2}\\ -\Pi_2 & -\Pi_2(1-\lambda c)-\frac{1}{2}\end{bmatrix},\quad \mathbf{M_4}=e^{-\lambda(2h+d)}\begin{bmatrix}1 & \lambda d\\ 1 & (\lambda d-1)\\ 0 & -\frac{1}{2}\\ 0 & -\frac{1}{2}\end{bmatrix},$$

$$\mathbf{M_3}=e^{-\lambda c}\begin{bmatrix}-e^{-2\lambda d} & -\lambda d e^{-2\lambda d} & -1 & -\lambda d\\ -e^{-2\lambda d} & (1-\lambda d)e^{-2\lambda d} & 1 & (1+\lambda d)\\ -\Pi_2 e^{-2\lambda d} & (-\Pi_2\lambda d+\frac{\Pi_1}{2})e^{-2\lambda d} & -\Pi_2 & -\Pi_2\lambda d-\frac{\Pi_1}{2}\\ \Pi_2 e^{-2\lambda d} & (\Pi_2(\lambda d-1)+\frac{\Pi_1}{2})e^{-2\lambda d} & -\Pi_2 & -\Pi_2(\lambda d+1)+\frac{\Pi_1}{2}\end{bmatrix}.$$

The vectors containing the known displacement gradient mismatch at $x = -d$ and $x = c$ are given by [23]:

$$\mathbf{v_1} = -\frac{1}{\pi}\frac{2\mu_2\Pi_1}{\kappa_2+1}e^{-2\lambda(h+c)}\begin{bmatrix}0\\0\\-\frac{\alpha(1-\lambda c)+\beta\lambda c}{1+\alpha}\\\frac{\beta(1-\lambda c)+\alpha\lambda c}{1+\alpha}\end{bmatrix},$$

$$\mathbf{v_2} = -\frac{1}{\pi}\frac{2\mu_2\Pi_1}{\kappa_2+1}e^{-2\lambda(h+d)}\begin{bmatrix}0\\0\\\frac{\alpha(1-\lambda d)+\beta\lambda d}{1+\alpha}\\\frac{\beta(1-\lambda d)+\alpha\lambda d}{1+\alpha}\end{bmatrix},$$

$$\mathbf{w_1} = -\frac{1}{\pi}\frac{2\mu_2\Pi_1}{\kappa_2+1}e^{-2\lambda(h+c)}\begin{bmatrix}0\\0\\\frac{-\beta(1+\lambda c)+\alpha\lambda c}{1+\alpha}\\\frac{-\alpha(1+\lambda c)+\beta\lambda c}{1+\alpha}\end{bmatrix},$$

and

$$\mathbf{w_2} = -\frac{1}{\pi}\frac{2\mu_2\Pi_1}{\kappa_2+1}e^{-2\lambda(h+d)}\begin{bmatrix}0\\0\\\frac{-\beta(1+\lambda d)+\alpha\lambda d}{1+\alpha}\\\frac{\alpha(1+\lambda d)-\beta\lambda d}{1+\alpha}\end{bmatrix}.$$

Here α and β are Dundur's bi-material parameters and the parameters Π_1 and Π_2 are functions of Dundur's bi-material parameters α and β, and are defined as:

$$\Pi_1 = \frac{1+\alpha}{1-\alpha}, \quad \Pi_2 = \frac{\alpha-\beta}{1-\alpha}.$$

For the stress analysis of a crack which is completely embedded in region '2', only the constants D_i and G_i need to be determined. Explicit expressions for these constants can be obtained by partitioning the matrices $\mathbf{M}_1, \mathbf{M}_2, \mathbf{M}_3$ and $\mathbf{M}_4$ into smaller 2-row units ([31]), such that

$$\begin{bmatrix}[M_{111}] & [M_{112}] & [M_{21}] & [0]\\ [M_{121}] & [M_{122}] & [M_{22}] & [0]\\ [M_{311}] & [M_{312}] & [0] & [M_{41}]\\ [M_{321}] & [M_{322}] & [0] & [M_{42}]\end{bmatrix}\begin{bmatrix}\{D_{12}\}\\ \{D_{34}\}\\ \{E\}\\ \{C\}\end{bmatrix} = \begin{bmatrix}\{v_{11}\}\\ \{v_{12}\}\\ \{v_{21}\}\\ \{v_{22}\}\end{bmatrix}. \tag{C12}$$

The vectors $\{C\}$ and $\{E\}$ can be eliminated using Gaussian elimination, to obtain (Giurgiutiu et al., 1998):

$$\{D_{12}\} = \begin{bmatrix}D_1\\D_2\end{bmatrix} = \left([M_{21}^*] - [M_{22}^*][M_{12}^*]^{-1}[M_{11}^*]\right)^{-1} \left(\{v_{22}^*\} - [M_{22}^*][M_{12}^*]^{-1}\{v_{11}^*\}\right), \tag{C13}$$

$$\{D_{34}\} = \begin{bmatrix}D_3\\D_4\end{bmatrix} = \left([M_{12}^*] - [M_{11}^*][M_{21}^*]^{-1}[M_{22}^*]\right)^{-1} \left(\{v_{11}^*\} - [M_{11}^*][M_{21}^*]^{-1}\{v_{22}^*\}\right). \tag{C14}$$

Similarly, the vectors $\{F\}$ and $\{H\}$ can be eliminated to obtain (Giurgiutiu et al., 1998):

$$\{G_{12}\} = \begin{bmatrix}G_1\\G_2\end{bmatrix} = \left([M_{21}^*] - [M_{22}^*][M_{12}^*]^{-1}[M_{11}^*]\right)^{-1} \left(\{w_{22}^*\} - [M_{22}^*][M_{12}^*]^{-1}\{w_{11}^*\}\right), \tag{C15}$$

$$\{G_{34}\} = \begin{bmatrix}G_3\\G_4\end{bmatrix} = \left([M_{12}^*] - [M_{11}^*][M_{21}^*]^{-1}[M_{22}^*]\right)^{-1} \left(\{w_{11}^*\} - [M_{11}^*][M_{21}^*]^{-1}\{w_{22}^*\}\right), \tag{C16}$$

where

$$[M_{11}^*] = [M_{321}] - [M_{42}][M_{41}]^{-1}[M_{311}], [M_{12}^*] = [M_{322}] - [M_{42}][M_{41}]^{-1}[M_{312}],$$
$$[M_{21}^*] = [M_{121}] - [M_{22}][M_{21}]^{-1}[M_{111}], [M_{22}^*] = [M_{122}] - [M_{22}][M_{21}]^{-1}[M_{112}],$$
$$\{v_{11}^*\} = \{v_{22}\} - [M_{42}][M_{41}]^{-1}\{v_{21}\}, \{v_{22}^*\} = \{v_{12}\} - [M_{22}][M_{21}]^{-1}\{v_{11}\},$$

and

$$\{w_{11}^*\} = \{w_{22}\} - [M_{42}][M_{41}]^{-1}\{w_{21}\}, \{w_{22}^*\} = \{w_{12}\} - [M_{22}][M_{21}]^{-1}\{w_{11}\}.$$

The above dislocation solution can be utilized to solve problems involving an arbitrarily oriented crack which is completely embedded in the elastic layer. It is noted that the solution to the above problem was also provided by Omoike and Vilmann [32] using a series representation of the bounded kernels. The present work deals with the stress analysis of a crack located along $|x| \leqslant a, y = 0$ (see Fig. 1). The influence functions in the elastic layer along the line of the crack, $y = 0$ are be obtained by substituting $i = 2$ and $y = 0$ into Eqs. (C4)–(C9):

$$G_{xxy}^{(2)}(x,0) = \frac{\pi(\kappa_2+1)}{2\mu_2}\int_0^\infty [(G_1 - (\lambda x+1)G_2)e^{\lambda x} - (G_3 - (\lambda x-1)G_4)e^{-\lambda x}]d\lambda, \tag{C17}$$

$$G_{yxx}^{(i)}(x,0) = \frac{\pi(\kappa_2+1)}{2\mu_2}\int_0^\infty [-(D_1 - \lambda x D_2)e^{\lambda x} - (D_3 - \lambda x D_4)e^{-\lambda x}]d\lambda, \tag{C18}$$

$$G_{yyy}^{(2)}(x,0) = \frac{\pi(\kappa_2+1)}{2\mu_2}\int_0^\infty [(D_1 - (\lambda x+2)D_2)e^{\lambda x} + (D_3 - (\lambda x-2)D_4)e^{-\lambda x}]d\lambda, \tag{C19}$$

$$G_{xxx}^{(2)}(x,0) = G_{xyy}^{(2)}(x,0) = G_{yxy}^{(2)}(x,0) = 0. \tag{C20}$$

The integrals in Eqs. (C17)–(C19) need to be evaluated numerically over the interval 0 to λ_{max}, where λ_{max} is the upper limit of the integral. These integrals are rapidly convergent and the choice of λ_{max} would depend upon the desired numerical accuracy. The constants D_i and G_i are functions of the variable λ and must be evaluated at each value of λ either by using Eqs. (C13)–(C16) or by the direct numerical inversion of Eqs. (C10) and (C11).

Now consider a dislocation at $(x,y) = (t,0)$ with infinitesimal Burger's vector $\delta b_y = B_y(t)dt$, where $B_y(t)$ is the dislocation density. The stresses along the line of the crack due to this dislocation can be obtained by setting $b_x = 0$, $y = 0$, and by replacing x by $x - t$ in Eqs. (C1)–(C3):

$$\sigma_{xx}^{(2)}(x,0) = \frac{2\mu_2}{\pi(\kappa_2+1)}\left[\frac{1}{x-t} + G_{yxx}^{(2)}(x-t,0)\right]B_y(t)dt, \tag{C21}$$

$$\sigma_{yy}^{(2)}(x,0) = \frac{2\mu_2}{\pi(\kappa_2+1)}\left[\frac{1}{x-t} + G_{yyy}^{(2)}(x-t,0)\right]B_y(t)dt, \tag{C22}$$

$$\sigma_{xy}^{(2)}(x,0) = 0. \tag{C23}$$

The stresses due to a continuous distribution of dislocations along the crack-line are then given by

$$\bar{\sigma}_{xx}^{(2)}(x,0) = \frac{2\mu_2}{\pi(\kappa_2+1)}\int_{-a}^{+a}\left[\frac{1}{x-t} + G_{yxx}^{(2)}(x-t,0)\right]B_y(t)dt, \tag{C24}$$

$$\bar{\sigma}_{yy}^{(2)}(x,0) = \frac{2\mu_2}{\pi(\kappa_2+1)}\int_{-a}^{+a}\left[\frac{1}{x-t} + G_{yyy}^{(2)}(x-t,0)\right]B_y(t)dt. \tag{C25}$$

Note that the values of the constants and (see Fig. C1) would be $c = h - t$ and $d = h + t$ for a dislocation located at $x = t$. These values must be utilized when evaluating the influence functions appearing in Eqs. (C24) and (C25) at each value of t.

References

[1] Marshall DB, Cox BN, Evans AG. The mechanics of matrix cracking in brittle-matrix fiber composites. Acta Metall 1985;33(11):2013–21.

[2] Aveston J, Kelly A. Tensile first cracking strain and strength of hybrid composites and laminates. Philos Trans R Soc Ser A 1980;294:519–34.

[3] Baker AA, Jones R. Bonded repair of aircraft structures. Dordrecht (The Netherlands): Martinus Nijhoff Publishers; 1988.

[4] Bachir Bouiadjra B, Belhouari M, Serier B. Computation of the stress intensity factors for repaired cracks with bonded composite patch in mode I and mixed mode. Compos Struct 2002;56(4):401–6.

[5] Sabelkin V, Mall S, Hansen MA, Vandawaker RM, Derriso M. Investigation into cracked aluminum plate repaired with bonded composite patch. Compos Struct 2007;79(1):55–66.
[6] Szekrelnyes A, Uj J. Advanced beam model for fiber-bridging in unidirectional composite double-cantilever beam specimens. Eng Fract Mech 2005;72:2686–702.
[7] Rose LRF. Crack reinforcement by distributed springs. J Mech Phys Solids 1987;35:383–405.
[8] Marshall DB, Cox BN. Tensile fracture of brittle matrix composites: influence of fiber strength. Acta Metall 1987;35(11):2607–19.
[9] McCartney LN. Mechanics of matrix cracking in brittle-matrix fibre-reinforced composites. Proc R Soc Ser A 1987;409:329–50.
[10] Budiansky B, Hutchinson JW, Evans AG. Matrix fracture in fiber-reinforced ceramics. J Mech Phys Solids 1986;34:167–89.
[11] Selvadurai APS. On the Mode I stress intensity factor for an external circular crack with fibre bridging. Compos Struct 2010;92:1512–6.
[12] Dalgleish BJ, Lu MC, Evans AG. The strength of ceramics bonded with metals. Acta Metall 1988;36(8):2029–35.
[13] Akselsen OM. Diffusion bonding of ceramics. J Mater Sci 1992;27:569–79.
[14] Chen EP, Sih GC. Interfacial delamination of a layered composite under anti-plane strain. J Compos Mater 1971;5(12):12–23.
[15] Erdogan F. Fracture problems in composite materials. Eng Fract Mech 1972;4(4):811–40.
[16] Hills DA, Kelly PA, Dai DN, Korsunsky AM. Solution of crack problems: the distributed dislocation technique. Dordrecht (The Netherlands): Kluwer Academic Publishers; 1996.
[17] Lee JC. Analysis of a fiber bridged crack near a free surface in ceramic matrix composites. Eng Fract Mech 1990;37(1):209–19.
[18] Ni L, Nemat-Nasser S. Bridged interface cracks in anisotropic bimaterials. Philos Mag A 2000;80(11):2675–93.
[19] Kotousov A. Effect of plate thickness on stress state at sharp notches and the strength paradox of thick plates. Int J Solids Struct 2010;47:1916–23.
[20] Berto F, Kotousov A, Lazzarin P, Pook LP. On scale effect in plates weakened by rounded V-notches and subjected to in-plane shear loading. Int J Fract 2013;180(1):111–8.
[21] Berto F, Lazzarin P, Kotousov A. On the presence of the out-of-plane singular mode induced by plane loading with KII = KI = 0. Int J Fract 2011;167(1):119–26.
[22] Bilby B, Eshelby J. Dislocations and the theory of fracture. In: Liebowitz H, editor. Fracture: an advanced treatise, vol. 1. New York (USA): Academic Press; 1968.
[23] Fleck NA, Hutchinson JW, Suo Z. Crack path selection in a brittle adhesive layer. Int J Solids Struct 1991;27(13):1683–703.
[24] Kotousov A. Fracture in plates of finite thickness. Int J Solids Struct 2007;44:8259–73.
[25] Bortolan Neto L, Khanna A, Kotousov A. Conductivity and performance of hydraulic fractures partially filled with compressible proppant packs. Int J Rock Mech Mining Sci; submitted for publication.
[26] Rose LRF. An application of the inclusion analogy for bonded reinforcements. Int J Solids Struct 1981;17:827–38.
[27] Wang CH, Rose LRF. Crack bridging model for bonded plates subjected to tension and bending. Int J Solids Struct 1999;36:1985–2014.
[28] Muki R, Sternberg E. On the stress analysis of overlapping bonded elastic sheets. Int J Solids Struct 1968;4(1):75–94.
[29] Cox BN, Rose LRF. A self-consistent approximation for crack bridging by elastic/perfectly plastic ligaments. Mech Mater 1996;22:249–63.
[30] Haghani R, Al-Emrani M, Kliger R. Stress distribution in adhesive joints with tapered laminates – effect of tapering length and material properties. J Compos Mater 2010;44(3):287–302.
[31] Giurgiutiu V, Ionita A, Dillard DA. Details of the integral equation method applied to the analysis of an adhesive layer crack. Int J Solids Struct 1998;35:1099–130.
[32] Omoike G, Vilmann CR. Arbitrarily oriented cracks in a layered media. J Compos Mater 1983;17(4):316–29.

Chapter 5

Controlling the Height of Multiple Hydraulic Fractures in Layered Media

Statement of Authorship

Title of Paper	Controlling the height of multiple hydraulic fractures in layered media
Publication Status	☑ Published ☐ Accepted for Publication ☐ Submitted for Publication ☐ Unpublished and Unsubmitted work written in manuscript style
Publication Details	SPE Journal, Preprint, 8 pages, doi: 10.2118/176017-PA Submitted: 21 Apr 2014, Submitted in revised form: 13 Mar 2015, Accepted: 20 Apr 2015

Principal Author

Name of Principal Author (Candidate)	Aditya Khanna		
Contribution to the Paper	Performed all analyses and wrote manuscript.		
Overall percentage (%)	80		
Certification:	This paper reports on original research I conducted during the period of my Higher Degree by Research candidature and is not subject to any obligations or contractual agreements with a third party that would constrain its inclusion in this thesis. I am the primary author of this paper.		
Signature		Date	10/04/2016

Co-Author Contributions

By signing the Statement of Authorship, each author certifies that:

i. the candidate's stated contribution to the publication is accurate (as detailed above);

ii. permission is granted for the candidate in include the publication in the thesis; and

iii. the sum of all co-author contributions is equal to 100% less the candidate's stated contribution.

Name of Co-Author	Andrei Kotousov		
Contribution to the Paper	Supervised the development of the theoretical models and assisted in the preparation of the original and revised manuscripts.		
Overall percentage (%)	20		
Signature		Date	10/04/2016

Khanna, A. and Kotousov, A. (2016). Controlling the height of multiple hydraulic fractures in layered media. *SPE Journal, 21*(1), 256-263.

Chapter 6

A new predictive model for the onset of skier-triggered avalanches

Statement of Authorship

Title of Paper	A new model for skier-triggered onset of failure in snow-packs containing buried weak layers
Publication Status	☐ Published ☐ Accepted for Publication ☑ Submitted for Publication ☐ Unpublished and Unsubmitted w ork w ritten in manuscript style
Publication Details	Geophysical Research Letters. Originally submitted on: 15 Oct 2015. Revision submitted on: 10 Apr 2016.

Principal Author

Name of Principal Author (Candidate)	Aditya Khanna		
Contribution to the Paper	Performed all analyses and wrote manuscript.		
Overall percentage (%)	80		
Certification:	This paper reports on original research I conducted during the period of my Higher Degree by Research candidature and is not subject to any obligations or contractual agreements with a third party that would constrain its inclusion in this thesis. I am the primary author of this paper.		
Signature		Date	10/04/2016

Co-Author Contributions

By signing the Statement of Authorship, each author certifies that:

i. the candidate's stated contribution to the publication is accurate (as detailed above);

ii. permission is granted for the candidate in include the publication in the thesis; and

iii. the sum of all co-author contributions is equal to 100% less the candidate's stated contribution.

Name of Co-Author	Andrei Kotousov		
Contribution to the Paper	Provided major contribution towards the formulation of the problem. Assisted in the preparation of the manuscript.		
Overall percentage (%)	20		
Signature		Date	10/04/2016

A new predictive model for the onset of skier-triggered avalanches

A. Khanna* and A. Kotousov

School of Mechanical Engineering, The University of Adelaide, Adelaide, SA 5005, Australia.

*Corresponding Author. Tel: +61 8 8313 6385

Email addresses: aditya.khanna@adelaide.edu.au (A. Khanna), andrei.kotousov@adelaide.edu.au (A. Kotousov).

Key Points:

- Crack-like defects may be generated in the weak layer under skier loading
- Skier-triggered failure of the weak layer is examined in Mode III
- The theoretical model reasonably describes the failure conditions

Abstract: It is proposed that catastrophic failure of the weak layer occurs in Mode III when a skier travelling downslope induces a defect of critical size within the weak layer. Theoretical models are developed to calculate the size of the skier-induced defect as well as the critical defect size required for the onset of failure within the weak layer. The latter model utilizes the distributed dislocation technique in contrast to the previous approaches based on beam theories and energy balance equations, which are strictly applicable only when the defect length is significantly greater than the slab thickness. Case studies are conducted for typical snow-pack properties and realistic failure conditions are identified.

1. Introduction

The fracture sequence prior to the release of a skier-triggered dry snow slab avalanche is now well understood. A skier travelling along the snow surface initiates a defect in a buried weak layer. If the skier-induced defect exceeds a critical size, it propagates in an unstable manner, resulting in the loss of support and possible release of the overlying snow slab [van Herwijnen and Jamieson, 2007; Schweizer et al., 2003]. For the case of a stationary skier, experimental studies have demonstrated that localized collapse or failure may occur over an area of the weak layer directly underneath the skier [Schweizer and Camponovo, 2001]. Therefore, it is reasonable to expect that a skier travelling downslope would produce a defect which extends significantly along the direction of the skier's trajectory as illustrated in Fig.1, provided that the spatial variability in the snow cover properties is small and the healing time for the formed defect is sufficiently long.

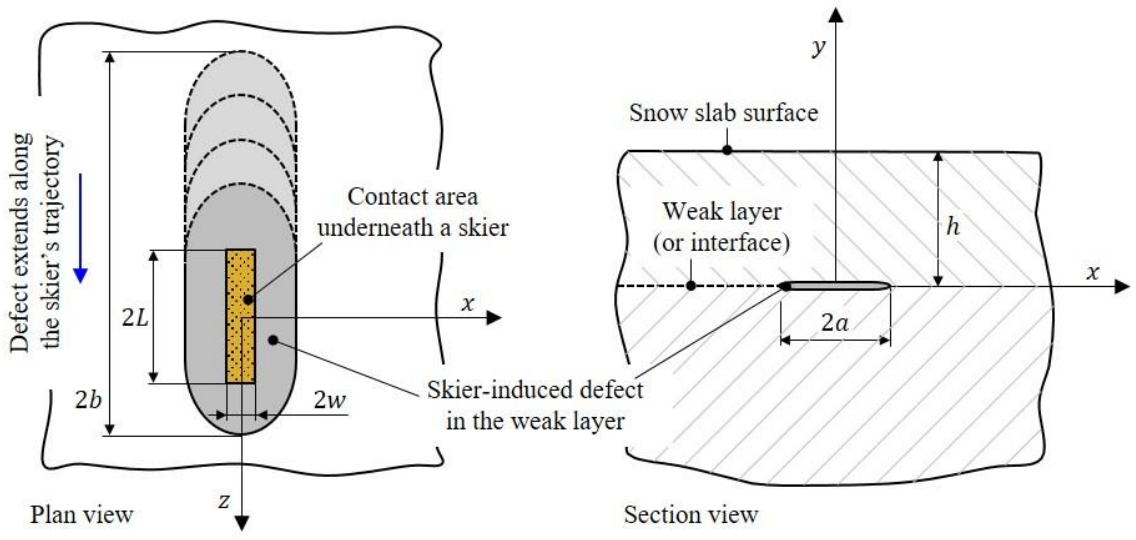

Fig. 1: Schematic representation of an elongated defect ($b \gg a$) induced in a buried weak layer by a skier travelling downslope.

The skier-induced defect can be idealized as a crack embedded within the snow-pack and fracture mechanics approaches may be utilized to identify the critical defect size required unstable failure of the weak layer. Several analytical and finite element fracture mechanical models have been developed in this context, notably the shear-slip model of McClung [1979], which assumes ductile crack propagation in pure mode II and the "anti-crack" model of Heierli et al. [2008], which permits both slope-parallel and slope normal displacements within the weak layer. However, it can be argued that these models are inadequate for analyzing the defect geometry shown in Fig. 1, as explained next.

Consider the simplified problem of an elliptical crack embedded in an elastic medium of infinite extent and subjected to uniform shear tractions along its major axis. The points along the crack front are subjected to a combination of mode II and mode III loading, with pure mode II loading at the two points which lie along the major axis of the crack and pure mode III loading at the two points which lie along its minor axis. Using the exact analytical solution, it can be shown that the ratio of the mode III stress intensity factor along the minor axis to mode II stress intensity factor along the major axis is proportional to $\sqrt{b/a}$, where b is the half-length of the crack along the major axis and a is the half-length along the minor axis [Saha and Roy, 2001].

This argument can also be extended to the present problem geometry in which a crack-like defect is embedded within the snow-pack and subjected to shear loading. The existing analytical models, which assume plane strain conditions (2D problem geometry) and consider failure of the weak layer in mode II, are indeed applicable for roughly circular shaped defects ($b \approx a$), or when the defects extend in the direction perpendicular to the shear loading ($a \gg b$). However, these models will provide a non-conservative assessment

of avalanche risk in the case of an elongated defect which extends along the direction of the shear loading ($b \gg a$) as shown in Fig.1. To address this gap, we formulate a conservative model in the present article and conduct the stress analysis of the problem within the two-dimensional anti-plane shear (mode III) formulation.

2. Modeling assumptions and problem formulation

Snow is a porous material with a complex microstructure and spatial variability in its material properties [Schweizer et al., 2003; Shapiro et al., 1997; Mellor, 1975]. There is also a significant variation in the material properties of snow over the depth of the snow-pack, attributed to the densification and the metamorphism of snow crystals [Jamieson and Johnston, 1999; Bradley et al., 1977]. Striving for simplicity, the snow-pack is idealized as a linearly elastic and brittle solid and the variations of the mechanical properties and density of the snow-pack are neglected. Although the deformation and failure of snow are highly rate and temperature-dependent, its behavior is largely elastic and brittle at high loading rates (dynamic loading) or low temperatures [Narita, 1980; Mellor, 1975]. Modelling of snow as a brittle, elastic and homogenous solid is quite common and normally required for the theoretical analysis of the problem.

The weak layer is idealized as an infinitesimally thin interface which experiences localized failure under the skier-induced loading. Experimental observations suggest that the nature of the initial localized failure within the weak layer is complex and depends upon the crystal structure of the weak layer, slope angle and loading rate [Reiweger et al., 2015; Reiweger and Schweizer, 2013; McClung and Schweizer, 1999]. Nonetheless, it is well known that weak layer failure mostly occurs by shear slip and that the shear strength of

snow increases proportionally with the normal compressive load [Reiweger et al., 2015; Jamieson and Johnston, 1998]. In order to identify the localized weak layer failure condition, the present study adopts the Mohr-Coulomb failure criterion since it reasonably describe the above mentioned experimentally observed trends. Other empirical failure criteria can also be implemented within the present framework, but at the expense of additional unknown material parameters. Another failure mechanism, mainly relevant to the failure of thick weak layers, is the crushing or collapse of the weak layer under compressive loading. The latter phenomenon is disregarded in the present study for simplicity reasons and is investigated elsewhere [Heierli et al., 2011; Heierli and Zaiser, 2008; Heierli et al., 2008].

The skier loading is idealized as a uniformly distributed normal load acting over a rectangular region on the surface of the snow slab. The skier's weight component parallel to the slope is neglected since the dynamic friction coefficient between the snow surface and the ski base is expected to be quite low [Mellor, 1975; Bowden and Hughes, 1939]. Although the skier loading is dynamic, Schweizer and Camponovo [2001] suggested that as a first approximation, it is appropriate to evaluate skier-induced stresses from the static elastic solution.

The stress analysis of the defect bearing snow pack is conducted within the two-dimensional anti-plane shear formulation. As shown in Fig. 1, the defect is idealized as a crack embedded in an elastic half-space and the disturbance in the stress state due to the presence of the crack is determined by solving an auxiliary problem in which the only external loads acting on the medium are the tractions applied to the crack surfaces. This is in accordance with Bueckner's superposition principle [Cartwright and Rooke, 1979;

105 Bueckner, 1958]. The variation of the elastic properties and density along the depth of the
106 snow pack can be incorporated into the present framework by modelling the snow-pack as
107 a layered medium and using the method presented by Khanna and Kotousov [2015].
108 However, this additional effort is outside the scope of the present article.

109 The critical defect size required for unstable failure initiation within the weak layer
110 is estimated using the brittle fracture criterion, i.e. when the strain energy release rate
111 exceeds the fracture energy of the material. Additional complexity may be introduced to
112 the current model by incorporating a process-zone of finite size around the crack tips, at
113 the expense of the introduction of additional fitting parameters [Bažant et al., 2003;
114 McClung, 2015, 1981, 1979]. Recent literature also reports the use of a volume-based strain
115 energy density approach to identify the brittle fracture conditions in a wide range of
116 materials under mixed-mode loading conditions [Berto and Lazzarin, 2014, 2009; Lazzarin
117 et al., 2009]. However, experimental data necessary to calibrate the models based on this
118 approach are lacking in the case of snow. The mathematical models for estimating the size
119 of the skier induced defect and the critical defect size required for unstable failure of the
120 weak layer are presented in following sections.

121 ## 3. Size of the skier-induced defect

122 The size of a skier induced defect would depend upon the strength of the weak layer
123 as well as the stress state within the weak layer. In order to determine the stress state, we
124 adopt an approach routinely utilized in civil engineering applications such as the design of
125 foundations and roadways [Selvadurai, 1979]. The snow slab is idealized as an elastic half-
126 space and only the slope normal component of the skier's weight is considered. The skier's

127 weight, mg, is uniformly distributed over a rectangular region of length $2L$ and width $2w$,
128 and the resulting normal stress on the slab surface is given by

$$\sigma_y(y=h) = \begin{cases} \sigma_o, & |x| \le w, |z| \le L, \\ 0, & |x| \le w, |z| \le L, \end{cases} \quad (1)$$

129 where $\sigma_o = mg\cos\theta/4Lw$ and θ is the slope angle. The corresponding stresses in the
130 interior of the slab are obtained by utilizing the fundamental solution for a concentrated
131 normal force acting on the boundary of an elastic half-space as the Green's function [Sadd,
132 2013]. The normal and shear stress components acting along the plane of the weak layer
133 ($y = 0$) under combined loading can be obtained as:

$$\sigma_y(y=0) = -\rho g h\cos\theta - \frac{3\sigma_o}{2\pi}\int_{-w}^{w}\int_{-L}^{L}\frac{h^3}{R^5}\,\mathrm{d}\xi\,\mathrm{d}\eta \quad (2)$$

$$\tau_{xy}(y=0) = -\frac{3\sigma_o}{2\pi}\int_{-w}^{w}\int_{-L}^{L}\frac{(x-\eta)h^2}{R^5}\,\mathrm{d}\xi\,\mathrm{d}\eta \quad (3)$$

$$\tau_{zy}(y=0) = -\rho g h\sin\theta - \frac{3\sigma_o}{2\pi}\int_{-w}^{w}\int_{-L}^{L}\frac{(z-\xi)h^2}{R^5}\,\mathrm{d}\xi\,\mathrm{d}\eta \quad (4)$$

134 where $R^2 = (x-\eta)^2+(z-\xi)^2 + h^2$, ρ is the density of the snow slab, h is the depth of
135 the weak layer from the slab surface and θ is the slope angle.

136 In order to identify the localized failure conditions within the weak layer, the Mohr-
137 Coulomb failure criterion is utilized. The failure criterion requires two material parameters,
138 namely the cohesive strength c, and the internal friction angle, ϕ of the weak layer.
139 Localized failure occurs by frictional slip if

$$|\tau| \ge c - \sigma\tan\phi \quad (5)$$

140 where σ and τ are the normal and shear stress components acting on the slip plane. It is
141 postulated that the slip plane must be aligned with the plane of the weak layer in order to

98

produce a defect at the macro-scale. Hence, the expression for normal stress given by Eq. (2) must be substituted into Eq. (5). For the shear stress component in Eq. (5), one must substitute the maximum shear stress acting on the slip plane, $y = 0$. Using stress transformation equations, the following simple expression for the maximum in-plane shear stress component is obtained

$$|\tau|_{\max} = \sqrt{\tau_{xy}^2 + \tau_{zy}^2}. \tag{6}$$

The right hand side of Eq. (6) is determined using Eqs. (3)-(4).

4. Critical defect size

The skier induced defect is idealized as a crack in an elastic half-plane subject to Mode III loading (see Fig. 1). The solutions for stresses and displacements near the crack tip and the critical defect size are obtained using the distributed dislocation technique. The displacement discontinuity along the crack faces is mathematically represented by a continuous distribution of screw dislocations. The unknown dislocation density is obtained in terms of the tractions prescribed along the crack line by solving a singular integral equation. The required solution for stress and displacement fields in the vicinity of the crack tip is then derived in terms of the dislocation density.

For the problem geometry shown in Fig. 1, the tractions arising on the crack faces due to the continuous distribution of dislocation can be obtained as follows [Erdogan and Gupta, 1971]

$$\hat{\sigma}_{yz}(s,0) = \frac{2\mu}{\pi}\int_{-1}^{1}\frac{b(t)\mathrm{d}t}{t-s} + \frac{2\mu}{\pi}\int_{-1}^{1}k(s,t)b(t)\mathrm{d}t\,, \quad |s|<1, \tag{7}$$

where $s = x/a$ is the normalized coordinate along the crack length, t is a dummy integration variable, $b(t) = \mathrm{d}B_z(t)/\mathrm{d}t$ is the dislocation density and $k(s,t)$ is given by the Fourier integral

$$k(s,t) = -a\int_{0}^{\infty} e^{-2\xi h}\sin\xi a(t-s)\,\mathrm{d}\xi = -\frac{(t-s)}{(t-s)^2+4(h/a)^2}. \tag{8}$$

The tractions along the crack faces due to the external loading can be obtained as $\bar{\sigma}_{yz}(s,0) = \tau_o = \rho g h\sin\theta$. The requirement of no-net tractions along the crack faces, i.e. $\hat{\sigma}_{yz}(s,0) + \bar{\sigma}_{yz}(s,0) = 0$, yields the integral equation for the unknown dislocation density as follows

$$\frac{1}{\pi}\int_{-1}^{1}\frac{b(t)\mathrm{d}t}{t-s} + \frac{1}{\pi}\int_{-1}^{1}k(s,t)b(t)\mathrm{d}t = \frac{2\tau_o}{\mu}, \quad |s|<1, \tag{9}$$

Eq. (9) must be solved under the following single-valuedness condition

$$\int_{-1}^{1} b(t)\mathrm{d}t = 0. \tag{10}$$

which represents the requirement of the continuity of displacements for $|s|>1$. The unknown dislocation density can be written as

$$b(s) = \omega(s)R(s), \tag{11}$$

such that aside from the analytic function $\omega(s)$, the behavior of $b(s)$ around $|s|=1$ is entirely determined by the fundamental function of the singular integral equation, $R(s)$. Since the crack opening displacement is parabolic in form rather than a cusp, at $s=\pm 1$, the dislocation density $b(s)$ must have a singularity. The latter situation arises when the stresses at the crack tips are finite, which is typical for various cohesive zone models

175 [Palmer and Rice, 1973; Barenblatt, 1962; Dugdale, 1960]. The appropriate form of the
176 function $R(s)$ is given by Erdogan and Gupta [1971] as

$$R(s) = (1 - s^2)^{-\frac{1}{2}}. \tag{12}$$

177 The Gauss-Chebyshev quadrature formulae for singular integrals can be employed to
178 reduce the singular integral equation of first kind, Eq. (9) and the side condition, Eq. (10)
179 to a linear system of algebraic equations [Erdogan et al., 1973; Hills et al., 1996]. For the
180 choice of fundamental function (singular at both ends), Eqs. (9) and (10) can be reduced to
181 the following algebraic system

$$\frac{2\tau_o}{\mu} = \frac{1}{N}\sum_{i=1}^{N} \omega(t_i)\left[\frac{1}{t_i - s_k} + ak(s_k, t_i)\right], \quad k = 1, \dots, N-1, \tag{13}$$

$$\frac{\pi}{N}\sum_{i=1}^{N} \omega(t_i) = 0\,, \tag{14}$$

182 where the set of N discrete integration points are given by

$$t_i = \cos\left(\pi\frac{2i-1}{2N}\right), \quad i = 1, \dots, N, \tag{15}$$

183 and the $N-1$ collocation points are given by

$$s_k = \cos\left(\pi\frac{k}{N}\right), \quad k = 1, \dots, N-1. \tag{16}$$

184 The system of algebraic Eqs. (13)-(14) can be solved, for example, by Gaussian elimination
185 to obtain a solution for the analytic function ω at discrete integration points, t_i. The mode
186 III stress intensity factor may be obtained in terms of the solution as [Hills et al., 1996]

$$K_{\mathrm{III}} = \frac{\mu}{2}\sqrt{\pi a}\,\omega(+1), \tag{17}$$

187 where the value of ω at the end-point $s = +1$ may be evaluated by using the interpolation
188 formula [Krenk, 1975]

$$\omega(+1) = \frac{1}{N}\sum_{i=1}^{N} \frac{\sin\left[\frac{\pi}{4N}(2i-1)(2N-1)\right]}{\sin\left[\frac{\pi}{4N}(2i-1)\right]}\omega(t_i)\,. \tag{18}$$

The energy release rate is related to the mode III stress intensity factor according to $G = K_{\mathrm{III}}^2/2\mu$ [Hills et al., 1996]. Based on the brittle fracture mechanics criteria, unstable crack propagation occurs when the energy release rate, G exceeds the specific fracture energy of the material G_c. Using Eq. (17), the critical crack length required for unstable crack propagation may then be expressed as

$$a_{\mathrm{cr}} = \frac{8G_c}{\pi\mu\omega^2(+1)}. \tag{19}$$

where $\omega(+1)$ can be calculated using Eq. (18). The critical crack length obtained using Eq. (19) can be used to identify the threshold strength of the weak layer, below which catastrophic failure is imminent.

5. Parametric study

In the following numerical calculations, the shear modulus and Poisson's ratio of the slab are set at $\mu = 1$ MPa and $\nu = 0.2$, respectively [Mellor, 1975]. The density of the slab is taken as $\rho = 200$ kg/m^3 and the slope angle $\theta = 40°$ [Perla, 1977]. The skier load defined in Eq. (1) is taken as $\sigma_o = 2$ kPa, which roughly corresponds to a skier of mass $m = 95$ kg, a ski area of 1.8 m × 0.2 m and a slope angle, $\theta = 40°$. The in-situ values of the strength and fracture resistance of the weak layer vary considerably due to their strong dependence on the weak layer microstructure. Therefore, an extensive parametric study is conducted in terms of these model variables.

Table 1. Critical defect size, a_{cr} (m) calculated using Eq. (19)

Weak layer depth, h (m)	Weak layer fracture energy, G_c (J/m^2)		
	0.01	0.05	0.10
0.1	0.241	0.653	0.970
0.3	0.044	0.203	0.356
0.5	0.016	0.079	0.156
1.0	0.004	0.020	0.040

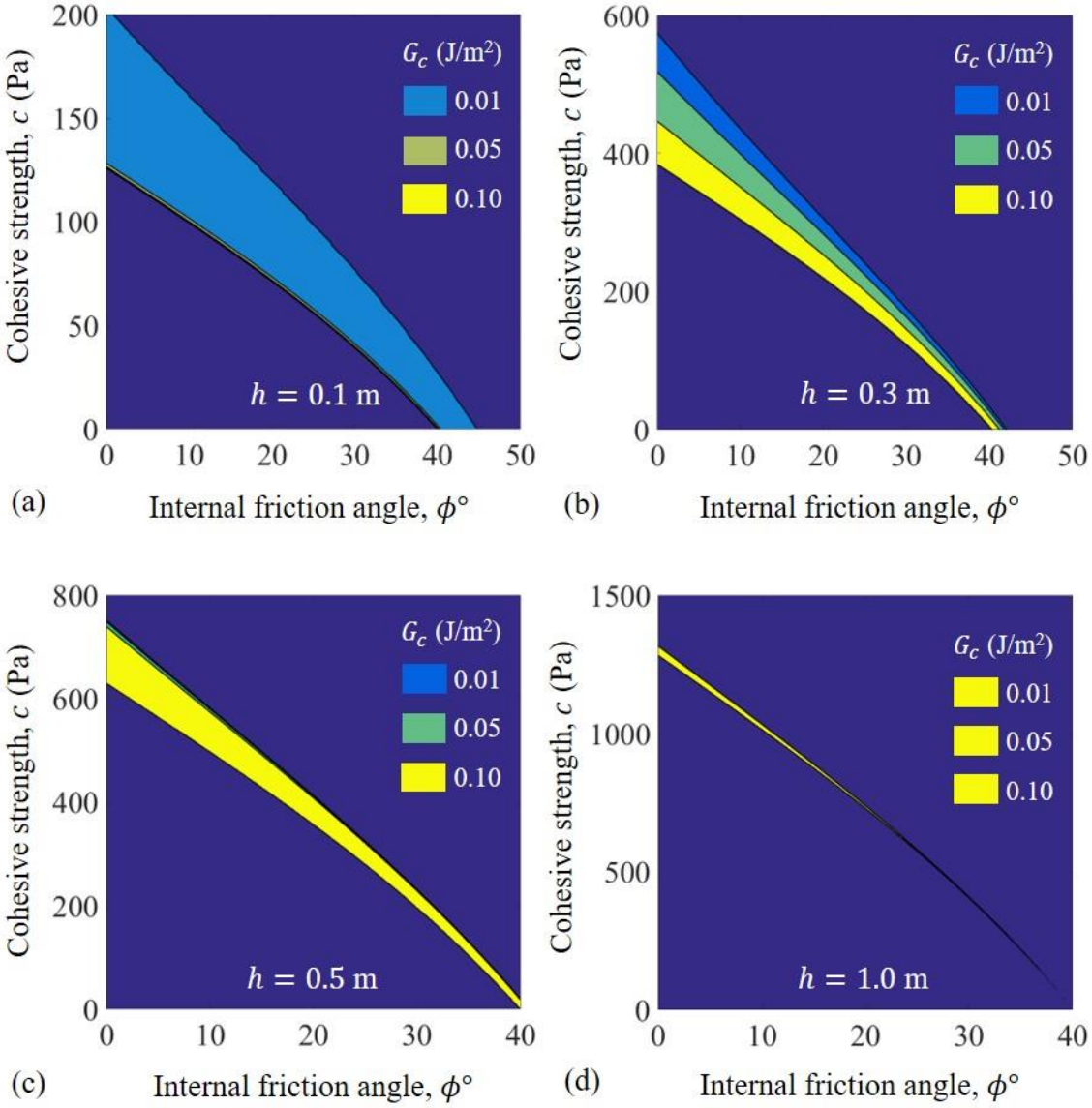

Fig. 2: Combinations of the weak layer strength parameters, c and ϕ which allow for the skier-induced defect to reach the critical size for avalanche onset.

212 Firstly, the critical defect size, a_{cr} is evaluated for various values of the weak layer
213 depth, h and the fracture energy, G_c using Eq. (19). The range of values selected for h and
214 G_c are representative of typical field measurements [Schweizer et al., 2011]. The calculated
215 values of a_{cr} are reported in Table 1 and span two orders of magnitude. As expected, the
216 critical defect size gets smaller with increasing depth and decreasing fracture energy. After
217 that, all possible combinations of c and ϕ are identified which allow for the skier-induced
218 defect to reach a size $a \geq a_{\mathrm{cr}}$. The results of the parametric study are presented in Figs. 2a-
219 d. In producing these figures, combinations of c and ϕ which lead to complete failure of
220 the weak layer under self-weight are ignored.
221 In the following discussion, the term 'failure' and 'failure onset' are used to
222 describe the unstable propagation of the skier-induced defect within the weak layer under
223 mode III conditions. The purple region in Figs. 2a-d indicates that failure does not occur
224 for that particular combination of c and ϕ. In all four sub-figures, the region corresponding
225 to failure at $G_c = 0.01$ J/m^2 is the largest and the region corresponding to failure at $G_c =$
226 0.1 J/m^2 is the smallest. The overlap of the various failure regions is quite obvious in Fig.
227 2b, but indistinguishable in Figs. 2a, c and d. For a particular combination of weak layer
228 depth and fracture energy, area of the failure region on the $c - \phi$ graph has a positive
229 correlation with the likelihood of failure. This is because a large area of the failure region
230 implies that failure can take place for a wide range of values c and ϕ in turn making it more
231 likely. The general tendencies which can be deduced from Figs. 2a-d are:
232 1. The failure onset in shallow weak layers requires the cohesive strength to be much
233 lower in comparison with weak layers which are buried deeper.

104

2. Failure onset is more likely at small values of the weak layer fracture energy. However, the influence of the weak layer fracture energy on the likelihood of failure diminishes with increasing depth of the weak layer.
3. Irrespective of the value of the weak layer fracture energy, the likelihood of failure onset first increases with increasing weak layer depth, but then decreases. This trend is in agreement with field observations of several hundred skier-triggered avalanche events reported in Herwijnen and Jamieson [2007] and Schweizer and Jamieson [2000].

The authors were unable to find experimental results or observations, which would confirm the first two general tendencies predicted by the analytical model. These might form a scope for future post-avalanche observations or experimental studies.

6. Conclusion

A new model for avalanche onset due to the skier-triggered failure of a buried weak layer is proposed. The model does not assume a pre-existing defect or deficit zone within the weak layer, but it instead incorporates the skier-induced defect into failure initiation conditions. A parametric study is conducted to demonstrate the plausibility of the proposed model and identify the conditions favorable for avalanche onset.

There is room for further analysis of the skier-triggered avalanche phenomenon based on the present model. For instance, the influence of snow densification on the likelihood of avalanche onset can be investigated in a future study. To facilitate such efforts, the computer routine used to obtain the results in Section 5 has been included in

255 the supplementary document. Refinement of the present model by removing some of its
256 simplifying assumptions would probably increase its accuracy as a predictive tool.

257 Acknowledgements

258 All experimental data used in this paper is properly cited and available in the cited
259 references. The numerical information provided in the figures is produced by solving the
260 equations in this paper.

References

Barenblatt, G.I. (1962), The mathematical theory of equilibrium cracks in brittle fracture, in Advances in applied mechanics, vol. 7, edited by H.L. Dryden and T. von Kàrmàn, pp. 55-129, Academic Press, New York.

Bažant, Z.P., G. Zi and D. McClung (2003), Size effect law and fracture mechanics of the triggering of dry snow slab avalanches, J. Geophys. Res., 108(B2), 2119, doi: 10.1029/2002JB001884.

Berto, F., and P.Lazzarin. (2014), Recent developments in brittle and quasi-brittle failure assessment of engineering materials by means of local approaches, Mater. Sci. Eng., R., 75, 1-48, doi: 10.1016/j.mser.2013.11.001.

Berto, F., and P.Lazzarin. (2009), A review of the volume-based strain energy density approach applied to V-notches and welded structures, Theor. Appl. Fract. Mech., 52(3), 183-194, doi: 10.1016/j.tafmec.2009.10.001.

Bueckner, H.F. (1958), The propagation of cracks and energy of elastic deformation, J. Appl. Mech., 80, 1225-1230.

Bowden, F.P., and T.P. Hughes (1939), The mechanism of sliding on ice and snow, Proc. R. Soc. Lond. Ser. A, 172 (949), 280-298.

Bradley, C.C., P.L. Brown and T.R. Williams (1977), Gradient metamorphism, zonal weakening of snow-pack and avalanche initiation, J. Glaciol. 12(81), 335-341.

Cartwright, D.J., and D.P. Rooke, (1979), Green's functions in fracture mechanics, in Fracture Mechanics: Current Status, Future Prospects, edited by R.A. Smith, pp. 91-123, Pergamon, Oxford.

Dugdale, D.S. (1960), Yielding of steel sheets containing slits, J. Mech. Phys. Solids, 8(2), pp. 100-104.

Erdogan, F., G.D. Gupta and T.S. Cook (1973) Numerical solution of singular integral equations, in Mechanics of Fracture, vol. 1, edited by G.C. Sih, pp. 368-425, Noordhoff International, Leyden, The Netherlands.

Erdogan, F., and G. Gupta (1971), The stress analysis of multi-layered composites with a flaw, Int. J. Solids Struct., 7(1), pp. 39-61, doi: 10.1016/0020-7683(71)90017-5.

Heierli, J., K.W. Birkeland, R. Simenhois and P. Gumbsch (2011), Anticrack model for skier triggering of slab avalanches, Cold Reg. Sci. Technol., 65(3), 372-381, doi: 10.1016/j.coldregions.2010.10.008.

293 Heierli, J., and M. Zaiser (2008), Failure initiation in snow stratifications containing weak
294 layers: Nucleation of whumpfs and slab avalanches, Cold Reg. Sci. Technol., 52 (3), 385-
295 400, doi: 10.1016/j.coldregions.2007.02.007.

296 Heierli, J., P. Gumbsch and M. Zaiser (2008), Anticrack nucleation as triggering
297 mechanism for snow slab avalanches, Science, 321, 240-243, doi:
298 10.1126/science.1153948.

299 Hills, D.A., P.A. Kelly, D.N. Dai and A.M. Korsunsky (1996), Solution of crack
300 problems: the distributed dislocation technique, Kluwer Academic Publishers, Dordrecht,
301 The Netherlands.

302 Jamieson, B., and C.D. Johnston (1999), Snowpack factors associated with strength
303 changes of buried surface hoar layers, Cold Reg. Sci. Technol., 30(1-3), 19-34, doi:
304 10.1016/S0165-232X(99)00026-9.

305 Jamieson, B., and C. Johnston (1998), Refinements to the stability index for skier-
306 triggered dry-slab avalanches, Ann. Glaciol., 26, 296-302.

307 Khanna, A., and A. Kotousov (2015), The stress field due to an interfacial edge
308 dislocation in a multi-layered medium, Int. J. Solids Struct., 72, 1-10, doi:
309 10.1016/j.ijsolstr.2015.06.030.

310 Krenk, S. (1975), On the use of the interpolation polynomial for solutions of singular
311 integral equations, Quart. Appl. Math., 32, 479-484.

312 Lazzarin, P., F. Berto, M. Elices and J. Gómez (2009), Brittle failures from U- and V-
313 notches in mode I and mixed, I + II, mode: a synthesis based on the strain energy density
314 averaged on finite-size volumes, Fatigue Fract. Eng. Mater. Struct., 32(8), 671-684, doi:
315 10.1111/j.1460-2695.2009.01373.x.

316 McClung, D.M. (2015), Mode II fracture parameters of dry snow slab avalanche weak
317 layers calculated from the cohesive crack model, Int. J. Fract., 193(2), 153-169, doi:
318 10.1007/s10704-015-0026-1.

319 McClung, D.M. (1981), Fracture mechanical models of dry slab avalanche release, J.
320 Geophys. Res., 86(B11), 10783-10790, doi: 10.1029/JB086iB11p10783.

321 McClung, D.M. (1979), Shear fracture precipitated by strain softening as a mechanism of
322 dry slab avalanche release, J. Geophys. Res., 84(B7), 3519-3525, doi:
323 10.1029/JB084iB07p03519.

324 McClung, D.M., and J. Schweizer (1999), Skier triggering, snow temperatures and the
325 stability index for dry-slab avalanche initiation, J. Glaciol., 45(150), 190-200.

326 Mellor, M. (1975), A review of basic snow mechanics, IAHS Publ., 114, 251-291.

Narita, H. (1980), Mechanical behaviour and structure of snow under uniaxial tensile stress, J. Glaciol., 26(94), 275-282.

Palmer, A.C., and J.R. Rice (1973), The growth of slip surfaces in the progressive failure of over-consolidated clay, Proc. R. Soc. Lond. Ser. A., 332, 527-548.

Perla, R. (1977), Slab avalanche measurements, Can. Geotech. J., 14(2), 206-213, doi: 10.1139/t77-021.

Reiweger, I., J. Gaume and J. Schweizer (2015), A new mixed-mode failure criterion for weak snowpack layers, Geophys. Res. Lett., 42(5), 1427-1432, doi: 10.1002/2014GL062780.

Reiweger, I., and J. Schweizer, Weak layer fracture: facets and depth hoar, Cryosphere, 7, 1447-1453, doi: 10.5194/tc-7-1447-2013

Sadd, M.H. (2013), Elasticity: Theory, Applications, and Numerics (Third Edition), Academic Press, doi: 10.1016/B978-0-12-408136-9.01001-1.

Saha, T.K., and A. Roy (2001), Weight function for an elliptic crack in an infinite medium - II. Shear loading, Int. J. Fract. 112 (1), 1-21, doi: 10.1023/A:1013527528837.

Selvadurai, A.P.S. (1979), Elastic Analysis of Soil-Foundation Interaction, Elsevier, Amsterdam, The Netherlands.

Schweizer, J., A. van Herwijnen and B. Reuter (2011), Measurements of weak layer fracture energy, Cold Reg. Sci. Technol., 69(2-3), 139-144, doi: 10.1016/j.coldregions.2011.06.004.

Schweizer, J., J.B. Jamieson and M. Schneebeli (2003), Snow avalanche formation, Rev. Geophys., 41(4), 1016, doi: 10.1029/2002RG000123.

Schweizer, J., and C. Camponovo (2001), The skier's zone of influence in triggering slab avalanches, Ann. Glaciol., 32(1), 314-320, doi: 10.3189/172756401781819300.

Schweizer, J., and J.B. Jamieson (2000), Field observations of skier-triggered avalanches, Proceedings International Snow Science Workshop, Big Sky, Montana, U.S.A., 2-6 October 2000.

Sigrist, C., and J. Schweizer (2007), Critical energy release rates of weak snowpack layers determined in field experiments, Geophys. Res. Lett., 34, L03502, doi: 10.1029/2006GL028576.

Shapiro, L.H., J.B. Johnson, M. Sturm and G.L. Blaisdell (1997), Snow mechanics: Review of the state of knowledge and applications, Rep. 97-3, U.S. Army Cold Reg. Res. Eng. Lab., Hanover, NH.

van Herwijnen, A., and B. Jamieson (2007), Snowpack properties associated with fracture initiation and propagation resulting in skier-triggered dry snow slab avalanches, Cold Reg. Sci. Technol., 50(1-3), 13-22, doi: 10.1016/j.coldregions.2007.02.004.

Geophysical Research Letters

Supporting Information for

A new predictive model for the onset of skier-triggered avalanches

A. Khanna[1], and A. Kotousov[1]

[1]School of Mechanical Engineering, The University of Adelaide, Adelaide, Australia, SA 5005.

Contents of this file

Introduction

The rigidity of the rocky substratum is several orders of magnitudes higher than the rigidity of the snowpack. For a weak layer located very close to the rocky substratum, the strong mismatch in the elastic properties would significantly affect the size of the skier induced defect or the critical defect size required for avalanche release. Within this supplementary document, we derive the elastic solutions which were incorporated in the present models to account for the presence of the rigid substratum. In these solutions, the snowpack is idealized as an elastic layer bonded to a rigid substratum.

In Section S1, we develop a solution for stresses in the elastic layer due to a concentrated line load acting normal to its free surface. This solution is used within Section 3 of the main article to obtain the size of the skier induced defect in the weak layer. In Section S2, we obtain the solution for stresses due to a screw dislocation for the same geometry. The latter solution is utilized within the framework of the Distributed Dislocation Technique to model the anti-plane crack in Section 4 of the main article.

Text S1. Stresses in an elastic layer bonded to a rigid substrate and subjected to a concentrated line load perpendicular to its free surface

Following the general approach presented in [Khanna and Kotousov, 2015] the solution to the plane problem of interest is obtained by superposing the solutions to two auxiliary problems, as shown in Fig. S1. Problem 1 involves finding the displacement gradient along $y = h$ due to a concentrated line load acting normal to the surface of an elastic half-plane. Problem 2 involves finding the corrective stresses which yield displacement gradients equal in magnitude and opposite to those obtained in Problem 1 along $y = h$ and which satisfy traction-free boundary condition is specified along $y = 0$. The solution approach utilizes the Airy's stress function formulation and Fourier transform techniques.

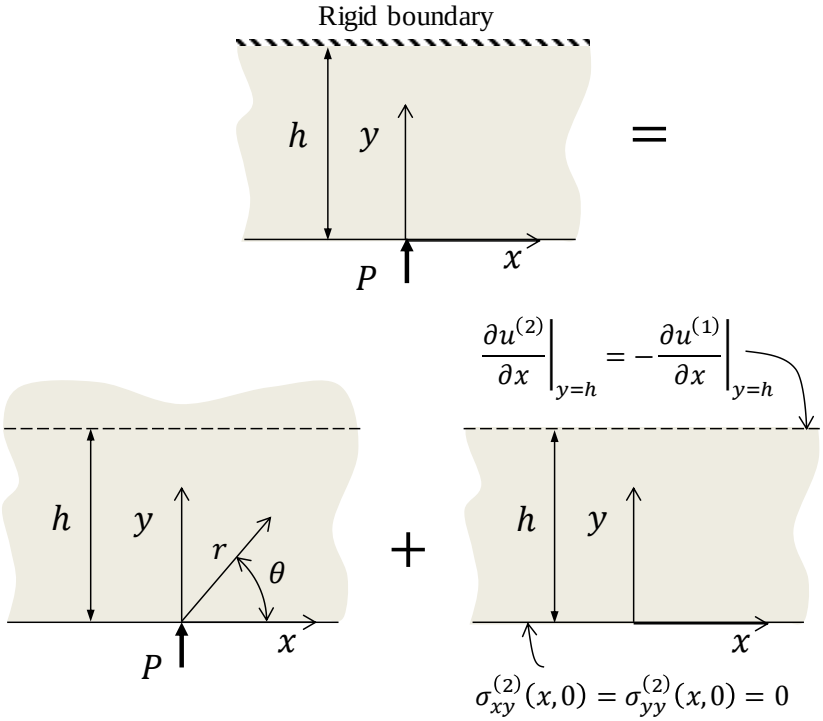

Figure S1. Principle of superposition applied to the plane problem an elastic layer bonded to a rigid substrate and subjected to a concentrated line load.

The solution to Problem 1 is derived from the fundamental solution for a wedge loaded by a force at its vertex, which was originally obtained by Flamant in 1892. In accordance with Barber [2010] the Airy's stress function for Problem 1 is

$$\Phi^{(1)} = -\frac{P}{\pi} r\theta \cos\theta = -\frac{P}{\pi} x \tan^{-1}\left(\frac{y}{x}\right). \tag{S1}$$

The corresponding stresses are

$$\sigma_{xx}^{(1)} = -\frac{2Px^2y}{\pi(x^2+y^2)^2}, \quad \sigma_{yy}^{(1)} = -\frac{2Py^3}{\pi(x^2+y^2)^2}, \quad \sigma_{xy}^{(1)} = -\frac{2Pxy^2}{\pi(x^2+y^2)^2}. \tag{S2}$$

Using Hooke's law to find the strains and then integrating, the displacement field can be obtained, correct to a constant, as

$$2\mu u_x^{(1)} = -\frac{P}{2\pi}\left\{(\kappa-1)\tan^{-1}\left(\frac{x}{y}\right) - \frac{2xy}{x^2+y^2}\right\}, \tag{S3}$$

$$2\mu u_y^{(1)} = -\frac{P}{2\pi}\left\{\frac{2x^2}{x^2+y^2} + \frac{(\kappa+1)}{2}\log(x^2+y^2)\right\}, \tag{S4}$$

where μ is the shear modulus of the elastic layer and κ is Kolosov's constant. These elastic constants can be related to the Young's modulus E and Poisson's ratio ν of the layer according to:

$$\mu = \frac{E}{2(1+\nu)}, \tag{S5}$$

$$\kappa = \begin{cases} 3-4\nu, & \text{in plane strain,} \\ \dfrac{3-\nu}{1+\nu}, & \text{in plane stress.} \end{cases} \tag{S6}$$

In the present problem it is convenient to express the displacements in gradient form to remove constants associated with the rigid body motion. The corresponding displacement gradients are

$$\frac{\partial u_x^{(1)}}{\partial x} = -\frac{P}{4\pi\mu}\frac{y}{(x^2+y^2)^2}\{(\kappa+1)x^2 + (\kappa-3)y^2\}, \tag{S7}$$

$$\frac{\partial u_y^{(1)}}{\partial x} = -\frac{P}{4\pi\mu}\frac{x}{(x^2+y^2)^2}\{(\kappa+1)x^2 + (\kappa+5)y^2\}. \tag{S8}$$

The solution to Problem 2 can be obtained by using Fourier transform techniques. The appropriate Airy's stress function, which satisfies the biharmonic equation can be written as the Fourier integral

$$\Phi^{(2)} = \frac{P}{4\pi}\int_0^\infty \left[\left(\frac{A}{\xi^2}+\frac{B}{\xi}y\right)e^{-\xi y} + \left(\frac{C}{\xi^2}+\frac{D}{\xi}y\right)e^{\xi y}\right]\cos(\xi x)\,d\xi. \tag{S9}$$

From (S9), the corrective stresses can be obtained as

$$\sigma_{xx}^{(2)} = \frac{P}{4\pi}\int_0^\infty \left[(A+(\xi y-2)B)e^{-\xi y} + (C+(\xi y+2)D)e^{\xi y}\right]\cos(\xi x)\,d\xi, \tag{S10}$$

$$\sigma_{yy}^{(2)} = -\frac{P}{4\pi}\int_0^\infty \left[(A+\xi y B)e^{-\xi y} + (C+\xi y D)e^{\xi y}\right]\cos(\xi x)\,d\xi, \tag{S11}$$

$$\sigma_{xy}^{(2)} = \frac{P}{4\pi}\int_0^\infty \left[(-A+(1-\xi y)B)e^{-\xi y} + (C+(1+\xi y)D)e^{\xi y}\right]\sin(\xi x)\,d\xi. \tag{S12}$$

The corresponding displacement components are given in the gradient form as

$$\frac{\partial u_x^{(2)}}{\partial x} = \frac{1}{2\mu}\frac{P}{4\pi}\int_0^\infty \left[\left(A+\left(\xi y-\frac{\kappa+1}{2}\right)B\right)e^{-\xi y} + \left(C+\left(\xi y+\frac{\kappa+1}{2}\right)D\right)e^{\xi y}\right]\cos(\xi x)\,d\xi, \tag{S13}$$

$$\frac{\partial u_y^{(2)}}{\partial x} = \frac{1}{2\mu}\frac{P}{4\pi}\int_0^\infty \left[\left(-A+\left(1-\xi y-\frac{\kappa+1}{2}\right)B\right)e^{-\xi y} + \left(C+\left(1+\xi y-\frac{\kappa+1}{2}\right)D\right)e^{\xi y}\right]\sin(\xi x)\,d\xi. \tag{S14}$$

The unknown constants A, B, C and D can be determined using the appropriate boundary conditions along $y = 0$ and $y = h$. Since the stresses and displacements corresponding to Problem 2 are given in terms of Fourier integrals, the boundary conditions can be expressed in the Fourier domain to obtain a system of linear equations in terms of the unknown constants. The traction-free boundary condition along $y = 0$ can be written as

$$\tilde{\sigma}_{yy}^{(2)}(x,0) = 0, \tag{S15}$$

$$\tilde{\sigma}_{xy}^{(2)}(x,0) = 0, \tag{S16}$$

where the tilde over-bar represents the Fourier transform with respect to the variable x. The displacement boundary condition along $y = h$ can be written in the Fourier domain as

$$\frac{\partial \tilde{u}_x^{(2)}}{\partial x}(x,h) = -\frac{\partial \tilde{u}_x^{(1)}}{\partial x}(x,h), \tag{S17}$$

$$\frac{\partial \tilde{u}_y^{(2)}}{\partial x}(x,h) = -\frac{\partial \tilde{u}_y^{(1)}}{\partial x}(x,h). \tag{S18}$$

Substituting Eqs. (S11) and (S12) into boundary conditions (S15) and (S16), respectively yields

$$-A - C = 0, \tag{S19}$$

$$-A + B + C + D = 0. \tag{S20}$$

Similarly, substituting Eqs. (S13) and (S7) into (S17) yields

$$\begin{aligned} \frac{1}{2\mu}\frac{P}{4\pi}\left[\left(A + \left(\xi h - \frac{\kappa+1}{2}\right)B\right)e^{-\xi h} + \left(C + \left(\xi h + \frac{\kappa+1}{2}\right)D\right)e^{\xi h}\right] \\ = -\frac{\partial \tilde{u}_x^{(1)}}{\partial x}(x,h), \end{aligned} \tag{S21}$$

and substituting Eqs. (S14) and (S8) into (S18) results in

$$\begin{aligned} \frac{1}{2\mu}\frac{P}{4\pi}\left[\left(-A + \left(1 - \xi h - \frac{\kappa+1}{2}\right)B\right)e^{-\xi h} + \left(C + \left(1 + \xi h - \frac{\kappa+1}{2}\right)D\right)e^{\xi h}\right] \\ = -\frac{\partial \tilde{u}_y^{(1)}}{\partial x}(x,h). \end{aligned} \tag{S22}$$

The right hand side of Eqs. (S21)-(S22) can be obtained as

$$\begin{aligned} \frac{\partial \tilde{u}_x^{(1)}}{\partial x}(x,h) &= \frac{2}{\pi}\int_0^\infty \frac{\partial u_x^{(1)}}{\partial x}(x,h)\cos(\xi x)\,dx \\ &= -\frac{1}{2\mu}\frac{P}{4\pi}\{(\kappa+1)(2-\xi h)h + (\kappa-3)(1+\xi h)\}e^{-\xi h}, \end{aligned} \tag{S23}$$

$$\begin{aligned} \frac{\partial \tilde{u}_y^{(1)}}{\partial x}(x,h) &= \frac{2}{\pi}\int_0^\infty \frac{\partial u_y^{(1)}}{\partial x}(x,h)\sin(\xi x)\,dx \\ &= -\frac{1}{2\mu}\frac{P}{4\pi}\{(\kappa+1)(2-\xi h) + (\kappa+5)\xi h\}e^{-\xi h}. \end{aligned} \tag{S24}$$

Eqs. (S21)-(S22) can be further simplified to

$$e^{-2\xi h}A + \left(\xi h - \frac{\kappa+1}{2}\right)e^{-2\xi h}B + C + \left(\xi h + \frac{\kappa+1}{2}\right)D = \{(\kappa+1)(2-\xi h)h + (\kappa-3)(1+\xi h)\}e^{-2\xi h}, \tag{S25}$$

$$-e^{-2\xi h}A + \left(1 - \xi h - \frac{\kappa+1}{2}\right)e^{-2\xi h}B + C + \left(1 + \xi h - \frac{\kappa+1}{2}\right)D = \{(\kappa+1)(2-\xi h) + (\kappa+5)\xi h\}e^{-2\xi h}. \tag{S26}$$

Together, Eqs. (S19), (S20), (S25) and (S26) form a system of four linear equations which can be solved to find the unknown constants in the general solution for $\Phi^{(2)}(x,y)$. The solution to the problem under consideration is given by $\Phi = \Phi^{(1)} + \Phi^{(2)}$. In particular, the normal compressive stress at the location of the weak layer, $\sigma_{yy}(x,h_1)$ can be obtained from Eqs. (S2) and (S11) as

$$\sigma_{yy}(x,h_1) = -\frac{2Ph_1^3}{\pi(x^2+h_1^2)^2} - \frac{P}{4\pi}\int_0^\infty \left[(A+\xi h_1 B)e^{-\xi h_1} + (C+\xi h_1 D)e^{\xi h_1}\right]\cos(\xi x)\,d\xi. \tag{S27}$$

Text S2. Stresses due to a screw dislocation in an elastic layer bonded to a rigid substrate

A screw dislocation in an elastic layer produces a two-dimensional stress state, in which the in-plane displacements, u_x,u_y are zero everywhere, while the out-of-plane displacement, u_z is independent of the z-coordinate. The non-zero stress components are related to the out-of-plane displacement according to

$$\sigma_{xz} = \mu\frac{\partial u_z}{\partial x}, \quad \sigma_{yz} = \mu\frac{\partial u_z}{\partial y}. \tag{S28}$$

In the absence of body forces, the out-of-plane displacement must satisfy the Laplace equation, i.e.

$$\nabla^2 u_z = 0, \tag{S29}$$

to ensure that the stresses given by Eq. (S28) satisfy the three-dimensional equilibrium equations. Such a stress state is known as anti-plane shear.

The solution to this problem proceeds in the same manner as the solution obtain in Section S1. The principle of superposition is used to decompose the problem under consideration into two auxiliary problems, as illustrated in Fig. S2.

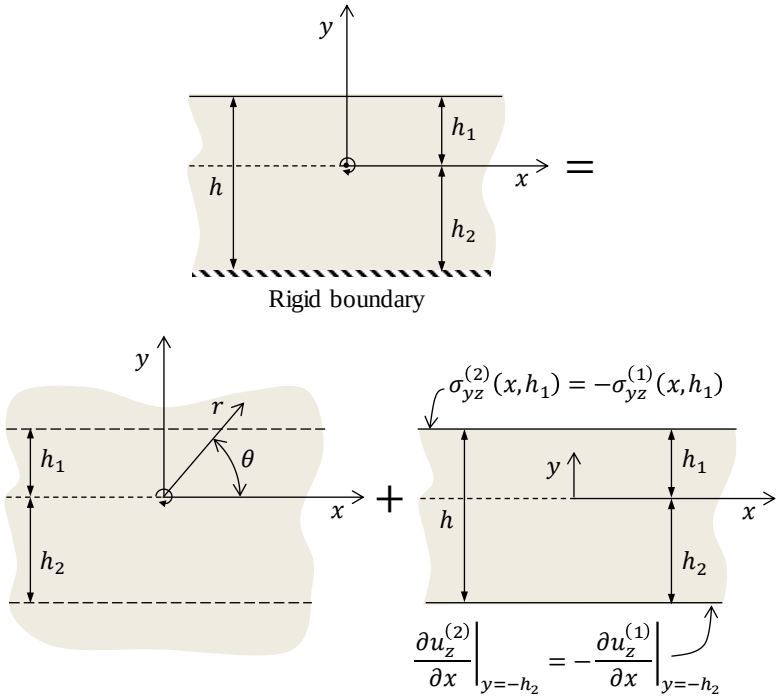

Problem 1: Screw dislocation in an infinite space

Problem 2: Boundary-value problem on an elastic strip

Figure S2. Notation for the bonded multi-layered medium.

Problem 1 considers a screw dislocation in an infinite body, which represents a cut along $x > 0, y = 0$, such that the two faces of the cut experience a relative out-of-plane displacement, $u_z^{(1)}(r,0) - u_z^{(1)}(r,2\pi) = B_z$. A suitable solution which satisfies Eq. (S29) is given by [Barber, 2010]

$$u_z^{(1)} = \frac{B_z}{2\pi}\tan^{-1}\left(\frac{y}{x}\right), \quad \sigma_{xz}^{(1)} = -\frac{\mu B_z}{2\pi}\frac{y}{x^2+y^2}, \quad \sigma_{yz}^{(1)} = \frac{\mu B_z}{2\pi}\frac{x}{x^2+y^2}. \tag{S30}$$

From Eq. (S30), we obtain the out-of-plane shear component at $y = h_1$ as

$$\sigma_{yz}^{(1)}(x,h_1) = \frac{\mu B_z}{2\pi}\frac{x}{x^2+h_1^2}, \tag{S31}$$

and the out-of-plane displacement at $y = -h_2$ in gradient form as

$$\frac{\partial}{\partial x}u_z^{(1)}(x,-h_2) = \frac{B_z}{2\pi}\frac{h_2}{x^2+h_2^2}. \tag{S32}$$

The general solution for Problem 2 can be obtained using Fourier transform techniques as before, in this case by taking the Fourier transform of Eq. (S29) and solving

the resulting ordinary differential equation. Only the skew-symmetric (odd) part of the general solution needs to be considered, i.e.

$$u_z^{(2)}(x,y) = \frac{2}{\pi}\int_0^\infty \left(Ae^{\xi y} + Be^{-\xi y}\right)\sin(\xi x)\,d\xi. \tag{S33}$$

By differentiating Eq. (S33), we obtain

$$\sigma_{yz}^{(2)}(x,h_1) = \frac{2\mu}{\pi}\int_0^\infty \xi\left(Ae^{\xi h_1} - Be^{-\xi h_1}\right)\sin(\xi x)\,d\xi, \tag{S34}$$

and

$$\frac{\partial}{\partial x}u_z^{(2)}(x,-h_2) = \frac{2}{\pi}\int_0^\infty \xi\left(Ae^{-\xi h_2} + Be^{\xi h_2}\right)\cos(\xi x)\,d\xi. \tag{S35}$$

The corrective solution of Problem 2 must cancel out the shear tractions along $y = h_1$ as well as the out-of-plane displacement at $y = -h_2$, given by Eqs. (S31) and (S32), respectively. In Fourier domain, these boundary conditions can be written as

$$\tilde{\sigma}_{yz}^{(2)}(x,h_1) = -\tilde{\sigma}_{yz}^{(1)}(x,h_1), \tag{S36}$$

$$\frac{\partial}{\partial x}\tilde{u}_z^{(2)}(x,-h_2) = -\frac{\partial}{\partial x}\tilde{u}_z^{(1)}(x,-h_2), \tag{S37}$$

where the tilde over-bar represents the Fourier transform with respect to the variable x. After some algebraic manipulations, the boundary conditions (S36) and (S37) yields the system of two equations

$$A - e^{-2\xi h_1}B = -\frac{B_z}{4\xi}e^{-2\xi h_1}, \tag{S38}$$

$$e^{-\xi h_2}A + e^{\xi h_2}B = -\frac{B_z}{4\xi}e^{-2\xi h_2}, \tag{S39}$$

which can be solved simultaneously to obtain the unknown constants A and B. The solution to the problem of a screw dislocation in an elastic layer can then be obtained as a superposition of the solutions to Problems 1 and 2. For example, the expression for the out-of-plane shear traction along $y = 0$ due to a dislocation present at $x = t$ can be obtained as

$$\sigma_{yz}(x,0) = \frac{\mu B_z}{2\pi}\left\{\frac{1}{x-t} + \int_0^\infty \left(\frac{e^{-2\xi h_2} - 2e^{-2\xi h} - e^{-2\xi h_1}}{1+e^{-2\xi h}}\right)\sin\{\xi(x-t)\}\,d\xi\right\}. \qquad \text{(S40)}$$

Text S3. Influence of rigid boundary along $y = -h_2$ on the solutions for the critical crack length and threshold compressive strength of weak layer.

To identify conditions under which the presence of the rocky substratum, i.e. the parameter h_2, can be ignored, we perform some calculations based on the values of input parameters defined in Section 5, with $G_c = 0.1$ J/m^2, $f = 0$ and $h_1 = 0.5$ m. Fig. S3a shows the dependence of the critical crack length required for unstable crack propagation on the distance of the weak layer from the rocky substratum, obtained using Eq. (15). The solid curve was obtained by substituting the numerical value of the parameter h_2 in the Fredholm kernel given by Eq. (5). The dotted curve was obtained by setting $h_2 \to \infty$ in the same expression. For a weak layer located half-way along the depth of a snow-pack, i.e. for $h_2 = h_1$, only a 0.55% deviation was observed in the value of the critical crack length when the presence of the rigid substratum is ignored. The deviation is even smaller for $h_2 > h_1$. Based on the obtained values of the critical crack length, the dependence of the threshold value of the compressive strength on the distance of the weak layer from the rocky substratum was derived. The solid curve in Fig. S3b was obtained by using Eq. (3) and the dotted curve was obtained by ignoring the last term of the same equation. As in the case of Fig. S3a, a very small deviation of 2% or less was observed in the threshold value of the compressive strength for $h_2 \geq h_1$.

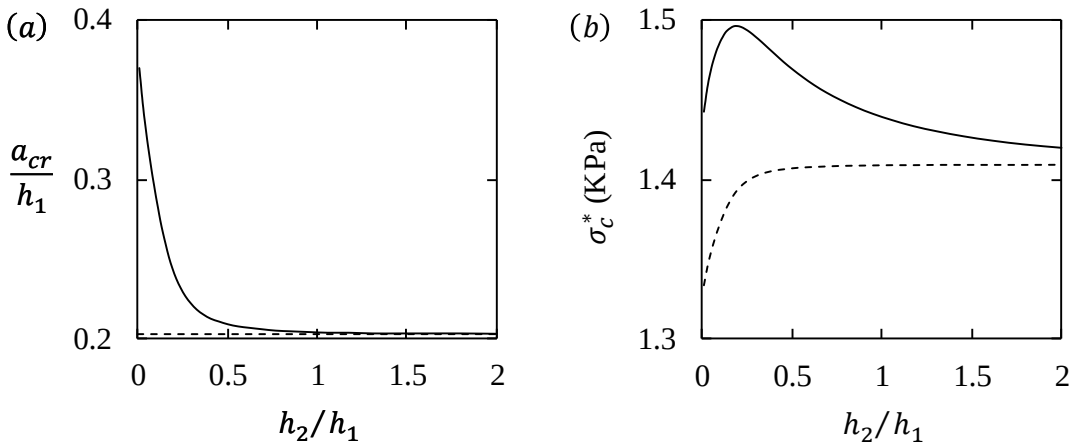

Figure. S3: Dependence of (a) the critical crack length, a_{cr} and (b) the critical value of the weak layer compressive strength, σ_c^* on the distance of the weak layer from the rocky substratum, h_2.

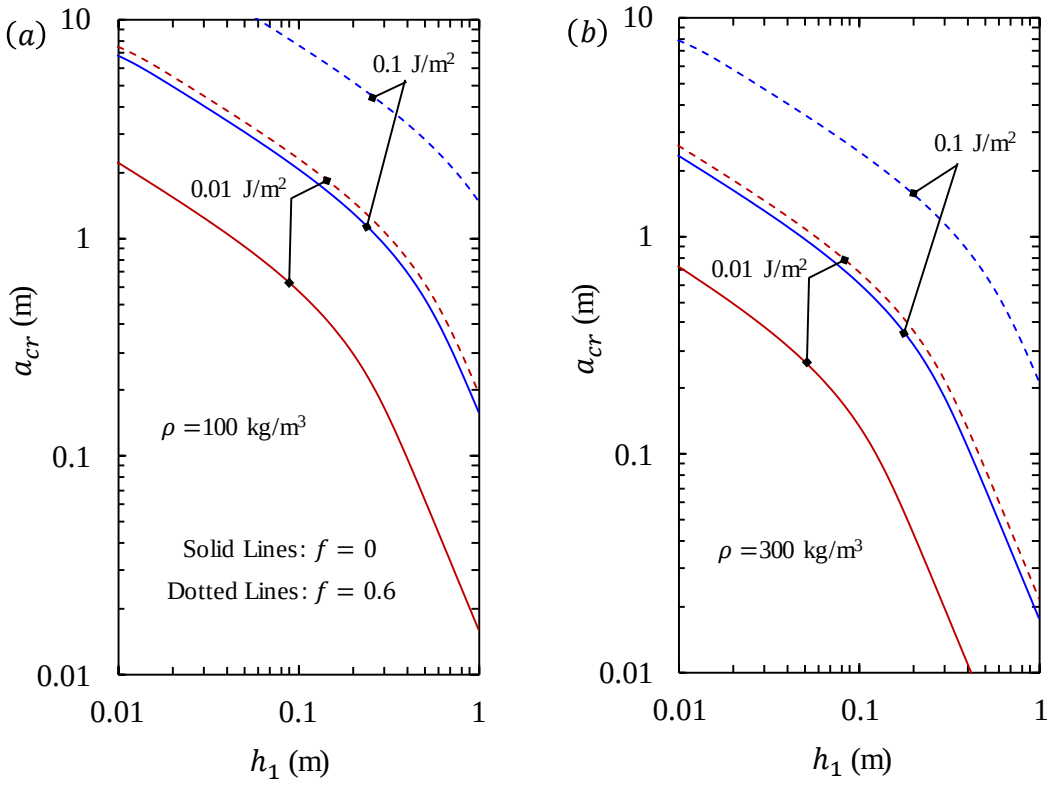

Figure. S4: Dependence of the critical crack length, a_{cr} on the weak layer depth, h_1, weak layer fracture energy, G_c, coefficient of friction between crack faces, f and snowpack density ρ.

References

Barber, J.R. (2010), Elasticity 3rd Ed., in Solid Mechanics and Its Applications, vol. 172, edited by G.M.L Gladwell, Springer Netherlands. doi: 10.1007/978-90-481-3809-8

Khanna, A., and A. Kotousov (2015), The stress field due to an interfacial edge dislocation in a multi-layered medium, Int. J. Solids Struct., 72, 1-10, doi: 10.1016/j.ijsolstr.2015.06.030.

Chapter 7

Summary and Recommendations

Chapter 7

Summary and Recommendations

The methodology and mathematical techniques utilised in the current work are largely based upon the pioneering contributions of several researchers, particularly Erdogan and his colleagues. The original contribution of the present thesis comes in the form of a newly formulated fundamental edge dislocation solution (Chapter 3), which can further extend the applicability of the adopted methodology. The novelty of the present thesis lies in the diverse applications and multi-disciplinary nature of the investigated problems. In this closing chapter, the main research outcomes of the thesis are summarised and recommendations for the extension of the current work are provided. The chapter concludes with a broader discussion on possible directions for future research.

7.1 Summary of the main outcomes

The publications which form the main body of the present thesis demonstrate the application of new and existing theoretical techniques and solutions for the analysis of practical problems related to the fracture of multilayered materials. Each of these publications represents an original and significant contribution to the respective area of research. A chapter-wise summary of the main research outcomes is presented below.

Chapter 3: The stress field due to an interfacial edge dislocation in a multi-layered medium

In this chapter, a solution for the stress field induced by an interfacial edge dislocation in a multilayered medium was obtained using the complex potential

method and Fourier transform techniques. It was demonstrated that the obtained solution is more general than all previously published solutions for edge dislocations in isotropic multilayered media. The new solution can be utilised to derive the governing integral equations for a wide variety of quasi-static crack problems in linearly elastic and isotropic multilayered materials. The obtained solution is applicable to the analysis of crack problems without any restrictions on the crack orientation or number of elastic layers, which represents one of the main advantages. Additionally, the derived solution is easy to implement and a supplementary computer code was provided in Khanna and Kotousov (2015).

Chapter 4: Stress analysis of a crack in a fiber-reinforced layered composite

In this chapter, a general approach was developed for the analysis of reinforced cracks in the vicinity of boundaries or interfaces in layered materials. The crack bridging reinforcements were modelled as a continuous distribution of displacement-dependant tractions along the crack faces. A numerical solution procedure based on the Newton-Raphson iterative scheme was utilized, since it does not impose any restrictions on the functional form of the relationship between the bridging tractions and the crack opening displacement. A parametric study was conducted to establish the dependence of the stress intensity factor upon the mismatch in elastic properties at the interfaces and the magnitude of the bridging tractions. The numerical results presented in this chapter can be applied for evaluating the residual strength of fiber-reinforced composites weakened by macroscopic cracks or cracked plates repaired by adhesively bonded composite patches.

Chapter 5: Controlling the Height of Multiple Hydraulic Fractures in Layered Media

In this chapter, fracturing-fluid pressure control was proposed as a possible mechanism for the containment of hydraulic fractures in hydrocarbon reservoirs. Subsequently, a simplified theoretical model was developed to evaluate the height

and the maximum opening of the hydraulic fractures during the fracturing stage as a function of the fracturing-fluid pressure. The effects of the spacing between adjacent fractures and the elastic mismatch in the layered reservoir were incorporated in the theoretical model. The feasibility of the suggested mechanism was demonstrated through a set of case studies in which the limiting values of the fracturing-fluid pressure were estimated. The obtained results can assist in the selection of the appropriate stimulation strategies during hydraulic fracturing.

Chapter 6: A new predictive model for the onset of skier-triggered avalanches

In this chapter, a new theoretical model was proposed for the onset of dry snow slab avalanches due to the skier-triggered failure of weak subsurface layers or interfaces. The model is based on the hypothesis that crack-like defects of high aspect-ratio can be generated in the weak layer or at interface under skier loading. The high aspect-ratio of the skier-induced defect would promote failure initiation of the weak layer in mode III rather than in mode II. Theoretical models were developed for calculating the size of the skier-induced defect and the critical defect size required for avalanche onset. The latter model utilised a new solution for a screw dislocation in an elastic layer, derived using the approach developed in Chapter 3. Case studies were conducted for typical snow-pack properties to identify the combination of snow-pack properties which provide the necessary conditions for unstable snow pack failure. The new model can be utilised as a forecast tool for skier-triggered avalanches and serve as a benchmark for numerical approaches.

7.2 Recommendations for future work

The theoretical models developed in the present thesis can be extended further for the examination of many related crack problems in multilayered media. In this section, recommendations regarding future works are provided in a chapter-wise form, focusing on the immediate extension of the work presented in the current thesis.

Chapter 3: The stress field due to an interfacial edge dislocation in a multi-layered medium

The governing integral equations for a variety of quasi-static crack problems in multilayered media can be derived in a straightforward manner using the dislocation solution obtained in Chapter 3. It would be of practical interest to analyse problems involving transverse cracking and crack path selection in multilayered materials using the DDT framework, which have not been attempted before. Previous works utilizing DDT are largely limited to simple two or three layer geometries (Romeo and Ballarini, 1995; Gupta et al., 1992; Fleck et al, 1991; He and Hutchinson, 1989; Erdogan and Biricikoglu, 1973; Gupta, 1973).

Another practical interest would be the further analysis of the obtained edge dislocation solution for some limiting cases of the geometry and material properties of multilayered materials. For example, many natural and engineering composites are comprised of multiple stiff and thin layers interleaved in a relatively soft matrix. It is believed that semi-analytical solutions or asymptotic approximations can be derived for these limiting and practically important cases. This will eliminate numerous difficulties with fracture analysis of such composites, in particular, analysis of transverse cracks intersecting a large number of layers.

Chapter 4: Stress analysis of a crack in a fiber-reinforced layered composite

The general approach presented in Chapter 4 can be extended to the analysis of several related problems involving reinforced materials and crack-bridging mechanisms, without imposing any restrictions on the orientation of the cracks or the functional form of the relationship between the bridging tractions and the crack opening displacement. One such problem is the stress analysis of delamination damage in laminate composites reinforced by transverse stitching (Dransfield et al., 1994). Another area of future work can involve the development of plasticity-induced fatigue crack growth models for multilayered materials, which are

currently widely implemented in fatigue life and damage tolerance analyses in metallic structures. The absence of such models significantly limits the wider utilisation of composites in many industries and applications.

Chapter 5: Controlling the Height of Multiple Hydraulic Fractures in Layered Media

The theoretical model developed in Chapter 5 could be extended for the analysis of problems involving fluid-driven fractures, such as dykes, mineral veins and pressurised joints, which penetrate several rock layers (Phillips et al., 2013). Several studies postulate that the variation in the magnitude of the in-plane stresses along the thickness of multilayered rock formations has a strong influence on propagation of fluid-driven fractures across several layers (Gudmundsson and Brenner, 2001; Warpinski et al., 1982). This additional consideration must be taken into account in the extended models.

The developed dislocation models can also be applied to many related problems in rocks, such as analysis of performance of hydraulic fractures partially filled with proppant packs. Some initial research has been published in articles by the applicant and included in the appendices (Bortolan Neto et al., 2015; Khanna et al., 2014; Kotousov et al., 2014). An immediate extension would be an incorporation of the layered structure of geological formations into these theoretical models.

Chapter 6: A new predictive model for the onset of skier-triggered avalanches

The snow pack, which was modelled as a homogenous elastic layer in Chapter 6, may also be composed of several layers with different elastic properties (Habermann et al., 2008). The theoretical approach can be readily extended for the latter case. Additional complexity can be introduced to the predictive model by considering a finite sized process-zone at the crack tips as suggested by several researchers (Bažant et al., 2003; McClung, 1979). The current work can be

extended to develop predictive models for other large-scale natural phenomena leading to humanitarian disasters. These include mud slides and naturally triggered snow avalanches.

7.3 Concluding remarks

Throughout the present thesis, a common methodology was utilised and further developed for the examination of crack problems of practical interest. The publications included in the main body of the thesis dealt with the analysis of crack problems in linearly elastic and isotropic multilayered materials. The significance of the main outcomes of these publications has been summarised in this closing chapter. The adopted methodology was also utilised by the candidate outside the context of the present research topic. The appendices to this thesis comprise of the candidate's publications on the latter problems.

A significant advancement beyond the scope of the current thesis would involve the application of DDT for the solution of crack problems in anisotropic multilayers, particularly for the examination of fatigue crack growth in laminate composites. Modelling fatigue crack growth and other composite related problems is challenging and computationally expensive, even in the isotropic case. The robustness and computational efficiency of currently available dislocation solutions and integral equation formulations for the more practical case of anisotropic multilayer has not been critically examined. Perhaps, future work could focus on the development of a robust framework for the analysis of practical problems such as the calculation of crack path, rate of fatigue crack growth and life of anisotropic laminate composites.

References

Romeo, A. and R. Ballarini (1995), A crack very close to a bimaterial interface, *J. Appl. Mech.*, 62, 614-619, doi: 10.1115/1.2895990.

Fleck, N.A., J.W. Hutchinson and Z. Suo (1991), Crack path selection in a brittle adhesive layer, *Int. J. Solids Struct.*, 27(13), 1683-1703, doi: 10.1016/0020-7683(91)90069-R.

He M.Y. and J.W. Hutchinson (1989), Crack deflection at an interface between dissimilar elastic materials, *Int. J. Solids Struct.*, 25(9), 1053-1067, doi: 10.1016/0020-7683(89)90021-8.

Gupta, G.D. (1973), A layered composite with a broken laminate, *Int. J. Solids Struct.*, 9, 1141-1154, doi: 10.1016/0020-7683(73)90108-X.

Erdogan, F. and V. Biricikoglu (1973), Two bonded half planes with a crack going through the interface, *Int. J. Eng. Sci.*, 11, 745-766, doi: 10.1016/0020-7225(73)90004-9.

Dransfield, K., C. Baillie, Y.-W. Mai (1994), Improving the delamination resistance of CFRP by stitching-a review, *Compos. Sci. Technol*., 50, 305-317, doi: 10.1016/0266-3538(94)90019-1.

Philipp, S.L., F. Afşar and A. Gudmundsson (2013), Effects of mechanical layering on hydrofracture emplacement and fluid transport in reservoirs, *Front. Earth Sci*., 1, 4, doi: 10.3389/feart.2013.00004.

Gudmundsson, A. and S.L. Brenner (2001), How hydrofractures become arrested, *Terra Nova*, 13, 456-462, doi: 10.1046/j.1365-3121.2001.00380.x.

Gupta, V., A.S. Argon and Z. Suo (1992), Crack deflection at an interface between two orthotopic media, *J. Appl. Mech.*, 59(2S), S79-S87, doi: 10.1115/1.2899511.

Warpinski, N.R., R.A.Schmidt, and D.A. Northrop (1982), In-Situ Stresses: The Predominant Influence on Hydraulic Fracture Containment, *J. Pet. Technol*., 34, 653-664, doi: 10.2118/8932-PA.

Bažant, Z.P., G. Zi and D. McClung (2003), Size effect law and fracture mechanics of the triggering of dry snow slab avalanches, *J. Geophys. Res*., 108(B2), 2119, doi: 10.1029/2002JB001884.

McClung, D.M. (1979), Shear fracture precipitated by strain softening as a mechanism of dry slab avalanche release, *J. Geophys. Res*., 84(B7), 3519-3525, doi: 10.1029/JB084iB07p03519.

Habermann, M., J. Schweizera and J.B. Jamieson (2008), Influence of snowpack layering on human-triggered snow slab avalanche release, *Cold Reg. Sci. Technol*., 54, 176-182, doi: 10.1016/j.coldregions.2008.05.003.

Khanna, A. and A. Kotousov (2015), Numerical implementation of an interfacial edge dislocation solution in a multi-layered medium, Proceedings of the 17th International Conference on Applied Mechanics and Mechanical Engineering (ICAMME 2015), 13-14 July 2015, Stockholm, Sweden.

Bortolan Neto, L., A. Khanna and A. Kotousov (2015), Conductivity and performance of hydraulic fractures partially filled with compressible proppant packs. *Int. J. Rock Mech.* Mining Sci., 74, 1-9, doi: 10.1016/j.ijrmms.2014.11.005.

Khanna, A., L. Bortolan Neto and A. Kotousov (2014), Effect of residual opening on the inflow performance of a hydraulic fracture, *Int. J. Eng. Sci*., 74, 80-90, doi: 10.1016/j.ijengsci.2013.08.012.

Kotousov, A., L. Bortolan Neto and A. Khanna (2014), On a rigid inclusion pressed between two elastic half spaces, *Mech. Mater*., 68, 38-44, doi: 10.1016/j.mechmat.2013.08.004.

Appendix A

Conductivity and performance of hydraulic fractures partially filled with compressible proppant packs

International Journal of Rock Mechanics & Mining Sciences 74 (2015) 1–9

Contents lists available at ScienceDirect

International Journal of Rock Mechanics & Mining Sciences

journal homepage: www.elsevier.com/locate/ijrmms

Conductivity and performance of hydraulic fractures partially filled with compressible proppant packs

Luiz Bortolan Neto*, Aditya Khanna, Andrei Kotousov

School of Mechanical Engineering, The University of Adelaide, Adelaide, SA 5005, Australia

ARTICLE INFO

Article history:
Received 3 March 2014
Received in revised form
27 August 2014
Accepted 20 November 2014
Available online 18 December 2014

Keywords:
Hydraulic fracturing
Proppant distribution
Compressible proppant
Residual fracture opening
Permeability–porosity relationship
Well productivity

ABSTRACT

Hydraulic or fluid-driven fracturing techniques are often utilised to enhance the production of oil or gas from hydrocarbon reservoirs. There are a number of engineering guidelines to identify the optimum fracture dimensions (i.e. length and average opening) and optimum fracture conductivity, which maximize the efficiency of a given hydraulic fracturing procedure. However, the fracture dimensions as well as conductivity during the production stage may be below the expected design values due to the compressive in-situ stresses, the non-uniform distribution of the proppant within the fracture, as well as the compressibility of the fractured rock and proppant pack.

In this paper, the performance of the hydraulic fracture, which is partially filled with a compressible proppant pack, is evaluated using a simple mathematical model. The mathematical model incorporates the aforementioned effects of proppant compressibility and in-situ stresses. A case study is conducted to investigate phenomena such as: the residual opening of fracture faces not supported by the proppant pack, the compaction of the proppant pack under the action of the confining stresses and the subsequent reduction in the permeability of the proppant pack.

1. Introduction

Hydraulic fracturing is a well stimulation technology used in the oil and gas industry for enhancing hydrocarbon recovery and alleviating near wellbore damage [1]. This technique consists of initiating, propagating and opening a fracture from the wellbore towards a hydrocarbon-bearing layer by a pressurised fluid. Granular particles called “proppants”, which range from natural sands to synthetic materials, are pumped into the created fracture along with the fracturing fluid. Once the injection pressure is relieved, they hold open, or “prop” the fracture and prevent its closure due to the in-situ compressive stresses. The proppant filled fracture provides a narrow but very conductive flow path towards the wellbore, increasing significantly the conductivity and production rate of the reservoir.

Several models have been developed in the past for estimating the conditions for fracture initiation and growth in rocks [1–6]. These models are used to predict the geometry of the hydraulic fracture for particular fracturing treatment conditions or to identify fracturing conditions which lead to an optimum fracture geometry. However, the increment in well productivity due to the hydraulic fracture ultimately depends upon the performance of the proppant pack, which controls the length, opening and conductivity of a fracture during the production stage [7,8]. During the proppant injection stage, the sedimentation and screen out of proppant particles may prevent the transport of proppant particles along the entire length of the fracture. As a result, the propped or effective length of the fracture can be much smaller than the length of the fracture initially created during the fluid injection stage [9–11]. During the production stage, the width of the propped fracture also diminishes due to the compaction of the proppant pack and the embedment of proppant particles into the fracture surface [12]. The conductivity of the proppant pack during the production stage may also decline by a few orders of magnitude, compared to the conductivity measured under laboratory conditions, due to several physical and chemical mechanisms [12]. By incorporating the effects of these phenomena, a more realistic estimate of the production rate from the fractured well can be obtained.

The authors have recently considered the some of these effects separately. For e.g. the problem of a fracture partially filled with an incompressible proppant pack has been considered in [13,14] and the effects of proppant pack compaction on the opening and conductivity of the fractures have been considered in [15–18]. In the present work, a more general problem of a fracture partially filled with a loose granular assembly of proppant particles is considered. The fracture is

* Corresponding author.
E-mail addresses: luiz.bortolanneto@adelaide.edu.au (L. Bortolan Neto), aditya.khanna@adelaide.edu.au (A. Khanna), andrei.kotousov@adelaide.edu.au (A. Kotousov).

http://dx.doi.org/10.1016/j.ijrmms.2014.11.005
1365-1609/

subjected to confining stresses, which result in the closure of the unpropped fracture segments as well as rearrangement of proppant particles in the pack, leading to a reduction in fracture opening and conductivity. In the next section, the mathematical formulation of the problem and the modelling assumption are described. Selected case studies and numerical results are presented which demonstrate the effect of the in-situ confining stresses, propped length and proppant pack compressibility on the performance of hydraulic fractures.

2. Problem formulation and modelling assumptions

Consider an isotropic, homogenous, linearly elastic rock formation with Young's modulus E and Poisson's ratio ν. It is penetrated by a vertical hydraulic fracture of length $2l_f$ and height $2h_f$. For the co-ordinate system shown in Fig. 1, the reservoir lies along the x–y plane, the wellbore lies perpendicular to the reservoir along the z-axis and the fracture is located along the x–z plane. The problem geometry is symmetric about the x and y axes.

The problem is formulated in 2D, as illustrated in Fig. 2, i.e. all parameters remain constant along the z-axis. In this 2D formulation, the fracture geometry is described by the Khristianovic–Geertsma–de Klerk (KGD) model [19,20] and the initial opening profile of the fracture, $\delta_0(x)$, is given in accordance with the linear elastic fracture mechanics, by

$$\delta_0(x) = \frac{4}{\overline{E}}\left(\sigma^{\infty} + p_f\right)\sqrt{l_{f0}^2 - x^2}, \tag{1}$$

where $\overline{E}$ is the reduced Young's modulus defined as $\overline{E} = E/(1-\nu^2)$ for plane strain conditions, σ^{∞} is the remote stress normal to the fracture and p_f is the fluid pressure within the fracture during the fracturing treatment. The stresses are assumed to be positive in tension and negative in compression. Since the KGD fracture geometry is based on the plane strain assumption, it implies that the opening or width of the fracture is independent of fracture height [3]. More sophisticated models describing the fracture geometry are available in the literature [2–6], however, the plane strain 2D model is more suitable for analytical studies, such as the present one [15,21]. The results based on the KGD model can be reasonably extended to other fracture geometries in the case of short fractures or in the near tip region, which can be modelled locally as a plane strain geometry [22]. Eq. (1) also assumes uniform fluid pressure in the fracture during the fracturing stage, which is the case when the fracture propagates in the toughness dominated regime and there is no significant fluid leak off into the reservoir [21,23].

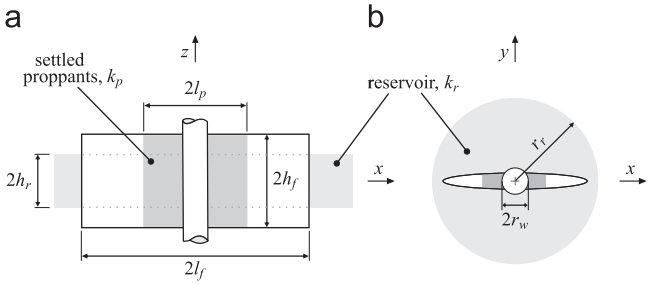

Fig. 1. Schematic diagram of a partially propped hydraulic fracture considered in the problem formulation (figure not to scale), (a) cross-sectional view and (b) plan view.

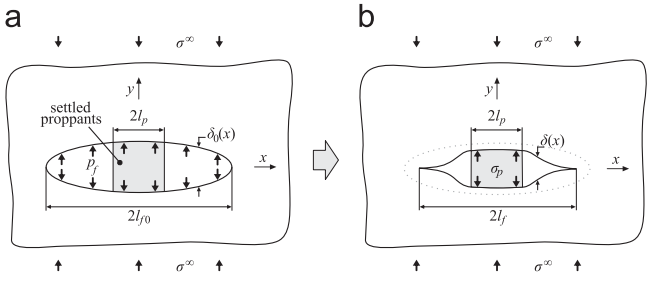

Fig. 2. The 2D approximated of a hydraulic fracture partially filled with proppant and subject to remote confining stress. (a) The initial opening and length of the fracture due to a uniform internal pressure p_f, (b) the residual opening and length of the fracture once the stimulating fluid pressure is removed.

The fracture is filled with a proppant pack of permeability k_p and porosity η, up to a length $2l_p \le 2l_f$. The proppant pack is assumed to be a granular assembly made up of proppant particles and the deformation of the proppant pack is linked largely to the rearrangement and densification of the loosely arranged particle assembly and the subsequent changes in pore volume. The deformation of the proppant pack is modelled by Terzaghi's soil consolidation model [23,24]. This model is chosen due to its simplicity, since only one parameter governs the deformation vs. stress behaviour or the overall compressibility of the proppant pack. More sophisticated compaction models can be used at the expense of additional empirical parameters or coefficients [25].

The compaction of the proppant pack and the subsequent reduction the porous space between the particles also lead to a reduction in permeability of the proppant pack. This dependence of the permeability on the porosity of the proppant pack is modelled using the empirical Kozeny–Carman equation [26]. It should be noted that the rearrangement of the proppant particles is only one of many mechanisms which lead to the reduction in permeability of the proppant pack during the production stage. Other mechanisms such as crushing and diagenesis of proppant particles and deposition of fines in the pore space [27–29], can also be incorporated into the empirical relationship between permeability and porosity.

During the production stage, it is assumed that the flow within the pore space of the proppant pack as well as the reservoir rock (i.e. at the micro-scale) occurs at small Reynolds number ($N_{\mathrm{Re}} < 1$) and can be described by the linearized form of Navier–Stokes equation [28]. Hence, the flow in the reservoir and the flow within the fracture are described by Darcy's law on the macro-scale. Conditions under which the macroscopic flow cannot be adequately described by Darcy's law as well as models which provide a better correlation between pressure drop and flow rate under these conditions, have been reviewed elsewhere [28,34,40]. Poro-elastic effects have also been excluded, which implies that the fluid flow in the reservoir is not coupled with the state of stress in the reservoir.

The aperture and length of the hydraulic fracture at the production stage are defined as the residual fracture opening, $2\delta(x)$ and length, $2l_f$, respectively. The residual opening and length of the fracture depend on the distribution and compressibility of the proppant pack, confining stresses, elastic properties of the reservoir, and on the initial fracture geometry. These are unknown and need to be determined as a solution to a mixed boundary value problem. The solution method that is developed and presented in the next section is based on the distributed dislocation technique, which is a quite standard tool in fracture mechanics modelling [30].

3. Residual opening and length of the hydraulic fracture

The solution for the residual opening and length of the hydraulic fracture can be obtained from the following boundary value problem:

$$\sigma_{yy}(x, \mathrm{y}) = \sigma^{\infty}, \quad x^2 + y^2 \to \infty; \tag{2a}$$

$$\sigma_{yy}(x, 0) = \sigma_p(x), \quad |x| < l_p; \tag{2b}$$

$$\sigma_{yy}(x,0)=0, \quad l_p<|x|\le l_f; \tag{2c}$$

$$\delta(x)=2u_y(x,0)=0, \quad |x|\ge l_f\,. \tag{2d}$$

The unknown residual length of the fracture, l_f lies in the interval $l_p \le l_f \le l_{fo}$, where l_p is the length of the proppant pack and l_{fo} is the initial length of the fracture. It is determined using the condition of zero stress intensity factor at the crack tips $|x|=l_f$.

Following the procedure of Bilby and Eshelby [31], the crack can be represented by a continuous distribution of dislocations along $-l_f \le x \le l_f$, such that the density of dislocations at a point x along the fracture is given by $b_y(x)$. The distributed dislocation density is related to the crack opening according to:

$$b_y(x)=-\frac{d\delta(x)}{dx}, \delta(x)=-\int_{-\infty}^{x} b_y(t)dt. \tag{3}$$

The normal stress along the location of the crack can be written as

$$\sigma_{yy}(x,0)=\sigma^{\infty}+\overline{\sigma}_{yy}(x,0), \quad |x|\le l_f\,, \tag{4}$$

where σ^{∞} is the normal stress in the absence of the crack and $\overline{\sigma}_{yy}(x,0)$ is the normal stress in the material due to a continuous distribution of edge dislocations of density $b_y(x)$ located along the crack line. The expression for $\overline{\sigma}_{yy}(x,0)$ is given by [32]:

$$\overline{\sigma}_{yy}(x,0)=\frac{\overline{E}}{4\pi}\int_{-l_f}^{+l_f}\frac{b_y(t)}{x-t}dt, |x|\le l_f. \tag{5}$$

The governing equation in terms of the unknown distributed dislocation density function can be obtained by substituting boundary conditions (2b) and (2c) into Eq. (4):

$$\frac{\overline{E}}{4\pi}\int_{-l_f}^{+l_f}\frac{b_y(t)}{x-t}dt=\sigma_p(x)-\sigma^{\infty}, |x|<l_p,$$
$$\frac{\overline{E}}{4\pi}\int_{-l_f}^{+l_f}\frac{b_y(t)}{x-t}dt=-\sigma^{\infty}, l_p<|x|<l_f. \tag{6}$$

The governing Eq. (6) is a non-linear singular integral equation containing the Cauchy kernel and is supplemented with the following single-valued condition for the dislocation density function:

$$\int_{-l_f}^{l_f} b_y(t)dt=0. \tag{7}$$

The condition given by Eq. (7) implies that the crack faces must physically come together at the crack tips [32].

The compressive behaviour of proppant pack i.e. the non-linear relationship between $\sigma_p(x)$ and $\delta(x)$ is described using Terzaghi's one dimensional soil consolidation model. The relationship between the deformation of the proppant pack and the compressive stress acting on the proppant pack $\sigma_p(x)$ can be written as

$$\sigma_p(x)=\exp\left(\frac{\lambda(x)}{C}\right)\sigma_{p0}, \tag{8}$$

where C is the proppant pack compressibility index and $\lambda(x)$ the proppant settlement ratio defined as

$$\lambda(x)=\frac{\delta_0(x)-\delta(x)}{\delta_0(x)}, \tag{9}$$

and σ_{p0} is the compressive stress at which the thickness of the pack is δ_0.

This model is empirical in nature and does not distinguish between various mechanisms leading to the compaction of the proppant pack. It simply provides a linearized dependence of the settlement ratio, λ on the logarithm of the compressive stress, σ_p according to Eq. (8). The value of the compressibility index, C is assumed to be constant over the range of applied compressive stresses and treated as an empirical constant. However, it should be noted that Eq. (8) is not suitable for modelling the deformation response of granular soils or proppant packs at very low or very high compressive stresses, since the behaviour of the proppant pack is nonlinear under these conditions and the compressibility of the pack is quite low [24].

Once the solution for the distributed dislocation density $b_y(x)$ along the crack length is known, the residual fracture opening is calculated using Eq. (3) and the residual fracture length is calculated by using the condition of zero stress intensity factor at the crack tips or at $|x|=l_f$. The solution procedure for the governing non-linear singular integral Eq. (6) is based on Newton–Raphson iteration scheme and Gauss–Chebyshev quadrature method and is described and validated in detail elsewhere [15].

4. Effect of proppant compressibility on the porosity and permeability of the proppant pack

The compaction of the proppant pack under the confining stresses of the reservoir leads to a reduction in the porosity of the proppant pack. The porosity, η, of the proppant pack can be defined as [28]:

$$\eta=\frac{V_p}{V_b}=1-\frac{V_s}{V_b}, \tag{10}$$

where V_b is the bulk volume of the proppant pack, V_p is the volume of the porous space within the proppant pack and V_s is the volume of the solid phase (comprising of proppant particles) and $V_b=V_p+V_s$. From Eq. (10) it follows that the residual porosity, η, is related to the initial porosity, η_0, according to:

$$\eta=1-\frac{V_{b0}}{V_b}(1-\eta_0), \tag{11}$$

where V_{b0} is the bulk volume of the proppant pack during the stimulation stage (before compaction) and V_b is the bulk volume of the proppant pack during the production stage (after compaction). The bulk volume of the proppant pack at these stages can be calculated from the geometry of the hydraulic fracture as:

$$V_{b0}=2h_f\int_{-l_p}^{l_p}\delta_0(x)dx, V_b=2h_f\int_{-l_p}^{l_p}\delta(x)dx. \tag{12}$$

The residual porosity of the proppant pack, η, can be calculated by substituting Eq. (12) into Eq. (11).

The model for proppant-pack compaction, given by Eqs. (8) and (9), must be used with care as it can provide physically meaningless values of η beyond a certain value of the ratio V_{b0}/V_b. To demonstrate this idea, consider the ideal case of a stable pack of equal sized spheres, for which the porosity lies in the range of $0.2595-0.4764$, depending on the pack arrangement [33]. Substituting $\eta_0=0.4764$ and $\eta=0.2595$ in Eq. (11) yields the critical value of the ratio $V_{b0}/V_b=1.4142$. For a given value of compressibility index C, if the ratio V_{b0}/V_b calculated using Eq. (12) exceeds the critical value of 1.4142, the porosity would be less than the minimum possible value of 0.2595. This is a limitation of the present formulation.

The relationship between the permeability and porosity of the proppant pack is modelled by the Kozeny–Carman equation, given by

$$k_p=\frac{F}{A^2}\frac{\eta^3}{(1-\eta)^2}, \tag{13}$$

where F is a geometric factor and A is the specific surface area [26,28]. The ratio between the residual permeability of the proppant pack (after compaction) and the initial permeability (before

compaction) can be obtained from Eq. (13) as:

$$\frac{k_p}{k_{p,0}} = \left(\frac{\eta}{\eta_0}\right)^3 \left(\frac{1-\eta_0}{1-\eta}\right)^2, \tag{14}$$

where it is assumed that the initial porosity, η_0, and the initial permeability, $k_{p,0}$, are known beforehand.

The effect of the in-situ compressive stress σ^∞ and the proppant pack compressibility on the porosity and permeability of the proppant pack can be obtained using the method described in this section. The change in permeability affects the fluid flow in the fracture, the governing equations for which are presented in the next section.

5. Steady flow of fluid within the hydraulic fracture

The governing equation for steady-state fluid flow within the fracture, as obtained by Zazovskii and Todua [35] is used here as it incorporates variable fracture opening and permeability along the length of the fracture. It can be written as:

$$S(x)k_f(x)\int_{-l_f}^{l_f}\frac{\psi(t)}{x-t}dt + 4\pi h_f k_r \int_{-l_f}^{x}\psi(t)dt = Q\mu\frac{\pi}{2}(1+\mathrm{sgn}(x-l_f)), \tag{15}$$

where the unknown function $\psi(x)$ multiplied by the constant $2k_r/\mu$ gives the fluid flux into the fracture. Eq. (15) is similar to the governing equation for crack opening, Eq. (6) in that both are singular integral equations containing the Cauchy kernel and an unknown density function. The numerical solution to the equation can be obtained using the Gauss–Chebyshev quadrature method. In the above equation, $2h_f$ and $2l_f$ are the height and length of hydraulic fracture, respectively, k_r is the permeability of the reservoir, μ is the viscosity of the fluid, Q is the fluid production rate at the wellbore and $S_f(x) = 2h_f\delta(x)$ is the cross-sectional area of the fracture. The fracture permeability $k_f(x)$ is defined as [12]:

$$k_f(x) = \begin{cases} k_p, |x| < l_p \\ \delta^2(x)/12, l_p < |x| \le l_f \end{cases}. \tag{16}$$

Eq. (16) implies that the permeability of the fracture is equal to the permeability of the proppant pack in the propped region of the fracture ($|x| < l_p$) and is given by Boussinesq's formula for flow in a narrow gap between two plates [36,37] in the un-propped region of the fracture ($l_p < |x| \le l_f$).

The governing Eq. (15) is supplemented by the following single-valued condition for the fluid flux distribution:

$$Q = 4\frac{h_f k_r}{\mu}\int_{-l_f}^{l_f}\psi(\xi)\mathrm{d}\xi. \tag{17}$$

Physically, Eq. (17) represents the conservation of mass of the reservoir fluid i.e. the net fluid flux into the fracture is equal to the fluid production rate at the wellbore, Q. The method for the selection of dimensionless variables and solution of the governing Eq. (15) is described in [13].

6. The well productivity index

The well productivity index, J is one of the main indicators of the performance of a well. The productivity index is classically defined as the ratio of the well production rate, Q and the pressure drawdown [1]:

$$J = \frac{Q}{p_r - p_w} = \frac{4\pi}{\alpha}\frac{h_r k_r}{B\mu}J_D, \tag{18}$$

where p_r is the reservoir pressure, p_w is the wellbore pressure, J_D is the dimensionless productivity index, B the formation volume factor and α a constant for appropriate units (i.e. $\alpha = 1$ for SI units and $\alpha = 887.22$ for traditional oilfield units). For a producing well of radius r_w lying at the centre of a circular reservoir of radius r_r, J_D is given by [1,38]:

$$J_D = \frac{1}{\ln(r_r/r_w)}. \tag{19}$$

For a well intersected by a hydraulic fracture of finite conductivity, the dimensionless productivity index is given by [35]

$$J_D = \left[\ln\left(\frac{1}{I_x}\right) - \int_{-1}^{1}\psi(X)\ln(X)dX\right]^{-1}, \tag{20}$$

where $I_x = l_f/r_r$ is the penetration ratio and $X = x/l_f$ is the normalised distance from the wellbore along the length of the fracture.

The above expression for dimensionless productivity index can be normalised against the value of J_D of a fracture with infinite conductivity, for which $\psi(X) = \pi^{-1}\left(1-X^2\right)^{-1/2}$ and the integral $\int_{-1}^{1}\Psi(X)\ln(X)dX = -\ln 2$. Hence, the normalised productivity index of the fracture is given by

$$\bar{J} = \left[\ln 2 - \ln\left(\frac{1}{I_{x,0}}\right)\right]\left[\ln\left(\frac{1}{I_{x,0}}\frac{1}{L_f}\right) - \int_{-1}^{1}\Psi(X)\ln(X)dX\right]^{-1}, \tag{21}$$

where $I_{x,0} = l_{f,0}/r_r$ is the initial or design value of the penetration ratio and $L_f = l_f/l_{f0}$ is the normalised residual length of the fracture. The normalised productivity index has a maximum value equal to 1 as the fracture conductivity tends to infinity.

7. Validation of empirical models against experimental results

The modelling outcomes of the present work, depend upon the validity of the empirical models as well as the chosen values for empirical constants such as the compressibility index, C, the initial porosity, η_o and initial permeability, $k_{p,0}$, of the proppant pack. The method for validating the empirical models and obtaining these properties from experimental data is described in this section. As an example, a particular set of experimental results obtained from [40] are considered. These results were obtained for a type of sintered ceramic proppant known as Carbolite®, manufactured by CARBO Ceramics Inc. The mesh size of the used proppant pack was 18/12, which means that the diameter of the proppant particles was in the range of 1000–1700 μm.

7.1. Terzaghi's soil consolidation model

The empirical consolidation model described in Section 4 is typically used for cohesive soils such as clays and provides a linearized dependence of the settlement ratio, λ on the compressive stress, $\log(\sigma_p)$ according to Eq. (8) [24]. The model is used in the present work to describe the compaction of the proppant pack and the value of the compressibility index of the proppant pack is assumed to be constant over the range of applied compressive stresses.

The actual deformation behaviour of a proppant pack can be observed by plotting experimental results for e vs. $\log_{10}(\sigma_p)$, where e is the void ratio of the sample at the compressive stress σ_p. The void ratio is related to the porosity of the proppant pack according to $e = \eta/(1-\eta)$. For the example of the Carbolite® 18/12 proppant, the experimental results are shown in Fig. 5. In this particular case, a straight line provides a reasonable fit for the e vs. $\log_{10}(\sigma_p)$ data, which implies that it is reasonable to use the empirical Terzaghi model to describe the compaction of the proppant pack. The value of compressibility index C is the slope of the e vs. $\log_{10}(\sigma_p)$ plot [39] and in this particular example, $C = 0.0583$. Based on the classification provided in Table 3, the given proppant pack is slightly compressible.

It should be noted that the empirical model is unable to distinguish between the various mechanisms which govern proppant pack deformation. These include: the rearrangement of particles in the pack, the elastic or plastic deformation of the individual particles, crushing of particles, etc. However, this does not severely limit the applicability of the model to practical problems since the empirical model can reasonably incorporate all of these deformation mechanisms, provided that an averaged value of the compressibility index C is taken over a wide range of compressive stresses.

7.2. Kozeny–Carman equation

The Kozeny–Carman relationship, which is given by Eq. (14), was used to predict the dependence of permeability on the confining stress. As an example, the predictions of the Kozeny–Carman equation are compared with the experimentally measured values of permeability at different values of confining stress (Fig. 6). In Eq. (14), the empirical constants denoting the reference values of porosity and permeability were chosen to be $\eta_0 = 0.338$ and $k_{p,0} = 171$ Darcy, respectively. These were the experimentally measured values of porosity and permeability at the lowest level of confining stress, which was 6.89 MPa (1000 psi) [40].

In general, a good agreement was observed between the Kozeny–Carman model and the experimental results, which suggests that the empirical model is appropriate for use in the present problem. However, it can be observed that the experimentally measured values of permeability are lower than the prediction of the Kozeny–Carman equation at high confining stresses (>20.68 MPa, 3000 psi). The maximum deviation is approximately 13.5%, and occurs at the highest value of confining stress, which is 34.47 MPa (5000 psi).

The discrepancy can partly be attributed to the experimental methods of porosity and permeability measurements. The porosity was calculated indirectly from the measurements of proppant pack compaction, whereas permeability measurements were made directly using accurate pressure transducers [40]. The production of fine debris at high confining stresses, could have potentially caused significant blocking of the porous space of the proppant pack without much compaction of the proppant pack. In this case, it is expected that the experimentally measured value of permeability would be lower than predicted value of permeability, which is based on indirect porosity measurements, even though the empirical model can potentially incorporate non-linear effects such as proppant crushing.

It should also be mentioned that the effect of other permeability reduction mechanisms such as the improper clean-up of fracturing fluid, fines migration from the reservoir, diagenesis of the proppant pack [27–29] can also be incorporated in the fluid flow model (Sections 5 and 6) without any modification of the analytical framework.

8. Results and discussion

In this section, the effects of proppant compressibility and compressive stresses on the residual opening and length of the fracture, proppant pack permeability as well as on the well productivity are demonstrated. The results are presented in terms of normalised and dimensionless parameters, which are summarised in Table 1. From Eq. (21), it can be observed that the normalised productivity index $\bar{J}$, depends upon the normalised residual length of the fracture, L_f and the normalised fluid flux along the fracture length, $\psi(X)$. The function $\psi(x)$ is obtained by solving the singular integral Eq. (15) and the solution depends upon the normalised residual opening profile $W(X)$ and dimensionless fracture conductivity C_{fd}.

The normalised residual length of the fracture L_f and the residual opening $W(X)$ depend upon the values of the dimensionless confining stress $\overline{\sigma}$, proppant pack compressibility C and normalised proppant length L_p. This dependence is described in Section 3. The value of the dimensionless fracture conductivity depends upon the residual length and opening of the fracture as well as the proppant pack permeability. It can be written as

$$C_{fd} = \frac{\delta(0)}{2\pi l_f}\frac{k_p}{k_r} = C_{fd,0}\frac{\delta(0)}{\delta_0(0)}\frac{k_p}{k_{p,0}}\frac{L_{f0}}{L_f}, \tag{22}$$

where $C_{fd,0}$ is the design value of the fracture conductivity defined in Table 1. The factor $\delta(0)/\delta_0(0)$ represents the reduction in the maximum opening of the fracture near the wellbore due to the compressibility of the proppant pack. The factor $k_p/k_{p,0}$ represents the reduction in permeability due to the compaction of the proppant pack under the effect of the confining stresses and is calculated in Section 4. The factor L_{f0}/L_f is the ratio of the initial and residual length of a partially filled fracture. The design value of fracture conductivity, $C_{fd,0}$ is multiplied by these factors to obtain the actual value of dimensionless fracture conductivity C_{fd}, as shown in Eq. (22).

For the purpose of the numerical study, the normalised productivity index, $\bar{J}$ is calculated as a function of the design value of the dimensionless fracture conductivity, $C_{fd,0}$ for different values of dimensionless confining stress $\overline{\sigma}$, proppant pack compressibility C, and normalised propped length of fracture, L_p. The range of these values covering the most common conditions in hydrocarbon reservoirs is summarised in Table 2 and a description of the chosen values is provided next.

For a typical sandstone reservoir with plane strain Young's modulus, $\overline{E} = 10$ GPa, the values of $\overline{\sigma}$ given in Table 2 corresponds to compressive stresses $\sigma^{\infty} = 1$, 10 and 100 MPa, respectively. According to the classification suggested by Coduto [39] as shown

Table 1
Normalised and dimensionless parameters.

Parameter	Definition
$X = x/l_f$	Normalised length coordinate
$L_p = l_p/l_{f0}$	Normalised propped length of fracture
$L_f = l_f/l_{f0}$	Normalised residual length of fracture
$W(X) = \delta(x)/\delta_0(0)$	Normalised residual opening of fracture
$\overline{\sigma} = \sigma^{\infty}/\overline{E}$	Dimensionless confining stresses
$C_{fD,0} = (\delta_o(0)/2\pi l_{f0})(k_{p,0}/k_r)$	Dimensionless fracture conductivity

Table 2
Normalised and dimensionless parameters.

Parameter	Numerical value		
$\overline{\sigma}$	10^{-4}	10^{-3}	10^{-2}
C	10^{-3}	10^{-2}	10^{-1}
L_p	1.0	0.5	0.1

Table 3
Classification of the proppant pack compressibility [39].

Compressibility, C	Classification
0–0.05	Very slightly compressible
0.05–0.10	Slightly compressible
0.10–0.20	Moderately compressible
0.20–0.35	Highly compressible
>0.35	Very highly compressible

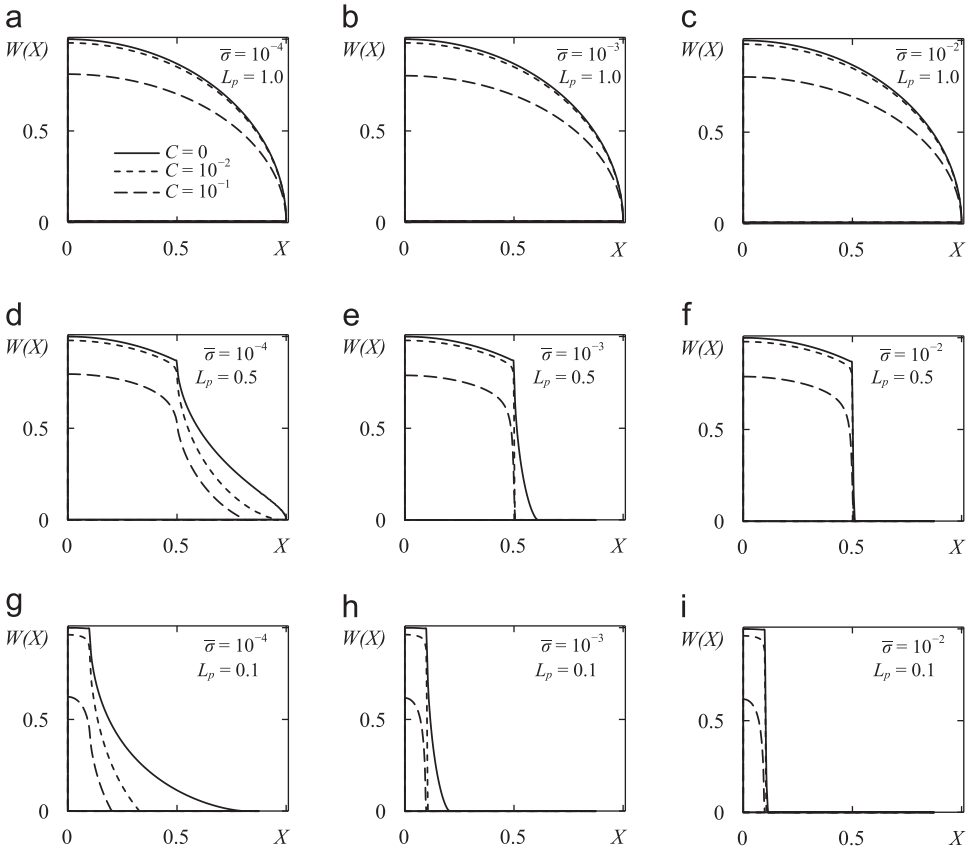

Fig. 3. Normalised residual opening of a hydraulic fracture filled with a compressive proppant pack.

Table 4
Numerical results for $L_p = 1.0$.

$L_p = 1.0$	$\overline{\sigma} = 10^{-4}$				$\overline{\sigma} = 10^{-3}$				$\overline{\sigma} = 10^{-2}$			
C	0	10^{-3}	10^{-2}	10^{-1}	0	10^{-3}	10^{-2}	10^{-1}	0	10^{-3}	10^{-2}	10^{-1}
$\delta(0)/\delta_0(0)$	1.000	0.998	0.980	0.810	1.000	0.998	0.980	0.801	1.000	0.998	0.980	0.800
$k_p/k_{p,0}$	1.000	0.989	0.897	0.267	1.000	0.989	0.897	0.246	1.000	0.989	0.897	0.244
l_f/l_{f0}	1.000	1.000	1.000	1.000	1.000	1.000	1.000	1.000	1.000	1.000	1.000	1.000
$C_{fd}/C_{fd,0}$	1.000	0.987	0.879	0.216	1.000	0.987	0.879	0.197	1.000	0.987	0.879	0.195
$\bar{J}(C_{fd,0} = 1)$	0.749	0.746	0.726	0.453	0.749	0.746	0.726	0.437	0.749	0.746	0.726	0.435

Table 5
Numerical results for $L_p = 0.5$.

$L_p = 0.5$	$\overline{\sigma} = 10^{-4}$				$\overline{\sigma} = 10^{-3}$				$\overline{\sigma} = 10^{-2}$			
C	0	10^{-3}	10^{-2}	10^{-1}	0	10^{-3}	10^{-2}	10^{-1}	0	10^{-3}	10^{-2}	10^{-1}
$\delta(0)/\delta_0(0)$	1.000	0.997	0.979	0.795	1.000	0.997	0.979	0.788	1.000	0.997	0.979	0.788
$k_p/k_{p,0}$	1.000	0.980	0.877	0.189	1.000	0.980	0.877	0.163	1.000	0.980	0.877	0.162
l_f/l_{f0}	1.000	0.980	0.962	0.819	0.608	0.504	0.504	0.504	0.511	0.504	0.504	0.504
$C_{fd}/C_{fd,0}$	1.000	0.996	0.892	0.184	1.643	1.937	1.702	0.255	1.955	1.937	1.702	0.253
$\bar{J}(C_{fd,0} = 1)$	0.772	0.689	0.650	0.320	0.383	0.323	0.321	0.262	0.327	0.323	0.321	0.261

in Table 3, the values of $C = 10^{-3}$ and 10^{-2} correspond to very slightly compressibility of the proppant pack, whereas $C = 10^{-1}$ corresponds to a slightly compressible pack. Finally, the value of $L_p = 1.0$ implies that the fracture is fully filled with proppant, $L_p = 0.5$ implies that the fracture is half-filled with proppant and $L_p = 0.1$ implies that one-tenth of the fracture is filled with proppant.

Besides these main governing parameters, the values of three other parameters: the initial porosity of proppant pack η_0, the design value of penetration ratio $I_{x,0} = l_{f0}/r_r$ and the maximum initial opening of the fracture $\delta_o(0)$, also need to be chosen. These values are kept fixed and are chosen to be $\eta_0 = 0.4764$ (which is the porosity of a cubic assembly of spherical particles), $I_{x,0} = 1$ (which implies the initial fracture spans the entire

reservoir) and $\delta_o(0) = 10^{-4} \times 2l_{f0}$ (i.e. the initial fracture opening is four orders of magnitude smaller than the initial fracture length).

First, consider the numerical results for the residual opening profile of the fracture as shown in Fig. 3. The solid lines are taken from [13] and represent the residual opening of a fracture filled with incompressible proppant ($C = 0$). The broken lines represent the case of compressible proppant packs. The compressibility of the proppant pack affects the residual opening as well as the residual length of the fracture. As the proppant compressibility increases, the residual opening of the fracture decreases. This also leads to a reduction in the permeability of the proppant pack. Numerical values for the reduction in fracture opening as well as reduction in proppant permeability are given in Tables 4–6 for a range of values of the governing parameters. It can also be observed from Fig. 3, that the residual length of the fracture, L_f is essentially equal to the propped length of the fracture, L_p except for the case of very low confining stresses ($\overline{\sigma} = 10^{-4}$). Even at very low confining stresses, the residual length of a fracture partially filled with compressible proppant is much shorter when compared to the incompressible proppant case.

Next, consider the effect of proppant compressibility and confining stress on the normalised productivity index, $\bar{J}$ as shown in Fig. 4. The solid lines ($C = 0$) are taken from [13] and represent the productivity index of a fracture filled with incompressible proppant. The broken lines represent the results for the case of a compressible proppant pack. The value of the normalised productivity index is governed by the dimensionless fracture conductivity, C_{fd} and the normalised residual length of the fracture, L_f and is calculated using Eq. (21). It can be observed from Fig. 4 that for a given design value of the dimensionless fracture conductivity $C_{fd,0}$, the value of the normalised productivity index decreases with increasing proppant compressibility, C and increasing dimensionless confining stress, $\overline{\sigma}$. In Fig. 4(g)–(i), the results corresponding to $C = 0.1$ are omitted.

Table 6
Numerical results for $L_p = 0.1$.

$L_p = 0.1$	$\overline{\sigma} = 10^{-4}$				$\overline{\sigma} = 10^{-3}$				$\overline{\sigma} = 10^{-2}$			
C	0	10^{-3}	10^{-2}	10^{-1}	0	10^{-3}	10^{-2}	10^{-1}	0	10^{-3}	10^{-2}	10^{-1}
$\delta(0)/\delta_0(0)$	1.000	0.994	0.962	0.623	1.000	0.994	0.962	0.617	1.000	0.994	0.962	0.623
$k_p/k_{p,0}$	1.000	0.961	0.761	–	1.000	0.961	0.760	–	1.000	0.961	0.760	–
l_{f0}/l_f	0.809	0.348	0.334	0.206	0.206	0.105	0.105	0.100	0.113	0.105	0.105	0.100
$C_{fd}/C_{fd,0}$	1.234	2.738	2.191	–	4.851	9.050	6.933	–	8.821	9.050	6.93	–
$\bar{J}(C_{fd,0} = 1)$	0.508	0.238	0.228	–	0.176	0.131	0.131	–	0.135	0.131	0.131	–

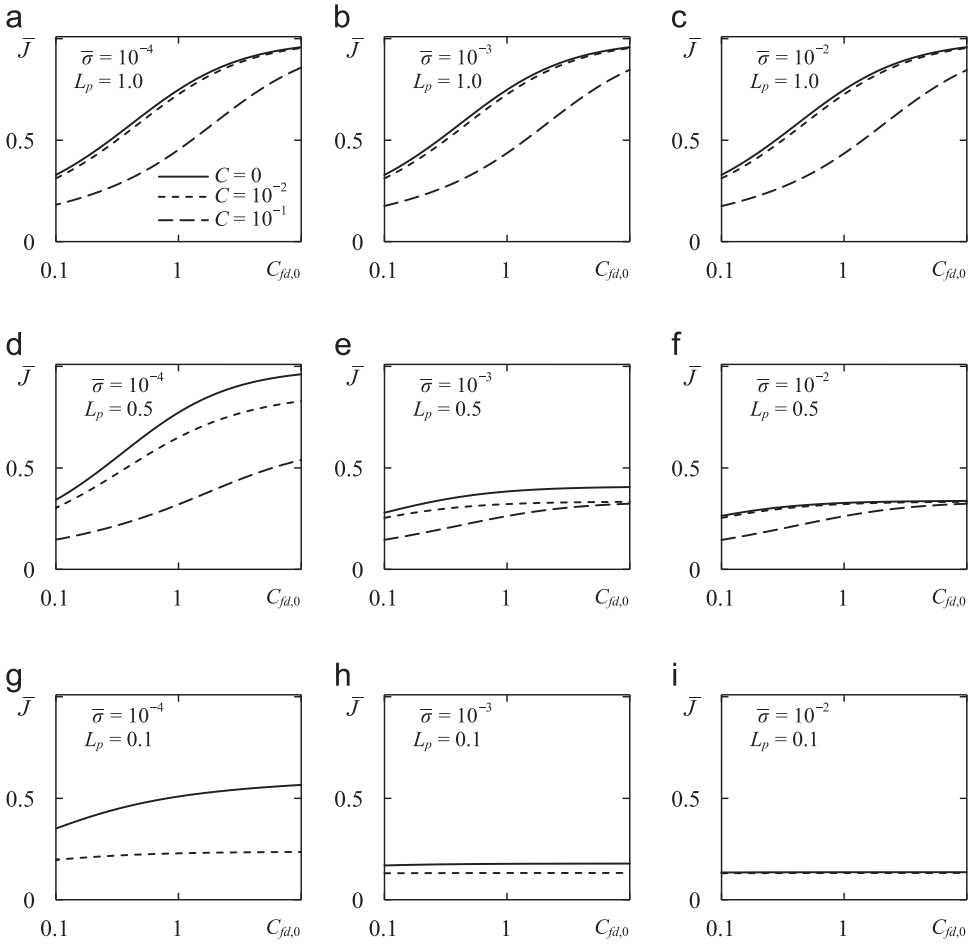

Fig. 4. Normalised productivity index vs. the design value of dimensionless fracture conductivity.

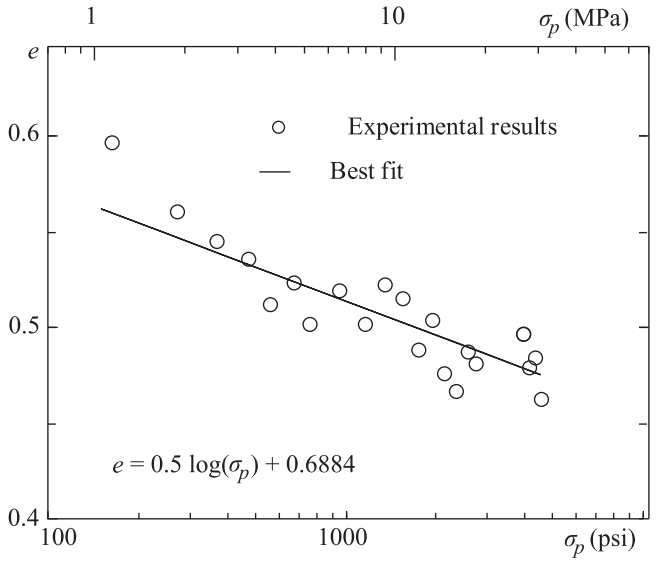

Fig. 5. Experimental results for e vs. log σ_p obtained by Lopez–Hernandez [40] for Carbolite® 18/12 ceramic proppant. The slope of a straight line fitted through the experimental data can be taken as the compressibility index C of the proppant pack over a particular range of compressive stresses.

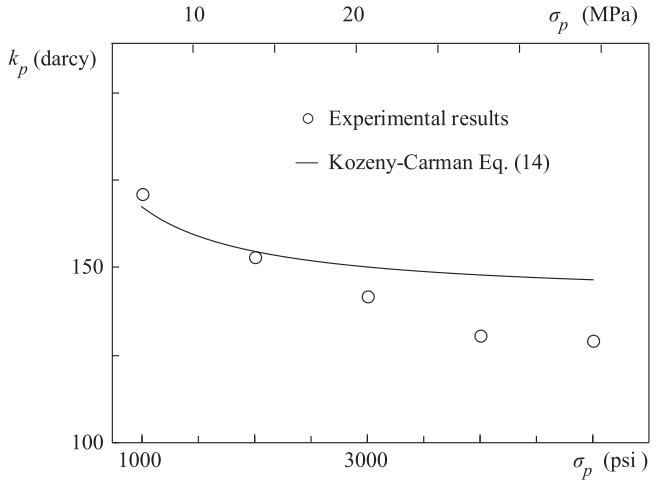

Fig. 6. Experimental results for k_p vs. σ_p obtained by Lopez–Hernandez [40] for Carbolite® 18/12 ceramic proppant. The Kozeny–Carman equation predicts similar trend as the experimental results and the maximum variation in permeability is 13.5% at 34.47 MPa (5000 psi).

This is because the model of proppant pack permeability provides physically meaningless values for this set of parameters (see discussion in Section 4).

9. Conclusion

In the present work, the fracture mechanics problem of a hydraulic fracture partially filled with a compressible proppant pack is studied. The confining stress leads to the partial closure of the unpropped fracture segments as well as the compaction of the proppant pack. The compaction of the proppant pack, in turn, also leads to a reduction of the average fracture opening as well as a reduction in the proppant pack permeability. A simple fluid flow model is utilized to quantify the effect of confining stress and partial filling of the fracture on the productivity index of the well.

The developed mathematical model provides a balance between the complexity and comprehension, which is crucial for engineering applications. The numerical results are obtained using the well-established and reliable solution techniques such as Gauss–Chebyshev quadrature method and Newton–Raphson iteration scheme. It is believed that the presented numerical results are reproducible and can be independently verified. The latter is often impossible with sophisticated numerical approaches, which currently dominate the research area.

It was found that the residual length of a fracture partially filled with proppant is essentially the same as the propped length of the fracture, at moderate to high values of confining stress. This means that any unpropped regions in the fracture will most likely close during the production stage. The aim of a fracturing treatment must be to maximize proppant transport in the fracture, since the productivity index of a fully filled fracture is greater than a partially filled fracture. There should be some means to estimate the extent of propped transport in a fracture in order to determine the residual length of the fracture and the productivity index of the fractured well, for example, with the help of radioactive tracer particles.

It was demonstrated in the present work that the residual opening of the fracture and the permeability of the proppant pack might be significantly lower than the expected or design values (see Tables 4–6). A method for obtaining the dependence of the residual opening and permeability on the confining stress, using experimental results, was also presented. We believe that the outcomes of this work can guide the design of hydraulic fracturing stimulations and aid in the selection of appropriate proppant for achieving the maximum efficiency of fracture stimulations.

References

[1] Economides MJ, Nolte KG. Reservoir stimulation. 3rd ed. . Chichester, England: Wiley; 2000.
[2] Rahman MM, Rahman MK. A review of hydraulic fracture models and development of an improved pseudo-3D model for stimulating tight oil/gas sand. Energy Sources Part A. 2010;93:1416–36.
[3] Adachi JI, Siebrits E, Peirce A, Desroches J. Computer simulation of hydraulic fractures. Int J Rock Mech Min Sci 2007;44:739–57.
[4] Mahrer KD. A review and perspective on far-field hydraulic fracture geometry studies. J Pet Sci Eng 1999;24:13–28.
[5] Yew CH. Mechanics of hydraulic fracturing. Houston, Texas: Gulf Professional Publishing; 1997.
[6] Warpinski NR, Moschovidis ZA, Parker CD, Abou-Sayed IS. Comparison study of hydraulic fracturing models—test case: GRI staged field experiment no. 3. SPE Prod Facil 1994;9:7–16.
[7] Clark PE, Güler N. Prop transport in vertical fractures: settling velocity correlations. In: SPE/DOE low permeability gas reservoirs symposium. Denver, Colorado; 1983.
[8] Clark PE, Quadir JA. Prop transport in hydraulic fractures: a critical review of particle settling velocity equations. In: SPE/DOE low permeability gas reservoirs symposium. Denver, Colorado;1981.
[9] Barree RD, Cox SA, Gilbert JV, Dobson M. Closing the gap: fracture half length from design, buildup, and production analysis. In: SPE annual technical conference and exhibition. Denver, Colorado; 2003.
[10] Cutler RA, Enniss DO, Jones AH, Swanson SR. Fracture conductivity comparison of ceramic proppants. SPE J 1985;25:157–70.
[11] Montgomery CT, Steanson RE. Proppant selection: the key to successful fracture stimulation. J Petrol Technol 1985;37:2163–72.
[12] Barree RD, Cox SA, Barree VL, Conway MW. Realistic assessment of proppant pack conductivity for material selection. In: SPE annual technical conference and exhibition. Denver, Colorado; 2003.
[13] Khanna A, Bortolan Neto L, Kotousov A. Effect of residual opening on the inflow performance of a hydraulic fracture. Int J Eng Sci 2014;74:80–90.
[14] Kotousov A, Bortolan Neto L, Khanna A. On a rigid inclusion pressed between two elastic half spaces. Mech Mater 2014;68:38–44.
[15] Bortolan Neto L, Kotousov A. Residual opening of hydraulic fractures filled with compressible proppant. Int J Rock Mech Min Sci 2013;61:223–30.
[16] Bortolan Neto L, Kotousov A. On the residual opening of hydraulic fractures. Int J Fract 2013;181:127–37.
[17] Bortolan Neto L, Kotousov A. Residual opening of hydraulically stimulated fractures filled with granular particles. J Pet Sci Eng 2012;100:24–9.
[18] Bortolan Neto L, Khanna A. The performance of hydraulic fractures partially filled with compressible proppant. Aust J Mult Eng 2013;10:185–97.
[19] Geertsma J, de Klerk F. A rapid method of predicting width and extent of hydraulically induced fractures. J Petrol Technol 1969;21:1571–81.

[20] Khristianovic SA, Zheltov YP. Formation of vertical fractures by means of highly viscous liquid. In: Fourth world petroleum congress. Rome, Italy; 1955. p. 579–586.
[21] Mokryakov V. Analytical solution for propagation of hydraulic fracture with Barenblatt's cohesive tip zone. Int J Fract 2011;169:159–68.
[22] Papanastasiou P. The effective fracture toughness in hydraulic fracturing. Int J Fract 1993;96(2):127–47.
[23] Garagash DI. Plane-strain propagation of a fluid-driven fracture during injection and shut-in: asymptotics of large toughness. Eng Fract Mech 2006;73(4):456–81.
[24] Terzaghi K, Peck RB, Mesri G. Soil mechanics in engineering practice. 3rd ed.. New York, NY: John Wiley & Sons; 1996.
[25] Pestana JM, Whittle AJ. Compression model for cohesionless soils. Geotechnique 1995;45:611–31.
[26] Mavko G, Nur A. The effect of a percolation threshold in the Kozeny–Carman relation. Geophysics 1997;62:1480–2.
[27] Lee DS, Elsworth D, Yasuhara H, Weaver JD, Rickman R. Experiment and modeling to evaluate the effects of proppant-pack diagenesis on fracture treatments. J Pet Sci Eng 2010;74:67–76.
[28] Tiab D, Donaldson EC. Petrophysics: theory and practice of measuring reservoir rock and fluid transport properties. 2nd ed.. Boston, Massachusetts: Gulf Professional Pub; 2004.
[29] Penny GS. An evaluation of the effects of environmental conditions and fracturing fluids upon the long-term conductivity of proppants. In: SPE annual technical conference and exhibition, SPE-16900-MS, 27–30 September, Dallas, Texas; 1987.
[30] Kotousov A. Fracture in plates of finite thickness. Int J Solids Struct 2007;44:8259–73.
[31] Bilby B, Eshelby J. Dislocations and the theory of fracture. In: Treatise H Liebowitz, editor. Fracture: an advanced. New York, NY: Academic Press; 1968. p. 99–182.
[32] Hills DA, Kelly PA, Dai DN, Korsunsky AM. Solution of crack problems: the distributed dislocation technique. London, England: Kluwer Academic Publishers; 1996.
[33] Conway JH, Sloane NJA. Sphere packings, lattices, and groups. 3rd ed.. New York, NY: Springer; 1999.
[34] Macdonald IF, El-Sayed MS, Mow K, Dullie FAL. Flow through porous media-the Ergun equation revisited. Ind Eng Chem Fundam 1979;18(3):199–208.
[35] Zazovskii AF, Todua GT. Steady inflow into a well with a long vertical fracture. Fluid Dyn 1990;25:584–93.
[36] Balueva AV, Zazovskii AF. Elastic–hydrodynamic problem of inflow of fluid to a crack in a porous media. Mech Solids 1985;20:151–60.
[37] Snow DT. A parallel plate model of fractured permeable media. University of California; 1965 (PhD thesis).
[38] Barenblatt GI, Entov VM, Ryzhik VM. Theory of fluid flows through natural rocks. 1st ed.. Amsterdam, Netherlands: Springer; 1990.
[39] Coduto DP. Foundation design: principles and practices. Upper Saddle River, New Jersey: Prentice Hall; 2001.
[40] Lopez-Hernandez HD. Experimental analysis and macroscopic and pore-level flow simulations to compare non-Darcy flow models in porous media. Golden, Colorado: Colorado School of Mines; 2007 (PhD thesis).

Appendix B

Effect of residual opening on the inflow performance of a hydraulic fracture

International Journal of Engineering Science 74 (2014) 80–90

Contents lists available at ScienceDirect

International Journal of Engineering Science

journal homepage: www.elsevier.com/locate/ijengsci

Effect of residual opening on the inflow performance of a hydraulic fracture

Aditya Khanna *, Luiz Bortolan Neto, Andrei Kotousov

School of Mechanical Engineering, The University of Adelaide, Adelaide, SA 5005, Australia

ARTICLE INFO

Article history:
Received 17 May 2013
Received in revised form 29 August 2013
Accepted 30 August 2013
Available online 29 September 2013

Keywords:
Hydraulic fracturing
Distributed dislocation technique
Finite conductivity
Residual opening profile
Well productivity index

ABSTRACT

The problem of steady state fluid production from a hydraulic fracture subject to remote compressive stresses is considered. The fracture is partially filled with proppant and the distribution of proppant is symmetric about the wellbore. The unpropped fracture segments can provide additional length to the fracture and highly conductive pathways for fluid flow. However, these fracture segments are susceptible to closure due to the confining stresses. The governing equations for fracture opening and fluid flow into the fracture are solved numerically using the Gauss–Chebyshev quadrature technique and a sensitivity study is conducted to investigate the effect of the residual opening of the unpropped fracture segments on the performance of a hydraulic fracture. The range of governing parameters is identified for which the residual opening of a fracture leads to production enhancement.

1. Introduction

Hydraulic fracturing is a widely applied technique in oil and gas industries for enhancing the productivity of wells drilled in low-permeability reservoirs (Valkò & Economides, 1995). Among many parameters, the increase in well productivity due to the fracturing treatment also depends upon the residual opening of the fracture which incorporates the length, width and shape of the fracture during the production stage. Typically, a fracture is only partially filled with proppant due to the plugging of proppant particles between the asperous fracture walls or their sedimentation during the proppant injection stage. Partial filling of a hydraulic fracture can lead to a complex residual opening profile during the production stage (Bortolan Neto & Kotousov, 2012b; Bortolan Neto & Kotousov, 2013) and complete closure of the unpropped fracture segments. Such effects have not been incorporated in the existing analytical solutions for fluid production from hydraulic fractures (Diyashev & Economides, 2006; Entov & Murzenko, 1994; Kanevskaya & Kats, 1996; Valkò & Economides, 1995). The presence of unpropped fracture segments with much higher conductivity than the sand-filled or propped fracture may significantly alter the inflow performance of the fracture and subsequently the production rate. It is of practical importance to investigate the effect of residual opening of a partially filled fracture on the well productivity. In particular, the range of governing parameters for which fracture residual opening has a significant impact on production must be identified (McLennan et al., 2008; Mukherjee et al., 1995).

In this paper, a hydraulic fracture which is partially filled with proppant is modelled as a straight crack opened by a rigid inclusion and subject to remote compressive stresses as illustrated in Fig. 1. The solution to the mechanical problem is obtained by using the distributed dislocation technique (Bilby and Eshelby, 1968, chap. 2). This solution for the residual opening profile is substituted into the governing equations for fluid production to evaluate the effect of residual fracture

* Corresponding author. Tel.: +61 8 8313 6385.
E-mail address: aditya.khanna@adelaide.edu.au (A. Khanna).

0020-7225/$ - see front matter © 2013 Elsevier Ltd. All rights reserved.
http://dx.doi.org/10.1016/j.ijengsci.2013.08.012

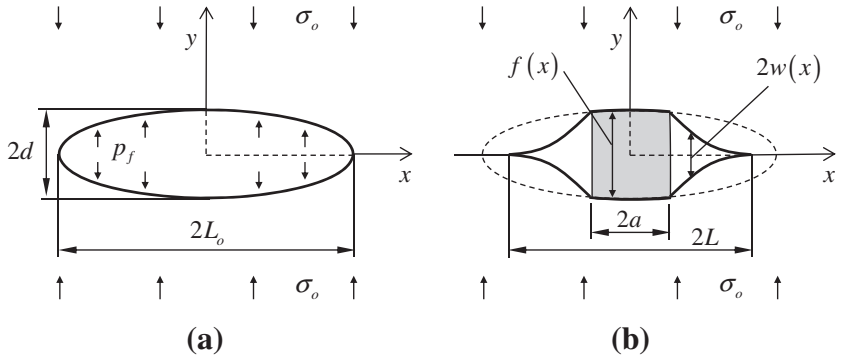

Fig. 1. Schematic representation of a partially filled hydraulic fracture as a 2D crack opened by a rigid inclusion and subject to remote compressive stresses (a) The initial crack geometry prior to the injection of proppant and (b) The residual opening profile of the crack upon the removal of the fracturing fluid pressure.

opening on the inflow performance of a hydraulic fracture. The main objective of the simplified modelling is to evaluate the effect of the residual opening on the production rate and to investigate general tendencies of the numerical solution by conducting a case study.

2. Mathematical model

Consider a fracture of initial length $2L_o$ and maximum opening $2d$ as shown in Fig. 1(a). The fracture is partially supported by a proppant pack and subject to remote confining stresses. Due to the confining stresses, closure of the un-propped segments of the fracture occurs and the equilibrium crack length $2L$ needs to be determined (Fig. 1(b)). The coordinate x is aligned with the length of the fracture and the problem is symmetric about $x = 0$. The symmetry of the problem is utilized in the mathematical model and the governing equations are written over the interval $-L \leq x \leq 0$.

2.1. Residual opening profile

The opening profile of a crack subject to uniform internal pressure is given by:

$$f(x) = 2d\sqrt{(1-(x/L_o)^2} \tag{1}$$

The elliptical opening profile defined in Eq. (1) is commonly used to model the opening of hydraulic fractures and is referred as the KGD fracture geometry (Valkò & Economides, 1995). It is used to represent the initial opening profile of the fracture as shown in Fig. 1.

The residual opening profile of a crack opened by a rigid inclusion over $|x| \leqslant a$ can be calculated by considering the following boundary value problem:

$$2w(x) = f(x), \quad |x| \leqslant a, \tag{2a}$$

$$w(x) = 0, \quad |x| \geqslant L, \tag{2b}$$

$$\sigma_{yy}(x,0) = -\sigma_o, \quad a < |x| < L, \tag{2c}$$

$$\sigma_{xy}(x,0) = 0, \quad |x| < \infty, \tag{2d}$$

where $2w(x)$ is the residual opening profile and σ_o is the remote confining stress. The sign convention for stress is positive under tension. The unknown equilibrium crack length L is determined using the condition of no stress singularity at the crack tips i.e. $x = \pm L$.

The boundary value problem (2) can be formulated in terms of the function $b(x)$ associated with the edge dislocation density (Hills et al., 1996). The edge dislocation density function $b(x)$ is related to the crack opening as follows:

$$b(x) = -2\frac{dw(x)}{dx}, \quad w(x) = -\frac{1}{2}\int_{-\infty}^{x} b(t)dt. \tag{3}$$

For the coordinate system shown in Fig. 1, the edge dislocation density is an odd function of x i.e. $b(x) = -b(-x)$. Utilising the symmetry of the problem, the following Föppl integral equation can be written for the edge dislocation density function (Kotousov et al., 2013):

$$\frac{2}{\pi}\int_{-L}^{-a}\frac{t_2 b(t_2)}{x^2-t_2^2}dt_2=\frac{2}{\pi}\int_{-a}^{0}\frac{t_1 f'(t_1)}{x^2-t_1^2}dt_1+\frac{4\sigma_o(1-\nu^2)}{E},\quad -L\leqslant x\leqslant -a, \tag{4}$$

where t_1 and t_2 are dummy integration variables, σ_o is the confining stress and E and ν are the Young's modulus and Poisson's ratio of the rock. In the limit $x\to a^+$, the crack opening must be continuous i.e. the following additional condition must be satisfied:

$$f(a+)=-\int_{-L}^{-a}b(t)dt. \tag{5}$$

The solution to equation (4) subject to condition (5) yields the unknown dislocation density $b(x)$ over the interval $-L\leqslant x\leqslant -a$ and the residual opening profile of the crack can be calculated using Eq. (3).

2.2. Fluid flow into the fracture

The steady state two-dimensional flow from the reservoir towards the hydraulically fractured well is described by the following system of equations (Zazovskii & Todua, 1990):

$$\mathbf{u}(x,y)=-\frac{k}{\mu}\nabla p(x,y) \tag{6}$$

$$\operatorname{div}\mathbf{u}=0 \tag{7}$$

For the one-dimensional flow in a fracture with variable opening $2w(x)$, which is partially filled with proppant, the following system of equations can be written:

$$v(x)=\begin{cases}-\frac{k_f}{\mu}\frac{dp_f}{dx}, & 0\leqslant|x|<a\\ -\frac{w^2(x)}{3\mu}\frac{dp_f}{dx}, & a<|x|\leqslant L\end{cases}, \tag{8}$$

$$\frac{d}{dx}(w(x)v(x))+q(x)=0 \tag{9}$$

Here $\mathbf{u}$ and v are the seepage flow velocities in the reservoir and the fracture, p and p_f are the respective fluid pressures, μ is the fluid viscosity, k is the reservoir permeability, k_f is the permeability of the proppant pack, $w(x)$ is half of the residual opening of the fracture and $q(x)$ is the fluid flux per unit thickness which enters one of the faces of the fracture. Eqs. (7) and (9) are the continuity equations for flow in the reservoir and the fracture respectively. Eq. (6) is the Darcy's law for fluid flow in the porous reservoir and Eq. (8) is the governing equation for one-dimensional flow in the partially filled fracture. Darcy's law is used in the propped region of the fracture and Boussinesq's formula for laminar flow between two plates is used in the unpropped region of the fracture (Balueva & Zazovskii, 1995). In addition to Eq. (6)–(9), the conditions of continuity of fluid flux and fluid pressure at the fracture surfaces have to be fulfilled. These can be written as:

$$q(x)=u_y(x,0),\quad |x|<L, \tag{10}$$

$$P_f(x)=p(x,0),\quad |x|<L. \tag{11}$$

From Eqs. (6) and (7) it follows that the fluid pressure in the reservoir satisfies the Laplace equation

$$\nabla^2 p(x,y)=0, \tag{12}$$

the solution to which is obtained in terms of an auxiliary function $\psi(x)$ defined as:

$$\psi(x)=\frac{\partial p(x,0)}{\partial y},\quad \psi(x)=\begin{cases}\psi_1(x), & |x|<a\\ \psi_2(x), & a<|x|<L\\ 0, & |x|>L\end{cases} \tag{13}$$

The function $\psi(x)$ multiplied by the constant $-k/\mu$ yields the fluid flux $q(x)$ entering the fracture. Due to the symmetry of the problem, $\psi(x)$ is even, i.e. $\psi(x)=\psi(-x)$ and the unknown functions $\psi_1(x)$ and $\psi_2(x)$ represent the fluid flux entering the propped and unpropped regions of the fracture, respectively.

The general solution to the Laplace equation (15) subject to boundary condition (13) over the region $-\infty<x\leqslant 0, 0\leqslant y<\infty$ is given by Polyanin (2002):

$$p(x,y)=\frac{1}{\pi}\int_{-L}^{-a}\psi_2(t_2)\ln\sqrt{\left(x^2-t_2^2\right)^2+y^2}dt_2+\frac{1}{\pi}\int_{-a}^{0}\psi_1(t_1)\ln\sqrt{\left(x^2-t_1^2\right)^2+y^2}dt_1. \tag{14}$$

The pressure gradient along the fracture can be obtained by differentiating Eq. (14) with respect to x and by utilizing condition (11). This results into:

$$\frac{dp_f}{dx}=\frac{\partial p(x,0)}{\partial x}=\frac{2}{\pi}\int_{-L}^{-a}\frac{\psi_2(t_2)x}{x^2-t_2^2}dt_2+\frac{2}{\pi}\int_{-a}^{0}\frac{\psi_1(t_1)x}{x^2-t_1^2}dt_1,\quad -L\leqslant x\leqslant 0. \tag{15}$$

Eq. (15) is used to derive the governing equation for fluid flow in the fracture. The governing equation over the unpropped region $-L\leqslant x\leqslant -a$ is:

$$\frac{2w^3(x)}{3\pi}\left[\int_{-a}^{0}\frac{\psi_1(t_1)x}{x^2-t_1^2}dt_1+\int_{-L}^{-a}\frac{\psi_2(t_2)x}{x^2-t_2^2}dt_2\right]+k\int_{-L}^{x}\psi_2(t_2)dt_2=0 \tag{16}$$

and over the propped region i.e. $-a\leqslant x\leqslant 0$ is:

$$\frac{2k_f w(x)}{\pi}\left[\int_{-a}^{0}\frac{\psi_1(t_1)x}{x^2-t_1^2}dt_1+\int_{-L}^{-a}\frac{\psi_2(t_2)x}{x^2-t_2^2}dt_2\right]+k\left[\int_{-a}^{0}\psi_1(t_1)dt_1+\int_{-L}^{-a}\psi_2(t_2)dt_2\right]=0. \tag{17}$$

At $x=-a$, the right hand sides of Eqs. (16) and (17) become equal because of the continuity of the fluid flux at $|x|=a$. The derivation of the governing Eqs. (16) and (17) follows directly from Zazovskii and Todua (1990), hence the details are omitted. The integral equations (16) and (17) are supplemented by the condition of conservation of mass:

$$\frac{2k}{\mu}\left[\int_{-a}^{0}\psi_1(t_1)dt_1+\int_{-L}^{-a}\psi_2(t_2)dt_2\right]=Q, \tag{18}$$

i.e. the total fluid flux entering the fracture must be equal to the rate of fluid production at the wellbore.

2.3. Dimensionless form of governing equations

To obtain the dimensionless form of equations of the governing Eqs. (4), (5), (16), (17), and (18), the following dimensionless parameters are introduced:

$$\delta(x)=\frac{w(x)}{d},\quad A=\frac{a}{L},\quad \bar{\sigma}=\frac{4\sigma_o(1-\nu^2)}{E},\quad C=\frac{1}{\pi}\frac{k_f}{k}\frac{d}{L},\quad \Psi=\frac{kL}{Qu}\psi,\quad k=\frac{3k_f}{d^2}. \tag{19}$$

The parameter $\delta(x)$ is the normalized residual opening of the crack, A is the dimensionless propped length of the fracture, $\bar{\sigma}$ is the dimensionless confining stress, C is the dimensionless fracture conductivity, Ψ is the dimensionless fluid flux entering the fracture and κ is the dimensionless proppant pack permeability.

In addition, the scaled coordinates X_1 and X_2 are introduced over the intervals $-a\leqslant x\leqslant 0$ and $-L\leqslant x\leqslant -a$, respectively. The scale transformation $x=(X_1-1)a/2$ is performed over $-a\leqslant x\leqslant 0$ to provide $-1\leqslant X_1\leqslant 1$ and the scale transformation $x=X_2(L-a)/2-(L+a)/2$ is performed over the interval $-L\leqslant x\leqslant -a$ resulting in $-1\leqslant X_2\leqslant 1$. Two dummy integration variables ξ_1 and ξ_2 are introduced such that $t_1=(\xi_1-1)a/2$ and $t_2=\xi_2(L-a)/2-(L+a)/2$. Subsequently, the governing equations for fracture residual opening (4), (5) can be written in terms of dimensionless variables as:

$$\frac{2}{\pi}\int_{-1}^{1}\frac{[(1-A)\xi_2-(1+A)]b(\xi_2)d\xi_2}{[(1-A)(X_2+\xi_2)-2(1+A)](X_2-\xi_2)}=\frac{2}{\pi}\int_{-1}^{1}\frac{A^2(\xi_1-1)f'(\xi_1)d\xi_1}{[(1-A)X_2-A\xi_1-1][(1-A)X_2+A\xi_1-(1+2A)]}+\bar{\sigma} \tag{20}$$

and

$$\int_{-1}^{1}b(\xi_2)d\xi_2=-\frac{2f(a+)}{L-a}. \tag{21}$$

The normalized residual opening $\delta(X_2)$ over the interval $-1\leqslant X_2\leqslant 1$ is given by:

$$\delta(X_2)=-\frac{L-a}{4}\int_{-1}^{X_2}b(\xi_2)d\xi_2. \tag{22}$$

It follows from Eq. (1) that the normalized residual opening over the interval $-1\leqslant X_1\leqslant 1$ is simply given by $\delta(X_1)=\sqrt{1-X_1^2}$.

The governing equation for fluid flux distribution (16)–(18) can be re-written in terms of dimensionless parameters introduced by Eq. (19) as:

$$\frac{\delta^3(X_2)}{\kappa}\left[\int_{-1}^{1}\frac{A[(1-A)X_2-(1+A)]\Psi_1(\xi_1)d\xi_1}{[(1-A)X_2+A\xi_1-(1+2A)][(1-A)X_2-A\xi_1-1]}+\int_{-1}^{1}\frac{[(1-A)X_2-(1+A)]\Psi_2(\xi_2)d\xi_2}{[(1-A)(X_2+\xi_2)-2(1+A)](X_2-\xi_2)}\right]+\frac{1}{4C}\left[(1-A)\int_{-1}^{X_2}\Psi_2(\xi_2)d\xi_2\right]=0, \tag{23}$$

$$\delta(X_1)\left[\int_{-1}^{1}\frac{A(1-A)(X_1-1)\Psi_2(\xi_2)d\xi_2}{[AX_1+(1-A)\xi_2-(1+2A)][AX_1-(1-A)\xi_2+1]}+\int_{-1}^{1}\frac{(X_1-1)\Psi_1(\xi_1)d\xi_1}{(X_1+\xi_1-2)(X_1-\xi_1)}\right]+\frac{1}{4C}\left[A\int_{-1}^{X_1}\Psi_1(\xi_1)d\xi_1+(1-A)\int_{-1}^{1}\Psi_2(\xi_2)d\xi_2\right]=0 \tag{24}$$

and

$$A\int_{-1}^{1}\Psi_1(\xi_1)d\xi_1+(1-A)\int_{-1}^{1}\Psi_2(\xi_2)d\xi_2=1. \tag{25}$$

Finally, Eq. (13) can be written in dimensionless form as

$$\Psi(X)=\begin{cases}\Psi_1(X), & 0\leqslant|X|\leqslant A\\ \Psi_2(X), & A\leqslant|X|\leqslant 1\end{cases}, \tag{26}$$

where $X=x/L$ is the normalized coordinate along the fracture length.

A numerical procedure based on Gauss–Chebyshev quadrature method is utilized for obtaining the solution to the system of Eqs. (20)–(25). It is described in Appendix A. In the next section, the well productivity index is defined as a function of the fluid flux distribution $\Psi(X)$ along the fracture length.

3. Well productivity index

The well productivity index is a common parameter widely used to describe the inflow performance of a hydraulic fracture. For a well producing at a constant rate and located at the centre of a circular reservoir, the well productivity index J is given by (Valkò and Economides, 1995):

$$J=\frac{Qh}{p_e-p_w}=\frac{2\pi hk}{\mu}J_D, \tag{27}$$

where Q is the production rate per unit thickness, h is the thickness of the reservoir, p_e is the constant reservoir pressure at the outer boundary of the circular reservoir ($r=r_e$), p_w is the fluid pressure at the wellbore ($r=r_w$) and J_D is the dimensionless well productivity index. For a well with no fracture, the dimensionless well productivity index is simply given by $J_D=1/\ln(r_e/r_w)$ Valkò & Economides (1995) and for a well containing a symmetric hydraulic fracture, the dimensionless productivity index J_D is given by Zazovskii and Todua, (1990):

$$J_D=\left[\ln\frac{r_e}{L}-\int_{-1}^{1}\Psi(X)\ln X\,dX\right]^{-1}. \tag{28}$$

In order to evaluate the effect of residual opening on the performance of a hydraulic fracture, the hydraulic fracture is compared to a fracture of length $2L_o$ with an infinite conductivity $C\to\infty$. In practice, values of $C>100$ can be treated as infinite conductivity and this situation is referred as an ideal fracture. The fluid flux distribution for an ideal fracture is given by $\Psi(X)=\pi^{-1}(1-X^2)^{-1/2}$ and the dimensionless productivity index becomes $J_D=1/\ln(2r_e/L_o)$. Thus, the normalized productivity index of the hydraulic fracture is given by:

$$\bar{J}=\frac{\ln 2r_e/L_o}{\ln r_e/L-\int_{-1}^{1}\Psi(X)\ln X\,dX}. \tag{29}$$

The limit $\bar{J}\to 1$ implies that the equilibrium length of the fracture $2L$ is equal to the initial length $2L_o$ and the fracture has infinite conductivity. The closer $\bar{J}$ is to unity, the better is the performance of the hydraulically fractured well.

4. Numerical results and discussion

In this section, some interesting numerical calculations are presented for a fracture of an initial length $2L_o=100$ m and maximum opening $2d=1$ cm which lies at the centre of a circular reservoir of radius $r_e=500$ m. During a hydraulic fracturing treatment, the fracture dimensions can be estimated using a variety of mathematical models such as those provided in Valkò and Economides (1995) and Mikhailov et al., (2011). Three values of the dimensionless confining stress are chosen for the sensitivity study: $\sigma=10^{-4}$, 10^{-3} and 10^{-2}. For a typical sandstone reservoir with Young's modulus $E=20$ GPa and Poisson's ratio $\nu=0.25$, these value represent confining stresses in the range of 2–200 MPa. Further, two cases of proppant filling are considered: when only a small region in the vicinity of the wellbore is filled with proppant, say $a/L_o=0.1$ and when half of the fracture is filled with proppant i.e. $a/L_o=0.5$. For these parameters, the effect of residual opening on the well productivity index is investigated.

4.1. Normalized residual opening

The dependence of the residual opening upon the confining stress is shown in Fig. 2. At $\overline{\sigma}=10^{-4}$ (corresponding to very low confining stress) the deformation of the unpropped fracture segment is not significant whereas at $\overline{\sigma}=10^{-2}$ (corresponding to very high confining stress) almost complete closure of the unpropped fracture segment occurs. Table 1 contains the numerical values for the equilibrium crack length and the dimensionless propped length of the fracture corresponding to the curves in Fig. 2.

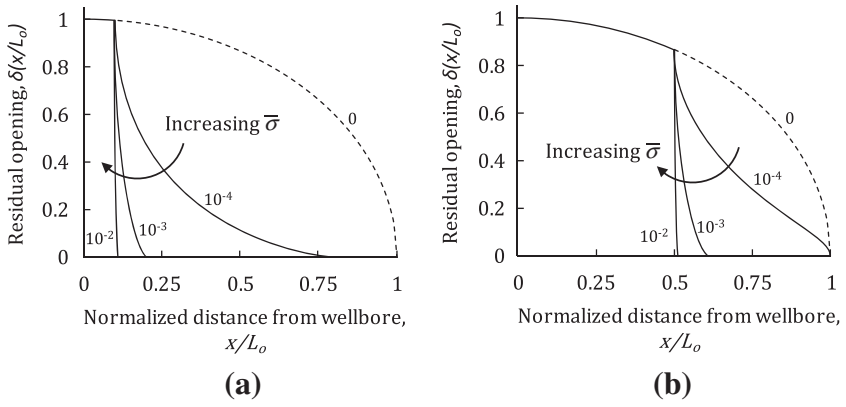

Fig. 2. The dependence of the residual opening profile on the confining stress (a) $a/L_o = 0.1$ and (b) $a/L_o = 0.5$. The dotted line represents the initial fracture opening profile.

Table 1
Equilibrium crack length L/L_o and dimensionless propped length A of the fracture.

a/L_o	$\bar{\sigma}$	L/L_o	$A = a/L$	a/L_o	$\bar{\sigma}$	L/L_o	$A = a/L$
0.1	10^{-4}	0.809	0.124	0.5	10^{-4}	1.000	0.500
	10^{-3}	0.204	0.490		10^{-3}	0.608	0.822
	10^{-2}	0.112	0.893		10^{-2}	0.511	0.978

4.2. Dimensionless fluid flux distribution

For given residual opening profile $\delta(X)$ and dimensionless propped length A, the dimensionless fluid flux distribution $\Psi(X)$ is governed by the dimensionless proppant pack permeability κ and the dimensionless fracture conductivity C. The range of these two parameters for which the sensitivity study is identified first.

The proppant pack comprises of several layers of spherical proppant particles packed between the walls of the fracture, hence fluid flow in the propped region of the fracture occurs via a network of interconnected pores within the proppant pack. On the other hand, the fluid flow path in the unpropped fracture segments is unrestricted i.e. there is negligible resistance to flow. It implies that the parameter $\kappa << 1$ (Khanna et al., 2012). Preliminary numerical calculations conducted in the present work suggests that the value of the parameter κ does not effect the solution for $\Psi(X)$ significantly for $\kappa \leqslant 10^{-2}$. Thus, all calculations for $\Psi(X)$ are performed for $\kappa = 10^{-2}$. Similar arguments can be made regarding the dimensionless fracture conductivity C. The solution for $\Psi(X)$ does not change significantly beyond $C > 100$, which corresponds to the ideal fracture. On the other hand, for values of $C < 0.01$, the fluid flux is concentrated in a very small region in the vicinity of the wellbore and the length of the fracture does not significantly affect the production. Hence, the range $0.01 \leqslant C \leqslant 100$ is considered in the present sensitivity study.

To demonstrate the effect of partial filling of the fracture on the fluid flux distribution $\Psi(X)$, numerical calculations are performed for a fracture with an elliptical opening profile $\delta(X) = \sqrt{1 - X^2}$. The values of dimensionless propped length are chosen to be $A = 0.1$ and 0.5 and the values of dimensionless fracture conductivity are chosen to be $C = 0.1$ and 10. The results are shown in Fig. 3. As expected, the partial filling of the fracture does not effect the fluid flux distribution at high fracture conductivity (Fig. 3(c) and (d)). For poor fracture conductivity, the partial filling of the fracture dramatically alters the fluid flux distribution along the fracture length. By comparing the solutions for $\Psi(X)$ for partially filled (solid line) and fully filled fractures (dotted line), see Fig. 3(a) and (b), it can be observed that in the case of partially filled fractures, the majority of the fluid enters the unpropped regions of the fracture. However, negative fluid flux near $|X| = A$ implies that a significant amount of the produced fluid leaks out of the fracture near the interface between the propped and unpropped region.

4.3. Simplified fluid flow model

It can be observed from Fig. 3(c) and (d), that for moderately high fracture conductivity the effect of permeability mismatch between the propped and unpropped fracture segments does not have a significant effect on the fluid flux distribution and hence, the well productivity. At low values of fracture conductivity (Fig. 3(a) and (b), the permeability mismatch leads to significant modification in the fluid flux distribution. However the well productivity given by Eq. (29) involves the integral of the fluid flux distribution over the length of the fracture. Thus, it can be expected that this quantity would be weakly sensitive to the permeability mismatch between the propped and unpropped fracture segments.

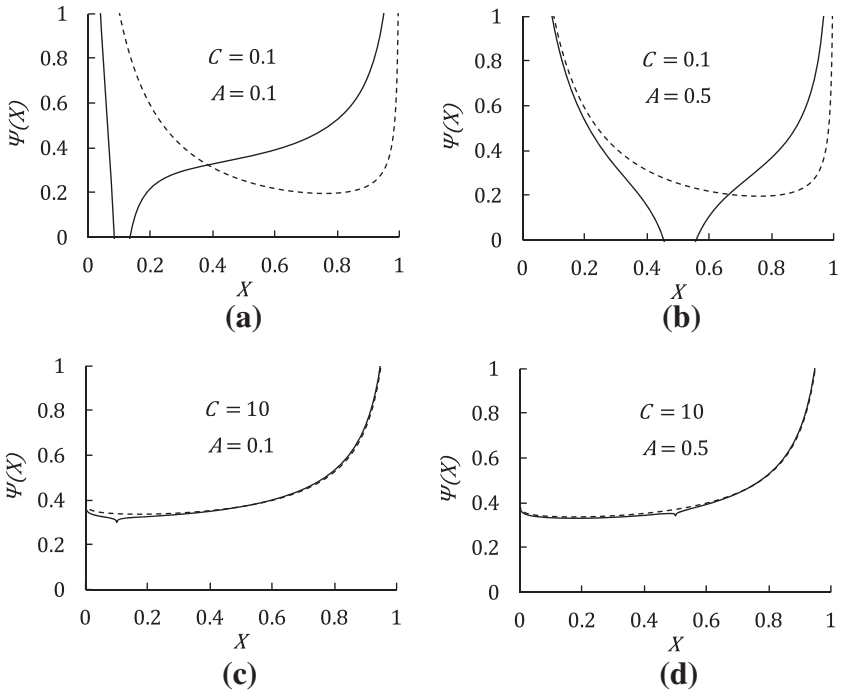

Fig. 3. Dimensionless fluid flux distribution along the fracture length. The dotted line corresponds to a fracture which is fully filled with proppant. It is identical for Fig. 3(a) and (b) and for Fig. 3(c) and (d).

It was also pointed out in Zazovskii and Todua (1990) that the well productivity is not significantly affected by the shape of the fracture especially at high values of fracture conductivity. Therefore, a much simpler model for fluid production is proposed by introducing the following assumptions:

1. The residual opening of the fracture over the length $2L$ is assumed to be constant, i.e. $2w(x) = 2d, \quad |x| \leqslant L$.
2. The permeability of the unpropped fracture length is assumed to be the same as the permeability of the propped length. Hence, the fracture permeability $k_f = \text{constant}, \quad |x| \leqslant L$.

Based on these assumptions, the governing equations of fluid flow (23)–(25) are reduced to the following equations given by Zazovskii and Todua (1990):

$$\int_{-1}^{1} \frac{\Psi(\xi)d\xi}{X-\xi} + \frac{1}{C}\int_{-1}^{X} \Psi(\xi)d\xi = \frac{1+\text{sgn}(X)}{2C} \tag{30}$$

and

$$\int_{-1}^{1} \Psi(\xi)d\xi = 1, \tag{31}$$

where the dimensionless coordinate $-1 \leqslant X \leqslant 1$ corresponds to $- - L \leqslant x \leqslant L$. The approximate solution obtained using Eqs. (30) and (31) is substituted into Eq. (29) and the results for well productivity index are compared to model developed in Section 2.2.

4.4. Well productivity index

Using Eq. (29), the effect of residual opening on the normalized well productivity index $\bar{J}$ can be investigated as well. In Fig. 4, the normalized well productivity index is calculated for the different residual opening profiles shown in Fig. 2. An increase in dimensionless confining stress leads to closure of the unpropped fracture segments and subsequent reduction in the productivity index of a partially filled fracture. By comparing Fig. 4(a) and (b), it can also be observed that the residual opening has a greater impact on well productivity when a shorter length of the fracture is filled with proppant.

The curves in Fig. 4 corresponding to $\overline{\sigma} = 10^{-2}$, essentially represent the productivity of a fracture with no residual opening. Conversely, the curves corresponding to $\overline{\sigma} = 10^{-4}$ represent the productivity of a fracture with negligible closure of the unpropped segments. A typical fracture is normally subjected to the confining stresses corresponding to the dimensionless confining stress of $\overline{\sigma} = 10^{-3}$ (Valkò & Economides, 1995). Accounting for the residual opening in such fractures leads to an

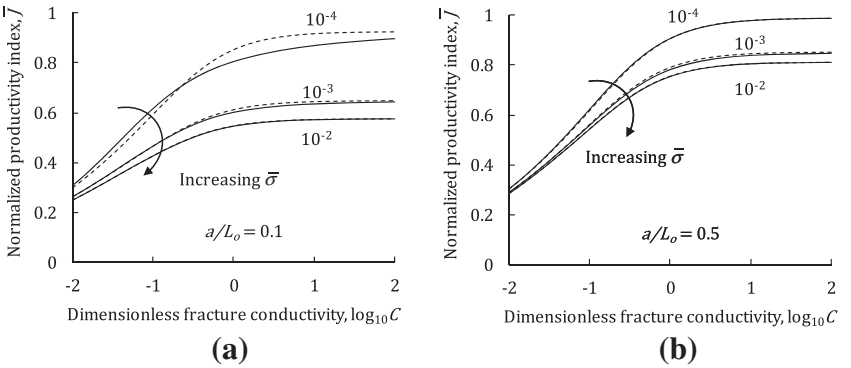

Fig. 4. The effect of residual opening on the inflow performance of a hydraulic fracture (a) only 10% of the fracture is filled with proppant (b) 50% of the fracture is filled with proppant.

increase of roughly 5–10% in the predicted well productivity index. For lower confining stresses the increase can reach up to 50% as shown in Fig. 4(a). This implies that the residual opening of a partially filled fracture is a secondary mechanism of productivity enhancement in fractures, specifically in low confining stress environment.

Fig. 4 also shows the comparison of the results for normalized well productivity obtained using the fluid flow model developed in Sections 2.2 (solid lines) and the simplified model proposed in Section 4.3 (dotted lines). The simplified model provides acceptable results for a wide range of the governing parameters, except for the situation when a fracture with small propped length a/L_o is subject to small dimensionless stress $\bar{\sigma}$. The comparison provides a useful result, namely the increase in well productivity is primarily due to additional fracture length rather than the shape of the fracture or the high conductivity of the un-propped fracture segments. Nonetheless, the fluid flow model developed in Section 2.2 should be viewed as non-trivial since:

1. The residual opening phenomenon is of significance only when the propped length a/L_o and dimensionless stress $\bar{\sigma}$ are small. It is in this range of governing parameters that we see the discrepancy between the developed model and its simplified version.
2. It was shown (as in Fig. 3(a) and (b) of the manuscript) that for a fracture with poor conductivity, the presence of highly conductive residual opening may not be beneficial. The proppant pack essentially acts as a plug in this situation leading to the leak-off of the fluid produced by the unpropped region back into the reservoir.

Another permeability enhancement mechanism which can lead to an increase of the production rate is the roughness induced opening of the fracture (Kotousov et al., 2011) in which case the height of the prominent surface asperities primarily governs the fracture conductivity (Zou et al., 2013). This mechanism is disregarded in the current study but can be also incorporated into the developed mathematical model (Bortolan Neto & Kotousov, 2012a).

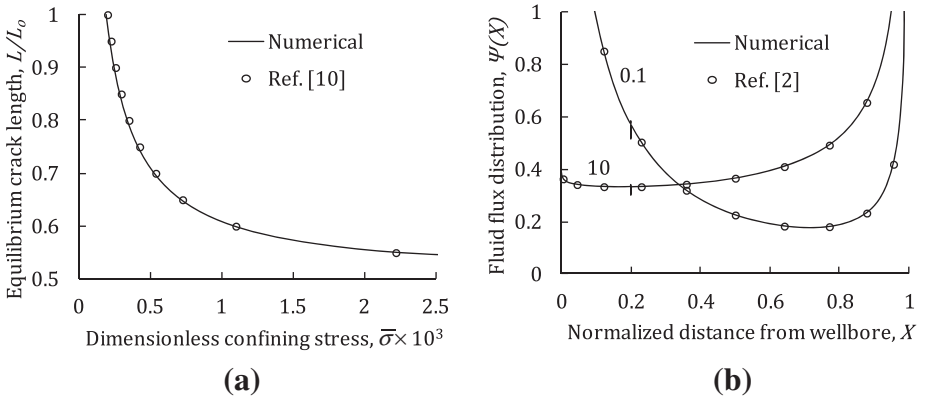

Fig. 5. Validation of numerical results: (a) Equilibrium crack length vs. dimensionless confining stress (b) Dimensionless fluid flux distribution along the fracture length.

5. Conclusion

The steady state fluid production from a partially filled hydraulic fracture was considered within a simplified mathematical formulation, which utilised the symmetry of the proppant distribution about the wellbore. The governing equation of the mechanical problem represents a Föppl-type integral equation, which was solved numerically. The solution for the residual profile was utilised in the fluid flow model, which provided a way for the calculation of the productivity index. The results indicated that the residual opening profile has a significant influence of the productivity rate at relatively low dimensionless confining stresses (ratio of the confining stresses to Young's modulus of the rock). The influence diminishes with an increase of the confining stresses. For typical or averaged conditions the effect of the residual opening on the productivity index is about 10%.

The considered model does not take into account many other non-linear effects. One of them mentioned above is the roughness induced opening of hydraulic fractures. Another important effect, which can significantly influence the flow in narrow fracture channels is the compressibility of proppant (Bortolan Neto & Kotousov, 2012b; Bortolan Neto & Kotousov, 2013). Accounting for the compressibility of the proppant pack will lead to the coupling of the mechanical and fluid problem and the solution can still be obtained numerically based in the method outlined in the Appendix A. However, this is a scope for future work.

Appendix A. Numerical solution technique

Gauss–Chebyshev quadrature method is utilized to obtain the numerical solutions to the system of singular integral equations (see Ref. Hills et al., 1996). By implementing the quadrature method, the singular integral equations can be converted to systems of linear equations which can be solved readily using Gaussian elimination.

The interval $-1 \leqslant X_1 \leqslant 1$ is discretized into N points, the interval $-1 \leqslant X_2 \leqslant 1j = 1\ldots M$ is discretized into M points and the following indices are defined: $i = 1\ldots N$, $k = 1\ldots N-1$ and $l = 1\ldots M-1$. The integration and collocation points over the interval $-1 \leqslant X_1 \leqslant 1$ are given by $s_i = \cos(\pi(2i-1)/2N)$ and $t_k = \cos(\pi k/N)$ respectively. The integration and collocation points over the interval $-1 \leqslant X_2 \leqslant 1$ are given by $S_j = \cos(\pi(2j-1)/2M)$ and $T_l = \cos(\pi l/M)$ respectively. The discretized form of the governing equations is presented next.

A.1. Residual opening profile

The governing equation for the edge dislocation density (20) contains the Cauchy kernel $(X_2-\xi_2)^{-1}$. The asymptotic behaviour is built into the solution for by writing the edge dislocation density function as $b(X_2) = W(X_2)\Theta(X_2)$ where $W(X_2) = (1-X_2)^{-1/2}$ is the fundamental solution and $\Theta(X_2)$ is an unknown regular function to be determined at M points along the interval $-1 \leqslant X_2 \leqslant 1$. The Eqs. (20) and (21) are discretized as:

$$\frac{2}{M}\sum_{j=1}^{M}\frac{[(1-A)S_j-(1+A)]\Theta(S_j)}{[(1-A)(T_l+S_j)-2(1+A)](T_l-S_j)} = \frac{2}{\pi}\int_{-1}^{1}\frac{A^2(\xi_1-1)f'(\xi_1)d\xi_1}{[(1-A)T_l-A\xi_1-1][(1-A)T_l+A\xi_1-(1+2A)]}+\bar{\sigma} \tag{A1}$$

and

$$\frac{\pi}{M}\sum_{j=1}^{M}\Theta(S_j) = -\frac{2f(a+)}{L-a}. \tag{A2}$$

Together, Eqs. (A1) and (A2) form a system of M linear equations which are solved to obtain the unknown edge dislocation density function $b(X_2)$. The residual opening profile can be then calculated using Eq. (22).

The mode-I stress intensity factors at $x = -L$ and $x = -a$, i.e. at $X_2 = \pm 1$ are given by Hills et al. (1996):

$$K_I(\pm 1) = \mp\frac{4(1-\nu^2)}{E}\sqrt{2\pi(L-a)}\Theta(\pm 1). \tag{A3}$$

For given values of $\bar{\sigma}$, a and L_o, the equilibrium crack length L is found by trial and error such that the value of $K_I(-1) \sim 0$, i.e. there is no stress singularity at the crack tips.

A.2. Fluid flux distribution

The governing equations for fluid flow (23) and (24) also contain the Cauchy kernel and the fluid flux distribution can be written as $\Psi_1(X_1) = W(X_1)\Phi_1(X_1)$ and $\Psi_2(X_2) = W(X_2)\Phi_2(X_2)$ where $W(X) = (1-X^2)^{-1/2}$ as before and $\Phi_1(X_1)$ and $\Phi_2(X_2)$ are unknown regular functions to be determined. Eq. (23) can be written as a system of $M-1$ equations:

$$\frac{\delta^3(T_l)}{\kappa}\left[\frac{\pi}{N}\sum_{i=1}^{N}\frac{\Phi_1(s_i)A[(1-A)T_l-(1+A)]}{[(1-A)T_l+As_i-(1+2A)][(1-A)T_l-As_i-1]}+\frac{\pi}{M}\sum_{j=1}^{M}\frac{\Phi_2(S_j)[(1-A)T_l-(1+A)]}{[(1-A)(T_l+S_j)-2(1+A)](T_l-S_j)}\right]$$
$$+\frac{(1-A)}{4C}\frac{\pi}{M}\sum_{j=l}^{M}\Phi_2(S_j) = 0. \tag{A4}$$

Similarly, equation (24) can be written as a system of N - 1 linear equations:

$$\delta(t_k)\left[\frac{\pi}{M}\sum_{j=1}^{M}\frac{\Phi_2(S_j)A(1-A)(t_k-1)}{[At_k+(1-A)S_j-(1+2A)][At_k-(1-A)S_j+1]}+\frac{\pi}{N}\sum_{i=1}^{N}\frac{\Phi_1(s_i)(t_k-1)}{(t_k+s_i-2)(t_k-s_i)}\right]$$
$$+\frac{1}{4C}\left[A\frac{\pi}{N}\sum_{i=k}^{N}\Phi_1(s_i)+(1-A)\frac{\pi}{M}\sum_{j=1}^{M}\Phi_2(S_j)\right]=0. \tag{A5}$$

Two additional linear equations are provided by Eq. (25) and the condition of continuity of fluid pressure at $|x| = a$:

$$A\frac{\pi}{N}\sum_{i=1}^{N}\Phi_1(s_i)+(1-A)\frac{\pi}{M}\sum_{j=1}^{M}\Phi_2(S_j)=1, \tag{A6}$$

$$\Phi_1(-1)=\Phi_2(+1). \tag{A7}$$

Together Eqs. (A4)–(A7) represent a system of $N + M$ linear equations which can be solved to obtain the unknown fluid flux distribution in the fracture.

Appendix B. Validation of the numerical results

B.1. Residual opening profile

The analytical method for obtaining the solution to the problem of a crack opened by a rigid inclusion and subject to remote confining stresses was presented in Maiti (1980). The analytical method is suitable for calculating the unknown equilibrium crack length but faces computational difficulties when calculating the residual opening profile. Hence, a numerical approach was utilized in the present work. The numerical method is validated by comparing the obtained results for the unknown equilibrium crack length to the results obtained using the analytical solution. The comparison is shown in Fig. 5(a) where the calculations were performed for a crack with an aspect ratio $d/L_o = 10^{-4}$ and a normalized propped length $A = 0.5$.

B.2. Fluid flux distribution

The problem of flow towards a fracture which is fully filled with proppant was solved in Zazovskii and Todua (1990). The mathematical model was extended to the problem of a partially filled fracture in the present work. The numerical results can be compared against the solution obtained in Zazovskii and Todua (1990) by choosing $\delta(X) = 1$ and $\kappa = 1$. The former condition implies that the fracture has constant opening and the latter implies that there is no mismatch in the permeability of the propped and unpropped fracture segments. The comparison is shown in Fig. 5(b) for $A = 0.2$ and two different values of the dimensionless fracture conductivity C. The chosen values of C are indicated above the respective curves. The singularity in present solution for $\Psi(X)$ at $X = A$ is due to the numerical formulation.

References

Balueva, A. V., & Zazovskii, A. F. (1995). Elastic-hydrodynamic problem of inflow of fluid to a crack in a porous medium. *Mechanics of Solids, 20*(5), 151–160.

Bilby, B., & Eshelby, J. (1968). Dislocations and the theory of fracture. In H. Liebowitz (Ed.). *Fracture: An advanced treatise* (Vol. 1, pp. 99–182). New York: Academic press.

Bortolan Neto, L., & Kotousov, A. (2012a) On the residual opening of cracks with rough faces stimulated by shear slip. In *Proceedings of the 7th Australasian congress on applied mechanics, ACAM 7*. Presented at the 7th Australasian Congress on Applied Mechanics, ACAM 7, Engineers Australia, Adelaide, Australia. (p. 10).

Bortolan Neto, L., & Kotousov, A. (2012b). Residual opening of hydraulically stimulated fractures filled with granular particles. *Journal of Petroleum Science and Engineering, 100*, 24–39.

Bortolan Neto, L., & Kotousov, A. (2013). Residual opening of hydraulic fractures filled with compressible proppant. *International Journal of Rock Mechanics and Mining Sciences, 61*, 223–230.

Diyashev, I., & Economides, M. (2006). The dimensionless productivity index as a general approach to well evaluation. *SPE Production & Operations, 21*, 394–401.

Entov, V. M., & Murzenko, V. V. (1994). Steady flow of homogeneous fluid in an oil reservoir recovery element with a hydrofracture. *Fluid Dynamics, 29*, 81–87.

Hills, D. A., Kelly, P. A., Dai, D. N., & Korsunsky, A. M. (1996). *Solution of crack problems: The distributed dislocation technique*. London: Kluwer Academic Publishers.

Kanevskaya, R. D., & Kats, R. M. (1996). Exact solutions of problems of fluid inflow into a well with a vertical hydrofracture and their use in numerical models of flow through porous media. *Fluid Dynamics, 31*, 854–864.

Khanna, A., Kotousov, A., Sobey, J., & Weller, P. (2012). Conductivity of narrow fractures filled with a proppant monolayer. *Journal of Petroleum Science and Engineering, 100*, 9–13.

Kotousov, A., Bortolan Neto, L., & Khanna, A. (2013). On a rigid inclusion pressed between two elastic half spaces. *Mechanics of Materials*. http://dx.doi.org/10.1016/j.mechmat.2013.08.004.

Kotousov, A., Bortolan-Neto, L., & Rahman, S. S. (2011). Theoretical model for roughness induced opening of cracks subjected to compression and shear loading. *International Journal of Fracture, 172*(1), 9–18.

Maiti, M. (1980). On the equilibrium of a Griffith crack opened by a rigid inclusion. *SIAM Journal on Applied Mathematics, 38*(2), 209–214.

McLennan, J.D., Green, S.J., & Bai, M. (2008). Proppant placement during tight gas shale stimulation: Literature review and speculation. In *Proceedings of the 42nd U.S. Rock Mechanics Symposium*. Presented at the The 42nd U.S. Rock Mechanics Symposium, San Francisco. 14.

Mikhailov, D. N., Economides, M. J., & Nikolaevskiy, V. N. (2011). Fluid leakoff determines hydraulic fracture dimensions: Approximate solution for non-Newtonian fracturing fluid. *International Journal of Engineering Science, 49*, 809–822.
Mukherjee, H., Paoli, B. F., McDonald, T., Cartaya, H., & Anderson, J. A. (1995). Successful control of fracture height growth by placement of artificial barrier. *SPE Production & Facilities, 10*(2), 89–95.
Polyanin, A. D. (2002). *Handbook of linear partial differential equations for engineers and scientists*. Florida: CRC Press.
Valkò, P., & Economides, M. J. (1995). *Hydraulic fracture mechanics*. Chichester: John Wiley & Sons.
Zazovskii, A. F., & Todua, G. T. (1990). Steady inflow into a well with a long vertical fracture. *Fluid Dynamics, 25*, 584–593.
Zou, L., Tarasov, B. G., Dyskin, A. V., Adhikary, D. P., Pasternak, E., & Xu, W. (2013). Physical modelling of stress-dependent permeability in fractured rocks. *Rock Mechanics and Rock Engineering, 46*, 67–81.

Appendix C

On a rigid inclusion pressed between two elastic half spaces

Mechanics of Materials 68 (2014) 38–44

Contents lists available at ScienceDirect

Mechanics of Materials

journal homepage: www.elsevier.com/locate/mechmat

On a rigid inclusion pressed between two elastic half spaces

Andrei Kotousov *, Luiz Bortolan Neto, Aditya Khanna

School of Mechanical Engineering, The University of Adelaide, SA 5005, Australia

ARTICLE INFO

Article history:
Received 9 February 2012
Received in revised form 30 January 2013
Available online 27 August 2013

Keywords:
Rigid inclusion
Distributed dislocation technique
Contact
Föppl integral equation
Elasticity
Singularities

ABSTRACT

A solution to the problem of a rigid cylindrical inclusion pressed between two elastic half spaces is obtained using the distributed dislocation technique. The solution is compared with previously published analytical and numerical results for a rigid cylindrical inclusion bounded by two parabolic arcs with rounded corners. A simplified solution to the problem based on the classical contact theory and well-known results for crack problems is also suggested and validated. The simplified solution agrees well with analytical results in the case when the length of the opening around inclusion is much larger than the length of the contact zone.

1. Introduction

The problem of a rigid inclusion pressed between two elastic half spaces has many important applications, for example, in the investigation of friction properties of flat surfaces in the presence of contamination, in the design of various engineering components like fasteners and in various particle technologies such as hydraulic fracturing which involve the injection of small particles (proppant) into artificial fractures or natural cracks present in oil/gas bearing rocks.

The two dimensional problem of a crack opened by a rigid inclusion was first considered by Lowengrub and Srivastav (1970). These researchers used the theory of dual and triple integral equations based on Fourier transform techniques of Sneddon (1957) and obtained a solution by assuming that the length of the contact between the inclusion and the solid body is known. However, in these types of problems, the contact area is generally not known in advance and has to be determined from the smooth tangency of the crack surface at the inclusion ends (Barenblatt, 1962; Cherepanov, 1979). Maiti (1980) reduced the problem with unknown equilibrium contact length to a Föppl integral equation, for which the solution can be easily found in closed form, see Tricomi (1985). However, in the problems considered by Lowengrub and Srivastav (1970) and Maiti (1980), the elastic spaces were assumed to be free from stresses at infinity, so that the opened area and resultant stresses are due to the presence of the rigid inclusion only.

Alblas presented a closed-form solutions to the problem of a rigid cylindrical inclusion, bounded by two parabolic arcs with rounded corners and pressed between two identical elastic half spaces (Alblas, 1974) or two elastics layers of equal thickness (Alblas, 1975). The unknown contact region is calculated by solving a transcendental equation involving elliptic integrals. An approximate solution to these problems based on the Chebyshev polynomials was presented by Gladwell (1977). The latter solution converges to Alblas' closed form analytical solution when the depth of the elastic layers is roughly twice larger than the length of the opening. The numerical approach developed by Gladwell was specifically suitable for the parabolic shape of the rigid inclusion as many of the integrals involved in the solution may be computed explicitly. However, both solutions experience computational difficulties at a relatively small length of the contact between the

* Corresponding author.
E-mail address: andrei.kotousov@adelaide.edu.au (A. Kotousov).

0167-6636/$ - see front matter © 2013 Elsevier Ltd. All rights reserved.
http://dx.doi.org/10.1016/j.mechmat.2013.08.004

inclusion and half spaces, which corresponds to large opening areas or relatively thin elastic layers (Gladwell, 1977).

A related axisymmetric problem in which a rigid oblate spheroidal inclusion is pressed between two dissimilar elastic half-spaces was considered by Gladwell and Hara (1981). The problem is quite relevant to the analysis of a rigid spherical proppant pressed between the faces of a crack in an oil/gas bearing rock; however the analysis of Gladwell and Hara (1981) was based on the assumption that the contact radius between the inclusion and the elastic half space is known in advance. An axisymmetric inclusion problem with an unknown equilibrium contact length between the half spaces was first solved by Selvadurai (1993) in terms of Hankel transforms for a rigid disc-shaped inclusion of constant thickness. The analysis was intended to serve as a simplified model for the fracture and proppant interaction scenario (Selvadurai, 1993, 1994). Selvadurai (1993) also presented an alternative method in which the problem of a rigid disc inclusion between two elastic half-spaces was decomposed into two auxiliary problems which are: (1) the problem of a penny shaped crack opened by rigid disc inclusion and (2) an annular crack subject to uniform tensile stress. The two methods were found to be in excellent agreement.

Several other similar problems have been considered more recently. These include the problem of a non-axisymmetric inclusion of constant thickness pressed between elastic half-spaces (Gladwell, 1995), the indentation of a pre-compressed penny shaped crack by a rigid disc (Selvadurai, 2000), the separation of dissimilar elastic half spaces due to axisymmetric stress fields (Selvadurai, 2003) and the separation of dissimilar piezoelectric half spaces by a rigid disc inclusion (Eskandari et al., 2009).

In this paper, the class of plane strain problems initiated by Alblas (1974) is revisited and two solution techniques are described for the problem of a rigid cylindrical inclusion pressed between two identical half-spaces. Firstly, an approximate solution to the problem is obtained based on the assumption that the length of the opened region between the half spaces is much larger than the size of the inclusion. In this simplified solution, it is also assumed that the stress distribution over the zone of contact is described by the classical Hertz theory of contact stresses between a rigid circular cylinder and an elastic half space (Johnson, 1985). Secondly, a method is developed based on the approach of Maiti (1980), which is reformulated in terms of unknown distributed dislocation densities (Codrington and Kotousov, 2007; Hills et al., 1996). The solution is obtained by the superposition of analytical results for the Föppl integral equation and the analytical solution for two collinear cracks in an infinite plate subjected to uniform remote stress on infinity given by Willmore (1949). This approach is analogous to Selvadurai's solution for disc shaped inclusions. The two solution methods are compared with the previously published analytical and numerical results for rigid inclusions of parabolic shape. The dislocation solution also confirms the applicability of the simplified approximate solution in the case of large openings around parabolic and circular rigid inclusions.

2. Problem formulation

Consider a rigid cylindrical inclusion with the shape, which permits a snug and smooth contact, squeezed by two semi-infinite elastic spaces. The elastic spaces are subjected to remote compressive stress, σ_o as illustrated in Fig. 1. As a result of elastic deformations, an area $(|x| \leqslant a, y = 0)$ between two elastic half spaces is open. The shape of the inclusion determines the profile of the opening over the contact region between the spaces and the inclusion given by $|x| \leqslant c$. Due to absence of the cohesion between the elastic half spaces and between the half spaces and inclusion, there must be no stress singularities in the problem solution, in particular at the end of the inclusion contact zone $(|x| = c)$ and at the point where the half spaces join together $(|x| = a)$. Moreover, the half opened length a, and the length of contact c are not known in advance and have to be determined from the solution of the problem.

The solution to the problem can be obtained as a superposition of the applied stress $\sigma_{yy} = \sigma_o$ and a corrective solution, which negates the induced stresses along the opening, $c < x < a$ (Codrington and Kotousov, 2007; Hills et al., 1996). The corrective solution in the case of frictionless contact can be found from the consideration of the following mixed value boundary-value problem:

$$\delta_y(x,0) = 2u_y(x,0) = f(x), \quad |x| \leqslant c, \tag{1a}$$

$$u_y(x,0) = 0, \quad |x| > a, \tag{1b}$$

$$\sigma_{yy}(x,0) = -\sigma_o, \quad c < |x| < a, \tag{1c}$$

$$\sigma_{xy}(x,0) = 0 \quad |x| < \infty, \tag{1d}$$

where $\delta_y(x,0) = \delta_y(x)$ is the crack opening.

The formulated boundary-value problem (1) can be significantly simplified if one assumes that the length of the contact area is much smaller than the characteristic size of the inclusion and the length of the opening. In this case, in accordance with the Saint–Venant principle, the distribution of the contact stresses between elastic half spaces and the rigid inclusion has to follow the classical Hertz theory (Johnson, 1985). An approximate solution based on these simplifications will be developed next.

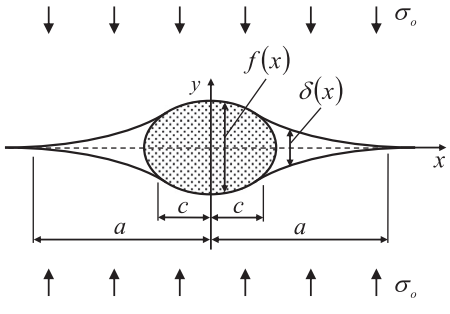

Fig. 1. Problem geometry and coordinate system.

3. Long crack approximation

In the simplified solution, it is assumed that the local geometry of the contact area can be approximated by a second order polynomial (Alblas, 1974), which can be written as

$$f(x) = d - \frac{x^2}{2R}, \tag{2}$$

where d and R are constants. The first constant d represents the depth of the inclusion and the second constant R – the local radius of curvature at the origin of the coordinate system, $x = 0$, which is also the axis of symmetry of the problem, see Fig. 2.

The stress intensity factor at the end of the opening ($|x| = a$) has to vanish as there is no cohesion between half spaces as described above. When the length of the opening area is much larger than the length of the contact i.e. $a \gg c$ the distribution of the contact pressure can be replaced by a concentrated force, P for the purpose of stress intensity factor calculations at $|x| = a$. This results into the following equation (Sanford, 2003):

$$\frac{P}{\sqrt{\pi a}} - \sigma_o \sqrt{\pi a} = 0. \tag{3}$$

In the previous equation, the first term represents the stress intensity factor due to a couple of opening forces of magnitude P applied in the centre of the crack. The second term is the stress intensity factor is due to the remote stress σ_o. From Eq. (3) the force acting on the inclusion is simply

$$P = \sigma_o \pi a. \tag{4}$$

The distribution of the contact stresses can be approximated by the equation derived from the classical Hertz theory (Johnson, 1985). For the contact between a rigid cylinder and elastic half space, the distribution of the contact stresses is given by the following expression:

$$\sigma_c(x) = \frac{2P}{\pi c}\sqrt{1 - \frac{x^2}{c^2}}. \tag{5}$$

Combining (5) and (4), the length of the contact area can be determined from the following equation:

$$c = \sqrt{\frac{P}{\pi}\frac{1+\kappa}{2\mu}R} = \sqrt{\sigma_o \frac{1+\kappa}{2\mu}Ra}, \tag{6}$$

where μ is the shear modulus and κ is the Kolosov's constant, $\kappa = 3 - 4\nu$ in plane strain and $\kappa = (3 - \nu)/(1 + \nu)$ in plane stress and ν is Poison's ratio. However, it seems, only the plane strain case is relevant to practical applications.

From the previous equation, the applied remote stress can be found as a function of the material properties and the geometry of the problem as

$$\sigma_o = \frac{2\mu}{1+\kappa}\frac{c^2}{Ra}. \tag{7}$$

Substitution of the last equation into the contact stress distribution (5) results in the relationship

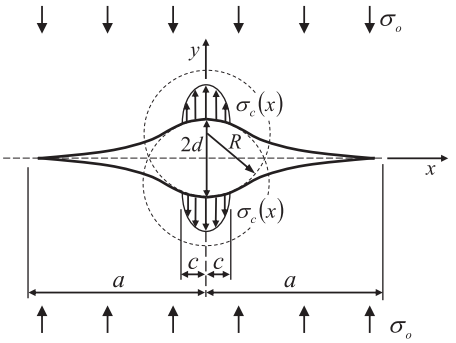

Fig. 2. Decomposition of the problem.

$$\sigma_c(x) = \frac{4\mu}{1+\kappa}\frac{c}{R}\sqrt{1 - \frac{x^2}{c^2}}. \tag{8}$$

The displacement of the crack faces (half of the crack opening displacement) due to the contact stress applied to the crack faces (8) can be found as

$$v_P(x) = -\frac{1}{\pi}\frac{1+\kappa}{8\mu}\int_{-c}^{c}\sigma_c(\xi)\ln\frac{a - x\xi - \sqrt{a^2 - \xi^2}}{a - x\xi + \sqrt{a^2 - \xi^2}}d\xi. \tag{9}$$

The displacement of the crack faces due to the applied remote stress σ_o can be expressed as

$$v_\sigma(x) = -\frac{1+\kappa}{4\mu}\sigma_o\sqrt{a^2 - x^2}. \tag{10}$$

The continuity condition at $x = 0$ requires that

$$v_P(0) - v_\sigma(0) = d, \tag{11}$$

or, finally,

$$-\frac{1}{\pi}\int_0^c \sqrt{1 - \frac{\xi^2}{c^2}}\ln\frac{a^2 - \sqrt{a^2 - \xi^2}}{a^2 + \sqrt{a^2 - \xi^2}}d\xi - \frac{c^2}{2Ra} = d. \tag{12}$$

A system of two Eqs. (6) and (12) can be utilised to find unknown parameters of the problem a and c. However, it is clear that the obtained approximate solution does not satisfy some boundary conditions, such as (1a) or (1c). The use of the continuity equation (11) is ambiguous to some extent and it can be replaced, for example, by a similar continuity equation for an arbitrary point located in the contact area. However, it is expected that Eqs. (6) and (12) provide an accurate solution to the problem when ratio a/R is sufficiently large. The analysis of this equation and a comparison with exact solutions will be presented later in this paper. In the next section, inclusion problem is formulated in terms of the distributed dislocation technique.

4. The distributed dislocation approach

To solve the boundary-value problem (1) let us introduce the function $b(\xi)$ associated with the edge dislocation density (Bilby and Eshelby, 1968; Hills et al., 1996).

$$b(\xi) = -\frac{\partial\delta(\xi)}{\partial\xi}, \tag{13}$$

and utilising the symmetry of the problem, the following integral equation can be written

$$\frac{2}{\pi}\int_c^a \frac{\xi b(\xi)}{x^2-\xi^2}d\xi = \frac{2}{\pi}\int_0^c \frac{\xi f'(\xi)}{x^2-\xi^2}d\xi + \sigma_0\frac{(\kappa+1)}{2\mu}. \tag{14}$$

Further, from Eq. (13) it follows that

$$\delta(x,y) = \int_x^a b(\xi)d\xi. \tag{15}$$

In the limit $x \to c^-$ the following additional continuity condition, similar to Eq. (11) has to be satisfied:

$$f(c-) = \int_c^a b(\xi)d\xi. \tag{16}$$

To determine a and c, the smooth tangency of the crack surface with the inclusion at $|x| = c$ and zero slope at $|x| = a$ is utilised in the solution method. Once the dislocation density is found, the normal stresses arising along the crack line due to a continuous distribution of dislocations are given by Hills et al. (1996)

$$\sigma_y(x,0) = \sigma_y(x) = \frac{2\mu}{\pi(\kappa+1)}\int_{-a}^a \frac{b(\xi)}{x-\xi}d\xi. \tag{17}$$

The solution to the problem under consideration can be obtained as a superposition of solutions of two supplementary problems shown in Fig. 3. The approach is analogous to a previously obtained solution for disc shaped inclusions (Selvadurai, 1993).

The first problem is a straight crack in an infinite solid opened by a rigid inclusion. This problem was considered by Maiti (1980). The second problem represents two collinear cracks occupying the region $c \leqslant x \leqslant a$ and subjected to remote tensile stress σ_o. It was first solved by Willmore (1949) using the complex variable approach. To superpose these two solutions both of them are represented through the dislocation densities (Kotousov, 2007). Then, the dislocation density function $b(x)$ of the problem under consideration can be found as a difference between the dislocation density functions of the inclusion problem, $b_\rho(x)$ and the collinear cracks problem $b_\sigma(x)$, i.e.

$$b(x) = b_\rho(x) - b_\sigma(x). \tag{18}$$

where $b_\rho(x)$ can be obtained from the Föppl integral equation

$$\frac{2}{\pi}\int_c^a \frac{\xi b(\xi)}{x^2-\xi^2}d\xi = \frac{2}{\pi}\int_0^c \frac{\xi f'(\xi)}{x^2-\xi^2}d\xi, \tag{19}$$

The dislocation density function $b_\sigma(x)$ can be determined from the following integral equation

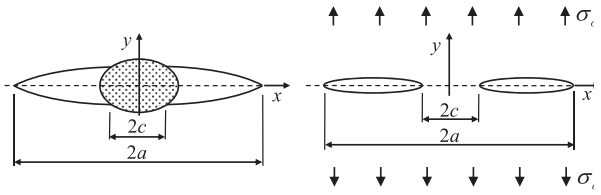

Fig. 3. Approximation of contact problem.

$$\frac{2}{\pi}\int_c^a \frac{\xi b(\xi)}{x^2-\xi^2}d\xi = -\sigma_0\frac{(\kappa+1)}{2\mu}. \tag{20}$$

The solution to the Föppl integral equation (19) can be written in two alternative forms (Maiti, 1980), as follows

$$b_{1\rho}(x) = -\frac{2}{\pi}\left(\frac{a^2-x^2}{x^2-c^2}\right)^{1/2}\int_c^a \left(\frac{\xi^2-c^2}{a^2-\xi^2}\right)^{1/2}\frac{\xi F(\xi)}{x^2-\xi^2}d\xi + \frac{C_1}{(x^2-c^2)^{1/2}(a^2-x^2)^{1/2}}, \tag{21}$$

and constant

$$C_1 = \frac{a}{K(k)}\left(f(c-) + \frac{2}{\pi}\int_c^a\int_c^a \left(\frac{a^2-x^2}{x^2-c^2}\right)^{1/2}\left(\frac{\xi^2-c^2}{a^2-\xi^2}\right)^{1/2}\frac{\xi F(\xi)}{x^2-\xi^2}d\xi dx\right), \tag{22}$$

where the parameter

$$k = \left(\frac{a^2-c^2}{a^2}\right)^{1/2}. \tag{23}$$

The second alternative form of the solution of the Föppl integral equation (19) is

$$b_{2\rho}(\xi) = -\frac{2}{\pi}\left(\frac{x^2-c^2}{a^2-x^2}\right)^{1/2}\int_c^a \left(\frac{a^2-\xi^2}{\xi^2-c^2}\right)^{1/2}\frac{\xi F(\xi)}{x^2-\xi^2}d\xi + \frac{C_2}{(x^2-c^2)^{1/2}(a^2-x^2)^{1/2}}, \tag{24}$$

with

$$C_2 = \frac{a}{K(k)}\left(f(c-) + \frac{2}{\pi}\int_c^a\int_c^a \left(\frac{x^2-c^2}{a^2-x^2}\right)^{1/2}\left(\frac{a^2-\xi^2}{\xi^2-c^2}\right)^{1/2}\frac{\xi F(\xi)}{x^2-\xi^2}d\xi dx\right). \tag{25}$$

The solution to the collinear crack problem is well known and can be written in terms of the dislocation density as:

$$b_\sigma(x) = \sigma_o\frac{\kappa+1}{2\mu}\frac{x^2-a^2\frac{E(k)}{K(k)}}{(x^2-c^2)^{1/2}(a^2-x^2)^{1/2}}, \tag{26}$$

where $K(k)$ and $E(k)$ are the complete elliptic integrals of the first and second kind with parameter k given by Eq. (23).

Similar to the solution of the Föppl integral equation (21)–(26), the solution of the superposed problem can also be written in two alternative forms:

$$b(x) = b_{1\rho}(x) - b_\sigma, \tag{27a}$$

and

$$b(x) = b_{2\rho}(x) - b_\sigma. \tag{27b}$$

These solution must be free from stress singularities, in particular at $|x| = c$ and $|x| = a$. The condition of the smooth tangency of the crack surface with the inclusion at $|x| = c$ applied to Eq. (27a) leads to the following relationship:

$$\left(\frac{a^2-c^2}{\pi c}\right)^{1/2}\left(\int_0^c \frac{2\xi f'(\xi)}{(c^2-\xi^2)^{1/2}(a^2-\xi^2)^{1/2}}d\xi - \frac{\pi C_1}{a^2-c^2}\right) - \sigma_o\frac{\kappa+1}{2\mu}\sqrt{\pi c}\frac{1}{k}\left(\frac{aE(k)}{cK(k)} - \frac{c}{a}\right) = 0. \tag{28}$$

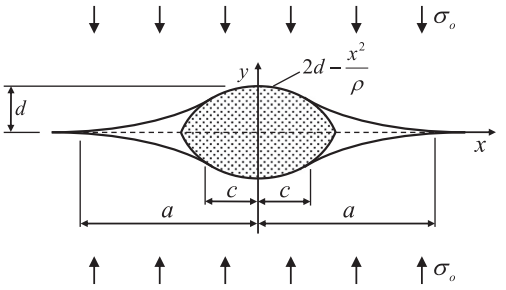

Fig. 4. Parabolic inclusion pressed between elastic half spaces.

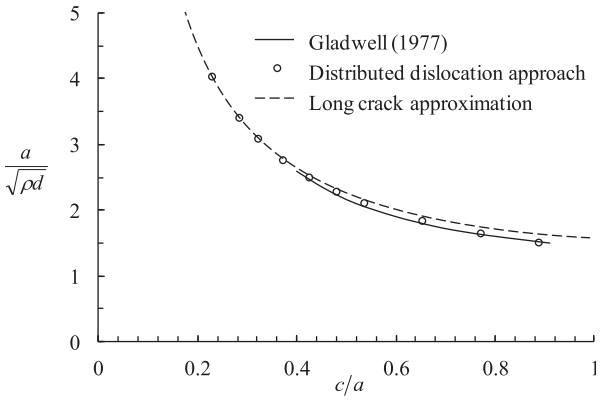

Fig. 5. Variation of dimensionless opening length with contact length parameter.

The absence of the stress singularity condition at $|x| = a$ applied to Eq. (27b) results into another integral equation:

$$\left(\frac{a^2-c^2}{\pi a}\right)^{1/2}\left(\int_0^c \frac{2\xi f'(\xi)}{(c^2-\xi^2)^{1/2}(a^2-\xi^2)^{1/2}}d\xi + \frac{\pi C_2}{a^2-c^2}\right) + \sigma_o \frac{\kappa+1}{2\mu}\sqrt{\pi a}\frac{1}{k}\left(1-\frac{E(k)}{K(k)}\right) = 0. \tag{29}$$

The solution to the system of algebraic equations (28) and (29) can be obtained by using a simple iterative procedure as follows. At a fixed ratio c/R and a guess value of the ratio a/R, the required compressive stress σ_o is first found from Eq. (28) exactly. Then, all three values (c/R, a/R and σ_o) are substituted into Eq. (29). If Eq. (29) is satisfied with the desired accuracy then these values are taken as a solution to the problem at the specified c/R ratio. If the desired accuracy is not achieved then a new and corrected value of a/R and the new calculated value of σ_o from Eq. (28) are substituted again into Eq. (29). The left part of Eq. (29) demonstrates a monotonic behaviour if it is considered as a function of a/R, thus the classical dichotomy method can be applied in the selection of the corrected value of a/R. The procedure is to be repeated until the desired accuracy or a specified convergence condition is achieved. Monotonic functions a/R and σ_o from variable c/R can also be inverted to get the relationship of c/R and a/R as functions of the compressive stress σ_o.

Once c and a are obtained, the distributed dislocation density function $b(x)$ is fully determined. The crack opening displacement $\delta(x)$ can be found from Eq. (15), while the stress distribution can be evaluated from the dislocation density function solution $b(x)$ superposed with the applied stress as described earlier

$$\sigma_y(x,0) = \sigma_y(x) = \frac{2\mu}{\pi(\kappa+1)}\int_{-a}^{a}\frac{b(\xi)}{x-\xi}d\xi + \sigma_o. \tag{30}$$

5. Results

5.1. Parabolic cylindrical inclusion

Consider first a rigid cylinder bounded by two parabolic arcs with rounded corners and pressed between two elastic half spaces with compressive stress σ_o applied on infinity (see Fig. 4).

$$f(x) = 2d - \frac{x^2}{\rho}. \tag{31}$$

Solution to this problem can be obtained from the system of equations (28) and (29) by substituting into these equations the following expressions:

$$f'(x) = -2\frac{x}{\rho}, \tag{32}$$

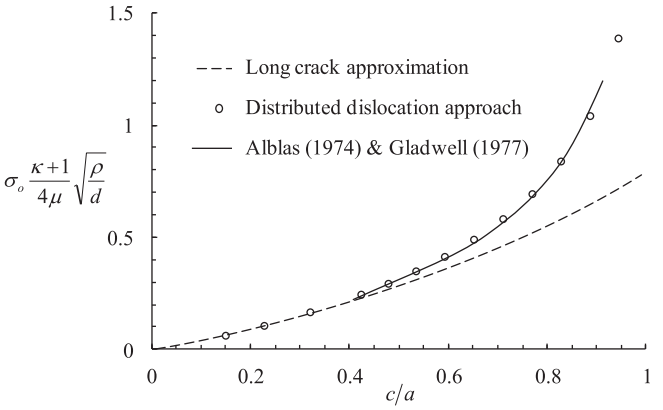

Fig. 6. Variation of dimensionless stresses at infinity with contact length parameter.

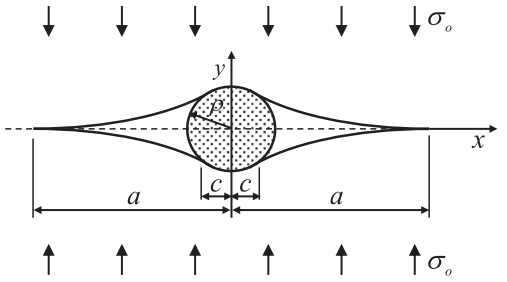

Fig. 7. Circular inclusion pressed between elastic half spaces.

and

$$F(x) = \frac{4}{\pi}\frac{\kappa+1}{2\mu}\frac{c - x\tanh^{-1}(c/x)}{\rho}. \tag{33}$$

A comparison of the present solution with the previously published results and with the simplified Eq. (12) is shown in Figs. 5 and 6.

From the above figures, it is seen that the present solution and the results obtained by Gladwell (1977) agree very well and the simplified equation provides a very good approximation to the problem for ratios $c/a < 0.5$. It is worth to note that Gladwell's solution was obtained for a relatively limited range of ratios c/a ($0.4 \leqslant c/a \leqslant 0.9$) because of difficulties associated with the computational procedure at low values of the nondimensional contact length parameter as described in the Introduction. The present approach does not experience such difficulties and can be easily generalised for other shapes of cylindrical inclusions. However, it must also be noted from Fig. 6 or otherwise that in order to approach a c/a ratio of one, the required compressive stress σ_o would tend to infinity. A more interesting problem of practical interest, which is a circular shape inclusion pressed between two elastic half spaces will be considered next.

5.2. Circular cylindrical inclusion

The shape of circular inclusion (Fig. 7) can be written as

$$f(x) = 2\sqrt{\rho^2 - x^2},\ |x| \leqslant c, \tag{34}$$

which leads to the following expressions for functions $f'(x)$ and $F(x)$

$$f'(x) = -\frac{2x}{\sqrt{\rho^2 - x^2}}, \tag{35}$$

and

$$\begin{aligned} F(x) &= \frac{2}{\pi}\int_0^c \frac{\xi f'(\xi)}{x^2 - \xi^2}d\xi \\ &= -\frac{4}{\pi}\frac{x}{\sqrt{\rho^2 - x^2}}\tanh^{-1}\frac{c\sqrt{\rho^2 - x^2}}{x\sqrt{\rho^2 - c^2}} \\ &\quad + \frac{4}{\pi}\tan^{-1}\frac{c}{\sqrt{\rho^2 - c^2}}. \end{aligned} \tag{36}$$

Similar to the previously considered case, the substitution of these functions into the system of equations (30) and (31) provides a solution to the problem, which is summarised in Figs. 8 and 9. To obtain the approximate solution in the case of cylindrical inclusion, which is valid for small c/a ratios, one has to substitute $d = R = \rho$ and solve the transcendental equation (12) in order to find the geometric parameters of the problem while the applied stress corresponding to this geometry can be calculated using Eq. (6).

From Figs. 8 and 9, it is seen that the simplified equation still provides a good evaluation of the dimensionless opening and stress on infinity, but at smaller ratios of the dimensionless contact length parameter c/a in comparison with the case of a parabolic shaped inclusion considered previously. Comparing Figs. 5 and 6 obtained for parabolic shape inclusion with Figs. 8 and 9 for circular inclusion one can conclude that the shape of the inclusion significantly affects the convergence of the approximate and exact solutions.

6. Discussion and conclusion

The exact inversion of Föppl integral and distributed dislocation approach were combined to obtain a closed form solution in integrals to the problem of rigid cylindrical inclusion pressed between elastic half spaces. This method was validated against previously published

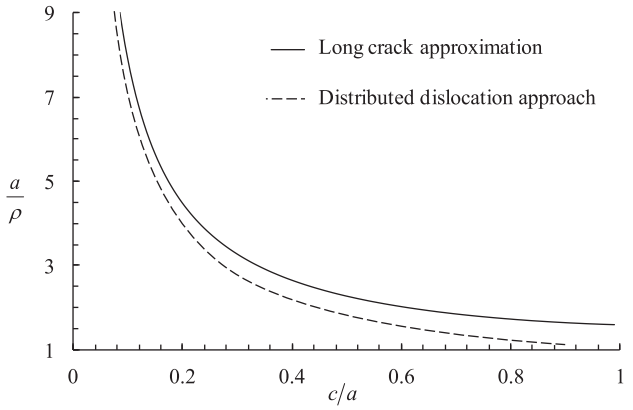

Fig. 8. Variation of dimensionless opening length with contact length parameter.

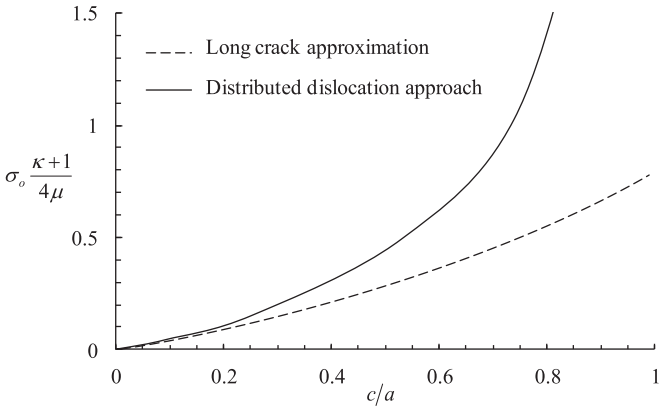

Fig. 9. Variation of dimensionless stresses at infinity with contact length parameter.

results for a rigid cylindrical inclusion bounded by two parabolic arcs with rounded corners. A very good agreement was observed between the present method and past approaches.

The present analytical method has few advantages. It does not experience any computational difficulties and results are readily obtained for a wide range of problem's geometries. However, for other than rubber-like materials, the developed method as well as the previous results can reasonably be applied only for relatively small ratios of the dimensionless opening length, c/a, as the large deformations around the rigid inclusion at moderate values of dimensionless opening ratios can violate the fundamental assumptions of the linear theory of elasticity. Nevertheless, from the Saint Venant's principle, the obtained results, such as stress and strain fields, are expected to be accurate away from the inclusion contact zone, which can experience large deformations as a result of contact stresses.

In addition we developed an approximate solution to the problem under consideration for relatively small values of dimensionless opening ratios. This approximate solution is practically identical to the exact solution at $c/a \sim 0.4$ for parabolic and 0.1 for circular inclusions. This approximate solution, unlike the accurate approaches, can be easily extended to other geometries of cylindrical inclusions and incorporate friction, crushing, plasticity and other non-linear effects, which were neglected in the current study. In order to incorporate these effects, one needs to establish a local deformation law and incorporate it into the solution procedure, similar to the Hertz equation utilised in the present paper.

Acknowledgment

Support of the Australian Research Council through research Grants DP1094299 and LP100100613 is gratefully acknowledged.

References

Alblas, J.B., 1974. On the two-dimensional contact problem of a rigid cylinder, pressed between two elastic half-planes. Mech. Res. Commun. 1, 15–20.

Alblas, J.B., 1975. On the two-dimensional contact problem of a rigid cylinder pressed between two elastic layers. In: De Pater, A.D., Kalker, J.J. (Eds.), The Mechanics of the Contact between Deformable Bodies. Delft University Press, p. 110.

Barenblatt, G.I., 1962. The mathematical theory of equilibrium cracks in brittle fracture. In: Dryden, H.L., Von Karman, T., Kuerti, G. (Eds.), Advances in Applied Mechanics, vol. 7. Academic Press, New York, pp. 55–129.

Bilby, B., Eshelby, J., 1968. Dislocations and the theory of fracture. In: Liebowitz, H. (Ed.), Fracture: An Advanced Treatise. Academic Press, New York, pp. 99–182.

Cherepanov, G.P., 1979. Mechanics of Brittle Fracture. McGraw-Hill, New York.

Codrington, J., Kotousov, A., 2007. The distributed dislocation technique for calculating plasticity-induced crack closure in plates of finite thickness. Int. J. Fract. 144, 285–295.

Eskandari, M., Moeini-Ardakani, S.S., Shodja, H.M., 2009. Inclusion embedded at the interface of a piezoelectric biomaterial. Q. J. Mech. Appl. Math 62 (3), 281–295.

Gladwell, G.M., 1977. The contact problem for a rigid cylinder pressed between two elastic layers. ASME J. Appl. Mech. 44, 36–40.

Gladwell, G.M.L., Hara, T., 1981. The contact problem for a rigid obstacle pressed between two dissimilar elastic half-spaces. Q. J. Mech. Appl. Math. 34, 251–263.

Gladwell, G.M.L., 1995. On contact problems for a medium with rigid flat inclusions of arbitrary shape. Int. J. Solids Struct. 32, 383–389.

Hills, D.A., Kelly, P.A., Dai, D.N., Korsunsky, A.M., 1996. Solution of Crack Problems – The Distributed Dislocation Technique. Kluwer Academic Publishers, Dordrecht, the Netherlands.

Johnson, K.L., 1985. Contact Mechanics. Cambridge University Press, Cambridge.

Kotousov, A., 2007. Fracture in plates of finite thickness. Int. J. Solid. Struct. 44, 8259–8273.

Lonwengrub, M., Srivastav, R.P., 1970. Effect of rigid inclusions in Griffith cracks. SIAM J. Appl. Math. 18, 887–893.

Maiti, M., 1980. On the equilibrium of a Griffith crack opened by a rigid inclusion. SIAM J. Appl. Math. 38, 209–214.

Sanford, R.J., 2003. Principles of Fracture Mechanics. Prentice Hall, Upper Saddle River, New Jersey.

Selvadurai, A.P.S., 1993. A unilateral contact problem for a rigid disc inclusion embedded between two dissimilar elastic half-spaces. Q. J. Mech. Appl. Math. 47 (3), 493–510.

Selvadurai, A.P.S., 1994. Separation at a pre-fractured bi-material geological interface. Mech. Res. Commun. 21, 83–88.

Selvadurai, A.P.S., 2000. The indentation of a precompressed penny-shaped crack. Int. J. Eng. Sci. 38, 2095–2111.

Selvadurai, A.P.S., 2003. On an invariance principle for unilateral contact at a bimaterial elastic interface. Int. J. Eng. Sci. 41, 721–739.

Sneddon, I.N., 1957. Fourier Transforms. McGraw-Hill, New York.

Tricomi, F.G., 1985. Integral Equations. Dover Publications, New York.

Willmore, T.J., 1949. The distribution of stress in the neighbourhood of a crack. Q. J. Mech. Appl. Math. 2, 53–63.